Identification of tumour microenvironment-derived signals that modulate the development and functionality of MDSCs

Carlo Zimarino

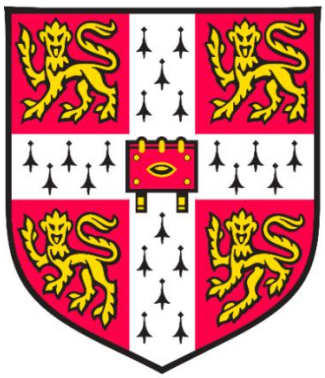

St Catherine's College
Cambridge

MRC | Cancer Unit

This thesis is submitted for the degree of Doctor of Philosophy

Supervisor: Dr. Jacqueline Shields

March 2021

Students Name (CRSid): Carlo Zimarino (cz329)

Dissertation Title: Identification of tumour microenvironment-derived signals that modulate the development and functionality of MDSCs.

Abstract: Myeloid Derived Suppressor Cells (MDSCs) are a heterogeneous immune population found within the tumour microenvironment (TME). We sought to explore the potential role of microenvironment components on the suppressive behaviour, development and maintenance of MDSCs, focusing mainly on the role of the SIRPα-CD47 signalling axis. In an orthotopic melanoma model, we observed an increase in Ly6C-expressing myeloid cells (indicating monocytic-myeloid derived suppressor cells (M-MDSCs) and monocytic dendritic cells (moDC)) as tumours developed. These cells were suppressive, able to block T $CD8^+$ cell proliferation. To model the effect of tumour-derived factors on M-MDSCs and moDCs development and function, we developed a culture system using hematopoietic stem cells cultured with GM-CSF and melanoma tumour condition media (TCM). Similar to the in vivo setting, exposure to TCM skewed the myeloid compartment towards an M-MDSC and moDC phenotype (based on Ly6C expression) that potently suppressed $CD8^+$ T cell proliferation to a greater extent than GM-CSF induced MDSCs.

Further characterisation of the TME by single-cell RNA sequencing and flow cytometry revealed specific expression of the signal-regulatory protein alpha (SIRPα) in M-MDSC and moDC cells fraction and elevated expression of its cognate ligand, CD47 by other immune cells. Thus, we investigated the impact of CD47-SIRPα interaction on MDSC function. Engagement of SIRPα on moDCs and M-MDSCs by recombinant CD47 in vitro induced intracellular signalling via SHP2, and inhibited the phagocytic capability of these cells. Moreover, persistent activation of this programme translated to an increase in their suppressive phenotype quantified by elevated expression of immune checkpoint molecules, inhibitory factors and reactive oxygen species. Knowing this axis promoted a pro-tumour, suppressive phenotype, we then investigated the consequence of its disruption on tumour growth in vivo.

Neutralization of SIRPα on moDCs and M-MDSCs in established tumours resulted in a significant decrease in growth, which was driven by a reprogramming of moDCs and M-MDSCs. Disruption of the CD47-SIRPα axis was sufficient to rescue their phagocytic capability, which in turn enhanced their ability to process and present antigen to

tumour infiltrating T cells. These functional changes were accompanied by metabolic adaptations.

In summary, we report the CD47-SIRPα axis functions as a mechanism used to support moDC and M-MDSC suppressive function in the TME, and its disruption in early tumour-infiltrating monocyte progenitors shows potential to restore anti-tumour features of myeloid cells and in turn promote the T cell mediated anti-tumour immune response.

Acknowledgments

I would like to thank Dr. Jacqueline Shields for the opportunity and the support to work through this PhD as well as correcting and showing me the right way to write things. Hafsa for the scientific discussion which helped me taking decisions during this journey and friendship. Luisa to stir my mind allowing me to see things I couldn't.

Thanks, to the entire Shields lab. Jennifer and Sarah by helping with your kind and comforting chats and the analysis of single cells sequencing. Jake (Giacobbe), to have navigated with me in stormy waters and given me a shoulder to steam out. Will, to remind me that there are other important things out there. Corrado, to have a mate ready to deep in philosophical matters which makes us a bit more human. Leonor to be a person to count on and made me feel better when I was down. Thanks to James with your sharpness and bright mind and Tik to be nice. I will forever remember your contributions to this period of my life and hope to have left a good one to you.

I would like also to thank the guys in ARES (E23 and Quarantine) for the support to my work and being really cool. Plus, special thanks to the CIMR flow team which have been amazing and always super helpful. Thank you to the Hutchinson core staff, I am extremely grateful for all your hard work, without which we could not function.

Thanks to my friend Vasilis, you are very important to me. Thanks to Juju and Elisabeth for helping. Salvo and Paolo, just knowing that you are there makes me happy.

Thank you, Delphine, without you this wouldn't have been possible. Your support and existence are at the core of my achievements and the person I'm now. By the way, thanks for feeding me.

My family. You people are just amazing, literally, I couldn't be here without you. Maria and Giustiniano, Monica and Michele, you saved me, you supported, you love me. I couldn't ask for a better family and I'm deeply grateful.

TABLE OF CONTENTS

Abbreviations

MDSCs: Myeloid Derived Suppressor Cells

TME: Tumour Microenvironment

Ly6C: Lymphocyte antigen 6 complex, locus C1

Ly6G: Lymphocyte antigen 6 complex, locus G

M-MDSCs: Monocytic Myeloid Derived Suppressor Cell

moDCs: monocytic dendritic cells

G-MDSC: Granulocytic Myeloid Derived Suppressor Cells

CD8: Cluster of Differentiation 8

SIRPα: Signal-Regulatory Protein Alpha

CD47: Cluster of Differentiation 47

APC: Antigen Presenting Cells

CD4: Cluster of Differentiation 4

DC: Dendritic Cell

VISTA: V-domain Ig Suppressor of T cell Activation

GR1: granulocyte receptor-1 antigen

CD11B: Cluster of Differentiation 11B, integrin-M (ITGAM)

CD11C: Cluster of Differentiation 11C, integrin, alpha X (ITGAX)

GM-CSF: Granulocyte-macrophage colony-stimulating factor

G-CSF: Granulocyte Colony- Stimulating Factor

M-CSF: Macrophage Colony- Stimulating Factor

IMC: Immature Myeloid Cells

BM: Bone Marrow

IL-(x): Interleukin

STAT3: Signal Transducer and Activator of Transcription 3

NFkB: Nuclear Factor kappa-light-chain-enhancer of activated B cells

RORC1: Retinoic-Acid-Related Orphan receptor C1

C/EBPβ-α (CCAAT-enhancer-binding protein-β-α) and SOCS3 (suppressor of cytokine signalling 3)

S100A8: S100 Calcium Binding Protein A8

S100A9: S100 Calcium Binding Protein A9

VEGF: Vascular Endothelial Growth Factor

COX-2: Cyclooxygenase 2

PGE2: Prostaglandin E2

TAM: Tumour Associated Macrophage

TLR: Toll Like Receptor

ARG1: Arginase 1

TCR: T Cell Receptor

IDO: Indoleamine 2,3-Dioxygenase

ROS: Reactive Oxygen Species

T_{reg}: T Regulatory Cell

CD62L: L-selectin

ADAM17: metalloendopeptidases 17

NK: Natural Killer

TGF-β1: Transforming growth factor beta 1

NKG2D: Natural-Killer Group 2, member D

NKp30: Natural-Killer p 30

CD40/CD40L: Cluster of Differentiation 40 and Ligand

IFN-γ: Interferon Gamma

TCM: Tumour Condition Media

CCR2/CCL2: C-C chemokine receptor type 2 and Ligand

MHCII-I: Major Histocompatibility Complex II-I

CD80: Cluster of differentiation 80, T-lymphocyte activation antigen

CD86: Cluster of differentiation 86, T-lymphocyte activation antigen

eNOS: Endothelial Nitric Oxide Synthase

iNOS: Inducible Nitric Oxide Synthase

NOX2: NADPH oxidase 2

TNF-α: Tumour Necrosis Factor Alpha

TSP1: Thrombospondin-1

SIRPα: Signal Regulatory Protein α, CD172α

CD47: Cluster of Differentiation 47, integrin associated protein (IAP)

ER: Endoplasmic Reticulum

CRT: Calreticulin

CD91: Cluster of Differentiation 91, also known as Low density lipoprotein receptor-related protein 1 (LRP1)

SHP-1/2: src homology ½ domain

VISTA, PD-1H: V-domain Ig suppressor of T cell activation

Foxp3: Forkhead box P3

NO: Nitric Oxide

CTLA4: Cytotoxic T-Lymphocyte Associated Protein 4

PD-1/ PD-L1: Programmed Death Receptor/Ligand 1

SCA-1: Stem cells antigen-1

HSC: Hematopoietic Stem Cell

MPP: Multipotent Stem Cells

CD45: Cluster of Differentiation 45, Protein tyrosine phosphatise C (PTPRC)

MACS: Magnetic-Activated Cell Sorting

F4/80: EGF-like module-containing mucin-like hormone receptor-like 1

CD206: Cluster of Differentiation 206, mannose receptor (MR)

FAS/FASL: First apoptosis signal, Ligand

CXCL: Chemokine (C-X-C motif) Ligand

CCL: Chemokine (C-C motif) Ligand

PTGS2: Prostaglandin 2b

NADPH: Nicotinamide Adenine Dinucleotide Phosphate

CSF-1R: Colony Stimulating Factor 1 Receptor

CHAPTER 1

INTRODUCTION

1.1 The Tumour microenvironment

The complex ecosystem of the tumour microenvironment (TME) is produced by the interaction between malignant and non-malignant cells which to create an environment favourable to its growth and later, dissemination. Because of the types of cells and inflammation observed in the tumour ecosystem, they are often likened to wounds that never heal[1]. The TME is characterised by a dynamic interaction between tumour cells and a diverse array of host cells known as the stroma. The outcome of these intricate interactions is a continuous remodelling in which the tumour cells, the host cells, and the ECM acquire altered phenotypes. These phenotypes exert their functions, either positively or negatively, by regulating tumour survival, propagation and progression[2] (figure 1.1).

The dynamism in populations recruited to the TME can be exemplified by the type of T cell found, which can determine tumour fate. Early tumours are enriched in type 1 $CD4^+$T cells (TH1) aid $CD8^+$T cells to promote tumour control and clearance[3,4,5]. In contrast, in later more established lesions, type 2 $CD4^+$T cells (TH2) and $CD4^+$T regulatory cells (Tregs) block the activation of $CD8^+$T cells to suppress tumour immunity, and promote disease progression[6,7,8,9]. These cells are just one of the protagonists orchestrating the cancer immune response but, other immune and stromal cell types are implicated in the regulation and tumour progression. These include endothelial cells, which comprise the blood and lymphatic circulatory systems, fibroblasts and various bone marrow derived cells (BMDCs), including macrophages, neutrophils, and myeloid cell-derived suppressor cells (MDSCs). The TME is also characterised by specific environmental conditions such as hypoxia[10,11,12], low pH[13,14,15,16] and high interstitial pressure[2,17,18].

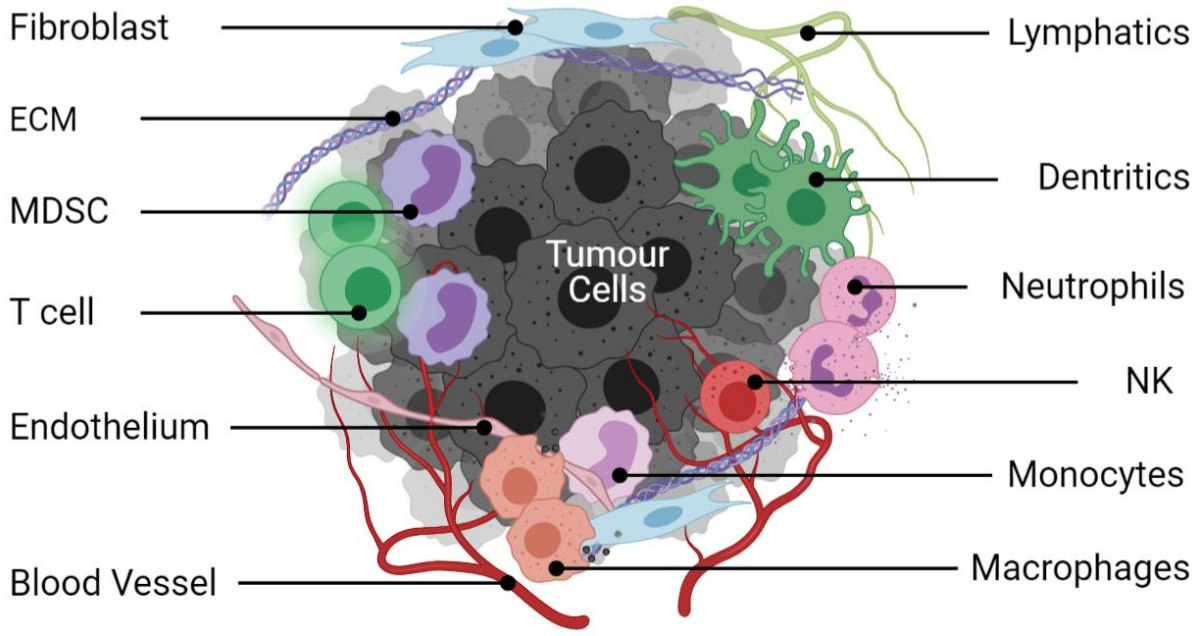

Figure 1.1. The tumour microenvironment. The tumour mass is composed by a heterogeneous population of cancer cells and a supporting niche of secreted factors, extracellular matrix proteins and resident and infiltrating host cells. These include both blood and lymphatic endothelial cells, fibroblasts and an assortment of immune cells such as dendritic cells, macrophage/monocyte, neutrophils, MDSC, natural killer and T cells. Collectively they determine the fate of cancer rejection or progression.

These contribute to the induction of angiogenesis which is crucial for tumour growth, and eventual metastasis. A growing number of cell types contribute to tumour angiogenesis[19,20,21] through their production of growth factors, cytokines and proteases, such as, vascular endothelial growth factor (VEGF), fibroblast growth factor (FGF), tumour necrosis factor-alpha (TNF-α), transforming growth factor-beta (TGF-β), angiopoietins (Ang) and matrix metalloproteinases (MMPs)[22].

The major components of TME play diverse roles to support disease. Here we introduce the ECM, cancer associated fibroblasts (CAFs) and endothelial cells. Immune cells will be discussed in more detail later[23].

1.1.1 The extracellular matrix (ECM)

The extracellular matrix (ECM) is defined as the non-cellular component (mostly fibrillar proteins and proteoglycans) of tissue that provides both biochemical and essential structural support for its cellular constituents, additionally it has a critical role in cell signalling and tissue homeostasis[24]. In tumours, ECM deposition and remodelling increases the stiffness compared to the surrounding normal tissue[25,26,27]. CAFs[28] are largely responsible for this remodelling[29], although macrophages can also exhibit remodelling properties[30,31]. This process involves increased deposition of collagens, fibronectin and proteoglycans, as well changes in their bio-mechanical properties[32,33,34]. Newly deposited and remodelled collagen and elastin fibres assemble and cross-link via the enzyme Lysyl Oxidase (LOX) which induces an increase in matrix stiffness[35,36,37]. The cross-talk between the fibrotic stroma and the tumour is characterised by cytoskeletal tension which causes the disruption of adherent junctions and tissue polarity perturbation resulting in tumour invasion and metastasis[25,38]. Indeed, reducing cytoskeletal tension, or disruption to the ECM surrounding in cancer cell has been reported to suppress their malignant behaviour[39,40]. Besides direct effects on tumour cell behaviour, the ECM acts as a reservoir for growth factors and cytokines which when cleaved, are released into the TME to exert their effects. Tumour cells, fibroblasts and some immune populations such as MDSC[41,42,43] over-express matrix metalloproteinases (MMPs)[44] remodel ECM release matrix bound VEGF that forms a gradient concentration for new angiogenic sprouting in the tumour niche[45,46], whereas release of TGF-β can go on to activate fibroblasts and induce phenotypic behaviour changes infiltrating immune cells[47].

ECM components can regulate immune cell recruitment and influence their phenotype. For instance, cleavage products of Collagen-1 and Elastin, as well as Hyaluronan (HA), act as chemotactic stimuli for myeloid cells[48,49,50] while Tenascin-C and Heparan Sulphate activate macrophages to produce inflammatory cytokines and

induce dendritic cells (DC) maturation[51,52]. Furthermore, the increased deposition of matrix has been reported to create a physical barrier for the infiltration of T cells as shown in pancreatic tumours[53], and T cell proliferation was significantly reduced in high density matrix favouring the formation of Tregs by TGF-β signaling[54]. Thus, the physical environment surrounding cells of a tumour can influence their behaviour dramatically.

1.1.2 Cancer associated fibroblasts (CAFs)

Fibroblasts are one of the most abundant cell types in local connective tissues and contribute to the maintenance of cellular homeostasis of the surrounding tissues. When tissues undergo pathological insult, the fibroblasts become activated and differentiate into myofibroblasts α-Smooth Muscle Actin (αSMA), which contract by actively producing ECM proteins to facilitate wound closure[55]. Once the wound is resolved, these cells undergo programmed cell death[56].

However, in cancer, this chronic wound healing response is hijacked. For instance, TGFβ family ligands and the lipid mediator lysophosphatidic acid promotes the expression of serum response factor (SRF) which drives activation and expression of αSMA[57,58,59]. Moreover, various inflammatory modulators can promote CAF activation such as interleukin-1 (IL-1) acting through the NF-κB pathway (nuclear factor kappa-light-chain-enhancer of activated B cells), and IL-6 acting primarily on signal transducer and activator of transcription (STAT) transcription factors[60,61].

CAFs are extremely heterogeneous and can be recognised diverse markers including Fibroblast-Specific Protein-1 (FSP-1), Fibroblast Activation Protein (FAP), the Platelet Derived Growth Factor Receptors α (PDGFRα) and β (PDGFRβ), Podoplanin (PDPN) and THY-1[62,63]. Our increasing understanding of CAF diversity thanks to single cell sequencing is beginning to help us understand the many pro-tumour functions the possess[64,65,66]; including production of growth factors that stimulate tumour growth,

development of angiogenesis, ECM remodelling, invasion and metastasis, and regulation of immune infiltrates[67,68]. CAFs can attract monocytes through the upregulation of vascular cell adhesion protein 1 (VCAM1) and induce their polarisation towards M2 tumour associated macrophages (TAM) releasing IL-8, thus suppressing Natural Killer (NK) cell function[69]. Similarly, the CAFs recruit myeloid derived cells such as monocytes, macrophages, MDSCs via secretion of CCL2[70] and contribute to their suppressive development by releasing CX-C motif chemokine 12 (CXCL12) and IL6[71,72] to support T-cell dysfunction and tumour immune escape[73]. Besides this indirect mechanism, CAFs were shown to directly inhibit T cells through multiple mechanisms such as decreasing antigen presentation, expressing co-inhibition programmed death ligand 2 (PD-L2), and inducing activation of cell death by Fas Ligand (FasL)[74].

In addition, CAFs secrete a number of pro-angiogenic factors such as VEGF which is a potent inducer of neovascularisation[75]. The release of VEGF is facilitated by the production of ECM remodelling enzymes such as matrix metalloproteinases (MMPs) and LOX[76,77], thus fibroblasts enzymatically and physically alter the ECM via contracting and stiffening matrix fibres[78].

1.1.3 Endothelial cells (ECs)

The lymphatic and blood vessel endothelium operate in parallel to control the distribution of nutrients and oxygen into tissue, maintain the flow of blood, and regulates the trafficking of immune cells[79,80]. The normal vasculature is hierarchical, arteries become arterioles which form into thin capillaries. The smooth muscle cells (SMCs) encapsulate the larger vessels to provide vessel stability, contractility and paracrine cues to the underlying endothelial cells. Small capillaries are sustained by pericytes regulated by PDGFB grow factor which, when genetically depleted causes vessel leakage and haemorrhages[81,82]. All vessels are embedded in the ECM, which as previously stated is rich in collagens, laminin and fibronectin[83].

In tumours, angiogenesis ultimately induces tumour cells intravasation and metastasis[84,85]. Newly formed blood vessels are abnormally tortuous, poorly perfused, and display altered endothelial morphology which results in intercellular gaps or holes, which leak fluid, blood, and fibrin into the surrounding tissue[86,87]. Angiogenesis is driven by hypoxia which upregulates VEGF. However, the poor vessel functionality leads to more hypoxia and more angiogenesis. In addition to VEGF, other angiogenic factors present in the TME include basic fibroblast growth factor (bFGF), angiopoietins (Ang), hepatocyte growth factor, epidermal growth factor (EGF), platelet-derived growth factor (PDGF), and placental-derived growth factor[88]. These factors disrupt endothelial integrity and contribute to the endothelial-mesenchymal transition (EndoMT) as characterised by the replacement of E-cadherin by VE-cadherin which in turn induces motility and invasive behaviours[89]. Furthermore, the EndoMT transition indicated enzyme labelled endothelial cells as possible source of CAFs[90]. ECs isolated from tumours expressed CD31[91], ICAM-2[92] and CD146[93] markers which are shared by normal ECs, and more recently were added more tumour specific CD276[94] and high mobility group box 1 protein HMBG1[95]. Unfortunately, this phenotype was not expressed under cell culture conditions thus, there aren't any known specific markers to identify the tumour associated endothelial cells. The ECs reshape the dynamics of nutrient distribution by creating immature blood vessels and accumulation of interstitial exudate which is advantageous to tumour growth.

The endothelium also recruits and provides immune cell entry via upregulation of adhesion molecules which allows their extravasation[96,97]. However, TME released angiogenic growth factors were shown to suppress the ECs expression of adhesion molecules involved in leukocyte binding (e.g., ICAM-1/2, VCAM-1, E-selectin and CD34)[98,99,100], thus preventing immune cell entry, thereby creating a 'immune privileged site' with few infiltrating immune cell[101]. Indeed, the tumour vasculature actively regulate immune populations they encounter and contribute to tumour

immune escape. Blood endothelium have been reported to present antigens to local leukocytes[102,103,104]. Moreover, they have been shown to express co-inhibitory molecules FASL and PDL1[105] to regulate immune cell entry into the tumour. Similar to blood endothelium, the lymphatic system is also expanded in the tumour stroma and provides a crucial link to tumour draining lymph nodes, in which immune responses are orchestrated[106,107] and a common site of metastasis. Like blood vessels, lymphatics also actively regulate immune function via expression of PDL-1[108,109,110] and regulating trafficking of immune cell to the draining lymph node.

The non-immune components of the TME exhibit a diverse array of functions, that adapt in response to local cues to help shape tumour development. The other protagonists within the TME are the immune cells comprising of lymphoid and myeloid cells which will be discussed later in this introduction. This project has focussed on the myeloid derived suppressor cells in melanoma and utilizes a syngeneic B16F10 mouse model.

1.2 Malignant melanoma

Malignant melanoma is one of the most common types of cancer and is associated with poor clinical outcome. Melanoma incidence in the EU reaches 90,000 new cases annually and melanoma of the skin is considered one of the fastest rising forms of cancer[111]. Melanoma accounts for 4% of all diagnosed forms of skin cancers, but it is responsible for more than 70% of deaths from such cancers[112]. Melanoma aggressively metastasize and the prognosis remains poor even with treatment using immunotherapeutics such as Ipilimumab (anti-CTLA-4), life expectancy remains an average between 10 to 17 months[113,114,115]. The rising incidence is connected to the decreased photoprotection from reduced melanin[116]. Diagnosis stage and prevention to UV exposure are critical in determining the therapy success and improve the chances of survival[117].

Cutaneous melanoma originates from melanocytes in a multistep process called melanomagenesis. The initial stages are known as radial growth phase (RGP), where melanocytes cluster forming a nevus and losing contact with the surrounding keratinocytes. This is followed by a vertical growth phase (VGP); the cells bypass senescence and actively proliferate, crossing the basement membrane and ultimately entering the bloodstream or lymphatic vessels to metastasize in the body[118].

Depending on the stage of the disease, different but limited, therapeutic approaches can be used, such as surgical resection, chemotherapy, radiotherapy, immunotherapy, or targeted therapy[119]. The combination of different chemotherapeutics was evaluated but the overall survival (OS) did not show improvement and is now mostly used as a palliative treatment[120]. This approach is associated to development of melanoma resistance to apoptosis as caused by chemotherapy[121]. Subsequently, a different approach was developed to target melanoma with small molecules inhibitors or antibodies targeting an oncogenic mutation affliated with melanoma. The BRAF (V600E or V600k) mutation is a key serine–threonine kinase from the mitogen-activated protein kinase (MAPK) pathway, which is a mutation occuring in 50% of cutaneous melanoma cases[122,123]. Targeting the tyrosine kinases improved the overall survival, however, the rapid development of multiple mechanisms of resistance made the benefits very limited[124]. In the attempt to reduce resistance mechanisms, the MEK dowstream signalling effectors of BRAF were also targeted[125]. Tremantinib is currently being tested against such targets in several clinical trials, both alone and in combination with other therapies[119]. For melanoma patients that are not presenting with the BRAF mutation the development of immunotheraphies represented a significant breakthrough. Checkpoint inhibitor antibodies such as anti-CTLA4 (Ipilimumab) and anti-PD-1 (Nivolumab and Pembrolizumab) were developed to harness the activation of the immune system against cancer[126,127]. However, even in responsive cancers, the immune checkpoint inhibitor success rate is often less than

50%[128]. Subsequently, a synergistic approach by combining the two inhibitors was tested but still a large portion of patients didn't respond[129]. As stated previously, there is still the need to overcome resistance mechanisms or identify new biomarkers to be exploited to further increase patient survival and cancer remission.

1.2.1 The melanoma microenvironment

An increasing body of evidence suggests that the melanoma microenvironment plays a significant role in limiting the efficacy of therapies. Melanoma is characterised by the prouction of specific antigens such as those expressed by the cancer germline genes MAGE, NY-ESO[130] and Tyrosinase . These are normally presented through MHCI to T cells which mount an immune response[131]. However, tumour cells tend to reduce the surface presentation of the antigen by downregulating MHCI[132,133,134,135]. Therefore, the T cells left unable to recognise cells as abnormal. The balance between co-stimulatory and co-inhibitory mechanimsms define the fate of this activation[136]. Melanoma is characterised by the expression of PD-L1 and PD-L2 which are associated with poor prognosis and greater disease progression[137,138]. In addition, the expression of Fas ligand (FasL) and PD-L1 in melanomas causes the apoptosis of effector T cells via Fas receptor and PD-1[139].

As melanoma progesses, there is an accumulation of Treg and MDSCs suppressive cells which in turn impairs T cells responses[140],[141]. Tregs are is frequently recorded in melanoma, and the ratio of CD8-positive T cells to Tregs is predictive of patient survival[142]. Their recruitment is suported by the CCR4-mediated interaction with the secretion of CCL2 from the tumour cells[143], whilst locally-produced TGF-β and IL-10 contributes to Treg expansion[144, ,145]. In parallel, myeloid suppressive cells are drawn in to the melanoma TME through chemokines and inflammatory mediators such as CCL2[146], CXCL12[147] and GM-CSF[148], G-CSF[149], IL-1b[150], IL-6[151], and prostaglandin E2[152,153], and their presence associated with poor pronosis; high numbers of MDSCs

were found in patients with metastatic melanoma but not their healthy counterparts[154]. Furthermore, CCL2 (MCP-1) is a potent chemoattractant for monocyte derived cells which differentiate into MDSCs and TAM[155]. The latter reported to promote angiogenesis by secretion of IL-8[156] and VEGFA[157], which is amplifed by release of ECM-bound protein by the MDSCs expression of MMPs[43]. CAFs in the melanoma TME are also rich sources of MMP1, MMP2 and MMP13[77,158,159], and at the same time increase deposition of matrix proteins such as osteopontin, SPARC and tenascin to remodel the physical environment[160,161]. The number of lymphatics in the melanoma TME are expanded, and as well as immune regulatry properties (described earlier) support the formation of the pre metatsic niche and lymph node metastasis[162,163].

1.2.2 Melanoma syngeneic model

Syngeneic models represent a versatile, tractable tool that allows studies of events within a rapidly changing niche. They have been useful to describe fundamental mechanisms, identifying potential theraputic targets, and testing new therapies whilst assessing the mechanisms of therapeutic resistance. Murine melanoma cell lines are subcutaneously injected into the strain of mice from which they were initially isolated. The B16 cell lines were derived from chemically induced spontaneous murine melanoma obtained in the C57BL/6 mice strain. The cell lines were denomitated from F0 to F10 and obtained by successive injections and isolations of cells from the tumour[164]. The F number corresponds to the level of aggressivity by which the tumour is able to colonise lungs and kill the host[165]. The major advantange of B16-F10 derived tumours is its rapid growth in vivo, leading to tumor-induced death within 2 to 4 weeks. This makes it a suitable model to study immune changes in a relatively short amount of time.

Another advange of using the melanoma syngeneic model is that the mouse strain is immunocompetent, thus is particularly suitable for studies involving immunotherapy.

For example, CTLA-4 blockade was shown to induce tumour rejection dependent on $CD8^+$ and $NK1.1^+$ cells[166]. Moreover, CTLA-4 was used in combination with PD-1 blockade which synergistically increased tumour rejection from 10% to 65%[167]. However, B16 cells ability to induce adaptive immune response has been questioned because they express relatively low amount of MHCI molecules[168,169]. Additionally, the B16F10 melanoma express tumour-associated antigens such as melanosomal protein TRP2 and gp100 sufficient for T cells recognition and activation[170]. Being lowly immunogenic and characterised by suppressive MDSCs infiltration[171,172], this model is suitable to successfully identify immune responses in immune checkpoint modulation studies[173]. The disadvantage of using this model is that the B16 cells don't present the BRAF mutation which is present in the 50% of the human melanomas[174]. Moreover, they express PTEN which is frequently lost in human disease[175]. Finally, while the rapid growth of B16 tumours does not fully re-capitulate the human disease it is still suitable to study immune responses to external stimulations.

1.3 The tumour immune microenvironment

1.3.1 Brief history of cancer immunology

"There is something unique about cancer that distinguishes it from normal cells, and that this difference can be recognised by the body's immune system"[176]. This was the foreseeing citation from Professor Lloyd J. Old postulated more than forty years ago, where he addressed the concept of cancer immunogenicity in biological context. In reality, cancer and cancer inflammation reports dated back to ancient Egypt; describing how a concomitant infection or fever was making tumours gradually disappear. Thus, it was the early recognition that inflammation could affect the tumour growth. In ancient Greece a recording showed that a persistent inflammatory lesion

could be ground for tumour formations, showing that even in the ancient world, analogies were being made between cancer and inflammation[177].

A long time passed between these observations and 1868, when the immune system was shown to directly modulate tumour growth. The German physicians, Busch[178] and Fehleisen, accidentally infected cancer patients with Streptococcus pyogenes, which is responsible of a common bacterial infection of the superficial layers of the skin. They duly noted a shrinkage of the tumour mass[179].

Towards the end of the nineteenth century, Elias Metchnikoff[180] stipulated the concept of phagocytosis which provided the basis for the study of humoral immunity. Almost simultaneously, Emil Behring and Shibasaburo Kitasato recognised that cell-free serum isolated from an immunised animal and injected in an infected one was curative[181,182]. This brought Behring to the discovery of neutralizing antibodies and opened the field to the identification of the cooperation between acquired and innate immunity[183]. This work led to the assignment of the first ever Nobel Prize in Medicine awarded in 1901 to Emil Behring "for serum therapy in therapeutic medical science".

Further contributions to this field was added by the work of William Bradley Coley, who tested the concept of immune infiltration in cancer by injecting different mixtures of inactivated bacteria in patients and ultimately achieving tumour remission[184]. His work was highly contested but in opening the debate this contributed to the identification of the mechanism behind his work and the therapeutic achievement[185]. Advances in understanding the immune system started to increase in frequency, with Ruth and Graham discovering the interferon[186] and the very first cancer vaccine[187], and the concept of cancer immunology as developed by Burnet and Thomas[188,189]. Their hypothesis of Cancer Immunosurveillance described the continuous patrolling of the immune cells which are able to discern different surface antigenic structure from normal cells and use this to eliminate the cancerous cells[190]. Furthermore in 1967, the existence of T cells and their crucial role in orchestrating the immune response was

published in "Nature" by Jacques Miller[191]. Subsequently, the dendritic cells were characterised by Ralph Steinman in 1973[192] and the description of MHC restriction was elucidated in the work of Zinkernagel and Doherty in 1974[193]. Almost coinciding with the publication on natural killer (NK) cell activity by Eva Klein in 1975[194]. All these elements combined, produced the first evidence of the immunosurveillance concept at the end of the last century.

Shankaran et al[195] created lymphocyte specific immunodeficient mice by disrupting the recombination-activating gene-2 (RAG2) to generate The $RAG^{-/-}$ mice, which developed tumours earlier than wild-type mice and with greater frequency. This work showed that lymphocyte release of IFN-γ and Perforin was essential to prevent the development of sarcomas and epithelial tumours. However, as the tumours developed in the presence of an intact immune system, the immunogenicity reduced and paradoxically favoured the eventual outgrowth of tumours that were more capable of escaping immune detection. This concept was well summarised by the work of Schreiber, Dunn, Old and their teams that truly introduced the concept of immune surveillance and cancer immunoediting[196].

1.3.2 Cancer immunoediting

The Cancer Immunoediting hypothesis refines the earlier cancer immunosurveillance hypothesis. The immune system wasn't only preventing the development of tumours but instead, it was directly shaping the neoplastic evolution[197]. As such, it was presented as a testable model composed by three distinct phases known as the "three E's": Elimination, Equilibrium and Escape[198]. The elimination phase was partially based on the early work of Paul Ehrlich, who conceived the idea that without the immune system the "overwhelming frequency" of cancerous cells couldn't be repressed[199]. Therefore, cancer cells are eliminated before they become clinically evident[200]; often without the requirement for immune cell patrolling and elimination, otherwise we would see a far higher frequency of malignancies. Thus, cancer cells circumvent their

intrinsic tumour-suppressor mechanisms[201] and increase in volume via angiogenesis[202] and tissue invasive-growth[203] mechanisms. This tissue remodelling induces the release of proinflammatory molecules and chemokines[204], which leads to the activation of the innate immune system and its recruitment to the dangerous lesion. Natural Killer cells (NK) present the NKG2D receptor which detects the increase in MHC class I-like self-molecules (MICA) as overexpressed by damaged cells and induces cytolysis causing the release of tumour associated antigens (TAAs)[205,206]. IFN-γ release is critical for the progression of the antitumor response[207], its secretion induces the production of Nitric Oxide (NO)[208] and Reactive Oxygen Species (ROS) by macrophages[209], which when combined with the NK TRAIL[210] or Perforin[211] dependent mechanisms induces apoptosis of the cancer cells. The TAAs released are detected by activated dendritic cells that migrate to the lymph node and subsequently activate naive tumour-specific Th1 $CD4^+$ T cells[212]. These and the antigen cross-presentation via the DC-MHCI create tumour-specific $CD8^+$ Cytotoxic T cells[213,214]. These cells infiltrate the tumour site recognise and kill the cancerous cells[215] a response sustained by $CD4^+$ T-cell IL-2 production. This series of events constitutes the elimination phase.

The equilibrium phase is perhaps the longest phase because highly genetically instable cancerous cells fail to be eliminated, and stay in a dynamic balance with IFN-γ production and the lymphocyte population. This phase is estimated to stand for nearly 20 years in the case of solid tumours[216]. The immune system actively prevents the tumour growth but also provides an evolutionary stimulus promoting the cancer cells in accumulating nucleotide-excision repair instability (NIN), microsatellite instability (MIN), and chromosomal instability (CIN)[217]. This results in a selective pressure towards the survival of the fittest, or in this case, those cells which can establish favourable conditions within the tumour microenvironment for the tumour to escape[218].

The escape phase is characterised by the rise of the selected cancer cells into active growth and expansion. To overcome the stationary state, tumour cells actively produce cytokines associated with immunosuppression such as transforming growth factor β (TGF-β) and interleukin-10 (IL-10). For example, TGF-β promotes the recruitment of suppressive T regulatory cells (Tregs)[219] and myeloid derived suppressor cells (MDSC)[220]. Whereas, IL-10 promotes the polarisation of macrophages towards an M2 phenotype [221]. Those cells are all associated with the promotion of an immunosuppressive environment. Gradually the tumour cells can also down-regulate the MHCI antigens and evade NK cell killing and also, assume a defective death receptor signalling (FasL and TRAIL)[222]. All those factors ultimately reduce the activated T cell infiltration and function, consequently, reducing the pressure on the selected tumour cells allowing tumour escape.

1.3.3 The "Cancer Immunity Cycle".

The Cancer Immunity cycle was proposed as a model to explain the necessary steps taken by the immune system to kill cancer cells[223]. This can be briefly summarised in a series of steps. The first stage is a consequence of the initial response to tumour escape when the NK cells instigate the production TAAs. Tolerance and immunity to necrotic and apoptotic cells is finely regulated by DCs. The phosphatidylserine cell membrane exposure triggers the release of inflammatory cytokines such as IL-10 and TGF-β, combined with the release of cell death degradation products (high mobility group box 1 (HMGB1), uric acid, heat shock proteins) stimulates the DC activation and subsequent TAAs processing[224,225].

This triggers the second step, characterised by the DCs activation of the T cells through MHCI and MHCII antigen presentation. The lymphoid organs host this event; the antigen presenting cells (APCs), which primed the Th1 $CD4^+$ T cells into producing proinflammatory IL-2 and IFN-γ, cross-present the antigen to the naïve T cells that

continuously traffic through secondary lymphoid organs. Both mature DC and naïve T cells express CCR7, allowing homing and colocalization in response chemokine (C-C motif) CCL9 and CCL21[226] and consequent antigen primed T cell expansion. The first characteristic of T cell maturation is the downregulation of CCR7 and the upregulation expression of receptors specific to chemokines expressed in target tissues, examples including CCR1, CCR2, CCR3, CCR5, and CXCR3[227].

At this stage, the matured antigen specific $CD8^+$ cytotoxic T cells traffic back to the tumour site following chemotactic cues. Optimal T cell recruitment was firstly associated with the production of CCR5 or CCL3 by the tumour in mice models[228]. However, the role of chemokines remains controversial because of variation between tumours and the content of immunosuppressive cells in the TME, indicating other factors also contribute to this axis. The primary chemoattractant for effector cells appears to be CXCR3 ligands, CXCL10 and CXCL9[229,230]. The latter was specifically described as inducing a potent infiltration in malignant melanoma by $CD8^+$ T cells and improvement in patient survival[231]. The balance between suppression and inflammation often produces chemokine levels which are sub-optimal for the full attraction of the T cell population. Recruited T cells must then infiltrate the tumour bed via interacting with the APCs expressing the cognate agonist peptide-MHC (pMHC). This interaction may depend upon upregulation of integrins molecules such as leukocyte function-associated antigen (LFA)-1[232] by the T cells and parallel binding on the DCs ICAM-1[233] to form the immunological synapse[234].

This integrin dependent rolling and infiltration brings the T cells to specifically recognise and bind to cancer cells via T cell receptor (TCR). This interaction triggers the recognition of the pathogenic cell. Some tumours may select a reduced pMHC expression phenotype to escape but, if successful the granule content and the IFN-γ release by the CTL should kill the tumour cells releasing more TAAs and repeating the cycle[235,236].

1.4 Innate and adaptive immune compartment in cancer

Our bodies are capable of inducing significant inflammation to destroy threats to its integrity, it has also developed potent suppressive mechanisms by which it returns to the normal status quo, evolving inhibitory receptor/ligand pairs, or immune checkpoints to avoid collateral damage. In cancer, these suppressive mechanisms are exploited causing inhibition of the immune system.

1.4.1 T lymphocytes

As described previously, the $CD8^+$ T cell response is due to activation by the TCR binding to the MHC molecules on the APCs. To achieve an inflammatory polarisation, the co-stimulatory interaction of CD28 with the DCs co-stimulatory molecules CD80 (B7-1) and CD86 (B7-2)[237] have to reinforce the signal, thus surpassing the threshold of activation. In the TME, T cell dysfunction can develop, a phrase commonly termed as T-cell exhaustion, which typically occurs as a result of a physiological protective mechanism against chronic inflammation[238]. The balance between costimulatory and immune checkpoint molecules results in either activation or inhibition of the T cell polarisation. The most well studied inhibitory checkpoints are the cytotoxic lymphocyte antigen-4 (CTLA-4) and the programmed cell death protein 1 (PD-1).

TCR stimulation promotes the membrane exposure of CTLA-4[239] which is also constitutively expressed by Tregs[240]. The inhibitory molecule competes with CD28 for binding to the B7 protein and causes inhibition of T cell proliferation and reduced IL-2 secretion[241]. PD-1 however, does not compete with CD28, but when engaged prevents the phosphorylation activation cascade required by the T cells. PD-1 is engaged by PD-L1 which is broadly expressed by both professional and non-professional APCs[242] including MDSCs, and several type of tumour cells[243,244,245].

Another ligand, PD-L2, is primarily expressed on DCs and monocytes its expression can also be induced different cells including CAFs [74,246].

Growing numbers of potential immune checkpoint molecules are being discovered, highlighting an intricate network of signals that regulates the balance between inflammation and suppression. Within the category of co-inhibitory molecules much interest was generated by LAG-3, TIM-3 and TIGIT[247]. They respectively bind on MHCII, Gal-9 and CD155 expressed by APCs and they are all involved in the regulation of T cell activation. For instance, lymphocyte-activated gene-3 (LAG-3) shares similar structure to CD4 but it has a strong affinity for MHCII. This competition causes the T cells to lose the CD4 co-stimulation and causes inhibition through LAG-3 signalling[248]. Since these checkpoint molecules are upregulated in suppressed T-cells, they can also be used as markers of "T-cell exhaustion"[249].

$CD8^+$ T cells receive support from the variety of $CD4^+$ T cell phenotypes that are present in the TME. The $CD4^+$ T helper 1 (Th1) cells sustain the proliferation of the $CD8^+$ cells by releasing IL-2 and IFN-γ, the production of which strongly correlate with good prognosis[250]. The contribution of $CD4^+$ Th2 and $CD4^+$ Th17 is less evident in the elimination of cancer. However, $CD4^+$ Th2 are important to achieve B cells responses through the release of IL-4, IL-5 and IL-13 and Th17 cells are favourable in fighting microbial insults by IL-17A, IL-17F, IL-21 and IL-22 release[250,251]. Generally, the cytokine signature of these populations correlate with a worse prognosis[250,251] but exceptions exist for Th2 in breast cancer[252] and Th17 in oesophageal cancer[253].

Most commonly associated with tumour progression and the inhibition of T cell inflammatory responses are the Tregs. Their specific marker phenotype comprise of the expression of CD4, forkhead box P3 (FOXP3) and CD25[254]. Their depletion has been correlated with the insurgence of auto-immune diseases[255] and in cancer, often correlates with poor prognosis, particularly when combined with reduced numbers of

cytotoxic lymphocytes [250,256,257]. Tregs constitutively express CTLA-4 and bind the CD80/86 on APCs impairing their maturation[258]. Moreover, they are even able to physically remove the co-stimulatory molecules from the APC through trogocytosis[259], hence inhibiting the activation of CD8 T cells and APCs. Furthermore, Tregs induce immune suppression through the production of TGF-β, a potent regulator of the CTL function[260], and IL-10, which is involved in macrophage suppression and MDSCs increase[261].

1.4.2 Obstacles posed by the TME to the T cells activity

As we saw in the cancer immunity cycle, there are many points at which an immune response can be hindered, contributing to the progression of disease. Defects in antigen release and tumour cell death may impair the uptake and antigen presentation by DCs and macrophages to T cells. These mechanisms are associated with DC activation impairment due to the correlation between tumour mutation burden (TMB) and decreased expression of tumour neoantigens on the MHCI[262]. Another mechanism of impairment has been associated with molecules that inhibit DC maturation such as IL-6[263], IL-10[264], IL-35, lipids[265] and tumours exosomes[266]. For instance, IL-6 has been shown to suppress the expression of MHCII and CD86 through activation of the STAT3 pathway, thus reducing T cell stimulation[267]. Due to the plasticity of immature DCs, stimulation of these pathways skew their maturation towards suppressive myeloid cells[268] and consequently dampen the T cell anti-tumour response.

T cell migration towards inflammatory sites is mainly driven by CX3CR1, CXCL9 and CXCL10. The abundant expression of these cytokines correlates with T cell recruitment and tumour infiltration[269]. However, it has been reported that melanoma metastases downregulate the secretion of these cytokines thus limiting the effectiveness of antitumor immunity[270]. Moreover, infiltration of T cells into tumours was reported to be affected by aberrant angiogenesis[271,272,273]; new blood vessels can act as a physical

barrier to the extravasation of T cells[274], while VEGF also affects T cell adhesion by reducing the expression of VCAM-1 and ICAM-1 on the surface of endothelial cells[275,276]. Additionally, the tumour endothelium barrier upregulates FASL as a result of VEGF, IL-10 and prostaglandin E2 (PGE_2) stimulation, thus inducing $CD8^+$ T cell death by Fas receptor engagement[277]. Another emerging growth factor that acts synergistically with VEGF in cancer is Angiopoietin-2 (ANGPT2). This is also partially contributes to the vasculature barrier formation[278]. A further barrier that prevents and traps T cells away from their targets is the dense matrix in which cancer-associated fibroblasts (CAFs) may also play a role[279].

1.4.3 NK cells

Natural killer cells (NK) are part of the innate lymphoid cell (ILC) family and their phenotype is characterised by the markers $CD3^-$ $NK1.1^+$ in mice[280], and $CD3^-CD56^+$ in humans[281,282]. Unlike ILC, NKs secrete IFN-γ and have cytosolic ability to counteract pathogens or pathologic insults[283]. In healthy individuals, NKs are "educated" in self-tolerance through the engagement of inhibitory receptors like CD94/NKG2A31 and Ly49 (or Killer cell immunoglobulin-like receptors in humans) with MHC-I. The latter is lost by damaged cells which also express stress ligands recognised by NKs, therefore NKs activate cytotoxic functions to destroy the cell and subsequently contribute to inflammation[284]. A common activating receptor in mice and humans is NKG2D, which binds with strong affinity to polymorphic MHC-I homologous ligands[285,286]. Once the activation is triggered, NKs can exploit several cytotoxic mechanisms such as the release of cytolytic granules into a target cell, induction of death ligand expression, or antibody dependent cell cytotoxicity (ADCC)[287].

Depletion of NKs correlates with higher tumour growth and metastasis, while reports indicate that infiltration correlates with good prognosis, at least in clear cell renal cell cancer (CCRCC) and in response to neoadjuvant treatment in breast cancer[288].

However, tumour cells can evade detection by upregulating ligands for inhibitory receptors, such as non-classical MHCI molecule Human Leukocyte Antigen (HLA) G[289], as well as shedding ligands that bind the activating receptor NKG2D[290]. Contributing to this evasion mechanism, stromal cells or MDSCs in the TME can secrete immunosuppressive mediators or can express NKG2DLs, which drive a chronic interaction with NKG2D on NK cells leading to a down-modulation of the receptor[291,287,292]. Tumours can also express immunoregulatory factors, such as transforming growth factor-β (TGFβ)[293] or release of glucocorticoid-induced TNFR-related (GITR) ligand which binds on NKs GITR receptor inducing tolerance[294].

1.4.4 Neutrophils

Neutrophils are polymorphonucleated cells and are the most abundant circulating leukocyte population, functioning as early responders to inflammatory insult[295]. When activated, they use mechanisms to destroy the pathogen such as phagocytosis[296], degranulation, the release of ROS through NADPH oxidase[297] and Neutrophil Extracellular Traps (NETs) [295]. In the tumour their role remains controversial. Neutrophils were reported to exert both anti- and pro-tumorigenic responses. For instance, TGFβ induced accumulation of neutrophils with protumour function while its blockade favoured an antitumour phenotype[298,47]. However, tumour-derived granulocyte-colony stimulating factor G-CSF induced maturation into immunosuppressive neutrophils[299]. Depending on the cues they engage with, neutrophils adopt an N1-inflammatory or N2-suppressive phenotype[47,300].

Neutrophils also promote tumour angiogenesis[301,302]. In the cancer setting, neutrophils are often associated with a granulocytic population of myeloid-derived suppressor cells (G-MDSCs). The latter share similar morphology and expression of cell surface markers with mature neutrophils, but the difference lies in the ability to suppress T-lymphocytes[303]. G-MDSC cells can promote tumour angiogenesis by remodelling the

ECM via MMP9 expression[304,19]. Even the recruitment of these cells through IL-8/CXCR2 as expressed by the tumour causes the release of elastase which contributes to structural support for cancer invasion[305,306]. In addition, cancer associated neutrophils can express PD-L1 and promote T cells suppression via the PDL1/PD1 axis[307]. Neutrophils increase ROS production when in contact with T cells which can induce epithelial damage and antigen-specific tolerance[308,309]. Therefore, these cells are associated with poor prognosis in melanoma[310] and several others cancers[311,312,313]. Neutrophils can also undergo the process of NETosis, where the release of DNA and chromatin decorated factors such as neutrophil elastase and MMP9 can capture circulating tumour cells to promote metastasis[314] or induce thrombosis through a G-CSF dependent mechanism[315]. In a breast cancer model, DNase digestion of NETs , reduced the number of metastatic lesions[316]. In addition, CAF-secreted Amyloid β was found to drive NETosis through a CD11b and ROS-dependent mechanism both within the TME and at systemic levels[317]. As stated, neutrophils remain a very plastic population dependent on the surrounding cues which can promote inflammatory or suppressive functions, thus are often denominated G-MDSCs.

1.4.5 Dendritic cells

The DCs have an important role in the initiation of antigen-specific immunity and tolerance by providing immunomodulatory signals through cell–cell contacts and cytokines[318]. Historically DCs have been divided by location, with resident DCs in the lymphoid organs and migratory DCs moving through the lymphatics. The resident DCs were also termed conventional DC (cDC) to distinguish from plasmacytoid DC (pDC), which were known to release high quantities of type I interferon in response to viral infection[319]. cDCs originate from DC precursors present in the bone marrow (BM) with maturation dependent upon stimulation of the growth factor fms-like tyrosine kinase 3 ligand (FLT3L) and its receptor FLT3[320], as well as GM-CSF and its receptor GM-CSFR[321]. This is important because they share similarities with monocytic-derived (MC)

cells which may fall under the moDC and M-MDSC definitions. Both the cDC and MCs present an overlapping phenotype, however, the inflammatory MC arise independent of both FLT3 and GM-CSFR[321] thus making them a distinct population of highly plastic cells.

DCs in cancer are composed of different subsets distinct by developmental, phenotypical and functional criteria[322]. The cDC are typically divided in to $CD11c^+$ cDC1 and $CD11b^+$, which is more heterogeneous than cDC2. The former originates from precursor DC by the expression of basic leucine zipper ATF-like transcription factor 3 (BATF3) and are associated with anti-tumour cytotoxic immunity demonstrated in BATF3-/- mice[323]. Moreover, the cDC1 expresses surface molecules XCR1 and Clec9a (DNGR1) in both mouse and human. XCR1 is crucial in the functional cross-talk for activation of CD8+ T cells and NK cells[324] while Clec9a has a role as a receptor for necrotic material[325]. Therefore, cDC1 cells are considered to induce cellular immunity against tumours due to their efficient processing and cross-presentation of exogenous antigens on MHCI molecules to activate $CD8^+$ T cells[326,327]. A study which supports this showed that mouse cDC1, when loaded with dead tumour cell antigen, proved to be a potent vaccine by using the same mechanisms mentioned before[328]. Abundance of cDC1 cells in tumour tissue is also associated with survival and responsiveness to immune checkpoint blockade[326].

The origin of cDC2 remains enigmatic, but they are distinguished from cDC1 by the expression of CD11b integrin and signal regulatory protein alpha (SIRPα)[329]. They are potent inducers of $CD4^+$ T cell mediated immunity in cancer[330, 331]. However, within the $CD11b^+$ DC there is a high grade context dependent plasticity and their function may differ[332]. Human cDC2s can induce the polarization of diverse subsets of $CD4^+$ Th cells and activate $CD8^+$ T cells through MHCII[333,334].

Monocytic derived moDCs are predominantly generated in response to inflammation and promote context-dependent differentiation of $CD4^+$ T cells towards a Th1, Th2, or IL-17-producing T helper (TH17) phenotype[335]. In mice, the lymphocyte antigen 6 complex locus C1 (Ly6C) is associated as a specific marker for the moDCs identification[336]. However, confusion on moDC origin and markers caused a gradual reinterpretation of these cells as 'moDC-like' cells generated during inflammation and are often classified as highly plastic or 'non- classical' monocytes rather than DCs[337,318].

1.4.6 DCs and APCs tolerance in the TME

Cues within the TME induce the development of tolerogenic DCs[338,339]. This can be driven via presentation of TAAs in absence of co-stimulatory molecules which promotes T cell anergy instead of activation. A vast network of co-stimulatory and co-inhibitory signals make the APCs dialog with the T cells through immune checkpoint receptor-ligand interaction. The removal of the CD80/CD86 by CTLA-4 on the T cells is one of the limiting factors for immune activation[340]. PD-L1 and PD-L2, both expressed by DCs and other cells in the TME, add further inhibitory signals to the PD-1 expressing T cells[341]. Another important inhibitory molecule is V-domain immunoglobulin suppressor of T cell activation (VISTA) which is part of the PD-1 family but expressed by APCs. It negatively regulates $CD4^+$ T cell proliferation and also decreases the production of inflammatory cytokines such as IL-2 and IFNγ[342]. Additionally the T cells and APCs co-expressing and co-interacting via CD31 induce a tolerogenic phenotype favouring T cell priming towards Tregs through the increased secretion of IL-10 and TGF-β [343].

Those immune checkpoints contribute in creating a permissive environment for the tumour and limit the recruitment of inflammatory DCs. Indeed, few cDC1 cells are found in the TME due to factors which limit their recruitment, infiltration, and

maturation. This is associated with worst prognosis[326]. It was well characterised in both human and mouse, how tumours rich in active β-catenin were reducing CC-chemokine ligand 4 (CCL4) expression, which resulted in diminished cDC1 infiltration and consequently enhanced tumour growth[344]. Moreover, the tumour decreases the recruitment and maturation of the cDC1 via eliciting NKs by release of prostaglandin E_2 (PGE_2). The NK recruits cDC1 through CCL5 and XC- chemokine ligand 1 (XCL1) and, are main producer of the cDC1 soluble FLT3L molecule which drive their survival. In addition to NK depletion, FLT3L is negatively modulated by VEGF released in the TME. Those factors highly impair the recruitment and survival of cDC1.

The maturation of cDC1 cells is also impacted by IL-6, one of the major cytokines in the TME[345], which preferentially differentiates the myeloid cells towards an MDSC suppressive phenotype[346]. IL-6 and the IL-10 produced by macrophages in the TME facilitate signalling through signal transducer and activator of transcription 3 (STAT3) which polarises the APCs towards immune-suppression[347].

Together the mechanisms described, select for tolerogenic DCs or MDSCs that are characterised by molecules which affect T cell phenotype and function. Furthermore, APCs within the TME display impaired activation and phagocytic function as demonstrated by the sequestration of the alarmin high mobility group protein B1 (HMGB1) through high expression of TIM3[348]. This protein sequesters HMGB1 which normally mediates the innate detection of nucleic acids released by dead tumour cells. Some tumours also express the phagocytosis inhibitory molecule, CD47, that engages the signal- regulatory protein-α (SIRPα) on the APCs and blocks the engulfment of TAAs[349].

1.4.7 Tumour Associated Macrophage (TAM)

Tumour associated macrophages, as with the other myeloid cell types, share the same plasticity, adapting to localised cues in a context dependent manner. Generally, they are defined at two extremes, classically activated M1 and alternatively activated M2 cells[350], although in reality cells exist along a spectrum of phenotypes [351,352]. A third class exists of non-polarised macrophages named M0 or monocytic macrophages[353]. The M1 type are more pro-inflammatory and associated with anti-tumour activity, whilst M2 macrophages display immunosuppressive features which contribute to tumour progression[354]. Accumulation of macrophages is associated with poor prognosis in breast, prostate, ovarian, cervical, lung cancer, follicular lymphoma as well as uveal and cutaneous melanoma[355].

In vitro, Lipopolysaccharide (LPS), IFN-γ and GM-CSF have been shown to polarize macrophages towards the M1 phenotype, as characterized by the expression of TLR-2, TLR-4, CD80, CD86, iNOS, and MHC-II surface molecules[356,357]. Through the release of cytokines such as TNF-α, IL-1α, IL-1β, IL-6, IL-12, CXCL9, and CXCL10, they produce a positive feedback loop maintaining an M1 pheontype[358,359]. The pathways of NF-κB and STAT1 are strongly activated in the process of M1 polarisation which results in tumoricidal functions[360,361].

In contrast, M2 macrophages are directly induced by IL-4 and IL-1, and are characterised by the surface expression of CD206, CD163, CD209 and cytosolic proteins FIZZ1 and Ym1/2[362,363]. They upregulate and use IL-10 and TGF-β as a paracrine polarisation signal[364]. STAT 6 is considered the transcriptional pathway involved in their formation[365].

TAMs are pro-tumour. They support angiogenesis[366,367] and ECM[30,31] remodelling. They represent a dominant immunosuppressive population and are highly influenced by local cytokines such as TGF-β[220], which is produced by M2 cells and induces their differentiation. Furthermore, macrophage-derived TGF-β inhibits the cytosolic activity

of NK cells[368] and inhibits DCs[369] . IL-10 is another interleukin secreted by the TAMs, where it impairs DC maturation by favouring the formation of MDSCs[261] and induces the reduction of antigen presentation[264]. The M2 macrophages are also characterised by the expression of Arginase-1 (ARG-1) which metabolizes L-arginine into polyamine and proline, causing arginine depletion. This is turn is important for the correct TCR formation on the $CD8^+$ T cells[370,371]. The latter are also affected by TAM expression of PD-L1 which sparks inhibition through PD-1 engagement[372]. Additional PD-L1 signalling is caused by the Tregs which are recruited by the TAMs[373]through the secretion of CCL22 . All these mechanisms contribute in polarising the TAMs towards immunosuppression[374] and highlight their high similarity to MDSCs.

1.4.8 Monocyte-Derived cells

As a consequence of their plasticity, monocytes entering a tumour can become different types of cells depending by the molecular milieu they encounter. Their plasticity was highlighted by supplementing in vitro cultures with GM-CSF which induced the monocytes to acquire a DC-like phenotype, long been referred to as moDC cells[375,376,377]. In contrast, cultures supplemented with macrophage-colony stimulating factor (M-CSF) alone caused cells to devolve into a more monocytic macrophage (moMΦ) which could be polarised towards the classic M1 or alternatively activated M2 phenotype via addition of IL-4 and IFN-γ[359]. Much confusion arose by the alternative maturation and intermediate states that these cells can assume. The lack of a clear definition makes it crucial to not only identify them by phenotype but also by function. In an attempt to create a classification system for monocytic-derived cells, they were grown in contact with a vast array of cytokines and TLR ligands, and tested for gene-expression[378]. This study used bioinformatics to reveal a complex array of different cells lying on the phenotype spectrum model[378]. The phenotypes were dependent on medium cues. Supporting this, further work indirectly inferred that

moDCs could be a direct maturation lineage originating from monocytic-derived cells dependent upon the stimulation with GM-CSF[334].

Monocytes mobilised in the bone marrow enter into the circulation and express high levels of the chemokine receptor CCR2. These cells are considered classic monocytes, which in mice express Ly6C^{hi} and corresponds in humans to CD14^{hi}CD16^{lo} [379]. When they extravasate in to a tissue a small percentage becomes similar to tissue-resident macrophages or forms a local monocyte reservoir[380]. Tissue resident monocytes and patrolling monocytes which remain in the blood are biologically intertwined. It remains unclear if this is a final differentiation or if they can interchange their phenotype[381]. This transition was partially addressed by studying the myeloid-determining interferon regulatory factor 8 (IRF8), and the downstream Kruppel-like factor (KLF4). Knock out mice for these molecules resulted in a significant reduction of inflammatory tissue resident monocytes, but had little effect on patrolling populations[382]. The patrolling format expresses the chemokine receptor CX3CR1 and low levels of Ly6C expression in mice, and in human the phenotype is CD14^{lo}CD16^{hi}. In normal physiological conditions they check the vessels by engagement of LFA/ICAM molecules with endothelial cells[383].

In pathological conditions, such as cancer, myeloid cells are rapidly recruited to the injured site causing "emergency" myelopoiesis, resulting in mobilisation and consequent entry into circulation[384] (figure 1.2). In this scenario, hematopoietic stem cells (HSCs) differentiate into common myeloid progenitors (CMPs). These can then differentiate into granulocyte-monocyte progenitors (GMP) leading to the creation of monocytes/macrophages, as well as the DC precursors (MDPs) which develop into monocytes and neutrophils[385]. Lineage determining factor PU.1, CCAAT/enhancer-binding protein beta (C/EBPβ) and C/EBPα are involved in the differentiation of monocytes. PU.1-/- mice were found to be a lethal phenotype and the transfer of PU.1

mutated stem cell resulted in altered myelopoiesis[386,387]. Therefore, PU.1 is a master regulator for the formation of monocytes and DCs that works in combination with the monocyte associated IRF8 and KLF4 transcriptional factors[388]. Moreover, PU.1 synergistically cooperates with C/EBP-α/β[389] to promote the production of the alternative monocyte phenotypes[390]. C/EBPβ-driven programs are also activated in cancer-educated MDSCs[391]. In the primary tumour. TME-derived factors such as CCL2[392] act as chemoattractant for monocytes expressing CCL3, CCL4, CCL5, CXCL12, and growth factors such as colony stimulating factor-1 (CSF1)[393]. CSF1 is secreted in both human and murine tumours, and it is involved in monocyte survival and differentiation into TAMs[394] or MDSC[395]. Altering this axis can induce tumour reduction[396]. VEGF is also implicated in educating monocytes, through enhancing proangiogenic capabilities[397], by acquiring immunosuppressive features, and generating M-MDSCs by upregulating both ARG1 and iNOS through hypoxia response elements and NF-kB[398].

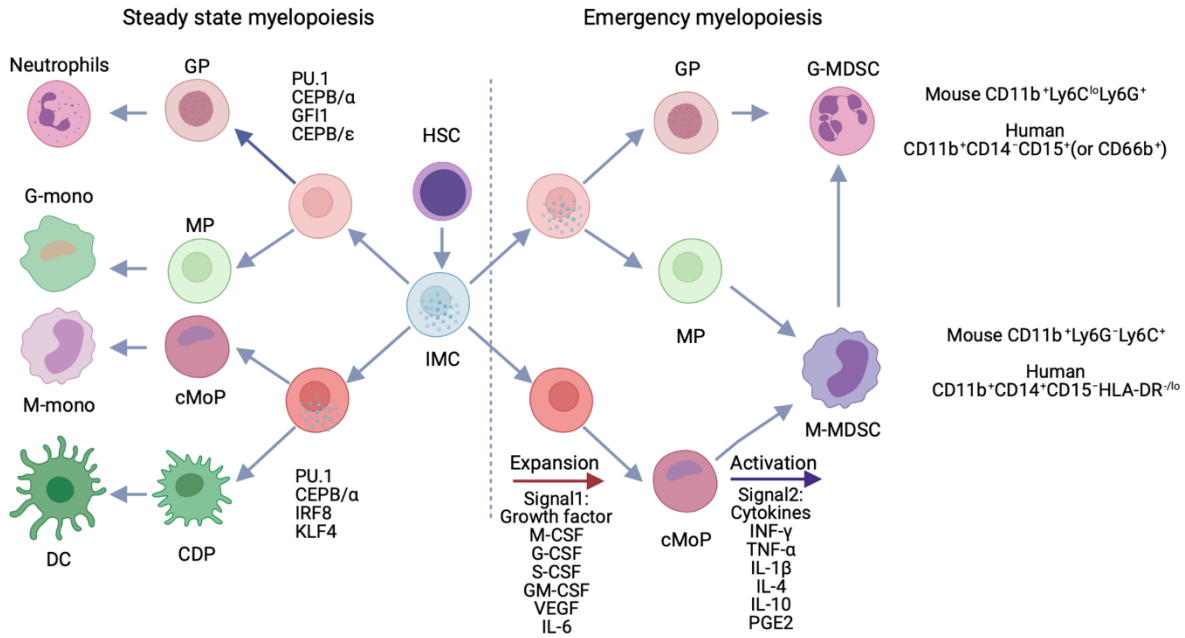

Figure 1.2. Steady state myelopoiesis and 'emergency myelopoiesis' and development of MDSC cells. MDSCs arise from immature myeloid cells (IMC) in the presence of several growth factors and cytokines during emergency myelopoiesis under inflammatory conditions. Growth

factors drive the expansion of myeloid cell progenitors. Then, a persistent second inflammatory signal composed of molecular cues from the TME induce progenitors to develop immunosuppressive function to generate M-MDSCs, and G-MDSCs[399]. Recently, it was found that GMP and MDP yielded distinct monocyte-committed progenitors which differentiated into different monocyte subsets at steady-state[400], respectively. Both monocyte progenitors can generate functional M-MDSCs and further acquire the ability to differentiate into G-MDSCs. Most common phenotype markers of MDSC subsets are illustrated here. HSC, hematopoietic stem cells; IMC, immature myeloid cells; GMP, granulocyte-monocyte progenitor; MDP, monocyte-dendritic cell progenitor; MP, monocyte-committed progenitor; cMoP, common monocyte progenitor; GP, granulocyte-committed progenitor; G-mono, GMP-derived monocyte; M-mono, MDP-derived monocyte.

1.5 The Myeloid Derived Suppressor Cells (MDSCs)

1.5.1 History of Myeloid Derived Suppressor Cells.

MDSCs are described as an immature myeloid population that undergo a transformation which contributes to subverting, inhibiting, and downregulating the immune response to cancer, rather than the conventional differentiation route. Originally it was described as an increase in the extramedullary haematopoiesis and neutrophilia[401] typically associated with the host macro environment; a colony stimulating activity resulting in an increased serum haematopoiesis and a general state of immune suppression[402]. It quickly became clear that MDSCs had a role in immune evasion. Initially, MDSCs were identified as "null cells" due to the lack of typical membrane markers for mature lymphoid and macrophage cells[403].

Their existence has been highly debated following much difficulty in characterising their phenotype. This is due to the high plasticity consistent with tumour heterogeneity and the varied tumour-dependent secreted cytokine-effects exercised on them[404]. However, over the years, the MDSC population has been extensively studied and a panel of markers are now accepted by the scientific community[405] Unfortunately, an obstacle encountered by those studying them is the different repertoire of markers

between human and mice[406]. Despite this, they share the same immunosuppressive behaviour. Thus, it is crucial to characterise them not only by phenotype but also by function, and the suppressive effect they exert on other cells of the immune system[405].

In mice, MDSCs were characterised by cell membrane protein markers, glutathione reductase (GR1) and the integrin-M (CD11b). Two subpopulations were later described as Ly6C and Ly6G, each of which have been investigated for specific phenotype and functions. Furthermore, MDSCs have been sub-divided as monocyte M-MDSC and granulocytic polymorphonuclear G-MDSCs populations by the opposed expression of the Ly6C and Ly6G integrins. This led to the classifications of $CD11b^{+}CD11C^{-}Ly6C^{hi}Ly6G^{-}$ and $CD11b^{+}CD11C^{-}Ly6C^{low}Ly6G^{+}$ cells respectively, each of which have been investigated for specific functionality[407,408,409]. In humans, G-MDSC are described as $CD14^{-}CD11B^{+}CD15^{+}$(or $CD66^{+}$) and M-MDSC $CD11b^{+}CD14^{+}HLA\text{-}DR^{low/-}$ $CD15^{-}$ [410,405].

1.5.2 Origins of Myeloid Derived Suppressor Cells.

All MDSCs derive from a common myeloid progenitor, and their development is most likely driven by the same growth factors that control normal myelopoiesis. The combination of GM-CSF, G-CSF, and M-CSF[411,412] plus persistent pathological signals from the tumour and tumour exudate result in MDSC maturation[402,413]. In cancer, elevated levels of CSFs induce emergency myelopoiesis that increases the survival, recruitment, proliferation and maturation of myeloid cells thus replacing the peripheral myeloid cells. Pathological conditions expose these cells to a prolonged signal marking the expansion in the bone marrow (BM) of immature myeloid cells (IMCs), which eventually migrate into the blood stream and become functionally active MDSCs[414,415,416] (figure 1.2).

The most accepted hypothesis for their activation is the "two signal model" that relies mainly on the activation of STAT3 transcription factor by CSFs and IL-6 to mobilise the IMCs from the BM[417,418]. This is followed by a second activation signal mediated by the pro-inflammatory transcription factor NFκB which is activated by both cytokines and TLR engagement[303]. Recently, it has been shown that RORC1 (retinoic-acid-related orphan receptor C1) was also involved in driving emergency myelopoiesis by acting on other crucial regulatory transcription factors such as C/EBPβ and SOCS3 (suppressor of cytokine signalling 3) the downstream regulators of the CSFs signals[419]. It is likely that both RORC1 and STAT3, together with NFκB, are critical inducers of MDSC generation and expansion[420]. Another study has also demonstrated that tumour-secreted IL-1β stimulated IMC migration from the BM to the periphery, where they proliferated and developed their suppressive phenotype, indicating that extramedullary myelopoiesis could be also responsible for MDSC maturation[419,421].

It is accepted that the IMCs arrest their maturation once subjected to inflammatory mediators such as S100A8, S100A9, VEGF, IL-10, and COX-2/PGE2 which are primarily linked to the activation of STAT3[422,423,424,425]. It also should be noted that the dissimilarities in phenotype could suggest that M-MDSC and G-MDSC have different origins[426,425]. Monocytes could undergo a reprogramming led by TLRs and PGE2 to generate M-MDSCs. Regardless the commonality that all the MDSCs share is the immune suppression directed at other cells of the immune system.

1.5.3 Mechanisms of suppression of MDSCs

MDSCs exercise their disruptive effects from the early stages of tumour development[427,428]. In combination with the tumour microenvironment, MDSCs unbalance the equilibrium stage in favour of tumour survival and spread[429,413 ,430,431]. Cytokine and chemokine gradients at the tumour directly contribute to the recruitment and activation of myeloid cells in the tumour microenvironment[432]. Here, the

continuous remodelling and cellular crosstalk shapes their differentiation and suppressive behaviour, the main feature of which, is their notable inhibition towards T cells.

MDSCs can exercise this inhibition through a variety of mechanisms [429].

Checkpoint molecules: MDSC express inhibitory immune checkpoint molecules. In various works, MDSC have been associated with PD-L1 expression, which, as explained previously engages PD-1 on the T cells to induce T cell anergy[433,434]. Patients that received ipilimumab immune therapy demonstrated G-MDSC cells in circulation, and higher PD-L1 expression by MDSCs was detected in the non-responders suggesting that they were selecting for a more suppressive MDSC population[435].

Altering metabolites: MDSCs also impact the availability of metabolites required by lymphocytes to perform their immunologic function. Specifically, L-arginine depletion through ARG1-dependent consumption[436] and L-cysteine deprivation via its consumption and sequestration[437] impact T cell receptor complex formation. This prevents the TCR from pairing with the ζ-chain which is downregulated, thus resulting in suppression of TCR signalling[438]. L-arginine is the substrate for enzymes expressed in MDSCs such as isoforms of nitric oxide synthases (NOS1, NOS2, and NOS3) and arginases (ARG-1 and ARG–2). NOS catalyse the conversion of L-arginine to NO and L-citrulline, whereas arginases support the reaction of L-arginine to L-ornithine and urea[439]. It was reported that L-ornithine is further metabolised to L-proline which is important for collagen synthesis, and it may have a role in tissue remodelling and tumour growth[439].

Another depleted metabolite that impacts the T cells is cysteine. This is considered an essential metabolite because T cells lack the enzyme cystathionine γ-lyase, which synthetizes cysteine from intracellular methionine[440,441,442,]. T cells are dependent upon macrophages and DCs that can gather cystine through their SLC7A11 transporters.

Intracellularly they reduce it to cysteine, and release cysteine into the extracellular space using the alanine–serine–cysteine (ASC) transporters[443]. The ASC is possessed by T cells to integrate the amino acid and, thus produce proteins[444]. MDSCs have been reported to express SLC7A11 but not the ASC transporter, causing a cysteine depletion in the intracellular space. This reduces the ability of T cells to produce proteins which are critical for proliferation and activation[437].

Reactive oxygen species: A further mechanism resulting in suppression includes the production of free radicals such as reactive oxygen species (ROS), which can drive several molecular changes in the T cell population. A state of oxidative stress occurs when the anti-oxidant system is overwhelmed by the oxidative burst causing a toxic insult[445]. The main source of ROS in MDSCs comes from intracellular mitochondria respiration and NADPH oxidases (NOX)[446], where NADPH transfers electrons to oxygen, creating superoxide radicals[447]. The NOX expression was found to be regulated by STAT3 in MDSCs, which, once extracted from NOX2-/- mice, produced lower amounts of ROS and failed to inhibit IFN-γ secretion and proliferation of antigen-specific $CD8^+$ T cells[448]. The ER and peroxisome (organelle that metabolizes long chain fatty acids) also contribute to the generation of ROS[449]. Despite the high levels of ROS, MDSCs survive through activation of NF erythroid 2-related factor 2 (Nrf2), which is linked to oxidative stress attenuation. Using Nrf2(+/+) and Nrf2(-/-) mammary carcinoma bearing mice, it was found that MDSCs survived and infiltrated more tumours, and also increased suppressive activity by H_2O_2 production[450]. The latter is formed from MDSC-derived superoxide, and impacts T cell activation by decreasing T cellular CD3ζ expression[451,452]. This also reduces the TCRs ability to bind the MHC-I[309]. Such interference, modifies signalling from the IL-2 receptor[453] and IFN-γ reduction resulting in TCR desensitization[454]. The homing of MDSCs is also enhanced by ROS, by inducing VEGF expression which, in a spontaneous melanoma mouse model was dependent on inducible NO synthesis[455]. In the same paper, mice injected

with tumour conditioned media boosted the production of VEGF in MDSCs, strongly indicating that NO produced by these cells acted as a positive feedback for VEGF driven MDSCs tumour infiltration.

As mentioned, MDSCs express a high level of inducible nitric oxide synthase (NOS2), which produces NO. NO was shown to inhibit antigen presentation by DCs and recognition by T cell receptor transgenic OT-II cells, consequently inhibiting proliferation via STAT1 nitration[456]. Moreover, Jak3/STAT5 required for T cell activation, was reversibly down-regulated by NO through inhibition of tyrosine phosphorylation[457]. $CD11b^+$ myeloid cells producing NO were also shown to induce T cell apoptosis, as detected by annexin V expression, which was prevented by blocking with NOS inhibitors[458]. Accumulating levels of NO induced increased expression of cyclooxygenase 2 (COX-2) and HIF-1α[459], and together with COX-1 modulated the production of PGE2. The latter was responsible for upregulating IDO, IL-10 and ARG1 expression, and inducing suppression in ex-vivo generated MDSCs [460].

Cytokine secretion: MDSCs also support the expansion of other immunosuppressive cells. $FoxP3^+$ Tregs have been expanded in vivo via IFN-γ and IL-10 secretion from MDSCs, but the expansion was independent from NO[461]. PBMC extracted MDSCs from patients with hepatocellular carcinoma (HCC) were also shown to induce the expression of $FoxP3^+$ when co-cultured with $CD4^+$ T cells[462]. This relation was also highlighted in ret melanoma mice where the dependence between MDSCs and Tregs was determined[141]. The presence of T regs increased MDSC expression of B7 family immune-regulatory ligands (B7-H1 (PD-L1), B7-H3 and B7-H4) and IL-10 and then, boosted suppression[141]. Moreover, MDSCs from B16 melanoma and from skin tumour–bearing ret transgenic mice greatly increased levels of the CCR5 ligands CCL3, CCL4, and CCL5 and promoted the recruitment of $CCR5^+$ Tregs to the tumour site[463]. In addition, there was an interdependence among TGF-β induced M-MDSCs and the increase in IL-10 and NOS2 expression, hence suppressive phenotype[464]. In other

studies the agonistic signal between CD40-CD40L[465] combined with the production of soluble factors such as IFN-γ, IL-10, TGF-β and ARG1 skewed pathways contributing to a differentiation towards Treg mediated immune suppression[466,467]. Another suppressive mechanism involves indoleamine 2,3-dioxygenase (IDO), an immunomodulatory enzyme that catalyses the breakdown of tryptophan to kynurenine. This enzyme was directly correlated with MDSC recruitment and maturation in mice in addition to associated Treg induction and consequent effector T cells inhibition[468]. MDSCs reduce the levels of tryptophan in the external environment by inducing IDO, which catabolizes this essential amino acid to N- formylkynurenine[469].

Other mechanisms: While the MDSCs are involved in formation of Tregs, the homing of activated lymphocytes is also impaired. Tumour induced MDSCs inhibited the expression of L-selectin (CD62L) on the naïve T and B cells reducing their ability to home to lymph nodes [470]. The concentration of MDSCs correlated with decreased L-selectin expression by a cell to cell contact mechanism due to the metalloprotease ADAM 17 (TACE) cleavage[471]. Supporting this mechanism, splenic M-MDSCs downregulated CD44, a receptor for the extracellular matrix component hyaluronic acid, and CD62L on $CD8^+$ T cells via a partial or total NO dependent mechanism[472]. Combined this impairs T cells extravasation and tissue infiltration.

Another example is the inhibition of NK cells through a membrane-contact dependent mechanism. Membrane-bound TGF-β1 on MDSCs is responsible for MDSC-mediated suppression and even blockade of the activating receptors, NKG2D and NKp30, which ultimately induces NK cell anergy[473,150].

More detailed analysis of the surface repertoires of MDSCs by surface mass spectrometry has identified 93 N-linked glycoproteins[474]. Among these were the leukocyte surface antigen (CD47) and its binding partners thrombospondin-1 (TSP1)[475] and the signal regulatory protein α (SIRPα or CD172α)[476], all of which are key proteins

involved in the "don't eat me signal"[477]. Expression of such signals function to prevent cells being phagocytosed by macrophages, MDSCs and phagocytes in general.

All these mechanisms highlight the severe impact that MDSCs have on immune evasion. Combined with their unclear origin and presence at the early tumour stage, they are a feasible candidate for research and new therapeutics.

1.5.4 Signalling pathways mediating immunosuppression

Intracellular signalling pathways are associated with the development and function of the suppressive behaviour of MDSCs. Of most relevance, the Janus kinase (JAK)–STAT signalling pathway is stimulated by the binding of several cytokines, chemokines and growth factors, resulting in the activation of the STAT protein.

MDSCs were characterised by the presence of activated STAT1 and 3. MDSC and Treg IL-10 production correlates with STAT3 activation in the MDSCs and consequent upregulation of PD-L1, driving T cells suppression[478]. In patients with chronic hepatitis C, M-MDSCs have higher levels of phosphorylated STAT3 and IL-10. Blocking the STAT3 signalling reduced M-MDSC expansion and IL-10 expression[479]. As previously mentioned, in cancer, the MDSC tend to increase their VEGF expression by an activated STAT3 dependency, allowing increased tumour infiltration and thereby support tumour growth and angiogenesis[480,481].

Moreover, the calcium-binding pro-inflammatory proteins S100A9 and S100A8 and NOX2 were proven to be directly regulated by STAT3[423,482]. These proteins are connected to the production of ROS and PGE2 increase in MDSCs, and both are involved in the mechanisms of T cell suppression[483]. In concomitance, STAT1 was showed to be activated by an IFN-γ-dependent signalling path, inducing expansion and activation of MDSCs via the anti-apoptotic molecule Bcl2a1[484]. Similarly, IL-6 produced in various tumours also reduced expression of the SOCS3 protein, leading

to phosphorylation of JAK1, JAK2, TYK2, STAT1 and STAT3 proteins[485]. Therefore, MDSCs expansion and suppressive ability is intertwined with the activation of phosphorylated STAT3.

1.5.5 Macrophage and MDSCs bidirectional crosstalk.

Tumours create a widespread tolerogenic environment by altering normal immune function through a constant and progressive release of tumour-derived factors. Indeed, the composition and concentration of these factors strongly perturb the normal steady state condition. In the tumour microenvironment, myeloid cells play a critical role in this disruption. TAMs infiltrate and exhibit many pro-tumour functions sharing similar activation features to macrophages involved in tissue repair. Mirroring these cells, MDSCs have myeloid origins and in tumours likely exist in various differentiation phases from monocytes/ M-MDSCs towards TAM. Molecularly, this process is accompanied by the upregulation of anti-apoptotic molecules cFLIP[486] and A1[487]. TAM can be distinguished from M-MDSCs by increased relative expression of F4/80[488], low-to-intermediate expression of Ly6C[489] and low or undetectable expression of S100A9 protein[490].

Although these population of cells are treated as separate entities, many features are shared; for example, the two populations exhibit immunosuppressive mechanisms and phenotypic markers. The altered myelopoiesis driven by metabolites, cytokines and chemokines lead to the recruitment of circulating $Ly6C^{+}CCR2^{+}$ inflammatory monocytes that accumulate and mature as TAMs. Interestingly MDSCs with monocytic features traffic from the BM to the tumour using the same CCR2/CCL2 pathway. Here, I will highlight the crosstalk characterising the two populations[491].

Macrophage composition differs depending on their location within a tumour, in response to localised cues, and the balance between recruitment and tissue-resident

turnover[492,493]. As with MDSC maturation, they require two types of signals; those that stimulate myeloid expansion followed by those that activate immune regulatory programmes. Both types of signal can be provided by the tumour. As for MDSCs, CSF1 is typical for macrophage maturation, G-CSF and GM-CSF induces their expansion. However, activated MDSCs within the tumour produce IL-10, which can impair macrophage antigen presentation capacity by MHC class II, CD80, and CD86[494]. Moreover, the ability of macrophages to directly clear tumour cells are also affected via enhanced eNOS and iNOS activity and depletion of Il-12 and TNF-α, further supporting an IL-6 and IL-10 MDSC expansion and M2 suppressive macrophage[495,496]. MDSC-macrophage-tumour cell crosstalk involves activation of STAT3 via IL-6 and IL-10. The relative amounts of these cytokines differ depending on the type of tumour, and are likely to contribute to the differential effects of IL-10 on tumour progression[497]. The most accepted theory is that there is a bidirectional crosstalk that comprises of a vast number of myeloid intermediate states which contribute to immunosuppression. This presents researchers with a significant advantage, as, due to their plasticity MDSCs represent strong therapeutic candidates. As targets they could impact multiple cell types and induce a strong phenotype-functional change towards tumoricidal action. Reducing MDSC number or function is also likely to increase T cell activation by macrophages since macrophage levels of MHC II will be restored. Antigen presentation by DC could also have the potential to improve since reduced numbers of MDSCs will eliminate the competition between MDSC and DC, promoting the expansion and maturation of immunocompetent DC[498].

1.5.6 Glucose metabolism impairment in MDSCs

Rapidly dividing mammalian cells such as cancer cells and immune cells require high glucose uptake. This enables cells to proliferate and mature, thus, they compete to acquire nutrients including glucose. Indeed, cancer cells and T cells upregulate the

glucose transporter GLUT1 via activation of glucose metabolism genes driven by hypoxia and oncogenic signalling[499]. In renal carcinoma, cancer cells outcompeted $CD8^+$ T cells, the overexpression of GLUT1 by the carcinoma correlated with low $CD8^+$ T infiltration[500501]. GLUT1 overexpression was also associated with poor prognosis in melanoma patients[502]. Low concentrations of glucose in the TME impacted the T cells by reducing proliferation capacity, cytokine production and TCR signalling[503]. Notably, the Tregs rely less on glycolysis and more on the oxidative mitochondrial pathway to produce energy, which may be an advantage to their accumulation in the TME[504].

The maturation and activation of MDSCs is characterised by an increase in glycolysis, the pentose phosphate pathway and tricarboxylic acid cycle during their differentiation and activation[505]. Consumption of carbon sources derived from high glycolytic flux was speculated to be a further mechanism of suppression against the T cells. This is supported by an increased uptake of glucose and glutamine needed for their maturation[506]. The upregulation of the glycolysis pathway was proved to protect against the damage caused by ROS producing MDSCs via antioxidant activity[507]. Moreover, in two triple-negative breast cancer (TNBC) mouse models, glycolysis restriction inhibited the release of G-CSF and GM-CSF reducing MDSC prevalence, and enhancing T cell cytotoxic activity[508]. Under glucose-restricted conditions, which may occur in TMEs, G-MDSC engage in oxidative mitochondrial metabolism and fatty acid oxidation (FAO) to support NADPH oxidase-dependent ROS production[509]. In vivo, tumour infiltrating MDSCs were reported to display unique phenotypes with increased mitochondrial mass and preferential use of FAO over glycolysis as a primary source of energy, unlike the peripheral MDSCs[510]. In contrast, M-MDSCs isolated from tumour tissue of patients with hepatocellular carcinoma had a dormant metabolic phenotype. These cells accumulated dicarbonil radical methylglyoxal in the cytosol which was transferred to $CD8^+$ T cells causing paralysis.

The majority of published data described the association between augmented glycolysis flux and the development of the MDSCs. Only the last paper cited was associating a dormant metabolic toxic phenotype to these cells. It is possible that glycolysis and metabolic disfunctions may be associated with MDSCs stage development and TME immersion.

1.6 Cancer immunotherapy

1.6.1 Conventional T cell approaches

Since the introduction of therapeutic immune-checkpoint inhibitors (ICIs), patient outcome for some tumour types has improved. Harnessing the immune response against the tumour focused on the activation of the potent $CD8^+$ cytotoxic T cells[511]. The blockade of CTLA-4 (ipilimumab), PD-1 (pembrolizumab and nivolumab) and PD-L1(atezolizumab, avelumab and durvalumab) acts to remove the inhibition on the T cells, shifting their phenotype from tolerogenic to inflammatory. These T-cell-targeted immunomodulators are now widely prescribed anticancer therapies, either alone or in combination, as a first or second line for treatment. This type of therapy has supported an extension in survival for patients previously considered terminal with melanoma[512,127], NSCLC[513], renal[514], urothelial[515] and head and neck[516]. Despite this, a suboptimal efficacy was seen and correlated to the development of resistance mechanisms[517] and ultimately in cancer recurrence[518].

Resistance has various possible explanations. For instance, insufficient tumour antigenicity could affect the activation of the T cells. It was demonstrated that high tumour cell mutational burden correlated with greater TAAs generation and, consequently improved the response to immune checkpoints blockade[519,520]. Moreover, anti-CTLA-4 therapy induced clonal expansion of TAA-specific T cells which were previously anergic in patients with melanoma[521]. From this research we

understand how poor antigenicity could impact the sensitivity to immune checkpoint blockade.

The loss of the IFN-γ receptor and impaired IFN-γ signalling was another mechanism associated with resistance to ICI, and cancer therapies in general[522]. In melanoma patients it was revealed how the mutation of proteins involved in IFN-γ signalling activity, JAK1/2, was selected for and consequently made the ICI therapy ineffective because it relied on IFN-γ T cell activation[523]. Instead of selecting a resistant IFN-γ tumour cell, another study highlighted how long exposure to IFN-γ was inducing epigenomic changes through STAT1, resulting in the upregulation of alternative T cell inhibitory receptors thus, exhaustion[524].

Normally, IFN-γ increases the expression of TAAs by MHCI and MHCII. Through these molecules, antigen presentation was modulated using anti-PD-1 and anti-CTLA-4 therapies[525]. CTLA-4 resistant patients were shown to have a decreased MHCI expression and the response to anti-PD-1 highlighted a T cell activation dependency upon MHCII expression. This bridges the importance of stimulating the innate immunity to obtain a full response. Defects in antigen processing was caused by β2-microglobulin (B2M) loss of function, hence the reduction of MHCI expression, in immunotherapy treated melanoma patients[526]. Also the gene MEX3B that encodes a post-transcriptional negative regulator of HLA-A, was reported to gain function in melanoma cells to evade T cells response[527].

These are just a few examples of resistance mechanisms to immunotherapy. In addition, the immune checkpoint inhibition, as with many other mechanisms in nature, is redundant. This means resident lymphocytes may upregulate other checkpoint inhibitors if one is blocked therapeutically[528]. The high heterogeneity of cells in the TME and their ability to exclude, suppress and exhaust the cytotoxic T cell responses requires a drug to shift the balance above a certain threshold, thus obtaining a potent therapeutic effect[529]. As such, most of the efforts to date have focused on boosting

the adaptive antitumor immune responses but it is equally important to understand and harness the power of innate immunity to overcome immunotherapy resistance.

1.6.2 Immune Checkpoint Inhibitors targeting myeloid cells

Patients respond to the T cell focused ICIs differently, however, cancer immunotherapy has improved the disease outcome for many forms of cancer, particularly melanoma[530]. Despite these advances, some patients present an inherent primary (never and non-responders) or acquired resistance after a period of response[531]. As previously mentioned, the suppressive impact of the myeloid cells contributes to the resistance against ICIs. Combinatorial approaches targeting both the innate and adaptive immune system offers a good strategy to improve therapeutic response rates[532,533]. Different strategies are being exploited and can be divided into two therapeutic categories: myeloid antagonist and agonist.

Therapies aiming to deplete myeloid suppressive accumulation

Colony-stimulating factor 1 (CSF-1R) is a member of the receptor protein tyrosine kinase family of growth factor receptors. It is expressed by myeloid cells and its activation is achieved by binding to the CSF-1 ligand[534], the expression of which has been correlated with poor prognosis in many cancer types including breast cancer[535,536]. The CSF-1/CSF-1R interaction stimulates proliferation, differentiation and recruitment of M2 TAMs and MDSCs in the TME[534]. CSF-1/CSF-1R blockade as a monotherapy resulted in the delay of tumour progression by reducing the suppressive myeloid phenotype and promoting M1 TAM and T cell responses at the tumour site[537]. Due to these encouraging results, CSF-1R blockade was used in combination the PD-1 blockade (Cabiralizumab and Nivolumab)[538]. This combination is currently tested in clinical trials[537,539] with advanced pancreatic cancer patients, working by stabilising the tumour growth through depletion of monocytes in circulation and simultaneous

increase in $CD8^+$ T cell activation/proliferation[540]. This promising approach is still under evaluation.

Blockers of the molecule Semaphorin 4D (CD100 or SEMA4D) are another promising approach to reduce the suppression caused by myeloid cells. The glycoprotein binds plexin receptors and is involved in immune regulation[541]. It is highly expressed in activated T and B cells, and APCs. When Semaphorin 4D binds to Plexin-B1 it inhibits the migration of monocytic and B-cell lineage cells. Moreover, when it acts as a receptor it modulates T cell activation and is involved in the terminal stages of B cell activation[542]. SEMA4D expression positively correlates with TME exclusion of $CD8^+$ T cells and the infiltration of immunosuppressive M2-polarized TAMs and MDSCs[543,544]. Its blockade in preclinical models has been shown to reduce CD206 M2-polarised macrophages favouring instead the $CD11c^+F4/80^+$ APC phenotype. When used in combination with anti-CTLA4 in colon26 tumour–bearing Balb/c mice, a dramatic reduction of tumour volume was associated with enhanced T cell activity supported by increases in IFN-γ, TNFα, and IL-6 and decrease of IL-10 and MCP-1[545]. Currently, a SEMA4D monoclonal antibody is being tested in combination with anti-PD-1 and anti-CTLA-4 in melanoma patients[546].

One of the first therapies tested for its ability to modulate MDSCs and monocytes towards a mature DC phenotype is called the all trans retinoic acid (ATRA). ATRA causes a glutathione synthase (GSS) increase, thus glutathione (GSH) accumulation in the MDSCs although, the precise mechanism of action remain elusive[547]. ATRA has been used in the clinic in combination with anti-CTLA4 for the treatment of melanoma, showing an increase in circulating HLA-DR^+ myeloid cells over time in together with $CD8^+$ T cells[548].

Additional therapies which modulate MDSCs include VEGF and angiopoitin-2 therapies. VEGF has a role in inhibiting DC maturation, antigen presentation and lymphocyte infiltration, whilst promoting Treg and MDSC expansion in the TME[549,550].

Pre-clinical models and a phase 1 study suggest that an anti-VEGF therapy combined with anti-PD-1 or anti-CTLA4 aided tumour reduction via MHCI upregulation and reduction of myeloid immunosuppressors.

Therapies aiming to reprogram myeloid suppressive cells towards inflammation

Another emerging therapy which targets the myeloid cells ability to create an immunosuppressive environment is CD73. Extracellular ATP or ADP is hydrolysed by CD39 (nucleoside triphosphate diphosphohydrolase) into AMP, which is in turn cleaved by CD73 (ecto-5'-nucleotidase) into adenosine. TGF-β was found to be responsible for inducing the expression of both enzymes by MDCSs in the TME[551]. The accumulation of adenosine in the extracellular space of melanoma tumours led to their absorption by T cells through surface G-protein-linked receptors: A1, A2A, A2B and A3[552]. Activation of A2A adenosine receptor inhibits IFN-γ production and cytotoxic killing by $CD8^+$ T cells and promotes the accumulation of Tregs[553]. Moreover, adenosis reduces the ability of T-cells to home to tumours through the downregulation of adhesion proteins such as ICAM-1, VCAM-1 or P-selectin[554]. Small molecule blockers of the A2A receptor (CPI-444) are currently being tested in clinical trials in combination with anti-PD-L1. Promising results showed that the blockade induced $CD8^+$ T cell infiltration in the tumour and Th1 inflammatory signatures[555] .

As discussed previously, IDO can be constitutively expressed by tumour cells or by macrophages, MDSCs and DCs at the tumour or in lymph nodes. Its expression negatively correlates with good prognosis[556]. IDO inhibition combined with anti-CTLA4 in a B16 murine model attenuated Treg and MDSC tumour infiltration, instead favouring T cell responses[557]. An oral inhibitor has been successfully tested in a Phase 1/2 study with advanced solid tumours[558] but unfortunately was disappointing in phase 3, possibly due to poor dosage. IDO blockade still remains a very attractive target to modulate myeloid cells and induce tumour toxicity.

The PI3-kinase γ was found to be expressed in myeloid cells and controls a critical switch between immune stimulation and suppression during inflammation and cancer. PI3Kγ signalling through Akt and mTOR inhibits NFκB activation while stimulating C/EBPβ activation, thus inducing an MDSC phenotype[559]. In pre-clinical models, PI3Kγ blockade was shown to reprogram myeloid cells towards inflammation[560]. The oral inhibitor IPI-549 combined with anti-PD1 was well tolerated by patients and resulted in a more inflammatory T cell phenotype as driven by the upregulation of IFN- γ[561].

Instead of blockade, an agonist approach is utilised to enhance and boost the antigen presentation and T cells activation which is obtained through CD40 stimulation. This is a costimulatory molecule expressed by myeloid cells that acts as an activator of APCs, T cells and B cells[562]. Once the antigen is presented in the lymph node via MHCII to the T cells, the CD40-CD40L interaction serves as effectively as CD28 in co-stimulating TCR-mediated activation[563]. A correlation between CD40 expression and colorectal cancer patient survival was reported. This was mediated via a reduction in suppressive myeloids and increasing TNF[564]. In a clinical trial, an increase in PD-L1 and PD-1 expression was detected following CD40 agonist therapy. This information was used to the patients advantage by using anti-PD-1 therapy to obtain a synergistic effect for tumour reduction[565].

Another agonist used in the clinic is the Stimulator of Interferon Genes protein (STING or transmembrane protein TMEM173)[566]. Nucleic acid released by cancer cells is detected by this protein. Upon detection, this mediates type I interferon production via STAT1 and 2 for activating the immune response[567]. Before STING identification as a binder, a chemotherapeutic agent 5,6-dimethylxanthenone-4-acetic acid (DMXAA) was shown to induce $CD8^+$ T cell activation in lung cancer and mesothelioma tumour bearing mice[568]. The STING signalling cascade remodels the tumour microenvironment

by antagonizing myeloid-derived suppressor cell expansion[569]. The production of interferon was also a direct effect of this therapy which was later correlated to the stimulation of STING. DMXAA also produced a reduction in tumour vasculature and consequent hypoxia resulting in tumour shrinkage of breast cancer models. This was achieved by a first wave of neutrophil activation followed by monocytes and finally, infiltration of $CD8^+$ T cells [570]. Unfortunately, DMXAA doesn't activate the human counterpart of STING but several specific human agonists are in development.

1.7 Phagocytosis checkpoints for cancer immunotherapy

The monocytes, macrophages and DCs, function as professional APCs. Their role is to bridge innate immune responses and activate adaptive immunity in pathogenic conditions[571]. Phagocytosis is the mechanisms by which the APCs acquire antigens which are processed and finally, presented on the cell surface by the MHCs. In cancer the process of phagocytosis is counter-balanced by anti-phagocytic signals or "do not eat me signals" (figure 1.3).

'Eat me signals'

Pro-phagocytic signals such as calreticulin, signalling lymphocytic activation molecule family member 7 (SLAMF7) and tumour-associated neoantigens induce antigen processing and presentation. Calreticulin is a chaperone molecule present in the endoplasmic reticulum that assists the correct folding of newly synthetized protein[572,573]. Apoptotic cells expose this at the membrane surface allowing its interaction with the prolow-density lipoprotein receptor-related protein 1 (LRP1or CD91) which is expressed by APCs to initiate phagocytosis[574,575]. This interaction with concomitant release of ATP and HMGB1 defines the damage-associated molecular patterns (DAMPs) that result in cancer immunogenicity[576]. Macrophages can also cause translocation of calreticulin to the cell surface after the activation and phosphorylation of expressed TLR such as TLR3, TLR4 and TLR7. Other proteins

participating in the activation of phagocytosis include the molecules SLAM7 and macrophage-1 antigen (MAC1). SLAM7 knockout mice demonstrated impaired phagocytosis activation against cancer cells lines[577]. In cancer this protein interacts with the macrophage-1 antigen (MAC1), a heterodimeric complement receptor composed of integrins CD11b and CD18 found on cDC2, moDC, MDCSs and macrophages. The heterodimer FcRγ and DAP12, proteins containing two ITAM motifs which elicit signalling via the SRC kinase, spleen tyrosine kinase (SYK) and BTK. The outcome of this pathway is the activation of phagocytic machinery[577].

Fc receptors are also involved in initiating phagocytosis through APCs. The FcγR comprises of the family members FcγRI, FcγRIIA, FcγRC, FcγRIIIA, and FcγRIIIB. The latter is the only receptor which transduces an inhibitory signal via phosphorylation of SHP1 and SHP2 proteins[578,579]. Fcγ receptors recognise and bind to the Fc domain of immunoglobulins. This generates an anti-tumour effect via ADCC and also, in mediating antibody-dependent cellular phagocytosis (ADCP)[580]. When engaged, the stimulatory ITAMs-SYC[581,582] signal transduction initiates the response.

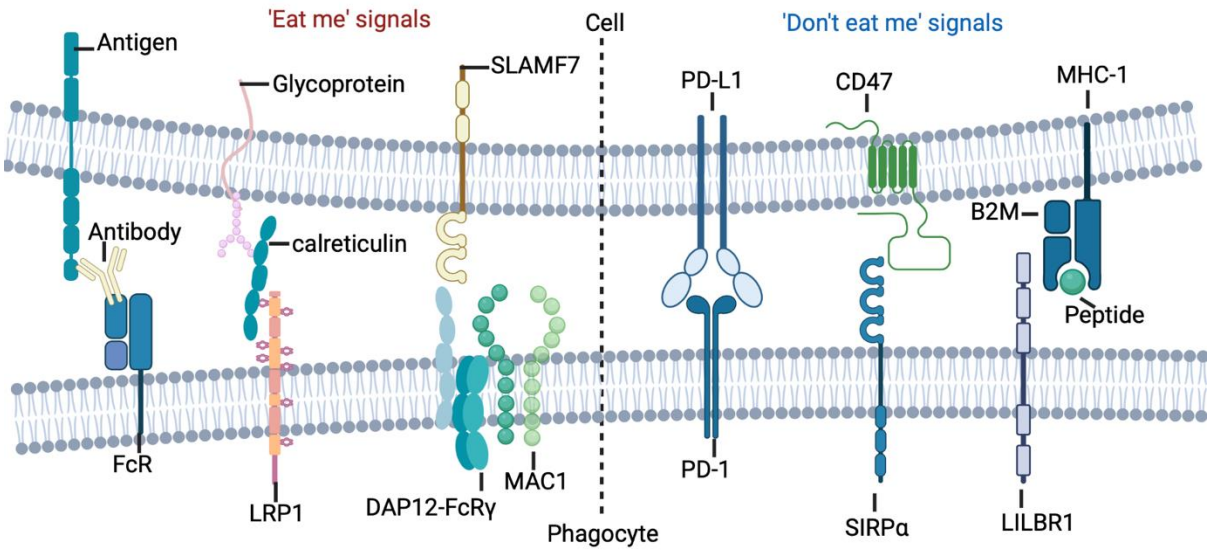

Figure 1.3. Regulation of tumour cell phagocytosis. Phagocytosis of tumour cells by phagocytes is regulated by pro-phagocytosis and anti-phagocytosis ('don't eat me'). The 'eat me' signals include tumour-associated antigens bound to and antibody and recognised by Fc receptors (FcRs)

on phagocytes; the endoplasmic reticulum chaperone protein calreticulin which binds the prolow-density lipoprotein receptor-related protein 1 (LRP1) receptor; the glycoprotein signalling lymphocytic activation molecule family member 7 (SLAMF7) which together with the macrophage-1 antigen (MAC1) are crucial to induce phagocytosis. In opposition, the 'don't eat me' signal includes CD47/SIRPα axes; the programmed cell death 1 ligand 1 (PD-L1); β2-microglobulin (B2M) which binds to the leukocyte immunoglobulin-like receptor 1 (LILRB1).

'Do not eat me signals'

MHC-I is a heterodimer composed by a heavy α-chain and β2-microglobulin (B2M). The α1-2 domains bind to the peptide and the α-3 domain to B2M, and this complex connects to the CD8 co-receptor to allow TCR docking for T cell activation[583]. MHC-I expressed by cancer cells was reported to interact with the leukocyte immunoglobulin-like receptor LILRBI on the APCs causing a reduction in phagocytosis. The B2M protein was responsible for this specific LILRBI-MHC-I interaction. The genetic disruption of MHC-I and CD47 in the tumour cells lead to a synergistic inhibition of tumour growth[584]. Despite the fact that the MHC-I dependent activation of the T cells is required for an immune response and a deletion of it causes tumour resistance[585]. A novel role for PD1-PD-L1 interaction as an inhibitor of TAM phagocytosis has also been highlighted. Here, TAMs displaying an M2-phenotype exhibited increased PD-1 expression correlated to tumour growth[586], and in this model, PD-1 negative TAMs showed better phagocytosis than PD-1^{+} These findings were supported by tumour reduction in PD-L1 knock out mice which were lacking T, NK and B cells. These findings might support that PD1-PD-L1 blockade not only induce T cell-mediated anti-tumour immunity but also phagocyte mediated[587].

Finally, the CD47-SIRPα phagocytic inhibition is the best studied of these mechanisms.

1.7.1 Physiological function of the CD47-SIRPα axis in different tissues.

The role of CD47 in inhibiting phagocytosis was discovered when red blood cells (RBCs) derived from CD47 knockout mice were rapidly cleared by macrophages when

transferred into wild-type (WT) recipient mice[476]. Moreover, the WT-RBCs triggered SIRPα phosphorylation in macrophages preventing phagocytosis. Phagocytosis was reactivated upon SIRPα blockade[476]. This was the first indication that the CD47–SIRPα axis was having a critical role in phagocytosis modulation. The SIRPα molecule is expressed by DC, macrophages and neutrophils but is barely expressed in NK and T cells[588,589,590]. In contrast, CD47 is expressed widely across immune cells[591,592,593], and its expression helps to ensure that self-tissues are not to be destroyed by the immune system, thus contributing to regulating normal tissue homeostasis.

For instance, the normal development of DCs in the spleen was found to be modulated by SIRPα. The spleen harbours two major categories of DCs; $CD11c^{high}$ conventional DC and $CD11c^{int}B220^{+}$ plasmacitoid DCs. The former is further subdivided into $CD4^{+}CD8^{-}$, $CD4^{-}CD8^{+}$ and double negative cDCs. The $CD8^{-}$ and $CD8^{+}$ cDCs are important for the priming of $CD4^{+}$ helper T (Th) and cytotoxic $CD8^{+}$ T cells respectively [594]. Indeed, in both SIRPα mutant and CD47-/- mice, a reduction in the number of $CD8^{-}$ and in particular $CD4^{+}$ cDCs indicated the importance of CD47-SIRPα interaction for their survival and trafficking[595,596,597]. Moreover, this interaction is thought to be important for T cell homeostasis in the spleen. In the SIRPα mutant mice, the T cell zone and the number of $CD4^{+}$ T cells was also reduced, in addition to CCL19 and CCL21 chemokines which are involved in their recruitment and circulation into the spleen[597,598].

Another tissue where the CD47-SIRPα interaction was found to be important was the bone. Derived from the same monocyte-macrophage lineage, osteoclasts mediate bone resorption, development and regeneration[599]. These and bone marrow stromal cells expressed CD47 and SIRPα ,and their development was markedly impaired by depletion of CD47 or disruption of the CD47-SIRPα interaction[600,601]. The stromal cells and osteoblasts support the formation of giant osteoclasts. This was impaired in CD47 deficient bone marrow cultures and mediated by the downregulation of M-CSF as well

as receptor activator of nuclear factor kB ligand (RANKL), both of which are important for osteoclastogenesis[602]. In addition, SIRPα mutant mice showed comparable effects on osteoclastogenesis to the CD47-/- mice[600].

1.7.2 Role of the CD47-SIRPα phagocytosis axes in cancer.

The CD47-SIRPα mechanism is exploited by tumour cells to avoid clearance by APCs. A large number of tumours were reported to overexpress CD47 including myeloma[603], leiomyosarcoma[604], acute lymphocytic leukaemia[605], non-Hodgkin's lymphoma[606], breast cancer[607], osteosarcoma[608], and head and neck squamous cell carcinoma[609]. The first paper that associated CD47-SIRPα disruption and phagocytosis enhancement used acute myeloid leukemia (AML) and Leukemia stem cells (LSC). A CD47-blocking antibody used on AML LSC-human engrafted mice supported an increase in phagocytosis[610], resulting in depletion of the cancerous cells. Subsequently, several studies demonstrated the same concept in different tumours[611,607].

CD47 expression in cancer cells was linked to the stimulation of transcription factor constituent enhancers. One of them was the tumour necrosis factor (TNF) inflammatory pathway that activates NF-κB, which bound directly on the enhancer[612]. In primary breast cancers, Hypoxia-inducible factor 1 (HIF1) showed binding on the CD47 promoter, correlating hypoxia with CD47 expression[613]. Moreover, in human and mouse leukaemia and lymphoma cells the MYC oncoprotein was also linked to the activation of the CD47 promoter. This case proved that depleting the MYC signal was sufficient to reduce the amount of CD47 expressed by the tumour, resulting in increased macrophage and $CD4^+$ T cell infiltration[614]. This research highlights the importance of the CD47–SIRPα axis involvement in tumour evasion.

As described, phagocytosis begins when the endoplasmic reticulum (ER) chaperone protein, calreticulin, is exposed on the cell surface due to an ER stress response. This

molecule is constitutively expressed in many cancers as a consequence of cellular stresses in the tumour microenvironment. The calreticulin ligand, CD91, is present on phagocytic cells including MDSCs, macrophages and dendritic cells[615,616]. As introduced earlier, CD47 is the signalling molecule that blocks and regulates this pathway, and it is the combination of calreticulin-CD47 that controls the balance between pro-and anti-phagocytic signal[616]. When CD47 binds its cognate inhibitory immunoreceptor SIRPα on myeloid cells, the anti-phagocytic signal is triggered.

Signal regulatory protein α (SIRPα) is a transmembrane protein also known as CD172a, SHPS-1, p84 (mouse homologue), or PTPNS1. The protein is formed from three immunoglobulin (Ig)-like domains in its extracellular region and four putative tyrosine phosphorylation sites in its cytoplasmic region[617]. When engaged, the tyrosine sites are phosphorylated followed by activation of the src homology-2 (SH2)-domain-containing protein tyrosine phosphatases; SHP-1 and SHP-2[618]. The former is predominantly expressed in haematopoietic cells and negatively regulates multiple functions of these cells. Instead, SHP-2 is expressed in most cell types modulated by the small guanosine triphosphate (GTP)-binding proteins Ras and Rho which contribute to cell growth and migration[619]. SHP-2 phosphorylation was associated with juvenile leukaemia where it was defined as a proto-oncogene and the product of tumour mutation[620].

CD47-SIRPα engagement via binding of the N-terminal IgV domain of SIRPα and the extracellular Ig-domain of CD47 promotes the phosphorylation of immunoreceptor tyrosine-based inhibitory motifs (ITIM) and consequent SHP-1-SHP-2 recruitment, triggering their enzymatic activity[621]. The signalling cascade leads to the dephosphorylation of myosin IIA. The resulting inhibition of cytoskeletal rearrangement consequently blocks the ability of macrophages to phagocytose[622] (figure 1.4). This activity was also correlated with the STAT3 pathway which was driving

IL-10 expression. In turn IL-10,regulates APC and in particular, MDSC maturation and function[623].

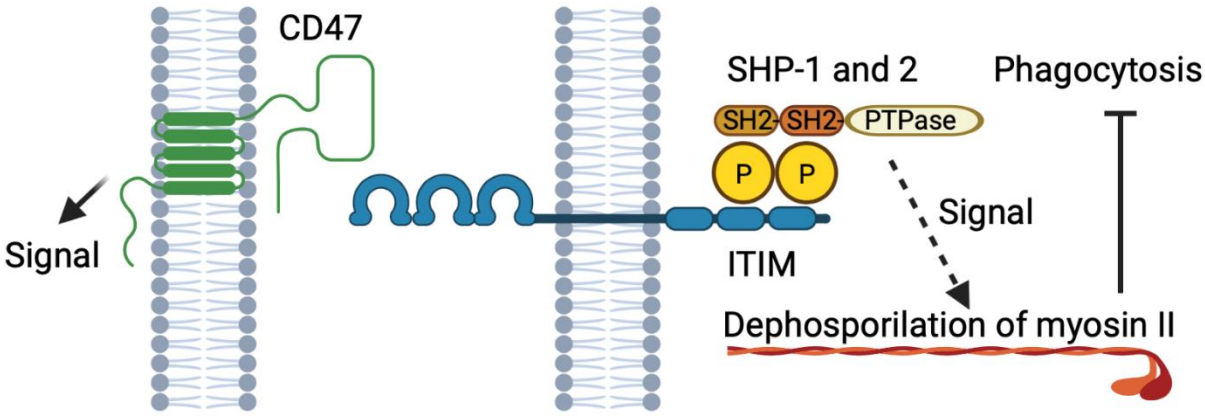

Figure 1.4. The CD47-SIRPα signalling system. CD47 is a member of the Ig superfamily, possessing a V-type Ig-like extracellular domain, five membrane-spanning segments and a short cytoplasmic tail. The extracellular domain interacts with SIRPα, also a transmembrane protein, which contains three Ig-like domains in its extracellular region and two tyrosine phosphorylation sites in its C-terminal cytoplasmic region. The tyrosine-phosphorylated sites of SIRPα (ITIM) bind to the protein tyrosine phosphatases SHP-1 and SHP-2 and activate signalling which induces myosin II dephosphorylation and consequent phagocytosis blockade. The binding of CD47 to SIRPα promotes tyrosine phosphorylation of SIRPα.

1.7.3 Targeting the phagocytosis checkpoint CD47-SIRPα

CD47- SIRPα blockade can be achieved by using antibodies directed either to one or the other molecule. Other methods include epitope competition with recombinant proteins comprising of the extra-cellular regions of CD47 or SIRPα; or targeting the pathways related to CD47 transcription-trafficking to the cell surface of cancer cells. Using those mechanisms the inhibitory signal on APCs is removed and the threshold of phagocytosis activation rendered more sensitive[624]. The use of such therapeutic antibodies increases the antibody-dependent cellular phagocytosis (ADCP) in pre-clinical patient-derived xenograft models[610,607,625,626,627,628].

In particular, anti-CD47 treatment in human glioblastoma cells grown in mouse xenografts induced an increase in infiltration of $CD80^{high}CD206^{low}$ M1-like myeloid cells, suggesting that the CD47-SIRPα interaction may be important in myeloid homeostasis[629]. In addition, blocking the axis was able to promote neutrophil-mediated breast cancer cell clearance when used in combination with trastuzumab[630]. In a similar study a SIRPα blocker was used to target MDSCs, which were allowing long-term kidney allograft tolerance, induced graft dysfunction and rejection. As a result, MDSCs numbers decreased and M1-like ($MHCII^{+}CD103^{+}$) cells increased in this model[631]. Further, the anti-SIRPα blockade promoted the infiltration of neutrophils and macrophages in a lymphoma xenograft mouse model[632].

Ongoing clinical trials are exploiting the potential of targeting the CD47-SIRPα axis for cancer therapy. The majority of trials are focused on the targeting of CD47 overexpression by the cancer cells to obtain ADCP. Primary AML patients were given an anti-CD47 antibody that unfortunately decreased AML cells in the spleen without reducing the overall burden of leukemia[633]. Despite this discouraging result, other drugs have reached clinical trials including Hu5F9-G4 (Forty-Seven), CC-90002 (Celgene), IBI188 (Innovent Biologics), SRF231 (Surface Oncology) and SHR-1603 (Hengrui) representing the anti-CD47 antibody class; and TTI-621 (Trillium), and ALX148 (Alexo Therapeutics) in the format of Fc-SIRPα fused proteins.

All those therapies are focused on the blockade of the CD47 overexpression by the tumour cells but, as we know CD47 is widely expressed by the majority of normal cells which increases the chance of unwanted off-target effects. In normal tissues CD47 is highly expressed in the bladder, prostate, fallopian tubes, mediumly in bronchus tissue, salivary glands, sex organs and lowly in a variety of other tissues of which skin, kidneys and stomach (source, the Human Protein Atlas, https://www.proteinatlas.org/). Further, we should bear in mind that this is a self-antigen marking the health status

and age of the cells. CD47 is expressed to avoid phagocytosis and re-cycle before time, thus allowing cells to exert their function before exhaustion.

Indeed, in trials, off-target binding induced anemia[634] and thrombocytopenia as side effects[635]. Nonetheless, the anti-CD47 therapeutic efficacy may be tumour-specific depending on drug compartmentalisation, stage of cancer progression, immune system responsiveness and acquired drug resistance[636]. Possible strategies to address the side effects may require anti-CD47 pre-loaded nanoparticles or vesicles to specifically deliver the payload to the tumour site or, as in the clinical trial Hu5F9-G4, give an initial low dose of CD47 antibody to induce transient anaemia followed by the therapeutic dose as shown to reduce RBCs depletion[637].

Because of this variability and the off-target effect, therapies targeting SIRPα expressed by the myeloid cells may be more advantageous. SIRPα is highly expressed in the bone marrow, placenta, the appendix, mediumly in the lung, stomach and colon and lowly on the skin, pancreas, vagina, endometrium, breast and prostate (source, the Human Protein Atlas, https://www.proteinatlas.org/). Generally, the expression is more localised compared to CD47 and we can assume that by blocking it, it won't affect the normal self-antigen and recycling cycle of the cells, while more probably it would lower the threshold to activate phagocytic and inflammation mechanisms.

Furthermore, although CD47-SIRPα targeting drugs have been assessed in preclinical models, the therapeutic benefit of selectively blocking SIRPα in humans remains unknown. An anti-SIRPα antibody which has reached the clinical trial stage is BI 765063 (OSE-172). This drug was shown to remodel the TME when used in combination with immune checkpoint blockade. The TME became enriched with M1-like inflammatory macrophage and demonstrated reduced T cell exclusion, ultimately causing tumour reduction[638]. The study of SIRPα blockade could be the solution to ensure targeting on myeloid cells, thus reducing off target effects, dimming inhibition from the CD47 binding and inducing a more inflammatory phenotype.

1.7.4 The P84 and MY-1 anti-mouse SIRPα antibodies.

In this study we will use the antibody anti-SIRPα-P84. This was initially discovered as a neural membrane glycoprotein but analysis of the cDNA sequence lead to the discovery that the P84 adhesion molecule was homologous of the human SIRPα[639]. P84 was later characterised to predominantly bind the integrin-associated protein (IAP/CD47)[640]. The monoclonal anti-SIRPα (clone P84) antibody was generated against this target and it has been used to characterise the phagocytic negative regulation of murine macrophages via SIRPα crosslinking with Src kinase family member[641]. Utilization of the P84 antibody was used to show the SIRPα-CD47 interaction was associated with phagocytosis inhibition[476], and also that SIRPα has a role in regulating the migration of tissue resident dendritic cells from the epidermis to draining lymph nodes[642]

Its therapeutic potential was previously studied in comparison with the antibody created by Miyasaka et al. called MY-1. The antibody was created by immunisation of rats with an eosinophil-enriched cell fraction, obtained from the mouse small intestinal lamina propria. The popliteal lymph nodes were used to generate hybridomas following standard methods, the culture supernatants were screened for Abs. From this process the MY-1 was generated and showed to inhibit eosinophil degranulation regulating their homeostasis and survival[643]. The therapeutic potential of this antibody and the P84 clone was described in solid tumours. Syngeneic mice were inoculated with CD47 high expressing renal cells carcinoma. An immunogenic effect was detected when the P84 antibody was injected in concomitance with the tumour cells but not when the tumour was established. The tumour growth curve showed that the P84 therapy was effective in reducing growth by one-third compared to control while MY-1 was effective in both cases. The latter was also shown to be better in increasing phagocytosis in a live cells microscopy experiments[644]. The anti-SIRPα (P84) was used for this research due to commercial availability and accessibility.

1.9 Project aims

Myeloid cells infiltration of the TME have been strongly associated with cancer progression and metastasis[645]. The plasticity of this highly heterogeneous group, particularly MDSCs, remains a debated topic because they share their principal markers with other populations of more mature myeloid cells. Nevertheless, whether they represent a myeloid specific lineage per se, or an intermediate differentiation state, they display potent pro-tumour properties[405]. Thus, to achieve tumour remission, there is the need to remodel the TME myeloid landscape back towards an inflammatory phenotype. Understanding the TME dynamic relation in determining the myeloid suppressive phenotype is crucial in order to act in moving the balance of inflammation/suppression towards therapy[646].

Embracing the activation of innate immunity against cancer has emerged as a possible approach to enhance the partial responses obtained by T cell-focussed checkpoint inhinibitors[647]. The identification of pathways involved in the regulation of phagocytosis and antigen presentation may prove an effective way to harness this potential and boost immune responses in a tolerogenic tumour[648]. One of the earliest to be discovered was the CD47-SIRPα dependent 'don't eat me' signal. Much work was done in blocking this interaction by occluding the access of CD47[649]. Despite the successes obtained, side effects were caused by off-target binding and antigen sinking. The CD47 is expressed in many tissues while the SIRPα is more limited, in particular myeloid cells[650].

Therefore, the goals of this PhD project are to define the myeloid remodelling towards suppression by interaction with a CD47 rich TME and, by blocking SIRPα, induce a myeloid response against cancer progression highlighting the mechanisms.

We will address the following specific aims:

1. Identify and characterise the myeloid suppressive cells remodelling in the melanoma TME.
    - Determine the evolution and remodelling of myeloid populations, defining the MDSCs phenotype in B16-F10 tumour bearing mice.
    - Measure the suppressive behaviour of *ex vivo* extracted moDC and M-MDSC cells towards T cells proliferation.
    - Develop an in vitro model that recapitulates in vivo observations to measure the suppressive function and phenotype of myeloid populations.

2. Determine the functional implications of the CD47-SIRPα interaction and disruption on myeloid cell suppressive phenotype and function.
    - Characterise the expression of CD47 receptor in the TME cells.
    - Determine the functional and phenotypic effects of CD47-SIRPα engagement on *in vitro* generated moDCs and M-MDSCs.
    - In parallel, determine impact of SIRPα blockade on myeloid characteristics.

3. Identify the impact of SIRPα blockade on tumour biology, determining the mechanism of action and associated immune changes.
    - Determine the therapeutic strategy and measure tumour responses with SIRPα blockade.
    - Quantify the changes in myeloid populations in the TME following therapy, and downstream inflammatory function.

Determine the mechanism of action by which the SIRPα blockade supports reduced tumour growth.

CHAPTER 2

MATERIALS AND METHODS

2.1 Cell Culture

2.1.1 Cell lines and cell maintenance

The C57BL/6 B16-F10 melanoma cell line was purchased from American Type Culture Collection (ATCC, Cat: CRL-6475). The cell line was maintained in Dulbecco's Modified Eagle Medium (DMEM, Life Technologies) with glucose and L-glutamine (Gibco, Cat: 41966-029) supplemented with 10% Foetal Bovine Serum (FBS) and 1% penicillin/streptomycin (p/s). FBS and p/s were supplied by the in-house media facility.

The B16-F10-OVA cell line was derived by B16-F10 melanoma cells. It was previously plasmid transfected to expresses a cytoplasmic form of full length chicken ovalbumin protein[74]. The cell line was maintained in DMEM (Life Technologies) with glucose and L-glutamine (Gibco, Cat: 41966-029) supplemented with 10% Foetal Bovine Serum (FBS) and 1% penicillin/streptomycin (p/s) and in the selective agent 50μg/ml Geneticin (Sigma-Aldrich, cat. A1720). FBS and p/s were supplied by the in-house media facility.

The B16-F10-GFP was generated by pLenti6/V5-DEST (ThermoFisher, cat. V49610) lentiviral transduction in the B16.F10 melanoma cells by a previous member of the laboratory. The cells line stably expresses the Green Fluorescent Protein (GFP). The cell line was maintained in DMEM (Life Technologies) with glucose and L-glutamine (Gibco, Cat: 41966-029) supplemented with 10% Foetal Bovine Serum (FBS) and 1% penicillin/streptomycin (p/s) and in the selective agent 8 ug/ml Blasticidin (Sigma-Aldrich, cat. 15205). FBS and p/s were supplied by the in-house media facility.

Cancer Associated Fibroblasts (CAFs) were isolated as previously described[74]. They were maintained in RPMI-1640, supplemented with 10% FBS, 1% penicillin-streptomycin, 10 mM HEPES and 15μM β-mercaptoethanol (β-ME, Sigma).

Primary T cell populations were isolated from murine spleens and cultured in Iscove's Modified Dulbecco's Medium (IMDM, Gibco, Cat: 12440053) supplemented with 5% fetal bovine serum (both Life Technologies), 1% penicillin-streptomycin and 15μM β-mercaptoethanol (both Sigma-Aldrich).

All cells in culture were routinely tested for mycoplasma contamination (MycoAlert Detection Kit, Lonza).

2.1.2 Cell passage

Cell lines were cultured in T75 or T175 cm^2 flasks (Thermo) and incubated at 37°C in a 5% CO_2 environment. At 80% confluency, media was removed, and the flasks washed with cell grade PBS. Cells were detached with 0.25% trypsin (Gibco) or Cell Dissociation Buffer Enzyme-Free PBS-based (Gibco, Cat:13151-014), which was neutralised by adding the appropriate culture media. The cells were counted by trypan blue exclusion and passage into separate T75 or T175 cm^2 flasks. All cell lines were used until passage 40 (P40), at which point an early passage stock was thawed.

2.1.3 Cryopreservation

1 and 1.5 x 10^6 cells were re-suspended in freezing media (90% FBS, 10% DMSO) and placed in a Nunc cryovial. Cryovials were transferred to a CoolCell® Freezing Container (Biocision) and stored at -80°C overnight before long-term storage in liquid nitrogen. For cell recovery, the cryovials were thawed at 37°C and the toxic freezing medium removed. The cells were resuspended in the appropriate culture medium and placed in a T75 flask for growth under standard conditions (37°C, 5% CO2).

2.2 Isolation of primary murine cells

2.2.1. Isolation of bone marrow murine cells

Wild-type age-matched male and female C57BL/6 mice were euthanized by cervical dislocation (MRC ARES, Cambridge). Femurs and tibias were removed and cleaned

from tissue residues. After, the bone edges were cut with surgical scissors and the bone marrow was flushed out with a syringe (25-gauge needle, 0.5mm x 25mm) injected PBS. The cells were collected in a 6 cm^2 petri dish (Thermo, Cat:150288) and resuspended to obtain a single cells solution. Then, the solution was passaged twice in clean 6 cm^2 petri dishes in order to sank and remove bone debris. At this point, the cells were collected in a 15 ml Eppendorf tube and washed with PBS. The single cell suspension was lysed in Red Blood Cell Lysis Buffer (RBC Buffer; 155 mM NH4Cl, 12 mM NaHCO3 and 0.1 mM EDTA in ddH2O) for 5 minutes, at room temperature (RT), before neutralisation with media.

2.2.2 Dissociation of murine spleens

Spleens were isolated from age-matched wildtype (WT) C57BL/6 mice (MRC ARES, Cambridge) and broken apart using a 25-gauge needle (0.5mm x 25mm). Broken tissues were passed through a 70µm strainer (Thermo), using a 1mL syringe plunger (Soft-Ject), to create a single-cell suspension. Remnant tissues was flushed through with PBS. For splenic tissues, the single cell suspension was lysed in Red Blood Cell Lysis Buffer (RBC Buffer; 155 mM NH4Cl, 12 mM NaHCO3 and 0.1 mM EDTA in ddH2O) for 5 minutes, at room temperature (RT), before neutralisation with media. RBC lysis was not conducted on LN samples.

2.2.3 MACS isolation of Sca-1^+ HSCs cell population.

The femur and tibia of the mouse were processed until a single-cell suspension was obtained as described in Section 2.2.1. The cells were counted with a haemocytometer and re-suspended at a density of 1 x 10^8 cells in 420µL of MACS Buffer (0.5% v/v BSA and 2mM EDTA in PBS). 80µL of mouse SCA-1-Biotin-Antibody (Miltenyi Biotec Cat: 130-101-885) was added to the suspension and incubated for 10 minutes at 4°C. 2 ml of MACS Buffer was added, and the cells were spun at 300 g for 2 minutes and the supernatant containing the antibody excess removed. The cells were re-suspended in 80 µL of anti-biotin MicroBeads and 420µL of MACS buffer and left for 10 minutes at

4°C. After, the MACS sorting apparatus was combined. A metal stand was used to support the QuadroMACSTM Separator (Miltenyi Biotec, Cat: 130-091-051). The LS Column were loaded into the magnet and primed with the MACS Buffer. Successively, the cells were loaded at the top of the column and flowed through using gravity. Other 3 ml of MACS buffer were used to wash the cells trapped by the magnetic field. After, the column was removed from the magnet and 4 ml of MACS buffer added. The plunge of the LS column was used to flush the SCA-1^+ cells in a collection tube.

2.2.4 MACS isolation of $CD3^+$ T cell populations.

Spleens were processed until a single-cell suspension was obtained as described in Section 2.2.2. To isolate $CD3^+$ T cells the magnetic activated cell sorting (MACS® Cell Separation) technology was used with the Pan T cell Isolation Kit II (Miltenyi Biotec, 130-095-130). The RBC^- extracted splenocytes were counted with a haemocytometer and re-suspended at a density of 1 x 10^8 cells in 400µL of MACS Buffer (0.5% v/v BSA and 2mM EDTA in PBS). 50µL of Pan T cell Biotin-Antibody Cocktail (Miltenyi Biotec Cat: 130-095-130) was added to the suspension and incubated for 5 minutes at 4°C. The cells were re-suspended in 100µL of anti-biotin MicroBeads and 300µL of MACS buffer and left for 10 minutes at 4°C. After, the MACS sorting apparatus was combined. A metal stand was used to support the QuadroMACSTM Separator (Miltenyi Biotec, Cat: 130-091-051). The LS Column were loaded into the magnet and primed with the MACS Buffer. Successively, the cells were loaded at the top of the column and flowed through using gravity. The column was washed with 3mL of MACS buffer to collect the unlabelled $CD3^+$ T cells. Flow cytometry was performed to confirm purity. Viable cells were counted using a haemocytometer and re-suspended at the desired concentration for *in vitro* assays.

2.2.5 MACS isolation of CD11b$^+$ly6C$^+$ cell population grown *in vitro*.

After in vitro HSC cell culture differentiation (Section 2.6.2), the CD11b$^+$Ly6C$^+$ were isolated. Initially, the grown myeloid cells were gently resuspended and collected to limit the presence of highly differentiated adherent cells. The wells were washed twice with MACS Buffer (0.5% v/v BSA and 2mM EDTA in PBS) and the solution added to the non-adherent myeloid. Those were counted with a haemocytometer spun at 300 g for 5 minutes and resuspended at a density of 1 x 10^7-10^8 cells in 450µL of MACS Buffer (0.5% v/v BSA and 2mM EDTA in PBS). 50µL of mouse CD11b-Biotin-Antibody (Miltenyi Biotec Cat: 130-113-233) was added to the suspension and incubated for 10 minutes at 4°C. 2 ml of MACS Buffer was added, and the cells were spun at 300 g for 2 minutes and the supernatant containing the antibody excess removed. The cells were re-suspended in 80 µL of anti-biotin MicroBeads and 420 µL of MACS buffer and left for 10 minutes at 4°C. After, the MACS sorting apparatus was combined. A metal stand was used to support the QuadroMACSTM Separator (Miltenyi Biotec, Cat: 130-091-051). The LS Column were loaded into the magnet and primed with the MACS Buffer. Successively, the cells were loaded at the top of the column and flowed through using gravity. Other 3 ml of MACS buffer were used to wash the cells trapped by the magnetic field. After, the column was removed from the magnet and 4 ml of MACS buffer added. The plunge of the LS column was used to flush the CD11b$^+$ cells in a collection tube. Those were spun and resuspended in 420 µL of MACS Buffer and 80µL of mouse Ly6C-Biotin-Antibody (Miltenyi Biotec Cat: 130-111-776) was added to the suspension and incubated for 10 minutes at 4°C. Same as for the CD11b separation from this point the same protocol was used. The plunge was used to flush and collect the positive Ly6C cells. Flow cytometry was performed to confirm purity. Viable cells were counted using a haemocytometer and re-suspended at the desired concentration for *in vitro* assays.

2.2.6 MACS isolation of CD11b$^+$ly6C$^+$ cell population from *in vivo* TME.

The tumour tissue was processed until a single-cell suspension was obtained as described in section 2.4.1. The cells were counted with a haemocytometer and re-suspended at a density of 1 x 10^8 cells in 420µL of MACS Buffer (0.5% v/v BSA and 2mM EDTA in PBS). 80µL of mouse CD11b-Biotin-Antibody (Miltenyi Biotec Cat: 130-113-233) was added to the suspension and incubated for 10 minutes at 4°C. 2 ml of MACS Buffer was added and the cells were spun at 300 g for 2 minutes and the supernatant containing the antibody excess removed. The cells were re-suspended in 80 µL of anti-biotin MicroBeads and 420 µL of MACS buffer and left for 10 minutes at 4°C. After, the MACS sorting apparatus was combined. A metal stand was used to support the QuadroMACSTM Separator (Miltenyi Biotec, Cat: 130-091-051). The LS Column were loaded into the magnet and primed with the MACS Buffer. Successively, the cells were loaded at the top of the column and flowed through using gravity. Other 3 ml of MACS buffer were used to wash the cells trapped by the magnetic field. After, the column was removed from the magnet and 4 ml of MACS buffer added. The plunge of the LS column was used to flush the CD11b$^+$ cells in a collection tube. Those were spun and resuspended in 420 µL of MACS Buffer and 80µL of mouse Ly6C-Biotin-Antibody (Miltenyi Biotec Cat: 130-111-776) was added to the suspension and incubated for 10 minutes at 4°C. Same as for the CD11b separation from this point the same protocol was used. The plunge was used to flush and collect the positive Ly6C cells. Flow cytometry was performed on an LSR Fortessa to confirm purity. Viable cells were counted using a haemocytometer and re-suspended at the desired concentration for *in vitro* assays. All these steps were made in accordance with manufacturer protocols.

2.2.7 Isolation of M-MDSC and moDC cell population by sorting *in vivo* TME.

Cells were sorted using the BD influx or BD Melody flow cytometer system. WT B16-F10 melanoma cells were injected into WT C57BL/6 mice and sacrificed after 11 days. Tumours were collected, processed and stained as described in section 2.4. Cells were sorted using the BD influx flow cytometer directly into Dulbecco's Modified Eagle Medium (DMEM, Life Technologies) with glucose and L-glutamine (Gibco, Cat: 41966-029) supplemented with 10% Foetal Bovine Serum (FBS) and 1% penicillin/streptomycin (p/s). Immune cells were selected using CD45 and separated into different populations based on expression of CD11c, CD11b, Ly6 and Ly6C.

2.3 In vivo Mouse models

2.3.1 Mouse strains

Animals were housed in accordance with UK regulations and experiments were performed under Project Licences P88378375 and Personal Licence I6BF82559. The mouse experiments were conducted at the MRC Ares Animal Facility (Cambridge, UK). The syngeneic tumour models, wildtype C57BL/6 mice were obtained from the in-house breeding facility and used for experimentation. All mice were house socially in individually ventilated cages with enrichment. Mice aged between 8 to 16 weeks of age upon tumour injection and female mice were used for experiments whilst male mice were used for bone marrow collection. Tumour inoculation, drugs preparation, culling and sample collection was conducted by me. Non-invasive tumour measurements and intraperitoneal (I.P.) drug injections were performed by trained animal technicians at Ares. Where possible technicians were blinded.

2.3.2 B16-F10 murine melanoma model

B16-F10, or B16-F10 OVA or B16-F10-GFP cells were passaged following standard protocol (Section 2.1.1) and counted by trypan blue exclusion. Cells were re-suspended at a density of $2.5x10^5$ or $4x10^5$ cells in 50µL of sterile PBS and transported to the Ares facility on ice. Mice were anesthetised by isoflurane inhalation and the right shoulder or both shoulders of the mice were shaved allowing a visual of the injection area. $2.5x10^5$ or $4x10^5$ cells were injected subcutaneously into the right shoulder or both shoulders depending on the experiment. Then, the mice were returned the to their cages for recovery. Once, the mice fully regain consciousness were moved in their assigned rack. At this point, the mice were continually monitored by the Ares staff and the mice were sacrificed after 5, 9 or 11 days; if the tumours were exceeding the 12mm in diameter which is the maximum permitted under the project license, the mice were culled before the end of the experiment and samples analysed. In a normal tumour development, the mice were culled at the end of the experiment by exposure to carbon dioxide, followed by neck dislocation or cardiac puncture exsanguination, if blood samples were required. Post-mortem the tumours were measured again on the skin and internally with Vernier callipers after extraction.

2.3.3 Mouse anti-SIRPα immunotherapy

The B16-F10 cells line was injected, and the tumour developed as described above (Section 2.3.2). The immunotherapy was administered twice along the 11 days long experiment. For each injection, the mice received 125µg (5 mg/Kg) of Ultra-LEAF™ Purified anti-mouse CD172a (SIRPα) Antibody or a rat IgG1 isotype control by I.P. injection (Table 2.1; Stock concentration of 1mg/ml, 125µl given per injection, resulting in a final concentration of 125µg of ICI or control). The first dose was administered once tumours reached 3mm in size (normally at Day 5). Three days later mice received a second dose of immunotherapy or isotype control, and a further three days later mice were killed by exposure to carbon dioxide, followed by neck dislocation or cardiac

puncture exsanguination. Tumours and blood were harvested and used for analysis. Dosing concentrations and regimes were based on current literature[644,632] and research purpose.

2.3.4 B16-F10-GFP cells and mouse anti-SIRPα immunotherapy for phagocytosis detection

$4x10^5$ B16-F10-GFP cells were injected, and the tumour developed as described above (Section 2.3.2). The immunotherapy was administered twice along the 9 days long experiment. For each injection the mice received 125µg (5 mg/Kg) of Ultra-LEAF™ Purified anti-mouse CD172a (SIRPα) Antibody or a rat IgG1 isotype control by I.P. injection (Table 2.1; Stock concentration of 1mg/ml, 125µl given per injection, resulting in a final concentration of 125µg of ICI or control). The first dose was administered once tumours reached 3mm in size (normally at Day 5). Three days later mice received a second dose of immunotherapy or isotype control, and the next day the mice were killed by exposure to carbon dioxide, followed by neck dislocation or cardiac puncture exsanguination. Tumours were harvested and used for analysis. Dosing concentrations and regimes were suggested by the experiments performed *in vitro*.

2.3.5 B16-F10-OVA cells and mouse anti-SIRPα immunotherapy for myeloid antigen presentation detection

$4x10^5$ B16-F10-OVA cells were injected, and the tumour developed as described above (Section 2.3.2). The immunotherapy was administered twice along the 9 days long experiment. For each injection the mice received 125µg (5 mg/Kg) of Ultra-LEAF™ Purified anti-mouse CD172a (SIRPα) Antibody or a rat IgG1 isotype control by I.P. injection (Table 2.1); Stock concentration of 1mg/ml, 125µl given per injection, resulting in a final concentration of 125µg of ICI or control). The first dose was administered once tumours reached 3mm in size (normally at Day 5). Three days later mice received a second dose of immunotherapy or isotype control, and the next day the mice were killed by exposure to carbon dioxide, followed by neck dislocation or

cardiac puncture exsanguination. Tumours were harvested and used for analysis. Dosing concentrations and regimes were suggested by the experiments performed *in vitro*.

2.3.6 Mouse anti-SIRPα and mouse anti-C3a immunotherapy

The B16-F10 cells line was injected, and the tumour developed for 11 days as described above (Section 2.3.2). Four mice groups were IP injected respectively 1) 125µg rat IgG1 and 20µg IgG2a isotype control, 2) 125µg (5 mg/Kg) anti-SIRPα, 3) 25µg (0.5 mg/Kg) anti-C3a and 4) anti-SIRPα plus and anti-C3a per injection (table 2.1). The first dose was administered once tumours reached 3mm in size (normally at Day 5). For group 2 anti-SIRPα immunotherapy was administered twice at day 5 and day 8. For group 3 anti-C3a was administered thrice at day 5, day 7 and day 9. For group 4 the drugs were combined at day 5 and after followed the respective patterns for a total of four injections. The same was for the isotype controls. The mice were killed at day 11 by exposure to carbon dioxide, followed by neck dislocation or cardiac puncture exsanguination. Tumours and blood were harvested and used for analysis. The anti-C3a dosing concentrations and regimes were based Davidson et al[651].

Antibody	Isotype	Clone	Species	Company	Cat No:
Ultra-LEAF™ Purified anti-mouse CD172a (SIRPα)	IgG1, κ	P84	rat	Biolegend	144037
C3a, Mouse, mAb 3/11	IgG2a	3/11	rat	HycultBiotech	HM1072
LEAF™ Purified Rat IgG1, κ isotype Ctrl	IgG1, κ	RTK2071	rat	Biolegend	400427
InVivoPlus IgG2a, κ Isotype Control	IgG2a	2A3	rat	Bio X Cell	BP0089

Table 2.1. Monoclonal Antibodies. Table detailing the isotype, clone, species, company, and catalogue number for the monoclonal and isotype control antibodies injected into experimental mice.

2.4 Flow cytometry

2.4.1 Processing of tumours and blood samples

Tumours were resected from the shoulder using surgical scissors maintaining the structural integrity. After, all tumours were mechanically dissociated using a blade and digested in 1mg/ml collagenase D (Roche), 1mg/ml collagenase A (Roche) and 0.4mg/ml DNase (Roche) in PBS, at 37^{O}C for 45 minutes. Then, to neutralise collagenase activity Ethylenediaminetetraacetic Acid (EDTA), was placed at a final concentration of 5mM at the top of a 70µm cell strainer (Falcon) just before to add all the samples. The digested tissues were gently passed through the filter using a 1 mL syringe plunger to further dissociate the cells and remaining tissue debris. PBS was used to wash, and the flow throw was collected in a 50 mL falcon tube. The single cells suspension was pelleted at 300g for 5 minutes, resuspended in sterile PBS and re-filtered using a second cells strainer (CellTrics, Cat: 04-0042-2317) to remove eventual fat residues obtaining a clean single cells solution. At this point the samples were distributed to a round-bottomed 96-well plates (Corning) ready for staining.

The blood samples were collected by cardiac puncture in an EDTA anti-coagulant tube to avoid blood clotting. The samples were transferred to a 15 mL Eppendorf tube and incubated in 5 mL of red blood cell lysis buffer (RBS, 150mM NH4Cl, 1mM KHCO3, 0.1mM EDTA in dH2O) at RT for 5mins. Then, the samples were pelleted at 300g for 5 minutes and re-suspended a second time in RBC buffer and incubated further 5 minutes at RT. After this second incubation the RBC buffer was neutralised using 45ml of PBS and centrifuged at 300g for 5 mins to remove debris. At this point the samples were distributed to a round-bottomed 96-well plates (Corning) reading for staining.

2.4.2 Staining samples for flow cytometry

Samples were washed with PBS and spun 2 minutes at 300g. The supernatant was discarded, and the cells were resuspended in PBS with viability dye, diluted 1:1000, for

15 minutes, to label dead cells. Live/Dead Fixable Violet (Thermo, Cat: 62248) was used depending on the flow cytometry panel. While the cells were being Live/Dead stained, the fluorophore-conjugated primary antibodies were prepared at 1:300 dilution in FACS buffer (0.5% Bovine Serum Albumin or 'BSA' in PBS). Cells were washed once with PBS before to add the primary antibodies, then they were incubated with the samples, for 40 minutes, at 4°C to avoid internalisation (Table 2.2). To mitigate non-specific binding of immunoglobulins to surface Fc receptors, FACS buffer was supplemented 1:1 with Fc blocker (generated in house from a rat 2.4G2 hybridoma cell line).

After surface membrane molecules staining, and if intracellular epitope detection was required, samples were fixed and stained in accordance with the FoxP3/ Transcription Factor Staining Kit (eBioscience, Cat: 00- 5523). The samples were washed once with PBS to eliminate the unbound primary antibody and resuspended in the fixation/permeabilization buffer for 1 hour, at RT. Then, cells were pelleted at 300g for 5 minutes and washed 3 times in permeabilization buffer. Cells were incubated with fluorophore-conjugated primary antibodies, diluted 1:300 in permeabilization buffer, for 30 minutes at RT. Finally, cells were washed with FACS buffer, to remove non-specific antibody, and transferred into polystyrene tubes (Corning), ready for flow cytometry. Samples were run on an LSR Fortessa cell analyzer (BD, Biosciences) and analysed using FlowJo version 10. (FlowJo, BD Biosciences).

Target	*Clone*	*Species*	*Company*	*Dilution*	*Conjugate*
Myeloid cells Markers					
CD45	30-F11	Rat	Biolegend	1:300	PerCP-Cy5.5, BV-785
CD11b	M1/70	Rat	Biolegend	1:300	PE, BV-785
CD11c	N418	Armenian Hamster	Biolegend	1:300	PE-Cy7
Ly6C	AL-21	Rat	BDBioscience s	1:300	AF488, APC, APC-Cy7
Ly6G	1A8	Rat	Biolegend	1:300	AF488, APC
SIRPα	P84	Rat	Biolegend	1:300	PE, APC
PD-L1	10F.9G2	Rat	Biolegend	1:300	PE
MHC II (I-A^b)	KH74	Mouse	Biolegend	1:300	PE
FasL	MFL3	Armenian Hamster	Biolegend	1:300	PE
CD47	miap301	Rat	Biolegend	1:300	APC, PE
VISTA	MIH63	Rat	Biolegend	1:300	PE
F4/80	BM8	Rat	Biolegend	1:300	FITC
CX3CR1	SA011F11	Rat	Biolegend	1:300	APC
XCR1	ZET	Rat	Biolegend	1:300	APC
ARG1	A1exF5	Rat	eBioscience	1:300	APC
NOS2	5CB52	Mouse	Biolegend	1:300	AF488
IDO	mIDO-48	Rat	Biolegend	1:300	PE
H-2K^b bound to SIINFEKL	25-D1.16	Mouse IgG1	Biolegend	1:300	APC
Stromal and Immune cells Markers					
Thy1	G7	Rat	Biolegend	1:300	APC-Cy7
Pdfrα	APA5	Rat	Biolegend	1:300	PE-Cy7
Pdfrβ	APB5	Rat	Biolegend	1:300	PE
CD31	MEC13.3	Rat	Biolegend	1:300	FITC
NK1.1	PK136	Mouse	Biolegend	1:300	BV-421
T cells Markers					
CD3ε	145-2C11	Armenian Hamster	Biolegend	1:300	BV-421
CD8a	53-5.8	Rat	Biolegend	1:300	BV-785
CD4	GK1.5	Rat	Biolegend	1:300	PE-Cy7
FoxP3	FJK-16s	Rat	Thermo	1:300	PerCP- Cy5.5

Thy1	G7	Rat	Biolegend	1:300	APC-Cy7

Table 2.2. Flow Cytometry Antibodies. Table detailing the clone, species, company, dilution and conjugates for each of the primary antibodies used for flow cytometric studies.

2.5 Immunofluorescent staining (IF)

2.5.1 Tissue sectioning

Tumours were placed in cryomolds, embedded in Optimal Cutting Temperature medium (VWR) and snap frozen on dry ice. Blocks were stored at -80°C for long-term storage and transferred to -20°C, 24 hours before sectioning to allow the blocks to acclimate to the cryostat temperature. Tumours were cut into 10µm sections, using a Leica CM1900 cryostat, and mounted onto superfrost-plus lysine coated slides (Thermo). The slides were stored at -80°C until use.

2.5.2 Immunofluorescent staining

Sections were air dried and fixed in a 1:1 mix of acetone (Fisher) and methanol (Fisher), for 2 minutes, at -20°C. Next, the sections were washed in PBS, for 10 minutes. To minimise non- specific binding, slides were incubated in a blocking solution containing 10% chicken or donkey serum (Alpha Diagnostics) and 2% BSA (Thermo) for 1 hour, at RT. The sections were then placed in a humidified chamber and incubated with primary antibodies, diluted in blocking buffer, at 4°C, overnight (Table 2.3). The following day, the antibodies were removed by 3 x 5 min washes in PBST (PBS with 0.1% Tween (NBS Biologics)) and the sections incubated with secondary antibodies for 1 hour, at RT (Table 2.4). If biotinylated primary antibodies were used, streptavidin conjugates were also added. After 3 further washes in PBST, the sections were counterstained with 1µg/ml of 4',6-diamidino-2-phenylindole (DAPI, Thermo, D1306), for 10 minutes, and mounted with 22 x 50 mm glass coverslips and SlowFade Gold Antifade Mountant (Life Technologies; Cat: S36936). The completed slides were imaged on a Zeiss 880 laser scanning confocal microscope using a 40x oil objective.

Target	Clone	Species	Company	Dilution	Conjugate

SIRPα	P84	rat	Biolegend	1:50	-
CD11b	M1/70	rat	eBioscience	1:100	biotin
Ly6C	AL-21	rat	BD pharmigen	1:60	AF 488

Table 2.3. Immunofluorescence Microscopy Primary Antibodies. Table detailing the clone, species, company, dilutions and conjugates for each of the primary antibodies used for IF studies.

Target	Company	Cat:	Dilution
Chicken anti-Rat Conjugated AF594	Life Technology	A21471	1:300
Streptavidin conjugated AF 647	Life Technology	S32357	1:300

Table 2.4. Immunofluorescence Microscopy Secondary Antibodies. Table detailing the company, catalogue number and dilution for each of the secondary antibodies used for IF studies.

2.6 Myeloid - T cell culture and co-culture assays

2.6.1 Generation of Tumour Conditioned Media

For tumour cell conditioned medium (TCM); B16.F10 cells were thawed from the same passage frozen batch and seeded at a density of $1.5x10^6$ cells in a T75 flask. They were left to recover and grown until 90% confluency and passaged once again and seeded in four T175 cm^2 flasks at a density of $3.5x10^6$ cells. Cells were grown until 60-70% confluent in full growth medium, successively the medium was changed with Dulbecco's Modified Eagle Medium (DMEM, Life Technologies) containing 10% FBS and p/s. After 24 hours it was harvested and centrifuged at 500 g for 10 minutes to kill eventual live cells and remove cellular debris. Then, the media was filter-sterilised using SteriFlip® vacuum filters (Merck, Cat: SCGP00525). The media collected was promptly aliquoted, snap frozen in dry ice to prevent protein degradation and stored at -80 °C.

2.6.2 *In vitro* conditioning of HSCs to obtain a myeloid cells culture

The HSCs were isolated as described in Section 2.2.3 Half of the total cells were resuspended in RPMI media, supplemented with 20ng/mL GM-CSF (Peprotech, Cat: 315-03) to generate our control. The other half was resuspended in 50% TCM (Section

2.5.1) and 50% RPMI media, supplemented with 20ng/mL GM-CSF full growth media. Cells were seeded in the respective cell culture media in a 12-wells plates. Each well containing a density of $2.5x10^5$ cells. Those were matured for five days changing the respective media each day. The culture media refreshment was obtained by inclining the plate of 45 degree and slowly removing the 95% of it, transferred in a 15 mL Eppendorf tube and centrifuged 5 minutes at 300 g. The supernatant was removed, and the eventual pellet resuspended in fresh media which was transferred back to the 12-wells plate in the respective slots. After 5 days the MDSC were harvested by gentle pipetting and isolated using the protocol in Section 2.2.5 or 2.2.7.

2.6.3 Coating with CD47 active protein

The recombinant mouse CD47 protein (Active) (cat: ab231160) was prepared in PBS at 5 µg/ml concentration. Then, 50ul of solution was used to coat the well in a 96 non-pyrogenic polystyrene flat or round (for T cell proliferation assay) bottom well plate. Plates were sealed with parafilm and kept overnight at 4°C to allow passive coating. The next day plates were washed with PBS and used for experiments.

2.6.4 Myeloid cells *in vitro* SIRPα blockade

The Ultra-LEAF™ Purified anti-mouse CD172a (SIRPα) Antibody (Cat: 144037) was prepared in the appropriate media and incubated with myeloid cells obtained as in Section 2.6.2, and $Ly6C^+$ cells isolated as in section 2.2.5, in ice for 30 minutes allowing SIRPα blockade. The antibody was used at the concentration of 115nM and in case of the phagocytosis experiment at 1nM or titrated 1:10 from 200nM. This incubation was made prior to contact with wells coated with CD47.

2.6.5 *In vitro* conditioning of myeloid cells culture with CD47 protein

The myeloid cells were obtained as in section 2.6.2. After 5 days of maturation in presence of GM-CSF or GM-CSF-TCM cells were washed with PBS and resuspended their respective media in a new plate were some of the wells were coated with CD47

protein (section 2.6.3). The cells were incubated for 2 days more at standard cell culture conditions (37°C + 5% CO2). At the end of the incubation cells were washed with PBS and stained according with the protocol described in Section 2.4.

2.6.8 CFSE and cell trace far red staining

For experiments assessing proliferation, T cells were stained with Cell-Trace CFSE (Thermo, Cat: C34554). For experiments assessing phagocytosis, B16.F10 and CAFs cells were stained with Cell-Trace Far red (Thermo, Cat: C345664). T cells were obtained as described in Section 2.2.4 and B16.F10 and CAFs were obtained as in Section 2.2.1. Cells were re-suspended at a density of 0.5–10 x 10^6 cells/ml in 1 mL of IMDM + 5% FCS + 0.5ul of β-mercaptoethanol (Sigma, Cat: M7522) + P/S and placed in a 15mL falcon tube. The tube was laid on its side and 110µL of PBS was placed near the top of the tube. 1.1µL of 5mM CFSE was added directly to the PBS droplet and the tube was closed and vortexed upside down for 5 seconds, flipped and vortexed again for 5 seconds. This process was made to evenly distribute the CFSE staining by the cells. Then, the tube was covered in aluminium foil to prevent UV light degradation and incubated for 7 minutes, at RT. After 5 minutes the cells were washed for a total of 3 times with a solution of 10mL of PBS + 5% FBS. Each time cells were centrifuged at 300g for 5 minutes and the supernatant discarded. After the last wash, the cells were resuspended in IMDM + 5% FCS + 0.5ul of β-mercaptoethanol (Sigma, Cat: M7522) + P/S, or RPMI + 10% FCS + P/S in case of B16.F10 and CAFS, and let rest for 20 minutes recovery at 37°C + 5% CO2. At this point the cells were stained and ready to be used.

2.6.9 T cell stimulation

A working concentration of 2.5mg/mL LEAF purified anti-mouse CD3e antibody (Biolegend, Clone: 145-2C11, Cat:14-0031) was prepared in PBS and added to a 96 flat-bottomed 96-well cell culture plate, then incubated for 2 hours at 37°C to allow the antibody passive coating. After this initial incubation, the plates were washed twice with PBS, to remove non-bound antibody. The CFSE-stained T cells (Section 2.6.3) were

re-suspended in IMDM + 5% FCS + 0.5ul of β-mercaptoethanol (Sigma, Cat: M7522) + P/S supplemented with 1µg/mL of soluble anti-CD28 antibody (Biolegend, Clone 37.51, Cat: 16-0281). 2 x 10^5 T cells were seeded per well and stimulated for 24 hours under standard culture conditions (37°C in a 5% CO2 environment). The next day the T cell proliferation was active and ready to be tested in experimental conditions.

2.6.10 *In vitro* MDSC T cells proliferation suppression

The MDSCs *in vitro* (Section 2.6.2) or *in vivo* (Section 2.4.1) were isolated following the protocols in section 2.2.5 or 2.2.6 or 2.2.7. The obtained myeloid cells were washed with PBS and resuspended at a density of 5x10^4 cells per 50ul of GM-CSF or GM-CSF-TCM media or treaded for SIRPα blockade (Section 2.6.4). 50ul were added to each well of a polystyrene clear round-bottomed 96-well cell culture plate with or without CD47 coating (Section 2.6.3) and incubated for recovery (20 minutes). In the meantime, the T cells CFSE stained (Section 2.6.8), seeded at a density of 2x10^5 cells per well and activated (Section 2.6.9) were also washed with PBS, resuspended in 50ul GM-CSF or GM-CSF-TCM media and transferred topping the myeloid in the same round-bottomed 96-well plate. In this manner a 1:4 ratio was obtained in each well (5x10^4 myeloid with 2x10^5 T cells). Then, the mixed cells were incubated at standard cell culture condition (37°C in a 5% CO2) for a total of 48 hours with the media replaced after 24 hours. At the end of the incubation cells were washed with PBS and stained according with the protocol described in section 2.4. After cells were washed twice and run on an LSR Fortessa cell analyzer (BD, Biosciences) and analysed using FlowJo version 10. (FlowJo, BD Biosciences).

2.6.11 Detection of Reactive Oxygen Species (ROS)

The myeloid cells were cultured (section 2.6.2) and Ly6C$^+$ cells were isolated (Section 2.2.5). Prior to the experiment, part of the cells was used to check the phenotype of the isolated cells by flow cytometry as control (Section 2.4). The rest of the cells were plated at 6x10^4 cells per well in a 96 nonpyrogenic flat bottom well plate where some

wells were CD47 coated (Section 2.6.3). Prior to CD47 contact some of the cells were treated for SIRPα blockade (Section 2.6.4). The cells were incubated 4 hours in GM-CSF control, GM-CSF-TCM, GM-CSF-TCM-CD47 and GM-CSF-TCM-CD47 media with prior SIRPα blockade of the cells. After the incubation cells were washed with PBS and treated with 10μM 2′,7′-Dichlorodihydrofluorescein diacetate (DCFDA; Sigma-Aldrich) in DMEM only for 25 minutes. Immediately after cells were washed twice with PBS and transferred in ice. Then, they were resuspended in PBS with viability dye, diluted 1:1000, for 3 minutes, to label dead cells. Live/Dead Fixable Violet (Thermo, Cat: 62248) was used. Immediately cells were washed once with PBS and run on an LSR Fortessa cell analyzer (BD, Biosciences).

2.6.12 T proliferation assay with transwell plates

The in vitro MDSC T cells proliferation suppression was performed as described in section 2.6.10 but cells were instead, plated in an HTS Transwell-96 well plate (Cat: 3381, Corning, 0.4 μm polycarbonate membrane) adding the MDSCs at the bottom and the T cells at the top of the well. the mixed cells were incubated at standard cell culture condition (37°C in a 5% CO2) for a total of 48 hours with the media replaced after 24 hours. At the end of the incubation cells were washed with PBS and stained according with the protocol described in section 2.4. After cells were washed twice and run on an LSR Fortessa cell analyzer (BD, Biosciences) and analysed using FlowJo version 10. (FlowJo, BD Biosciences).

2.6.13 Mass Spectrometry

The myeloid cells were cultured (section 2.6.2) and $CD45^{+}CD3^{-}NK1.1^{-}CD11c^{-}CD11b^{+}Ly6G^{-}Ly6C^{+}$ cells (M-MDSC from GM-CSF or GM-CSF-TCM culture) were sorted (Section 2.2.7) directly in lysis Pierce-RIPA buffer (Thermo Scientific) supplemented with protease-inhibitor cocktail (Roche), 1mM PMSF and 1mM Na3VO4 at 4°C. The protein fraction was quantified with Pierce BCA protein assay kit (Cat:SA244533) and

10ug of proteins from lysed cells were run on a 10% SDS page. Gel was divided in 12 sections and LC MS/MS was performed on each section and spectral analysis was performed. Data were analysed comparing the data from cells grown in GM-CSF and GM-CSF-TCM using Scaffold 4 software.

2.7 Phagocytosis and antigen processing

2.7.1 CD47 expressing cells and debris preparation for phagocytosis assay

The B16.F10 (CD47 low) cells and CAFs (CD47 high) cell cultures (Section 2.1.1) were stained using Cell Trace Far red (Thermo, Cat: C345664) using the same protocol in Section 2.6.3. The stained cells were resuspended to a concentration of $3x10^7$ cells/ml in 50% TCM (Section 2.6.1) and 50% RPMI media, supplemented with 20ng/mL GM-CSF (Peprotech, Cat: 315-03). Half of them were killed by heat induction in a thermomixer for 5 minutes at 98°C. The dead cells part was chilled in ice and mixed again with the live cells. With this method we obtained a mixture of live cells and debris.

2.7.2 Phagocytosis assay protocol

The moDC and MDSCs cultured *in vitro* (Section 2.6.2) were isolated following the protocols in section 2.2.5. Cells were seeded at $5x10^4$ cells per well in a 96 nonpyrogenic flat bottom well plate and kept in 100ul of 50% TCM (Section 2.5.1) and 50% RPMI media, supplemented with 20ng/mL GM-CSF (Peprotech, Cat: 315-03) for experimental condition. Cells were let recover overnight at standard cell culture condition (37°C in a 5% CO2). The next day, moDC and MDSC cells were washed and prepared according to condition: part of them were SIRPα blocked following the protocol in section 2.6.4, the others were resuspended in GM-CSF-TCM media (Section 2.6.1) and added to the CD47 coated plate (Section 2.6.3). In the meantime, the B16.F10

(CD47 low) cells and CAFs (CD47 high) were prepared (Section 2.7.1). Then, 50µl containing $7.5x10^4$ live cells and $7.5x10^4$ dead cells were added at top of the moDC and MDSC cells and incubated 4 hours at standard cell culture condition (37°C in a 5% CO2) to allow phagocytosis. At the end of the incubation cells were washed with PBS put in ice to block phagocytosis and stained according with the protocol described in Section 2.4.2. After cells were washed twice and run on an LSR Fortessa cell analyzer (BD, Biosciences) and analysed using FlowJo version 10. (FlowJo, BD Biosciences).

2.7.3 Processing of ova into peptide

The myeloid cells were generated as described in section 2.6.2. Cells were collected and washed in PBS. After, they were resuspended in GM-CSF-TCM media; if it was the case they were SIRPα blocked with 250nM antibody (Section 2.6.4) and after, plated at $2x10^5$ cells per well with or without CD47 coating (Section 2.6.3). The cells were incubated 3 hours in their respective conditions. Then, the cells were pulsed with DQ-Ovalbumin (Cat: D-12053, Thermo) at 100µg/ml for 10 min at 37°C and then washed 3 times with ice cold PBS, 5% FBS. After, cells were resuspended in pre-warmed full culture GM-CSF-TCM media and transferred to 37°C for 35 minutes. Immediately after, cells were washed twice with PBS and transferred in ice. Then, they were resuspended in PBS with viability dye, diluted 1:1000, for 3 minutes, to label dead cells. Live/Dead Fixable Violet (Thermo, Cat: 62248) was used. After this, cells were washed and stained for 15 minutes with fluorophore conjugated primary antibodies (Section 2.4). Immediately after, cells were washed once with PBS and run on an LSR Fortessa cell analyzer (BD, Biosciences).

2.8 Anti-SIRPα antibody study

2.8.1 The ultra-LEAF™ purified anti-mouse CD172a (SIRPα) antibody binding curve

The extracted bone marrow cells (Section 2.2.1) were resuspended at $5x10^4$ cells per well in PBS with viability dye, diluted 1:1000, for 15 minutes, to label dead cells. Live/Dead Fixable Violet (Thermo, Cat: 62248) was used. While the cells were being Live/Dead stained, the primary Ultra-LEAF™ purified anti-mouse CD172a (SIRPα) antibody (Cat: 144037) was titrated 1:20 starting from 500nM in FACS buffer (0.5% Bovine Serum Albumin or 'BSA' in PBS). Cells were washed once with PBS before to add the primary antibody, then they were incubated with the samples, for 40 minutes, at 4°C to avoid internalisation. Cells were washed once and incubated 20 minutes at 4°C with a secondary Alexa Fluor 647 chicken anti-rat IgG1 antibody (Cat: A21472) in FACS buffer. After cells were washed twice and run on an LSR Fortessa cell analyzer (BD, Biosciences) and analysed using FlowJo version 10. (FlowJo, BD Biosciences).

2.8.2 Competition between the PE conjugated and the unconjugated anti-mouse CD172a (SIRPα) clone p84

Bone marrow cells were extracted as described in section 2.2.1 and grown as described 2.6.2. Cells were washed twice and plated at $5x10^4$ cells per well in PBS with viability dye, diluted 1:1000, for 15 minutes, to label dead cells. Live/Dead Fixable Violet (Thermo, Cat: 62248) was used. Cells were washed and incubated with the unconjugated version of the anti-mouse CD172a (SIRPα) clone P84 Antibody (Biolegend, Cat: 144037) titrated 1:2 starting from a concentration of 100nM in FACS buffer (0.5% Bovine Serum Albumin or 'BSA' in PBS) for 40 minutes at 4°C. After, cells were washed with PBS and incubated with a secondary Alexa Fluor 647 chicken anti-rat IgG1 antibody (Cat: A21472) or, with PE anti-mouse CD172a (SIRPα) clone P84 antibody (Biolegend, Cat:144011) in FACS buffer for 30 minutes at 4°C. Unspecific

binding was washed away with 3 washes in PBS. Samples were run on an LSR Fortessa cell analyzer (BD, Biosciences) and analysed using FlowJo version 10. (FlowJo, BD Biosciences).

2.9 Immunoblotting

2.9.1 Myeloid cells preparation for immunoblotting

Myeloid cells were grown as in section 2.6.2 and Ly6C$^+$ cells isolated as in section 2.2.5. The cells obtained cells were resuspended in 50% TCM (Section 2.5.1) and 50% RPMI media, supplemented with 20ng/mL GM-CSF (Peprotech, Cat: 315-03) and seeded at 2x10^5 cells per well. After, cells were incubated in the respective conditions for 4 hours at standard cell culture condition (37°C in a 5% CO2). Then cells were washed in PBS and pelleted to be lysed 30 minutes in Pierce-RIPA buffer (Thermo Scientific) supplemented with protease-inhibitor cocktail (Roche), 1mM PMSF and 1mM Na3VO4 at 4°C. Then, they were stored in the freezer (-20°C).

2.9.2 Immunoblotting to detect SHP2 and STAT3

Samples were defrosted (Section 2.9.1) boiled at 99ºC for 5 min in protein loading buffer and loaded. Samples were then separated by a 10% SDS-PAGE and transferred onto a Nitrocellulose membrane (Millipore). The membranes were blocked with Odyssey blocking buffer (Li-Cor) for 1 hour and then incubated with a recombinant Anti-SHP2 antibody (Cat: ab187040, clone EPR17829-9, 68 kDa) or anti-SHP2 (phospho Y542) antibody (Cat: ab62322, clone EP508(2)Y, 60 kDa) or phospho-Stat3 (Tyr705) (D3A7) (Cat: 9145T, Cell Signaling, 80 kDa) or Stat3 (79D7) (Cat: 4904T, Cell Signaling, 80 kDa) and α-tubulin (Cat: T6074, clone B-5-1-2, Sigma, 50-55kDa) primary antibodies overnight at 4ºC in 5% BSA(w/v) in PBS and 0.1% Tween 20. After washing with PBS, membranes were incubated with the appropriate fluorescent-conjugated secondary

antibody (IRDye680RD Donkey anti-Mouse –925-68072; IRDye 800CW Donkey anti-Rabbit –925-32213) for 1 hour. Detection was performed using Odyssey CLx (Li-Cor).

2.10 Measure of specific metabolites

2.10.1 Cells glucose depletion

Myeloid cells were grown as in section 2.6.2 and Ly6C$^+$ cells isolated as in section 2.2.5. Cells were treated for SIRPα blockade (Section 2.6.4) and after, plated at 1x10^5 cells per well in a CD47 coated (Section 2.6.3) 96 nonpyrogenic flat bottom well plate. GM-CSF or GM-CSF-TCM grown cells were resuspended respectively in RPMI-1640 (Gibco, Cat: 41879-020), supplemented with 1% penicillin/streptomycin (p/s) or Dulbecco's Modified Eagle Medium (DMEM, Life Technologies) (Gibco, Cat: 41966-025) and 1% penicillin/streptomycin (p/s) in absence of Glucose and Foetal Bovine Serum (FBS). Cells were seeded at 2x10^5 cells per well incubated for 4 hours at standard cell culture condition (37°C in a 5% CO2).

2.10.2 Glucose uptake and GLUT-1

Cells were prepared as in section 2.10.1 (glucose depletion). 2-NBDG (2-(N-(7-Nitrobenz-2-oxa-1,3-diazol-4-yl) Amino)-2-Deoxyglucose) (Invitrogen, cat: N13195) was added in the well at 200 µM and incubated for 20 minutes at 37°C. In the meantime, the GLUT1 (Novus Biologicals, Cat: NB110-39113) antibody was preincubated with an Alexa-fluor-647 chicken anti-rabbit APC (Life technology, Cat: A21443) and after used at 35nM. Immediately after, cells were extensively washed and, once in ice, stained (Section 2.4) reducing the incubation time at 3 minutes for live/dead and 15 minutes for fluorophore-conjugated antibodies. Cells were washed once with PBS and run on an LSR Fortessa cell analyser (BD, Biosciences).

2.10.3 ATP assay

Cells were prepared and cultures in glucose deprived media as in section 2.10.1. Cells were washed with PBS and resuspended in full RPMI media, supplemented with 20ng/mL GM-CSF (Peprotech, Cat: 315-03) or in 50% TCM (Section 2.6.1) and 50% RPMI media, supplemented with 20ng/mL GM-CSF and incubated for 20 minutes at standard cell culture condition (37°C in a 5% CO2). The ATP level of cells was analysed using an ATP Assay Kit (Merck, Cat: 119107), according to the manufacturer's protocol.

2.10.4 NADH assay (hexokinase colorimetric assay)

Cells were prepared and cultures in glucose deprived media as in section 2.10.1. Cells were washed with PBS and resuspended in full RPMI media, supplemented with 20ng/mL GM-CSF (Peprotech, Cat: 315-03) or in 50% TCM (Section 2.6.1) and 50% RPMI media, supplemented with 20ng/mL GM-CSF and incubated for 20 minutes at standard cell culture condition (37°C in a 5% CO2). The activity of hexokinase in cellular lysates was analysed by measuring the NADH production per time in a colorimetric assay, according to the manufacturer's protocol (Sigma–Aldrich, Cat: MAK037).

2.11 Statistics

To evaluate statistical significance between two samples a T-test was performed. For multiple comparisons, a one way or 2-way ANOVA was employed with a Dunnett or Tukey post- hoc test. For growth curves 2-way ANOVA with Šidák correction was performed. Data are expressed as mean ± SEM, where a different cell isolates and batch of TCM was used for each experiment. Multi-variant data were analysed using analysis of variance (ANOVA), followed by Dunnett or Tukey post-hoc tests. The t-test was used to compare individual treatment conditions. $p < 0.05$ was considered statistically significant, giving a 95% confidence level. Data were analysed using Graphpad Prism 9 Software packages.

CHAPTER 3

PHENOTYPE CHARACTERISATION OF MYELOID DERIVED CELLS FROM ESTABLISHED MELANOMA TUMOUR

3.1 Introduction

A wide range of pathologies induce emergency myelopoiesis, an immune response against threats which results in rapid expansion of monocytes and neutrophils. When the insult is resolved and the tissue returns to a resting state, the myeloid cells go back to a normal level of myelopoiesis. This is not the case in pathologies such as cancer, where a persistent insult induces a continuous state of emergency myelopoiesis, expansion and accumulation of highly suppressive and highly diverse myeloid population[399].

This abnormal differentiation and function of myeloid cells exert its function by accumulating at the tumour site. These pathologically activated MDSC with potent immunosuppressive activity is common in tumours. MDSC have the ability to support tumour progression by promoting tumour cell survival, angiogenesis, invasion of healthy tissue by tumour cells[652], and metastases[653].

Myeloid derived suppressor cells play a key role from early stages of the primary tumour evolution, via immune modulation, angiogenesis, EMT and formation of the pre metastatic niche[654,655,656,657,658]. Their defining role is the contribution to tumour cell immune escape via the formation and maintenance of an immunosuppressive microenvironment. An increase of MDSCs correlates with poor prognosis and patient survival[659]. There is strong evidence that a higher circulating MDSC level is a potential prognostic parameter in patients with solid cancer, independent of MDSC subtype, cancer type, and cancer stage[659]. An increase in MDSCs was correlated to poor prognosis as the myeloid cells were suppressing the immune response in several solid tumours (melanoma[660], gastric[661], head and neck[662] and non-small cell lung[663] cancer and hematologic malignancies[664]). Furthermore, reducing the level of MDSCs could benefit clinical outcome in cancer therapy as elevated MDSC levels lead to resistance to hormone therapy[665], chemotherapy[666,667], radiotherapy[668] and

immunotherapy[669,670]. Thus, in light of their crucial role in cancer evolution, there remains a need to understand the evolving role of MDSCs alongside cancer progression.

In mice, MDSCs were initially characterised by cell membrane protein markers, the granulocyte receptor-1 antigen (GR1) and the integrin-M (CD11b, ITGAM)[405]. Later, two subpopulations were identified by expression of lymphocyte antigen 6 complex, locus C1 (Ly6C) and lymphocyte antigen 6, locus G (Ly6G) proteins. This lead to the division of MDSCs into monocyte M-MDSC and polymorphonuclear G-MDSCs displaying the marker profiles $CD11b^{+}CD11c^{-}Ly6C^{+}Ly6G^{-}$ and $CD11b^{+}CD11C^{-}Ly6C^{lo}Ly6G^{+}$ respectively, each of which have been investigated by specific functionality[408,671]. In humans, the G-MDSC are described as $CD14^{-}CD11b^{+}CD15^{+}$(or $CD66^{+}$) and M-MDSC $CD11b^{+}CD14^{+}HLA\text{-}DR^{low/-}CD15^{-}$ [410,405].

To examine the role of myeloid populations in tumour development, we used the well–characterised, syngeneic B16-F10 model that was originally obtained from a spontaneous chemical-induced tumour in a C57BL/6 mouse[672]. This model is characterised by a highly immunosuppressive environment, enriched in MDSCs[171,172]. In this first chapter, we sought to characterise the presence and changes in time of the myeloid landscape towards a suppressive phenotype able to block T cells proliferation. Furthermore, create an *in vitro* myeloid cells model to use for elucidating mechanism that could resemble and be correlated to the in vivo findings.

3.2 Results

3.2.1 Characterising the evolution of myeloid population as tumours develop.

To assess the prevalence of myeloid derived suppressor cells (MDSCs) in primary tumour, B16-F10 melanoma cells were orthotopically injected into wild type C57BL/6 mice and the tumours were grown for 11 days (figure 3.1 A). Tumours were then prepared for flow cytometry as described in section 2.4. Within the immune cell compartment ($CD45^+$), the lymphoid and natural killer cells were excluded ($CD3^+$ and $NK1.1^+$ cells respectively), and the proportion $Ly6G^+$ (polymorphonuclear MDSCs; G-MDSCs) and $Ly6C^+$ (monocytic MDSCs; M-MDSCs) within the $CD11b^+$ myeloid compartment was assessed (figure 3.1 B). The myeloid compartment (CD11b+ cells) composed about 40-50% of the total immune infiltrate within the tumour (Figure 3.1C), and of this, 60% were $CD11b^+Ly6C^+$ while only 3-5% were $CD11b^+Ly6G^+$ expressing (figure 3.1 C). Therefore, in established primary B16-F10 tumours, the predominant myeloid cell fraction were M-MDSCs ($CD11b^+Ly6C^+$), which have previously been shown to represent a suppressive population that dampens the anti-tumour immune response[405].

A

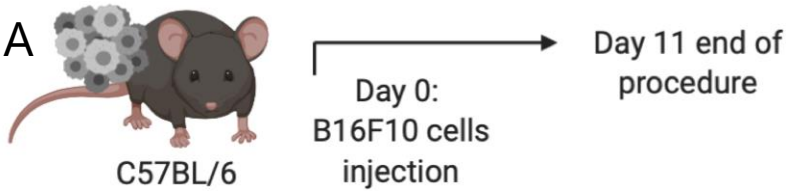

B

C

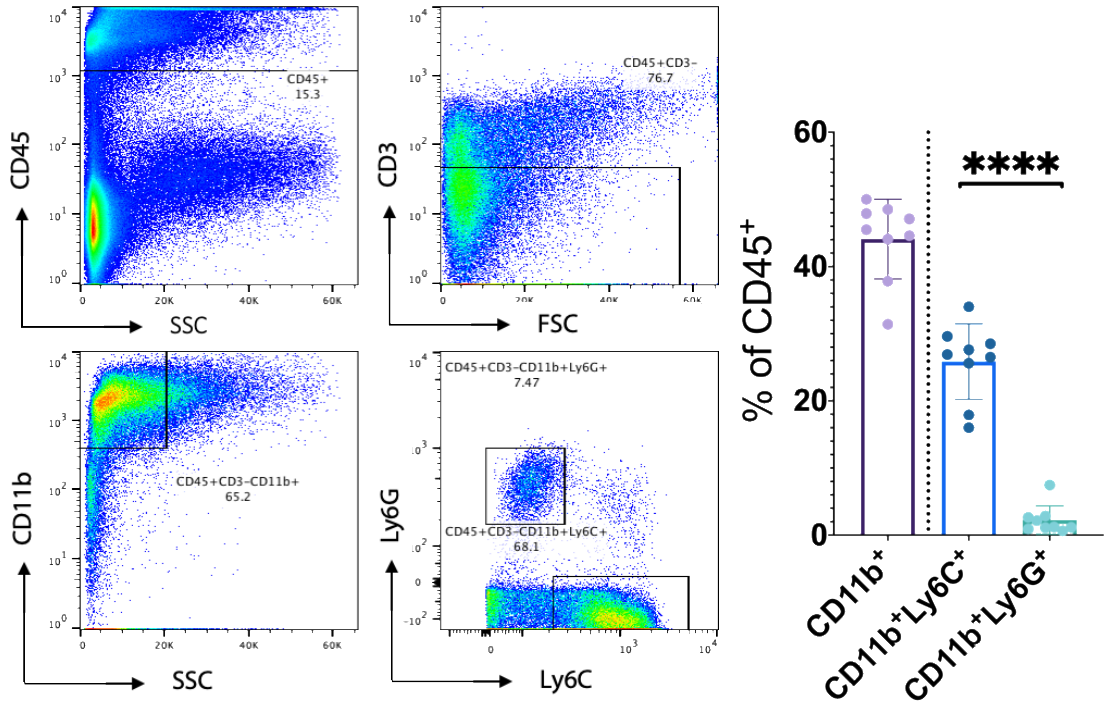

Figure 3.1. Ly6C-expressing cells are the dominant myeloid population in established B16-F10 melanoma. (**A**) Schematic of the in vivo experiment, B16-F10 cells were injected at day 0 and melanoma tumours collected the eleventh day. (**B**) Representative FACS plots showing the gating strategy, live cells were gated on $CD45^+CD11b^+Ly6C^+$ and $CD45^+CD11b^+Ly6G^+$ immune cells while T $CD3^+$ cells were excluded (**C**) Quantification of the myeloid cells as percentage of $CD45^+$ cells. Data are mean ± SEM; **** = $p<0.0001$ using ordinary one-way ANOVA with Tukey's post hoc test. Assays n=3 mice in each group, 3 independent experiment.

After determining that Ly6C expressing cells comprised the majority of the myeloid compartment in established tumours, we then determined whether these cells were present from an early stage of tumour development or appeared later. We thus examined composition in small day 5 tumours, intermediate day 9, or late stage day 11 tumours. Moreover, as CD11b is a generic marker for myeloid populations and contains cell types besides MDSCs, we also included CD11c. From this, 3 main clusters were identified and defined based on the expression of CD11b and CD11c and then by Ly6G and Ly6C (Figure 3.2 A). Based on this classification, we observed that in early

tumours, approximately 5% of the total immune infiltrate were $CD11c^{+}CD11b^{-}$, 50% were $CD11c^{+}CD11b^{+}$ and 30% were $CD11c^{-}CD11b^{+}$ (figure 3.2 B). Focusing within the $CD11c^{-}CD11b^{+}$ fraction, cells expressing Ly6G were almost completely absent whilst Ly6C accounted for 5% of all immune cells (figure 3.2 C). We defined these cells as M-MDSCs. Additionally, we observed that 7% $CD11c^{+}CD11b^{+}$ cells also expressed Ly6C. We defined these cells as monocytic dendritic cells, moDCs.

At the intermediate stage of development, day 9 tumours presented with a shift in the distribution of myeloid populations. We observed a drastic drop in $CD11c^{+}CD11b^{+}$ from 50% to 25%, whilst the $CD11c^{-}CD11b^{+}$ showed a slight increase to approximately 35% (figure 3.2 B). Within this population, the moDCs remained constant at 7% of total infiltrates and G-MDSC remained rare. However, M-MDSCs increased significantly from 5% to almost 20% to be the dominant population (figure 3.2 C). By day 11, late stage tumours contained approximately 5% $CD11c^{+}CD11b^{-}$, while $CD11c^{+}CD11b^{+}$ and $CD11c^{-}CD11b^{+}$ equilibrated to each comprise approximately 35% of the total immune infiltrate (figure 3.2 B). Consistent with earlier time points, G-MDSCs formed a negligible proportion of infiltrating immune cells while M-MDSCs comprised approximately 20% of the immune infiltrate, and moDCs formed 15% of the total infiltrate (Figure 3.2 C).

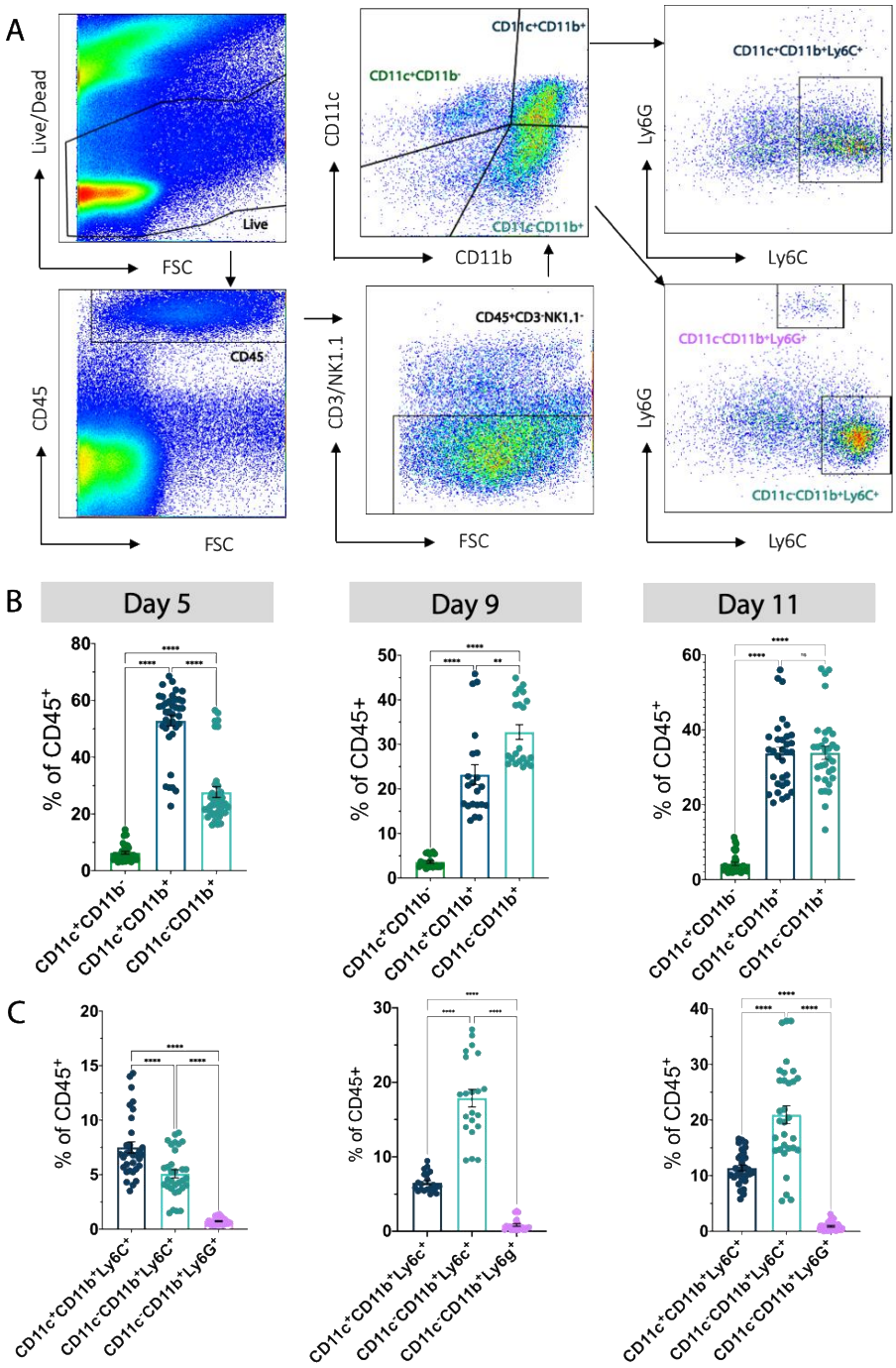

Figure 3.2. The composition of myeloid derived suppressive cells in B16-F10 tumours shifts as tumours develop. (A) Representative FACS plots of a day 11 tumours showing the staining strategy to identify MDSCs according to literature. Live cells were gated and $CD3^+$ and $NK1.1^+$ cells excluded. Within $CD11c^+CD11b^+$ and $CD11c^-CD11b^+$ gates, Ly6G (G-MDSC) and Ly6C (M-MDSC) markers identified $CD11c^+CD11b^+Ly6C^+$, $CD11c^-CD11b^+Ly6C^+$ and $CD11c^-CD11b^+Ly6G^+$. **(B)** Percentage of myeloid populations within $CD45^+$ cells. **(C)** Quantification of MDSCs populations expressing CD11b and CD11c (shown as % of CD45). (B-C) Data are mean ± SEM; * = $p < 0.05$, **

= p < 0.01, *** = p < 0.001, **** = p<0.0001 using one-way ANOVA with a Tukey's post hoc test. For day 5 and 9 n=5 mice in quadruplicate, for day 11 assays n=6 in quadruplicates.

Thus, an increase in Ly6C$^+$ cell populations was observed as tumours progressed, and while infiltration of Ly6G$^+$ cells was less, it remained constant along the time course. Indeed, although total myeloid infiltration decreased as tumours progressed, a concurrent expansion in Ly6C$^+$ M-MDSC and moDC fractions, which play a critical role in suppressing the anti-tumour immune response[673] likely contribute to the development of a suppressive environment during early tumour development.

3.2.2 Examining remodelled cDC1, cDC2, moDC, M-MDSC and G-MDSC landscape in melanoma

In order to determine the contribution of these cells to tumour progression, we then sought to characterise the components of the myeloid compartment in more detail at day 5 and day 11 post-tumour induction, where we previously observed the biggest changes in myeloid populations.

To classify myeloid components in more depth, we again divided cells based on CD11c and CD11b, confirming that the myeloid clusters remodel with time, dominated by a switch between CD11c$^+$CD11b$^+$ and CD11c$^-$CD11b$^+$ over time (figure 3.3).

In addition to M-MDSCs (CD11c$^-$CD11b$^+$Ly6C$^+$), G-MDSC (CD11c$^-$CD11b$^+$Ly6G$^+$) and moDCs (CD11c$^+$CD11b$^+$Ly6C$^+$) that are associated with immune-suppressive behaviors[330,322], conventional dendritic cells 1 (cDC1; CD11c$^+$XCR1$^+$) that play a role in activating cytotoxic T cells[674, 329], and conventional dendritic cells 2 (cDC2; CD11c$^+$CD11b$^+$Ly6C$^-$) which are key for induction of antitumor CD4$^+$ T cell immunity[330] were examined (figure 3.4 A). While cDC1-expressing cells were scarce at both time points examined (figure 3.4 B), the anti-tumour cDC2 fraction significantly reduced as tumours developed, dropping from 50% at day 5, to 20% at day 11 of the total immune

cells, and was replaced by moDCs and M-MDSCs which doubled (5% to 10% for moDCs and 5% to 20% for M-MDSCs) as tumours progressed (figure 3.4B). It is possible that moDCs may be a matured, more suppressive M-MDSC population developing in response to local cytokine cues.

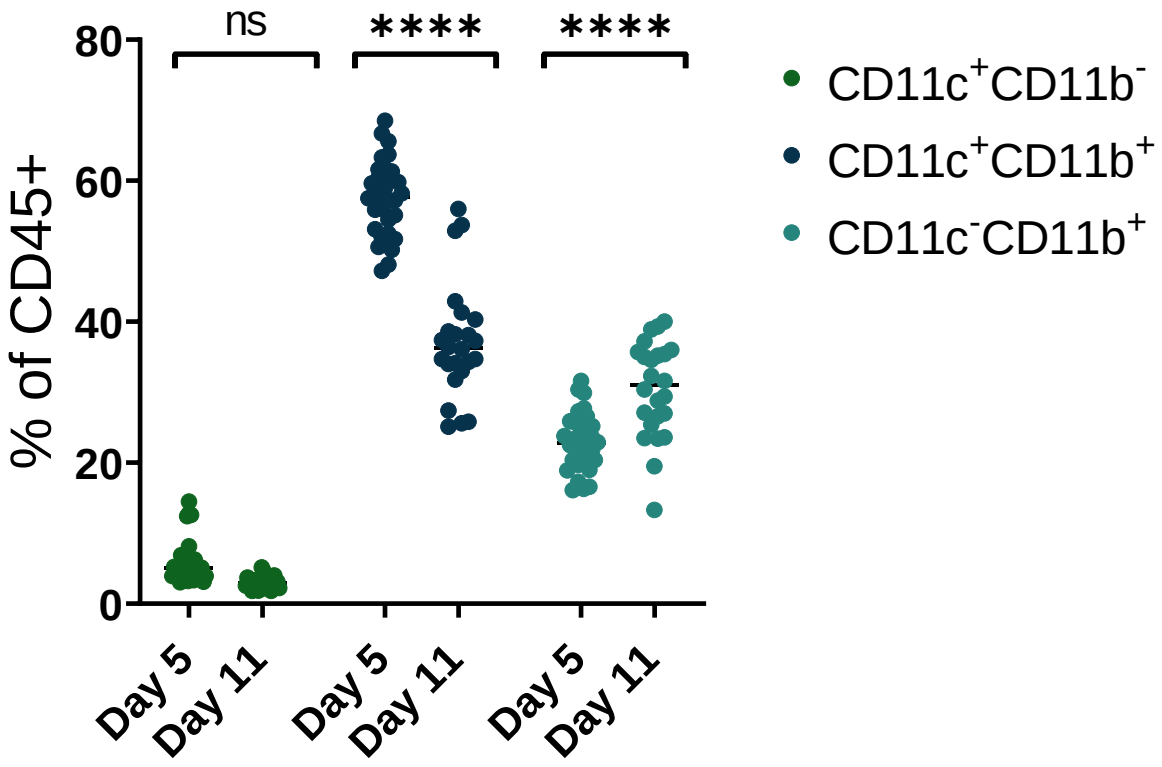

Figure 3.3. Analysis of the myeloid landscape remodeling along tumour evolution. (B) Flow cytometric quantification of infiltrating myeloid cells in day 5 and day 11 tumours subdivided according to the CD11c and CD11b markers. Expressed as % of $CD45^+$. Data are mean ± SEM; * = $p < 0.05$, ** = $p < 0.01$, *** = $p < 0.001$, **** = $p<0.0001$ using two-way ANOVA with a Sidak's multiple comparison post hoc test. For day 5 n=4 mice and for day 11 mice n=3, in duplicates.

Collectively, these data show that there is a distinct remodeling of the myeloid compartment along tumour growth from anti- to pro-tumour phenotypes. Although there was an overall stability in the proportion of myeloid cells in the tumour, we detected a clear expansion of M-MDSC and moDC fractions and a concurrent reduction of inflammatory DCs.

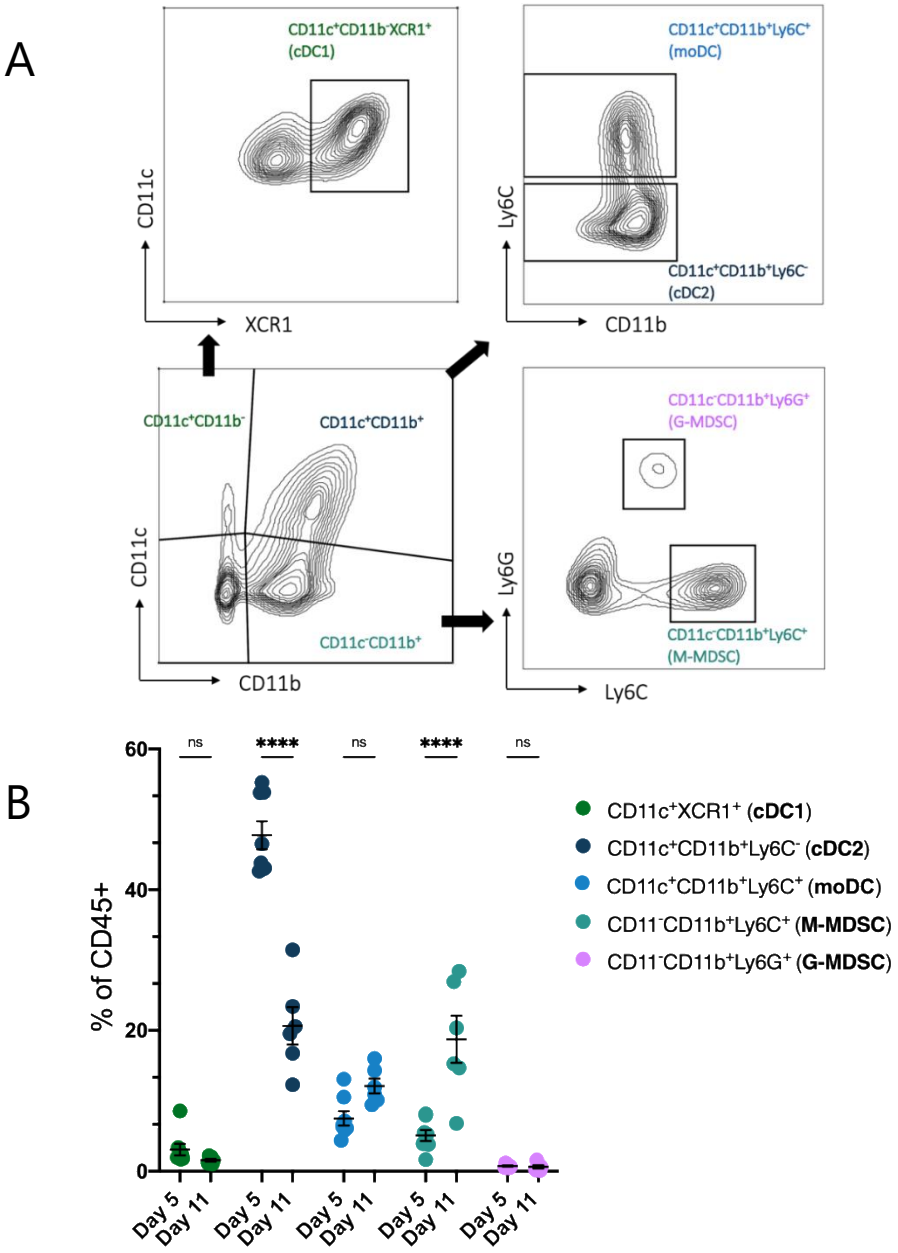

Figure 3.4. The myeloid landscape remodels from anti- to pro-tumour as tumours progress. **(A)** Representative FACS plots showing the gating to identify the myeloid populations; $CD11c^+CD11b^-XCR1^+$ (cDC1), $CD11c^+CD11b^+Ly6C^-$ (cDC2) and $CD11c^+CD11b^+Ly6C^+$ (moDC), $CD11c^-CD11b^+Ly6C^+$ (M-MDSC), and $CD11c^+CD11b^+Ly6G^+$ (G-MDSC). **(B)** Flow cytometry quantification of myeloid phenotypes in day 5 and day 11 tumours. Populations shown as percentage of $CD45^+$. Data are mean ± SEM; * = $p < 0.05$, ** = $p < 0.01$, *** = $p < 0.001$, **** =

p<0.0001 using two-way ANOVA with a Sidak's multiple comparison post hoc test. For day 5 n=4 mice and for day 11 mice n=3, in duplicates.

Having observed a switch in myeloid phenotype as tumours grow, we then sought to understand the contribution of the expanding myeloid components (M-MDSCs and moDCs) to the loss of a functional anti-tumour immune response. The signal-regulatory protein alpha (SIRPα) is generally used to define dendritic cells[322] and MDSCs[631]. SIRPα is the receptor for the protein CD47, and their interaction negatively influences phagocytosis and is known as "do not eat me signal"[617].

We therefore examined its expression to provide a snapshot of its distribution in early and late tumours. Nearly all cDC2, moDC and M-MDSC cell clusters expressed SIRPα at both time points examined, in contrast to only 10% of cDC1 and 25% of G-MDSCs (figure 3.5A). However, we did note an increase in expression in G-MDSCs at day 11, consistent with the development of a less functional, suppressive phenotype.

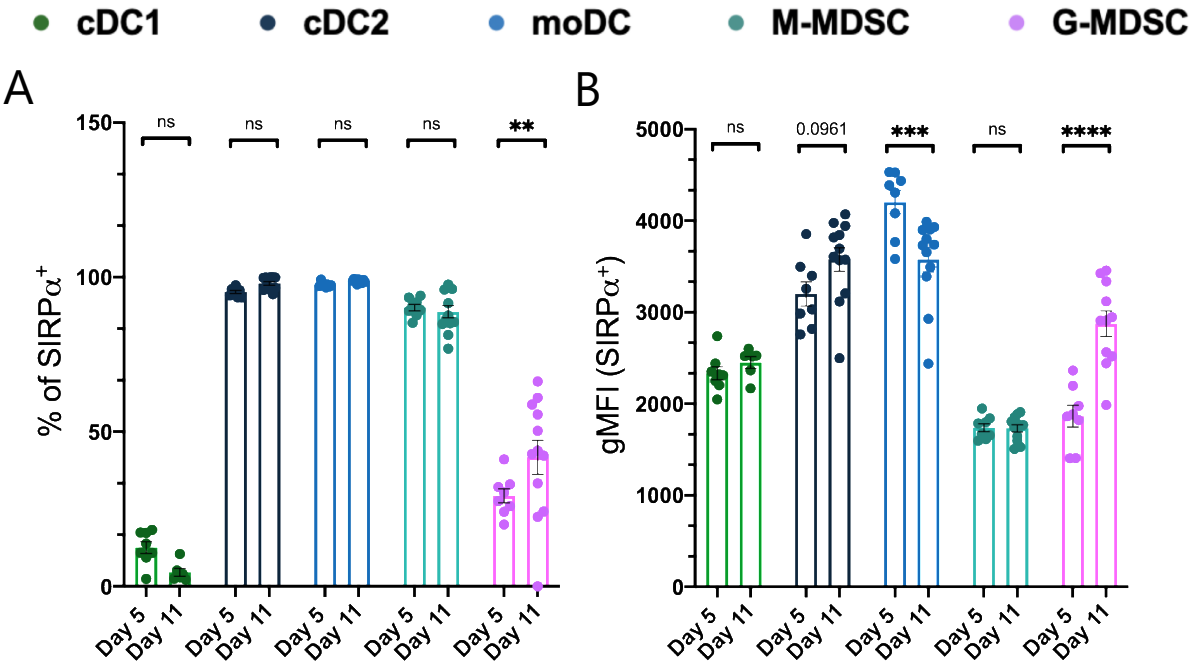

Figure 3.5. SIRPα expression identifies myeloid populations in the evolving TME. Quantification of **(A)** The prevalence and **(B)** expression levels of SIRPα, characterizing a mature myeloid phenotype, in cDC1, cDC2, moDC, M-MDSC and G-MDSC in day 5 and 11 tumours. Data are mean ± SEM; * = p < 0.05, ** = p < 0.01, *** = p < 0.001, **** = p<0.0001 using two-way ANOVA with a Sidak's multiple comparison post hoc test. Mice n=4 (day5) and n=4(day11) from two and three independent experiments.

Interestingly, although almost all M-MDSCs were positive for SIRPα, analysis of geometric mean fluorescence intensity (gMFI) showed that the level of expression was significantly lower than cDC2 and moDC (Figure 3.5B). Here it is important to note that the gMFI of SIRPα on the G-MDSCs and cDC1 was not reliable due to the scarcity of cells.

The presence of the myeloid cells expressing CD11b, Ly6C and SIRPα were also identified using a confocal microscope (figure 3.6A-D). The melanoma tumor microenvironment resulted infiltrated of CD11b cells which were also presenting Ly6C and SIRPα but also highlighted the myeloid heterogeneity as we saw in the FACS data.

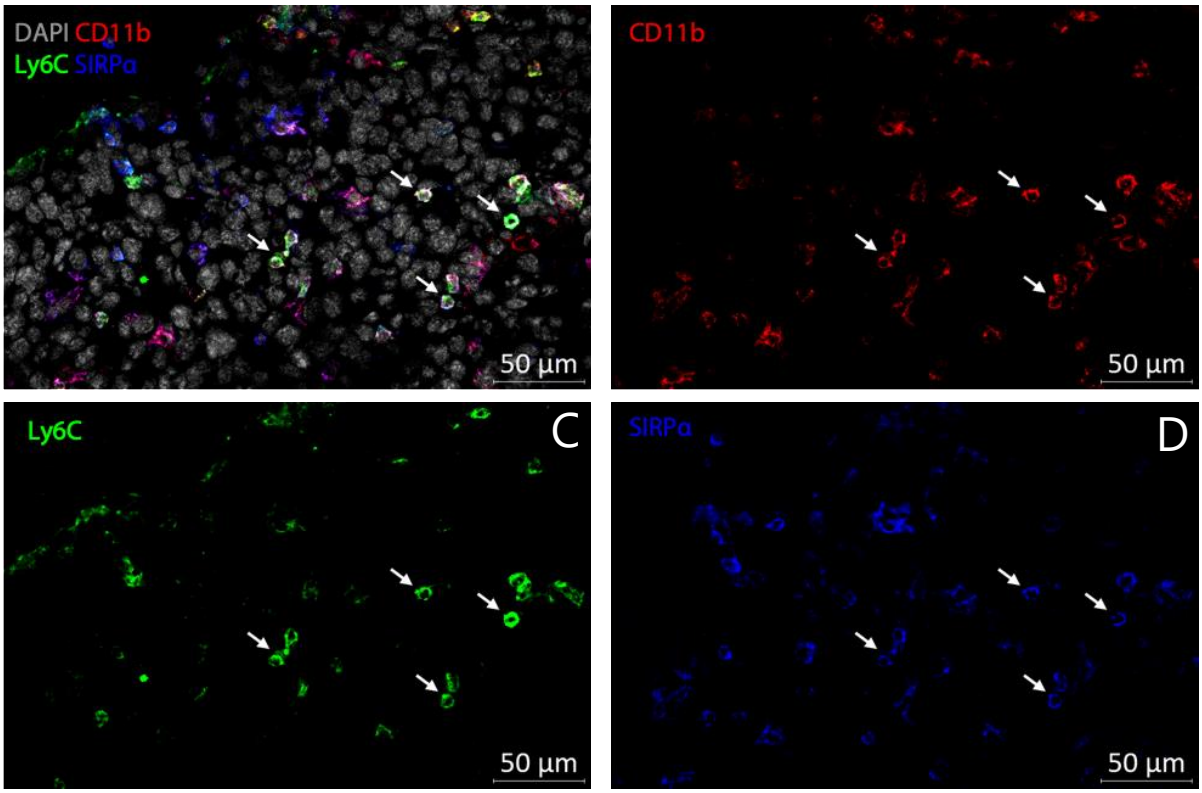

Figure 3.6. Confocal imaging of CD11b, Ly6C and SIRPα myeloid markers in B16F10 syngeneic C57BL/6 at day 11 of tumour development. Representative confocal image of a day 11 B16-F10 melanoma tumour showing myeloid cells. The arrows point to CD11b+Ly6C+SIRPα+ cells. **(A)** Image showing the combination of DAPI (Grey), CD11b (red), Ly6C (green), SIRPα (Blue). The image is shown for each single marker **(B)** CD11b, **(C)** Ly6C and **(D)** SIRPα.

After identifying the myeloid heterogeneity, we also measured CX3CR1 which marks monocytes and monocyte precursors, and F4/80 for mature macrophages[675,676]. Similar to SIRPα, CX3CR1 was widely expressed by the myeloid cells and again cDC2, moDC and M-MDSCs were most prevalent (Figure 3.7A), however, the proportion varied depending on tumour stage. Fewer CX3CR1^{+} moDCs and M-MDSCs were present at day 11 compared to day 5 of tumour development, and conversely, a significant increase in G-MDSCs expressing CX3CR1 were detected at day 11 (figure 3.7A). Moreover, for most populations the gMFI of CX3CR1 tended to increase while

the opposing effect was observed on moDC cells (Figure 3.7B). Interaction between CX3CL1 and CX3CR1mediates chemotaxis of immune cells to the tumour site[677] and moDCs expressing CX3CR1 were reported to induce T-cell-dependent antitumor immunity[678]. In addition, in a human hepatocellular carcinoma model, migration of suppressive MDSC into the hypoxia region was mediated through CCL26/CX3CR1and correlated with poor prognosis[679]. Taken together, these results explain what we observed, inflammatory moDC-CX3CR1^{+} decrease whilst M-MDSCs-CX3CR1^{+} suppressive increase.

F4/80 is reported to distinguish macrophages from DCs[680]. As expected, negligible F4/80^{+} cDC1 were detected. However, almost all cDC2 and moDC were positive for F4/80 in day 5 tumours, but this proportion significantly decreased by day 11 (Figure 3.7 C). The proportion of MDSC expressing F4/80 at day 5 was low in comparison (between 10 and 25%). However, while the prevalence of F4/80^{+} M-MDSCs further decreased by day eleven, G-MDSC showed a robust increase with almost 50% expressing this marker (figure 3.7 C). Interestingly, while the frequency of F4/80^{+} cells was reduced, the level expression determined by gMFI was increased on all remaining positive cells in each subset by day 11 (figure 3.7 D). Since levels of F4/80 have been correlated with induction of regulatory T cells in peripheral tolerance[681] and associated with tumour associated macrophages[682], its upregulation may be a further indicator in the switch to a more suppressive microenvironment.

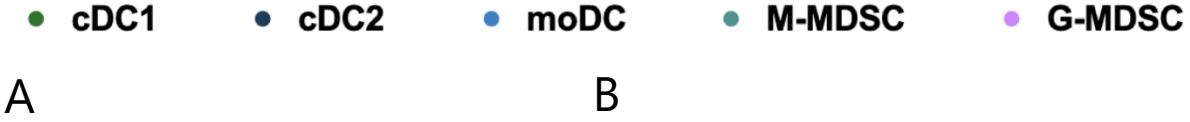

A B

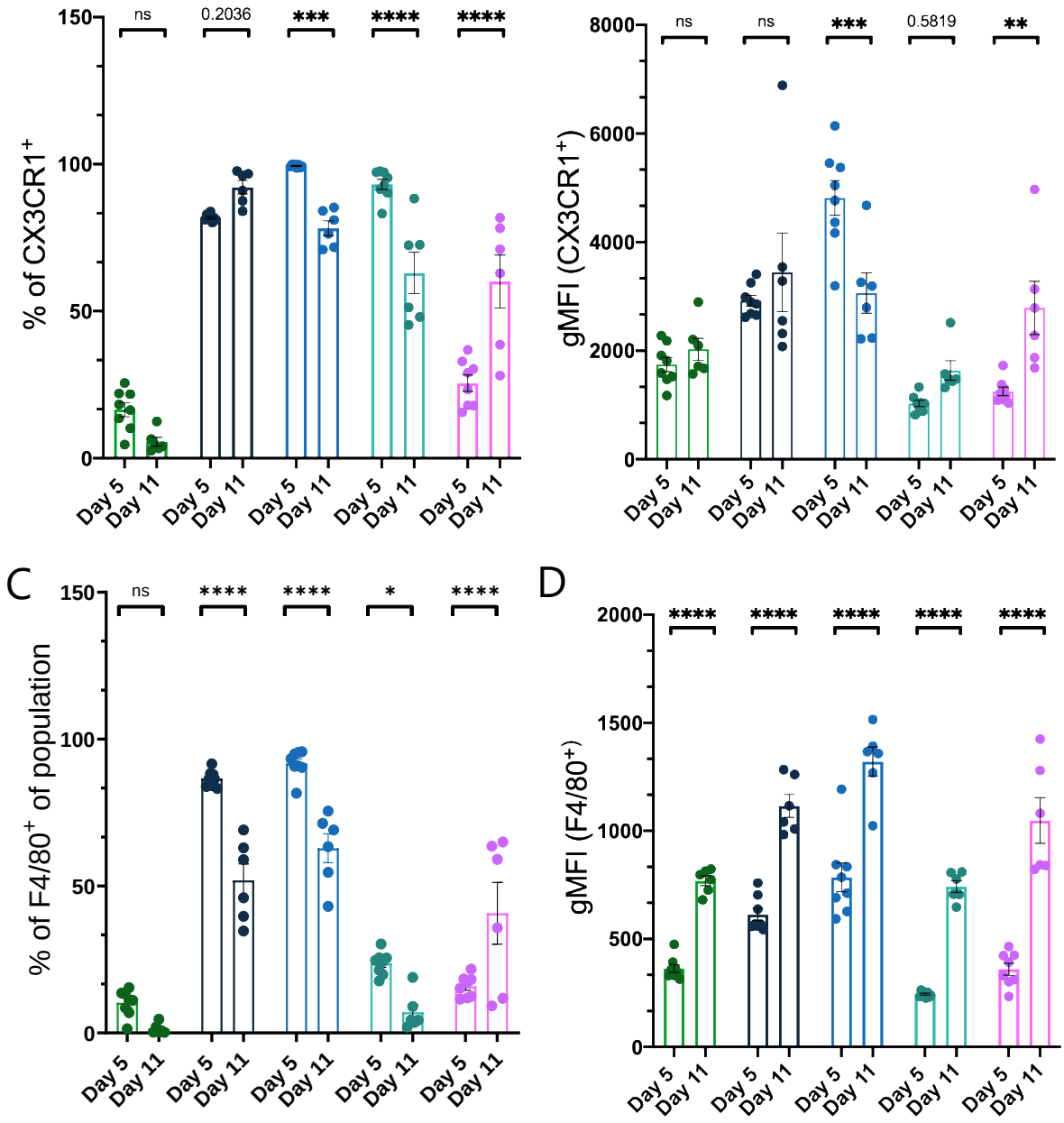

Figure 3.7. Analysis of the myeloid phenotypes associated with "mature" markers in the evolving TME. Quantification of **(A)** the prevalence and **(B)** expression levels of CX3CR1 (monocytes), and **(C)** the prevalence and **(D)** expression levels of F4/80 (macrophage) to characterize a mature myeloid phenotype, in cDC1, cDC2, moDC, M-MDSC and G-MDSC of day 5 and 11 tumours. Data are mean ± SEM; * = $p < 0.05$, ** = $p < 0.01$, *** = $p < 0.001$, **** = $p<0.0001$ using two-way ANOVA with a Sidak's multiple comparison post hoc test. Mice n=4 (day5) and n=3 (Day 11) in two independent experiments.

Together, these data showed that cDC2 maintained high expression of SIRPα and the monocytic marker CX3CR1, while the prevalence of F4/80+ cells was markedly reduced by day 11. In SIRPα+ moDCs, loss of the CX3CR1 monocytic marker and concurrent increase in F4/80 by day eleven, indicates that this population lost its undifferentiated monocytic phenotype to become more macrophage like as tumour progress. M-MDSCs, characterised by a strong Ly6C expression also frequently expressed SIRPα and CX3CR1 but as tumours progressed cells expressing CX3CR1 halved. Coupled with low F4/80, which was almost absent, these data suggested that the M-MDSCs were less differentiated than others myeloid populations, and because they shared the expression of the Ly6C it is possible that moDCs may be their precursor. Thus, as tumours grew, we measured a shift in the myeloid landscape and high levels of phenotypic plasticity towards pro-tumour populations, however SIRPα remained a common denominator.

3.2.3 Increased expression of immune modulatory molecules accompanies changes in myeloid populations

Having observed a significant shift in the composition of myeloid cells present as tumours progressed, we next began to examine if they were capable of suppressing the anti-tumour immune response. We first looked at markers that have previously been associated with T cell suppression. The programmed death-ligand 1 (PD-L1), when bound to PD-1 on activated T cells inhibits anti-tumour immunity by counteracting T cell-activating signal[683]. PD-L1 expression by myeloid cells has been associated with establishment of an immunosuppressive environment in pancreatic cancer[684] and as a predictive biomarker for immune checkpoint blockade[685].

In all populations examined, with the exception of cDC1, the gMFI of PD-L1 significantly increased by day 11 (Figure 3.8 A). Indeed, the cDC2 doubled the expression intensity from day 5 to day 11 while moDC and M-MDSCs increased by a

third. However, it should also be noted that PDL1$^+$ cDC1 and G-MDSC cells only made up a very small proportion of the total myeloid infiltrate (appendix 8.1 A), thus data may not accurately reflect protein levels.

Similarly, the Fas-FasL axis is implicated in myeloid cell-mediated immunosuppression and tumour progression[686,687,686], where engagement of FasL with Fas triggers apoptosis[688] and reduces T cell cytotoxic activity. As for PDL-1, the gMFI of FasL$^+$ myeloid cells showed a similar pattern of increasing expression (Figure 3.8 B). Importantly, the number of FasL$^+$ cells also increased from day 5 to day 11 post-tumour inductions (Appendix 8.1 B). The cDC2, moDC and M-MDSCs clusters exhibited more than doubled expression of the FasL (figure 3.8 B) but the positive M-MDSCs were low proportion (Appendix 8.1 B).

This higher expression of both PDL-1 and FASL over time confirms that myeloid cells shift towards a suppressive state as tumours progress and suggests a potential role in myeloid-mediated suppression of T cell function via activation of the apoptotic signal.

PD-L1 and FasL both induce suppression and apoptosis via cell-to-cell contact. However, this is not the only mechanism to induce suppression. T cell differentiation and activation also depends on nutrients availability and oxidation[689,690,445]. In cancer, Arginase 1 (ARG1) which is a critical regulator of amino acid metabolism that uses L-arginine to produce ornithine, has been shown to be involved in L-arginine depletion and nitric oxide production and this plays a critical role in progression. Myeloid cells have been shown to express ARG1, contributing to the suppression of T cells by decreasing inflammatory cytokine production, blocking the TCR formation and

eventually causing cell cycle and proliferation arrest[689]. Based on these reports, its correlation with myeloid-mediated immunosuppression was investigated.

With the exception of cDC1, ARG1 was almost undetectable in day 5 tumours. By day 11, expression increased by three-fold on cDC2 and moDCs and two-fold on M-MDSCs (figure 3.8 C). L-arginine depletion is also an important regulator of nitric oxide production. The catalysing enzyme, nitric oxide synthase 2 (NOS2) uses L-arginine to produce nitric oxide which in turn affects T helper cell differentiation and the effector functions of $CD8^+$ cytotoxic T cells[691]. These effects have previously been correlated with MDSC recruitment and NOS2, ARG1 and ROS upregulation[564,692].

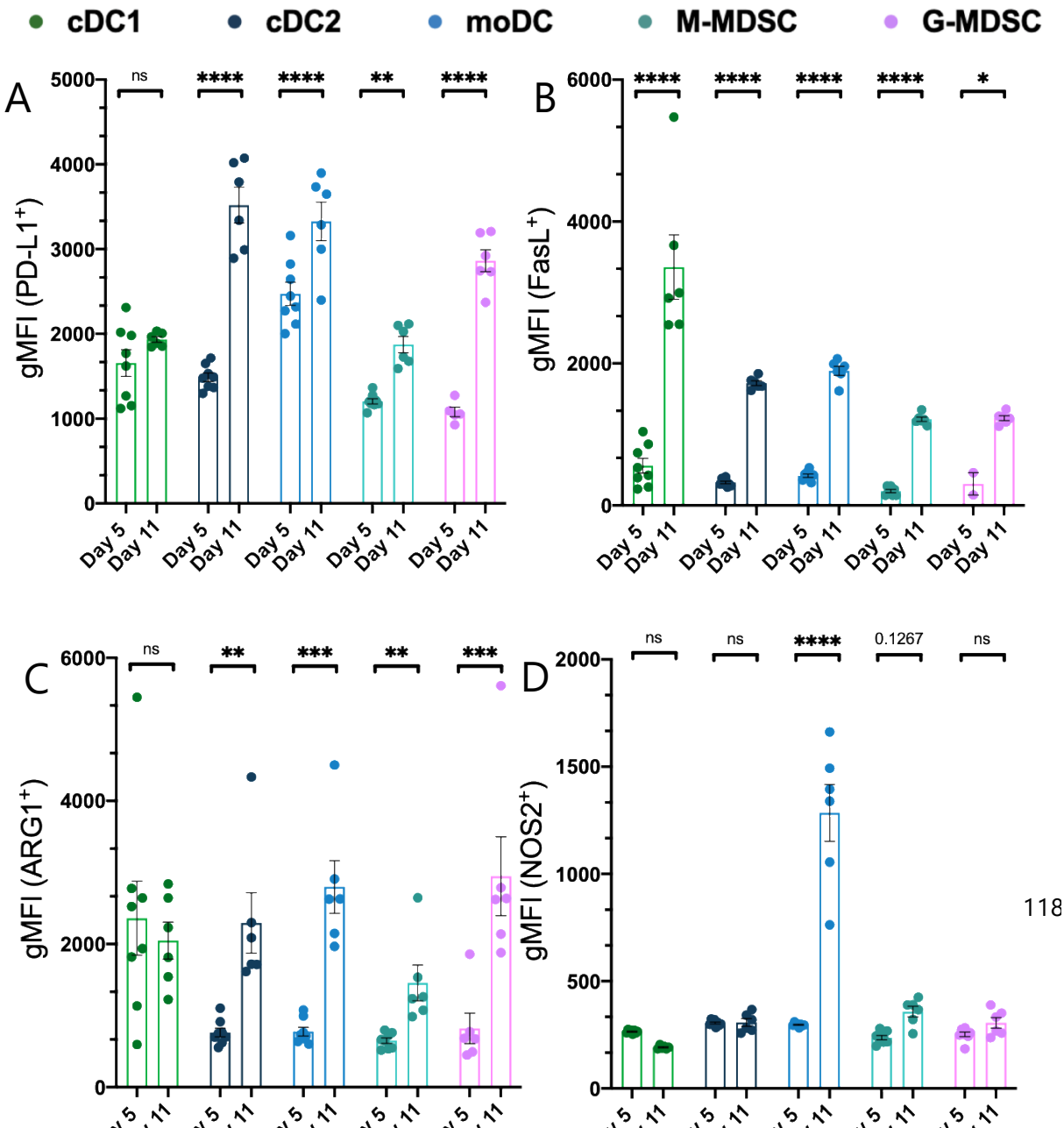

Figure 3.8. Analysis of function associated markers in the evolving myeloid cells increases along tumour evolution. Myeloid cells were extracted at the fifth and eleventh day of tumour development and markers associated with immunosuppression quantified by flow cytometry. The MFI geometric mean for **(A)** PD-L1 expression, **(B)** FasL expression, **(C)** ARG1 expression and **(D)** NOS2 expression in each myeloid cluster is shown. Data are mean ± SEM; * = $p < 0.05$, ** = $p < 0.01$, *** = $p < 0.001$, **** = $p<0.0001$ using two-way ANOVA with a Sidak's multiple comparison post hoc test. Mice n=4 (day5) and n=3 (Day 11) in two independent experiments.

Our flow cytometric analysis of the myeloid populations revealed that for moDC and M-MDSCs, only a small proportion of each myeloid subset was responsible for NO production, with $NOS2^+$ cells almost absent at day 5, however the proportion did increase at day 11 (appendix 8 .1 D). However, the gMFI of NOS2 expression was low on the majority of myeloid cell types, and it remained unchanged as tumours progressed with the exception of the moDCs, which presented with a 3-fold increase over time (figure 3.8 D).

These data indicate that NO production by most myeloid cells may not be an important contributing factor in this model for suppressing anti-tumour immunity but moDCs may provide a source of NO that contributes to the suppressive microenvironment. Thus, alongside direct interactions via PD-L1 and FasL, we confirmed that L-arginine depletion via ARG1 increase could be correlated with the myeloid cell's suppressive behaviour along tumour development.

3.3 Tumour associated myeloid cells inhibit proliferation

During tumour progression the myeloid compartment, particularly the Ly6C$^+$ populations, increased expression of immunosuppressive molecules. This observation made necessary to validate that the cells were in fact capable of suppressing T cell function. The gold standard method for determining the immunosuppressive capability of cells is to measure their capacity to suppress the proliferation of activated T cells. To perform this assay, we first extracted T cells from a spleen of a wild type C57BL/6 mouse. The cells were labelled with carboxyfluorescein succinimidyl ester (CFSE), a fluorescent compound able to permeate the cells and bind to intracellular lysine residues and other amine sources in the cytosol (figure 3.9 A). The covalently bound dye was used to monitor proliferation of CD3, CD28-stimulated T cells because the dye is divided equally between daughter cells and therefore the signal diminishes by half with each cellular division[693]. Gating on the T cells population and plotting the histogram of CFSE intensity will give a read out of picks that corresponds to the proliferative mitotic cycles. After the staining, the T cells were activated via TCR co-stimulatory molecules stimulation. The anti-CD3 antibody was coated on a well and successively an anti-CD28 was added in solution and incubated (figure 3.9 B). The procedure triggered the T cells proliferation that was measured over three days. The gating was set on the live CFSE positive cells and within, the T cells were detected using CD4 and CD8. Each T cell population was analysed by gMFI CFSE fluorescence.

Indeed, after 24h of stimulation, the signal produced by the CFSE labelled CD8$^+$ T cells was high and gradually diminished by 60h when they had undergone 4-5 mitotic cycles (figure 3.9 C). Interestingly, the CD4$^+$ T cells appeared to undergo fewer mitotic cycles over the 60h period, but the pattern of proliferation mirrored that observed with the CD8$^+$ T cells (Figure 3.9 C). This initial characterisation was used to determine the

experimental window for performing co-culture assays with the tumour-derived myeloid cells. Based on these proliferation optimisation studies we determined that an initial24h istimulation was needed to activate the T cells, followed by a further 48h in presence of the other cell type, to be compared to the proliferation of T cells alone. Thus, the experiment window was three days total.

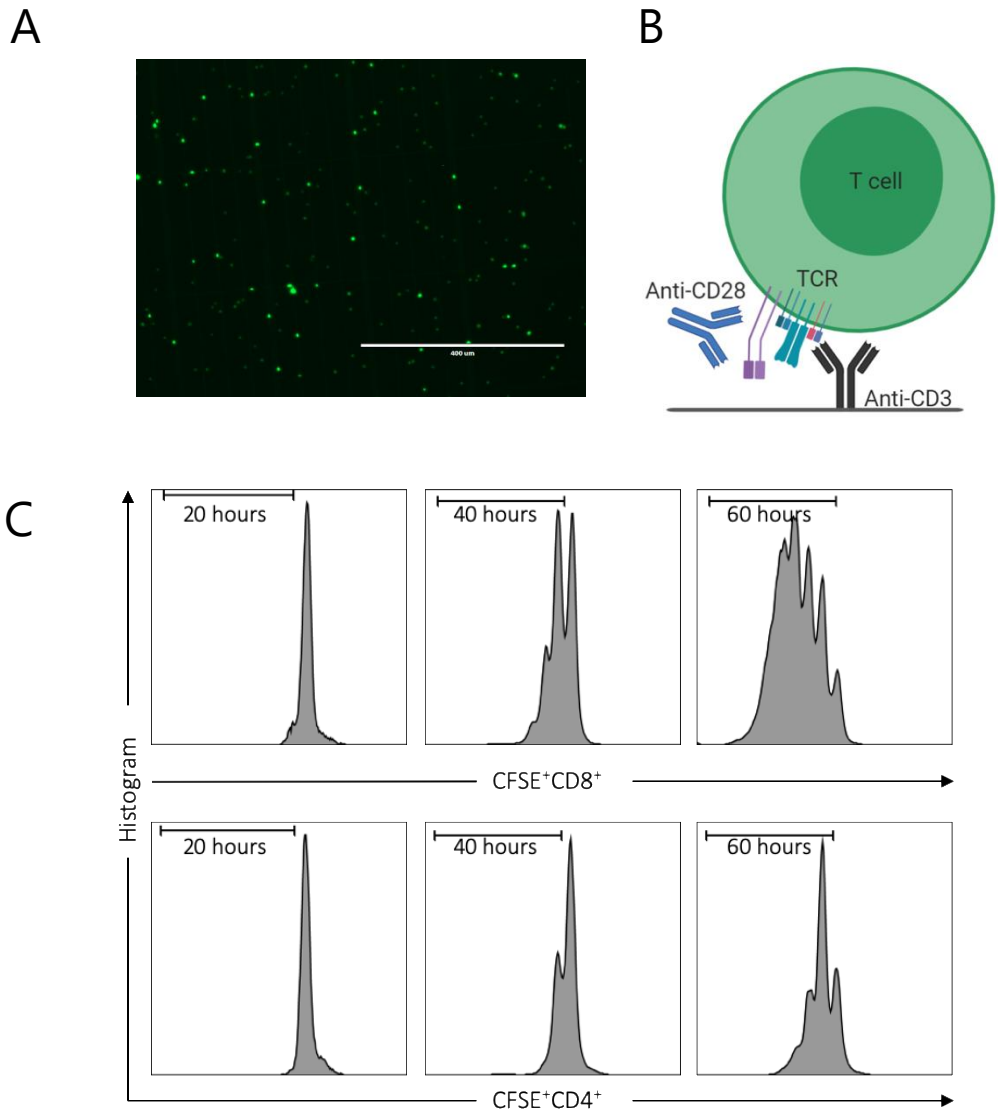

Figure 3.9 T cells CFSE staining and activation via TCR co-stimulatory receptors. (A) Image of T cells CFSE florescent cells (400µm resolution). (**B)** Representation of a T cells activation via stimulation of TCR co-stimulatory molecules with antibodies anti-CD3 and anti-CD28. **(C)** Representative T cells proliferation time course plots after stimulation at 20 hours, 40 hours and 60 hours.

3.3.1 Tumour-derived moDCs and M-MDSCs suppress t cells proliferation

Following optimisation, T cells were stimulated for 24h and subsequently mixed with M-MDSCs or moDCs isolated from day 11 tumours by MACS positive selection based on the expression of CD11b and Ly6C (figure 3.10 A). T cell suppression was then evaluated after 2 days by flow cytometry. MDSCs and moDCs were distinguished from T cells based on CD11b marker expression and absence of CFSE staining (Figure 3.10 B and C). The $CFSE^{+}CD11b^{-}$ T cell fraction was further subdivided into $CD4^{+}$ and $CD8^{+}$ fractions (Figure 3.10 D). Both CD4 and CD8 T cells propagated efficiently when cultured alone (Figure 3.10 E). However, In the myeloid cell co-cultures, only one bright peak of CFSE labelling was observed (Figure 3.10 E) indicating that isolated MDSCs were functionally suppressive. Indeed, when quantified, MDSCs induced almost complete inhibition of proliferation for both CD4 and CD8 cells (figure 3.10 F-G). The $CD11b^{-}Ly6C^{-}$ fraction had no impact on the capacity of T cells to proliferate (Figure 3.10 F-G). Of note, while the survival of $CD11b^{+}Ly6C^{+}$ cells isolated from tumours was low, suggesting that the process of extraction and incubation affected cell survival (Figure 3.10 H), the suppressive effect of isolated MDSCs was still exerted on both $CD4^{+}$ and $CD8^{+}$ cells.

Collectively, these data show that all Ly6C-expressing cells derived from melanoma express an array of immunosuppressive molecules that adapt as tumours develop, and are potent in their ability to functionally suppress the proliferation of activated T cells. Therefore, Ly6C expressing myeloid cells within tumours can be classed as MDSCs with potential to suppress T cells through various mechanisms.

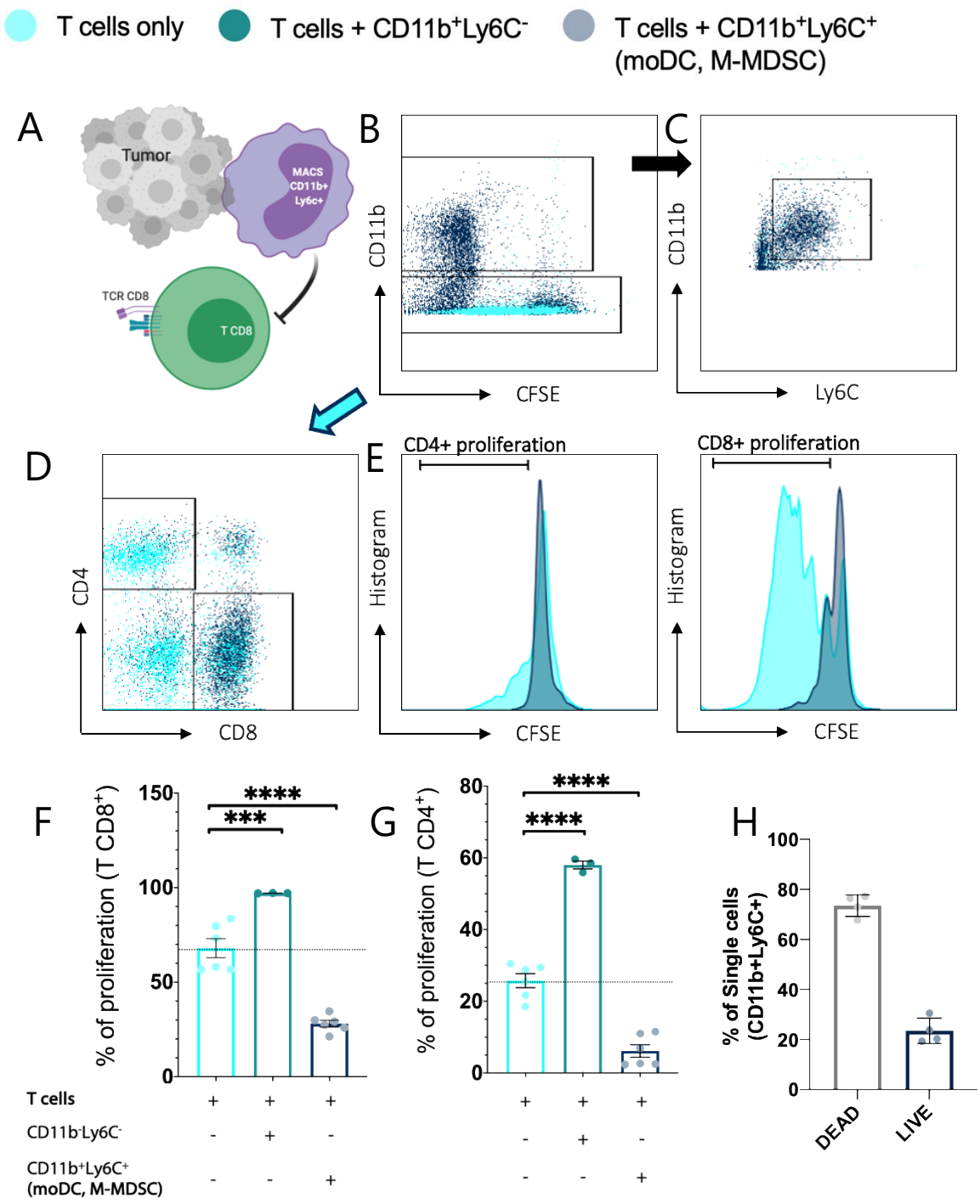

Figure 3.10. Tumour-derived moDC and M-MDSC inhibit proliferation of activated T cells. **(A)** Schematic representation of the experiment. **(B-E)** Representative FACS plots depicting gating strategy; light blue, T cell only control; dark blue, T cells from co-culture highlighting the myeloid population **(C),** The CFSE^{+} CD4 and CD8 **(D)** and CFSE plots of CFSE proliferation histograms compared to control **(E)**. **(F-G)** Quantification of the percentage of proliferated CD8 and CD4 cells alone, with CD11b^{+}Ly6C^{-} or CD11b^{+}Ly6C^{+}. **(H)** Percentage of CD11b^{+}Ly6C^{+} cells live and dead in

the T cell proliferation assay. Data are mean ± SEM; * = $p < 0.05$, ** = $p < 0.01$, *** = $p < 0.001$, **** = $p<0.0001$ using ordinary one-way ANOVA with a Dunnett's multiple comparison post hoc test. Assay n=3 in duplicate.

3.3.2 *Ex vivo* sorted $CD11b^+ly6C^+$ cells block T cells proliferation

To try and improve the survival of the $Ly6C^+$ myeloid cells isolated from the day 11 tumours, instead of using the MACS extraction method, cells were flow sorted based on the expression of the moDC and M-MDSC markers. This was potentially beneficial as it allowed further specificity for subset characterisation and isolation. Cells were stained and sorted based on their $Ly6C^+$ expression. Then, the $CD45^+CD11c^-CD11b^+Ly6C^+$ (M-MDSC) and $CD45^+CD11c^+CD11b^+Ly6C^+$ (moDCs) clusters were separated and added to cultures of CFSE-labelled activated T cells. After co-culture for 48h, the data were analysed separating populations as before (figure 3.11 A and B).

When examining at the $CD8^+$ cells proliferation, a noticeable suppressive effect was exercised with different potency by the two groups of myeloid cells. Interestingly, the M-MDSCs suppressed proliferation to a greater extent than the moDCs (figure 3.11 C-F). This was unexpected given the level of immunosuppressive molecules shown earlier to be expressed by the moDCs (Figure 3.8). One of the reasons could be the lower viability. Indeed again, the viability of $CD11b^+Ly6c^+$ cells were also affected by the sorting process, only 10% of M-MDSCs and 5% the moDCs were live by the end, despite an equal number of live cells being sorted in the wells (Appendix 8.2).

When co-cultured, moDCs suppressed $CD8^+$ T cells proliferation to slightly lesser extent than the M-MDSCs indicating, that the latter were more potent in delaying the T cells proliferation (figure 3.11 E). This difference was not detected regarding the $CD4^+$ cells which were equally suppressed when in contact with the two different myeloid cells populations (figure 3.11 F). This could have two explanations, the first could be

that effectively M-MDSCs are more suppressive despite having less suppressive molecules or the moDCs were more sensitive to the process of extraction. Overall, both clusters of cells were fragile and that translated in a milder suppression on the T cells proliferation compared to the MACS isolated cells shown in figure 3.10. As explained before, the inhibition of the mitotic cycle was equally propagated by both the myeloid cell clusters, hypothetically supporting a $CD8^+$ specific effect brought by the MDSCs higher suppressive potency.

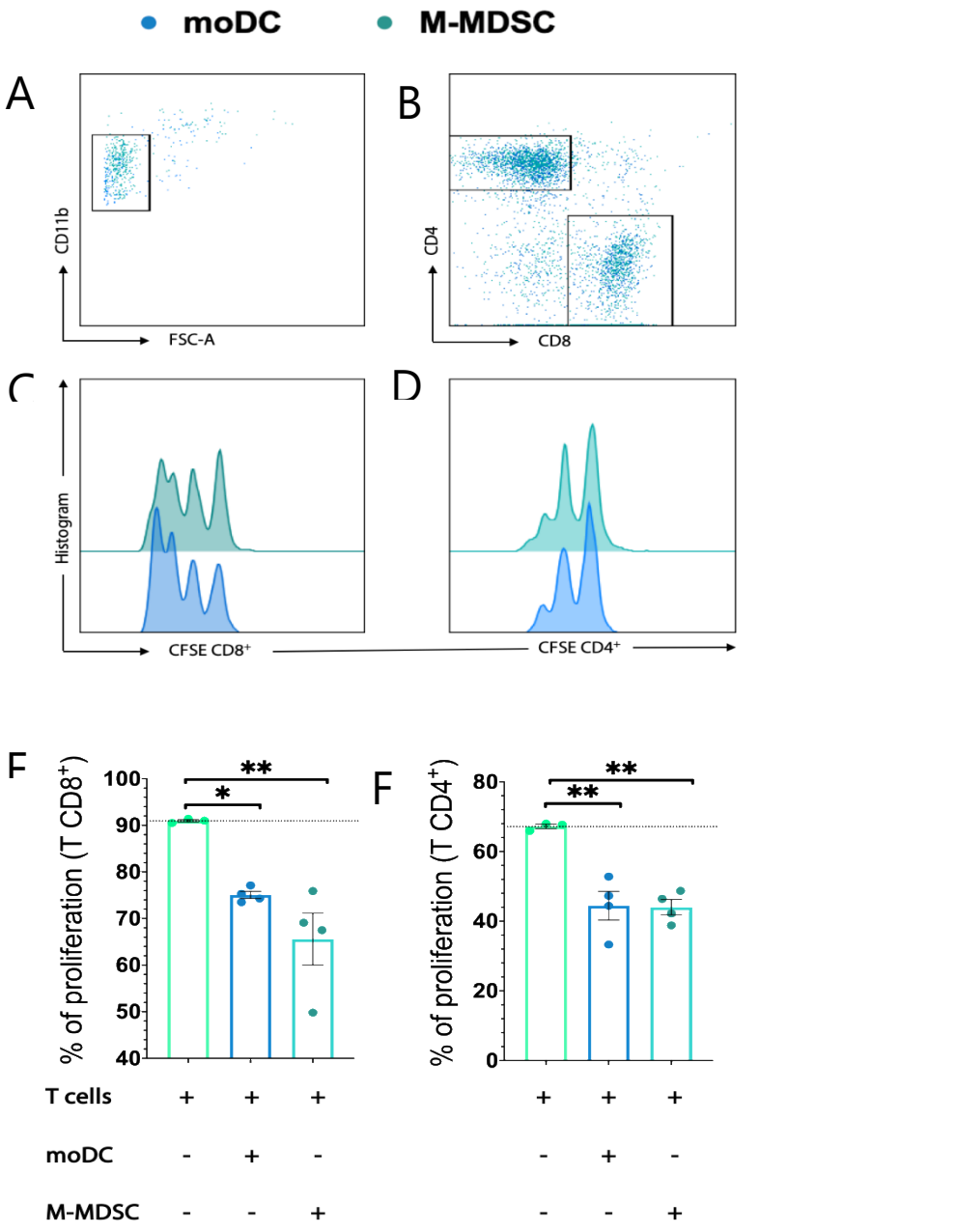

Figure 3.11. Tumour-derived sorted M-MDSCs are more suppressive than moDC. (A) Representative plots of the previously sorted moDCs and M-MDSCs expressing CD11b and **(B)** T cells present in the co-culture. **(C-D)** Representative proliferation histograms comparing T cells proliferation under the influence of moDC and M-MDSC. **(E-F)** Quantification of percentage of CD8 and CD4 of cells that proliferated when cultured with moDCs and M-MDCS cells compared to T cells only control. Data are mean ± SEM; * = $p < 0.05$, ** = $p < 0.01$, analyzed with one-way ANOVA with a Dunnett's multiple comparison post hoc test. Mice n=2 in duplicate from two different experiments.

With the data from two different myeloid isolation methods, we know that $CD11b^{+}Ly6C^{+}$ cells suppressed T cells proliferation and defined myeloid derived suppressor cells, MDSCs. It is not clear, however, which of the $CD11c^{+}$ or $CD11c^{-}$ myeloid cells suppresses more due to technical issues mentioned before. Due to the difficulties associated with the myeloid cell extraction process and potential impact on data analysis from poor viability, we set out to design an in vitro model system to model myeloid cells detected in the tumour.

3.4 Recapitulating tumour MDSCs in vitro.

Growing tumours strongly alter physiological myelopoiesis leading to the differentiation and expansion of MDSCs. Mature myeloid cells differentiate from hematopoietic progenitors, and based on the stimuli they encounter develop a suppressive nature. The most accepted theory is that immature myeloid cells (IMCs) from the bone marrow are mobilised by GM-CSF followed by a persistent second stimulus coming directly from the tumour that blocks their maturation inducing the immunosuppressive behaviour[694].

In vitro generation of MDSCs has been reported in many different protocols, however, the majority follow a three to five-day bone marrow cell culture in GM-CSF, IL-6 and IL-10 enriched media[376,464]. To simulate the soluble environment surrounding the B16 tumour, tumour conditioning media was generated and mixed in one to one ratio with complete culture media supplemented with GM-CSF to supply the growth and specific differentiation stimuli needed to generate the cells. Thus, to create a more solid tumour conditioning model, hematopoietic progenitors were extracted and cultured with TCM as described.

3.4.1 HSCs bone marrow isolation

Under the right stimuli, hematopoietic stem cells from the bone marrow differentiate to mature immune cells. HSCs are identified based on the marker SCA-1 in the bone marrow[695,696], thus we isolated bone marrow from femurs and tibias of healthy C57BL/6 mice and sorted using magnetic activated cell sorting (MACS) specific for the SCA-1 antibody. Flow cytometry confirmed that 60% of live cells extracted from the bone marrow had Sca-1 expressed on the surface, indicating that the isolation of HSCs was successful (figure 3.12 A and B).

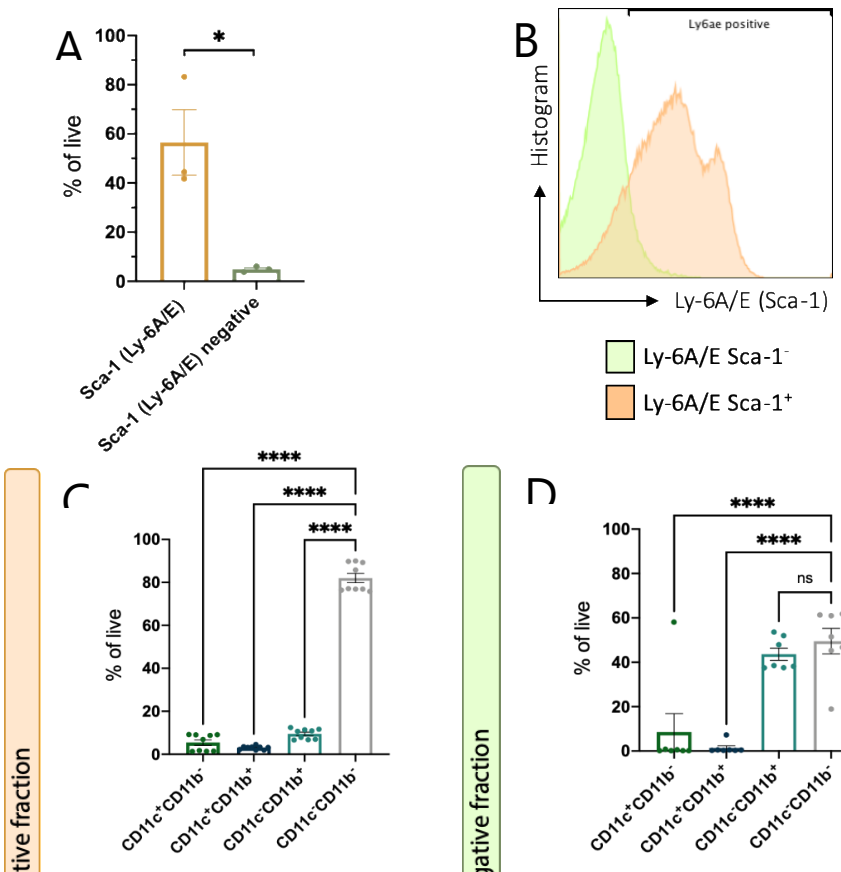

Figure 3.12. Successful isolation of SCA-1$^+$ hematopoietic stem cells from C57BL/6 bone marrow. (A) flow cytometry quantification of efficiency of extraction of SCA-1$^+$ HSCs as a percentage of live cells. **(B)** Representative plot of the SCA-1$^+$ extracted cells compared to the negative portion. Quantification of myeloid cells based on CD11c and CD11b cells in **(C)** SCA-1$^+$ and **(D)** SCA-1 negative fractions. Quantification of moDCs, M-MDSCs and G-MDSCs in **(E)** the SCA-1 positive fraction and **(F)** the negative fraction of extracted cells. Data are mean ± SEM; * = $p < 0.05$, ** = $p < 0.01$, *** = $p < 0.001$, **** = $p<0.0001$ (A) unpaired t test and C-F) one-way ANOVA with a Dunnett and Tukey's multiple comparison post hoc test. Total read out (A) n=3, (C) n=8, (D) n=7, (E) n=8, (F) n=5 at least in duplicates.

Further characterisation with the panel of myeloid cells markers was carried out to determine the starting point and purity of the cell culture system. The majority of SCA-1$^+$ samples were CD11c$^-$CD11b$^-$ indicating that the mature myeloid cells were not isolated (figure3.12 C). To notice that we couldn't deplete the entirety of the differentiated cells, between 10 and 20 % were still presenting a CD11b or CD11c phenotype while others were not identified by our panel.

However, the SCA-1 negative fraction contained significantly more CD11b and CD11c expressing cells (figure 3.12 D). The same results were recapitulated when looking at the previous markers plus the Ly6C and Ly6G. The SCA-1 positive fraction was scarcely populated with monocytes and neutrophils, and together composed only 7% of the total population after sorting (figure 3.12 E) while in the SCA-1 negative fraction they comprised almost 40% of the total (figure 3.12 F). This demonstrated that the SCA-1 positive sorting achieved the goal of isolating the HSCs rather than differentiated populations.

Subsequently, HSCs were maturated in the presence of GM-CSF that resemble the bone marrow mobilisation stimuli and a second persistent signal coming from tumour represented by the treatment with tumour condition media (TCM). With this system we aimed to obtain the same phenotype observed in vivo, and with the ability of suppressing T cells. As control the myeloid cells were grown in GM-CSF alone. The GM-CSF-TCM grown cells were supposed to have the closest phenotype to the M-MDSCs and moDCs described by the in vivo characterisation. The cells were treated for 5d to induce differentiation towards the cell types of interest. Due to the plastic nature of myeloid cells particularly during differentiation from HSCs, cell culture evolution was monitored over the differentiation period to assess the percentages of the various cells forming myeloid clusters.

3.4.2 HSCs differentiation into myeloid cells

The evolution of the cell cultures treated with GM-CSF alone or with GM-CSF and TCM was monitored and myeloid markers were analysed to explore how the cells differentiated at day 3 and day 5. At day 3, and compared with baseline isolates (figure 3.13), we observed the undifferentiated HSCs started to express CD11b. The shift was visible in the FACS plots but no major differences were detected when GM-CSF was compared to GM-CSF-TCM culture (figure 3.13 A and F). The three major myeloid clusters identified by CD11b and CD11c were similar in both cases, the undifferentiated $CD11b^{-}CD11c^{-}$ population went from 80-90% of the initial SCA-1 positive extraction to 30% after 3 days (figure 3.13 D and I). This reduction reflected the gain of more differentiated myeloid cells, 5% $CD11c^{+}CD11b^{-}$, 10% $CD11c^{+}CD11b^{+}$ and 50% $CD11c^{-}CD11b^{+}$ (figure 3.13 D and I). The expression of markers such as CD11b and CD11c increased gradually and may be already indicating a shift towards suppressive myeloid populations[697].

Furthermore, examination of the $CD11c^{+}CD11b^{+}$ and $CD11c^{-}CD11b^{+}$ compartments showed how the moDCs, M-MDSCs and G-MDSCs populations were starting to develop after day 3. The moDC increased from 0% to 10%, the M-MDSC from 2% to more than 25% and the G-MDSC remained fairly constant (figure 13 D-E and I-L). Three days in contact with GM-CSF and GM-CSF-TCM drove the expansion of the HSCs towards mainly moDCs and M-MDSCs. Indeed, the total 5-8 % of $CD11c^{+}CD11b^{+}$ were almost all moDCs (figure 13 D-E and I-L) and the 50% of $CD11c^{-}CD11c^{+}$ was mainly composed by M-MDSC (figure 13 D-E and I-L). Thus, by day 3 of maturation, in terms of population distribution, the cells seemed to start resembling the myeloid compartment detected in vivo, but there weren't any differences between the two culture conditions. Therefore, cultures were further expanded until day 5 post-isolation based on previous reports.

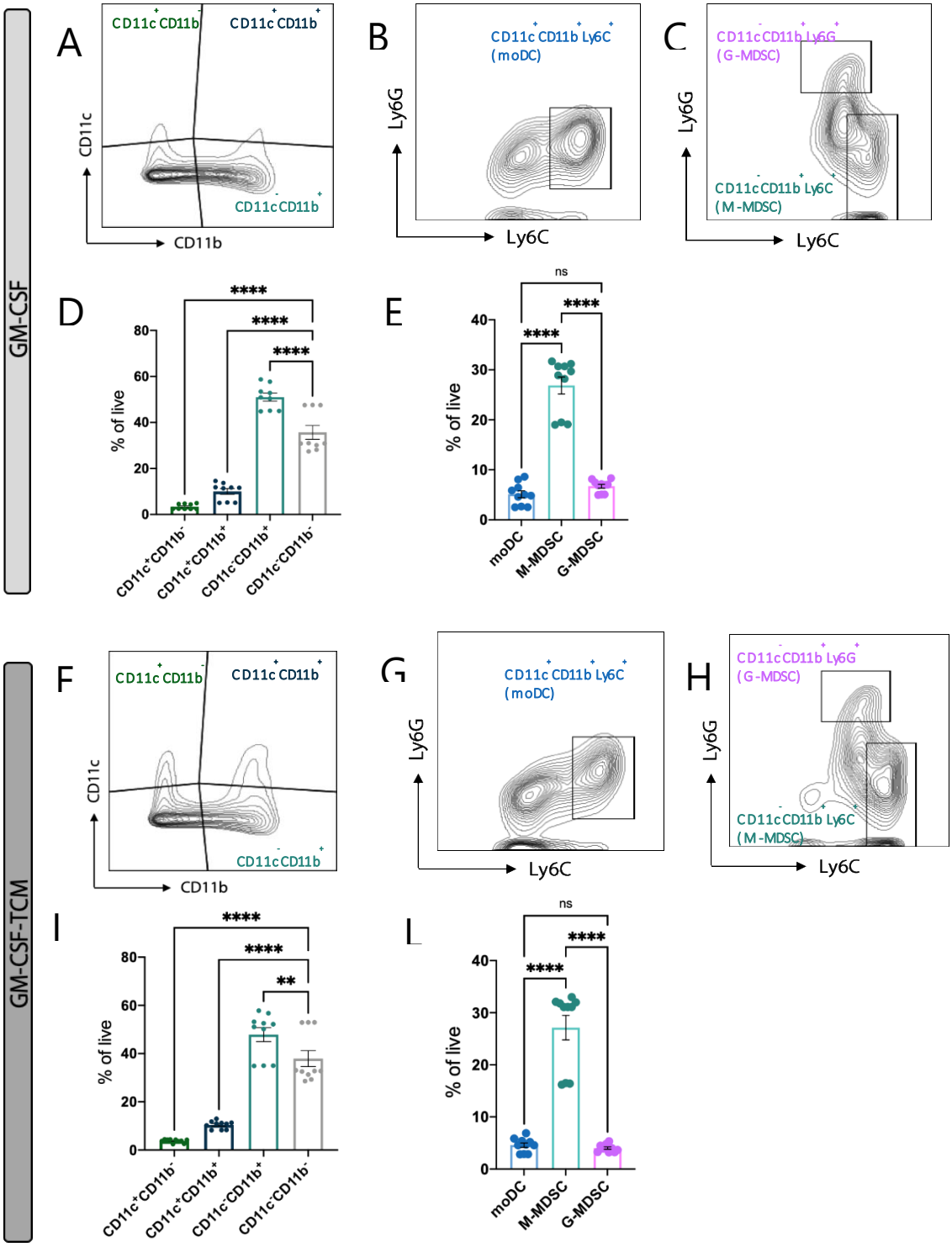

Figure 3.13. SCA-1⁺ HSCs start to differentiate after 3 days with GM-CSF, or GM-CSF-TCM. **(A-B-C)** Representatie plots showing the CD11b and CD11c populations and moDCs, M-MDSC and G-MDSCs at day 3 of GM-CSF exposure. **(D-E)** Quantification of live cells of CD11b and CD11c popluations, and moDCs, M-MDSC and G-MDSCs. **(F-G-H)** Representatie plots in GM-CSF-TCM. **(I-L)** Quantification of CD11b and CD11c populations and moDCs, M-MDSC and G-MDSCs at day

3 of cuture in GM-CSF-TCM. Data are mean ± SEM; * = p < 0.05, ** = p < 0.01, *** = p < 0.001, **** = p<0.0001 using one-way ANOVA with a Dunnett and Tukey's multiple comparison post hoc test. Assay n=3 in triplicates.

At day 5 post-isolation, the myeloid cells further matured, with an obvious reorganisation of CD11b and CD11c distribution compared to day 3 (figure 3.14 A and F). All the cells clearly differentiated in the two main clusters of $CD11c^{+}CD11b^{+}$ and $CD11c^{-}CD11b^{+}$ (figure 3.14 A and F), with $CD11b^{-}CD11c^{-}$ cells barely detectable in both GM-CSF and GM-CSF-TCM cultures. In TCM cultures, 40% cells were $CD11c^{+}CD11b^{+}$ and 60% were $CD11c^{-}CD11b^{+}$ while for the GM-CSF cultures, they were 30% and 70%, respectively (figure 3.14 D and I), suggesting that the cells grown in TCM differentiated more towards a $CD11c^{+}CD11b^{+}$ expressing phenotype which contains cDC2 and moDCs.

Further examination showed that moDCs, M-MDSCs and G-MDSCs were more defined compared to day 3 of cell culture in both treatment conditions. Following the kinetics of HSC maturation, we observed that CD11b was first upregulated by day 3 followed by expression of CD11c by day 5 to form the $CD11c^{+}CD11b^{+}$ population.

Interestingly, the composition of the myeloid compartment was similar between the two culture conditions (Figure 3.14 E and L). Nevertheless, the main cell population emerging in these cultures were the M-MDSCs which composed 40%, of the total population compared to 20% moDCs and only 5% G-MDSCs (figure 14 E and L).

Together, these data showed that cell culture systems were able to form myeloid matured populations from HSCs a predominantly moDCs and M-MDCSs composition, consistent with those that were detected in the tumour microenvironment. Further analysis was needed to understand if these represented suppressive myeloid cells differed in composition between GM-CSF and GM-CSF-TCM and, whether the addition of TCM influenced their suppressive nature in any way.

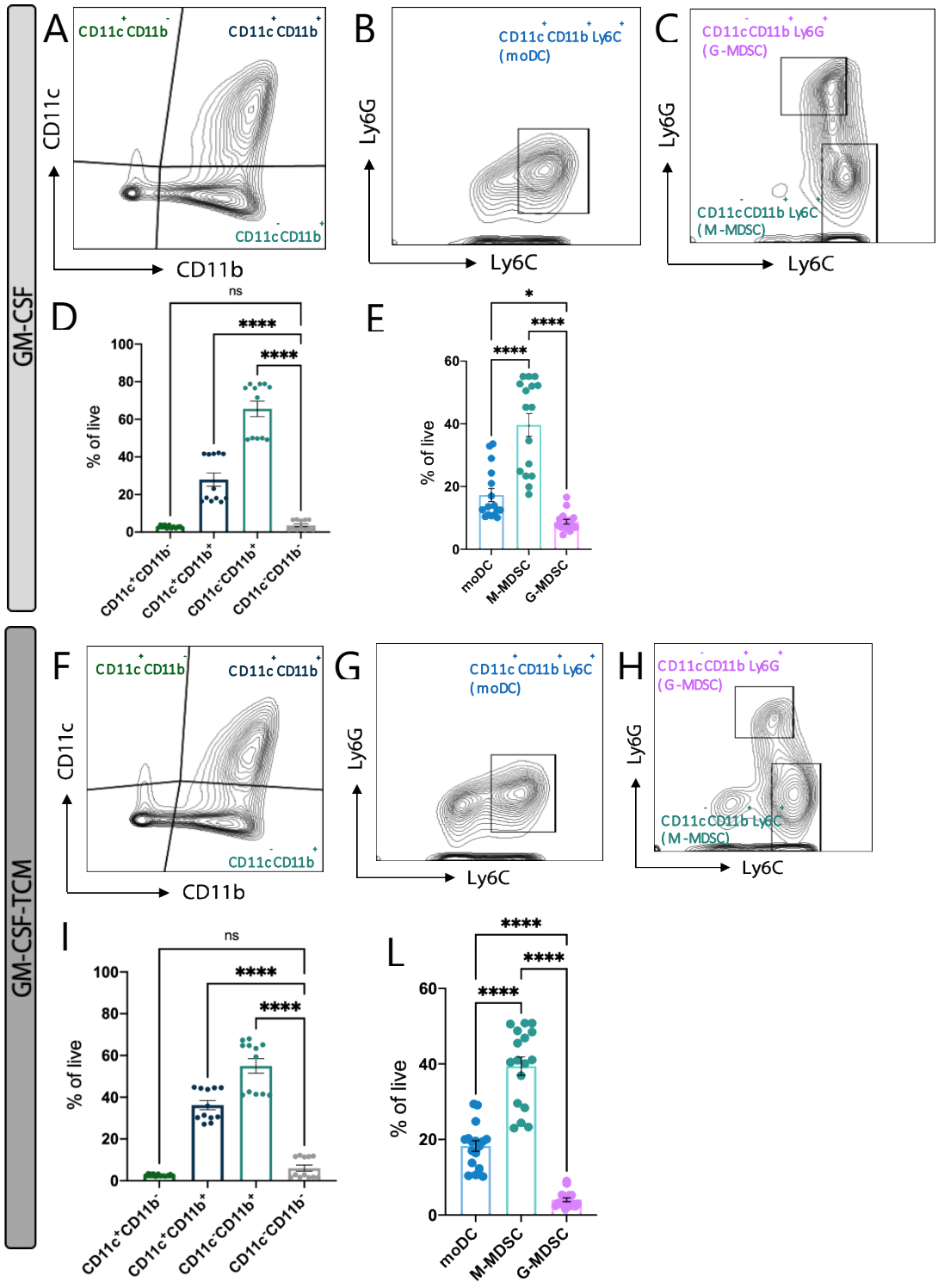

Figure 3.14. GM-CSF-TCM induces differentiation of SCA-1⁺ HSCs towards CD11b⁺CD11c⁺ phenotype. (A-F) Representative plots depicting distribution of CD11b and CD11c cells after 5 days of GM-CSF and GM-CSF-TCM cell culture. **(B-C and G-H)** Plots showing the moDC ($CD11c^+CD11b^+Ly6C^+$), M-MDSC ($CD11c^-CD11b^+Ly6C^+$) and G-MDSC ($CD11c^-CD11b^+Ly6g^+$) populations. **(D-E and I-L)** Quantification of myeloid populations after 5 days (percentage of live cells). Data are mean ± SEM; * = $p < 0.05$, ** = $p < 0.01$, *** = $p < 0.001$, **** = $p<0.0001$ using

one-way ANOVA with a Dunnett and Tukey's multiple comparison post hoc test. Assay n=2 for GM-CSF and n=2 for GM-CSF-TCM for eight independent experiments.

Directly comparing each population grown either in GM-CSF or GM-CSF-TCM, we observed an increasing trend for $CD11c^{+}CD11b^{-}$ (cDC1) and $CD11c^{+}CD11b^{+}$ (cDC2 and moDC) (figure 3.15 A-B), but there was a 10% reduction in GM-CSF-TCM $CD11c^{-}CD11b^{+}$ cluster that contains G-MDSC and M-MDSC (figure 3.15 C).

moDCs formed the majority of the $CD11c^{+}CD11b^{+}$ cluster but didn't change in presence of GM-CSF-TCM (figure 3.15 D), neither did the M-MDSCs resulted to cover around the 40% of the $CD11b^{-}CD11b^{+}$ (figure 3.15 E). However, a significant reduction in G-MDSCs was detected following TCM, explaining why we could see a reduction in the percentage of $CD11b^{-}CD11b^{+}$ cluster (figure 3.15 F). Since granulocytes are fast inflammatory cells, this effect we saw could mean that the GM-CSF-TCM would dampen the more reactive G-MDSC described in the literature[698], to further select the highly suppressive G-MDSC.

Having observed similar proportions of moDCs and M-MDSCs after TCM treatment, the key question then was to identify if TCM could drive any functional changes in the cells and enhance their suppressive nature. To test this, we tested the capacity of the in vitro myeloid cells to suppress T cell proliferation (as described earlier). From the HSC differentiated cultures, $Ly6C^{+}$ cells were isolated by MACS and co-cultured with T cells. These cells were therefore a mixed population of M-MDSCs and moDCs.

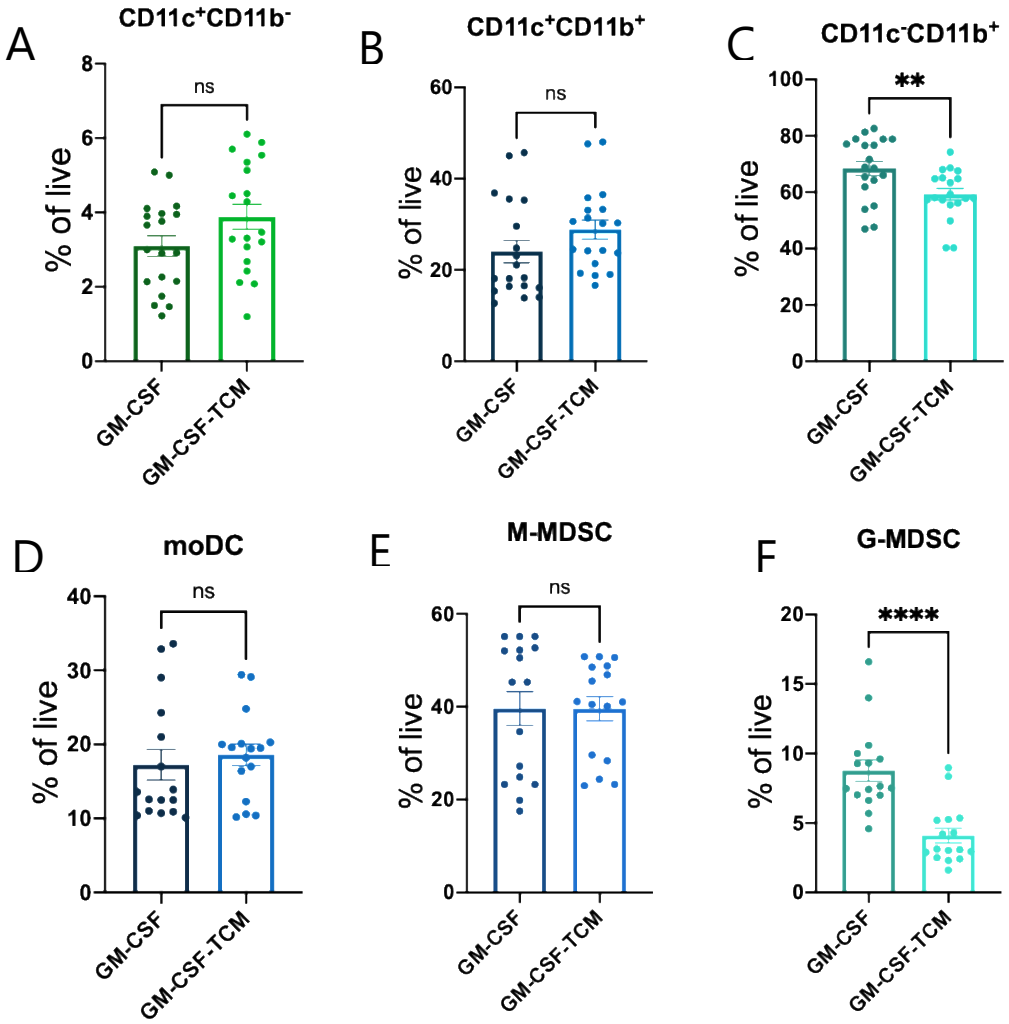

Figure 3.15. TCM induces a decrease in G-MDSC in vitro. Quantification of **(A)** CD11c^{+}CD11b^{-}, **(B)** CD11c^{+}CD11b^{+} and **(C)** CD11c^{+}CD11b^{-} myeloid clusters after treatment with GM-CSF or GM-CSF-TCM. Quantification of **(D)** moDC, **(E)** M-MDSC and **(F)** G-MDSC cells after treatment. The data shown in this figure a different visualisation of the figure 3.14 to highlight differences between GM-CSF and GM-CSF-TCM grown cells. Data are mean ± SEM; * = $p < 0.05$, ** = $p < 0.01$, *** = $p < 0.001$, **** = $p<0.0001$ using unpaired t test. Assay n=2 for GM-CSF and n=2 for GM-CSF-TCM for eight independent experiments.

3.4.4 TCM induced ly6C^{+} cells suppressed T cells proliferation in vitro

To measure the suppressive capacity of the different myeloid populations in vitro, we isolated the Ly6C^{+} population from the differentiated HSC cell culture. The process of extraction generated three different samples the Ly6G^{-}Ly6C^{-}, the Ly6G^{+}Ly6C^{int} and the Ly6G^{-}Ly6C^{+} population (figure 3.16 A-C), but as G-MDSCs, weren't the focus of this work, these cells were excluded from analysis by positively selecting for Ly6C highly expressing cells.

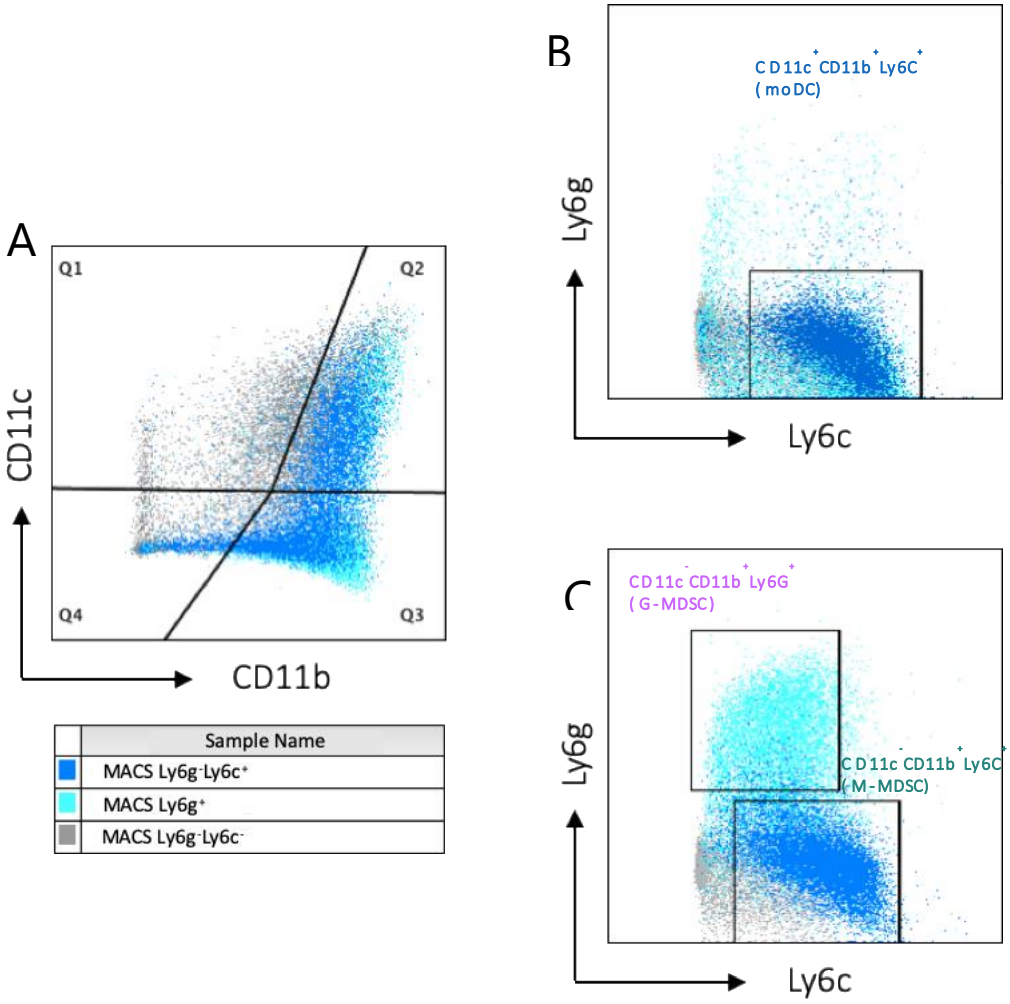

Figure 3.16. In vitro generated myeloid cells can be separated into moDCs, M-MDSC and G-MDSC populations. After five days cells culture Ly6C cells were isolated to be used in further experiments. Dark blue identifies the Ly6C$^+$ cells that were used for the in vitro experiments. Light blue identifies the depleted Ly6G cells and in grey the double negative cells. **(A)** Representative gating of CD11b and CD11c populations and **(B-C)**, expression of Ly6G and Ly6C within Q2 **(B)** and Q3 **(C)** to identify the moDCs, M-MDSC and G-MDSC populations.

With the Ly6C$^+$ cells purified from the in vitro cultures, a T cell proliferation assay was used to determine whether the different culture conditions drive changes in the immunosuppressive capacity of isolated cells. Based on the myeloid suppressor cells origin described in literature we supposed that the biochemistry of the TCM would induce a stronger suppressive phenotype when compared to the cells grown in the GM-CSF only. T cells were extracted and activated as described earlier and mixed with the MACS isolated Ly6C$^+$ cells from the GM-CSF or GM-CSF-TCM cultures. The experiment was incubated in the respective media where they were grown and incubated for two days. Then, the proliferation of CD4 and CD8 T cells was analysed.

CD11c CD11b Ly6C$^+$
(M-MDSC)

It was clear from the CFSE levels proliferation charts that both CD4$^+$ and CD8$^+$ T cells proliferation were suppressed compared to T cell only controls (figure 3.16 A). Firstly, the CD11b$^+$Ly6C$^+$ cells were quantified as percentage of CD45$^+$ to assess how many live cells were actively contributing to the suppressive effect for both GM-CSF and GM-CSF-TCM cultures. The CD11b$^+$Ly6C$^+$ number was consistent throughout the several experiments covering around the 25% of CD45 cells for both cells isolated by the two cell cultures. This meant consistency when assessing the effect observed on the T cells (figure 3.16 B). Quantification of CD8$^+$ T cell proliferation showed that compared to a 90% proliferation observed in the control, 60% of T cells proliferated in response to CD11b$^+$Ly6C$^+$ GM-CSF compared to just 40% co-cultured in the presence of GM-CSF-TCM cells (figure 3.16 C). A similar effect was measured with CD4$^+$ T cells (figure3.16

D). These experiments showed that the myeloid cells derived from HSCs of our culture system developed the ability to suppress T cells, but MDSCs from TCM treated cultures showed a marked increase in suppressive potency. This confirms that tumours condition the myeloid cells to a more suppressive phenotype, a feature that we can recapitulate *in vitro*.

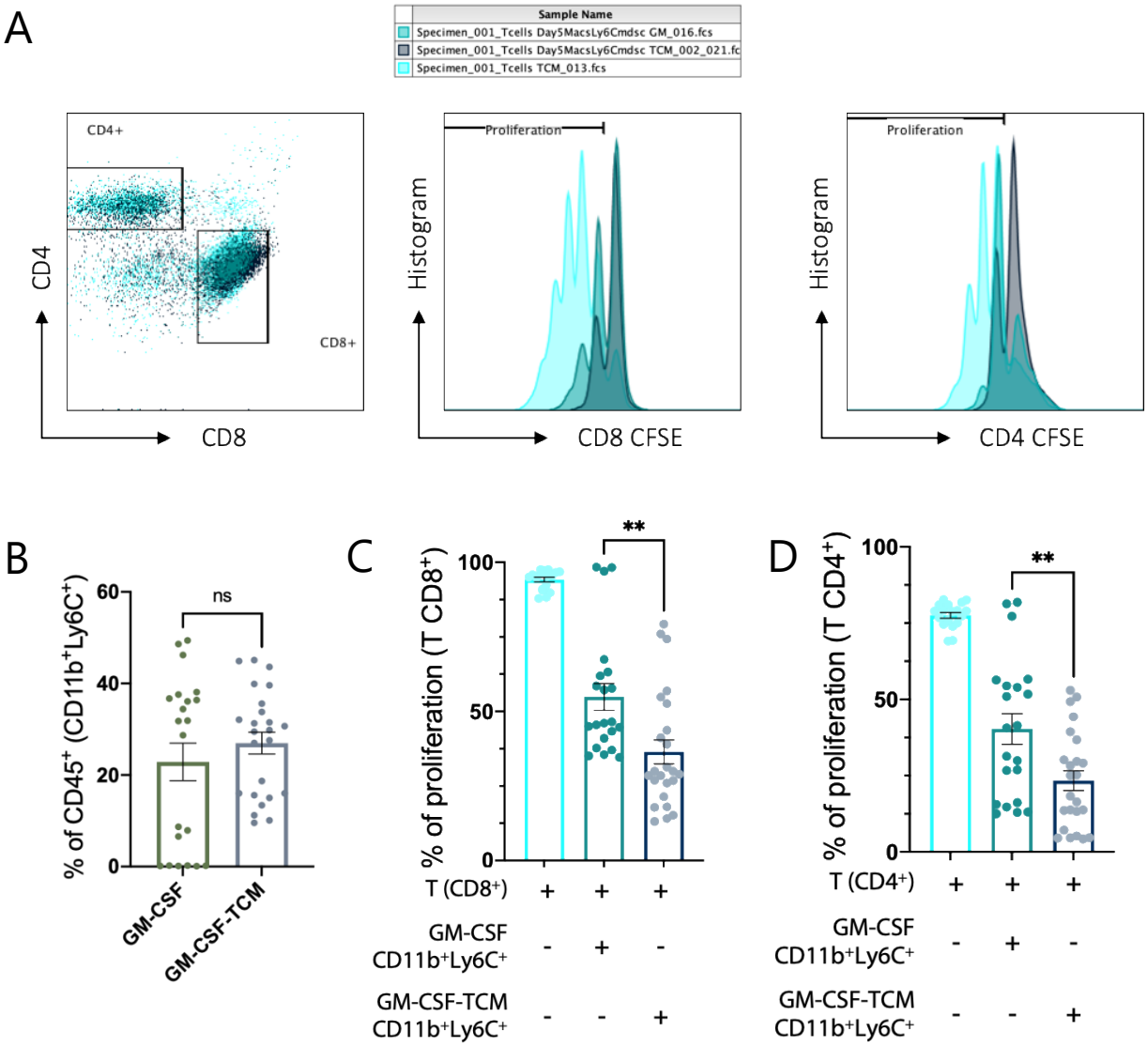

Figure 3.16. TCM-treated CD11b⁺Ly6C⁺ are more suppressive in vitro. (A) Representative FACs plots showing proliferation traces of the CD8⁺ or CD4⁺ in presence of the CD11b⁺Ly6C⁺ compared to T cells only control. T cell only light blue; GM-CSF mid blue; GM-CSF dark blue. **(B)** Quantification of live myeloid cells during the experiment. Quantification of **(C)** CD8 and **(D)** CD4 proliferation by GM-CSF or GM-CSF-TCM treated CD11b⁺Ly6C⁺ cells. (C-D) Data are mean ± SEM; * = $p < 0.05$, ** = $p < 0.01$, using ordinary one-way ANOVA with a Tukey's post hoc test. Experiments n=7 in triplicate.

3.5 TCM increases expression of immunomodulatory molecules

In the melanoma tumour microenvironment, immune cells are characterised by molecules involved in suppressive and inflammatory functions. At the beginning of this chapter we characterised the myeloid cells present in this niche for expression of molecules involved in immune escape.

Here we sought to explore if the in vitro myeloid derived cells grown in presence of GM-CSF and GM-CSF-TCM also expressed such molecules to mediate their suppressive effects. Based on the different potency in suppressing T cell proliferation, we supposed that the TCM grown cells would express more of these immunomodulators. MDSCs were grown with the methods described before and stained for their phenotype markers and additional suppressive molecules; SIRPα, PD-L1, FasL, VISTA, ARG1 and IDO.

Initially, to test if those molecules were indeed being expressed in the *in vitro* cell culture, we studied the expression levels of the molecules associated with immune suppression by measuring the gMFI on the GM-CSF-TCM grown moDCs and M-MDSCs. For both populations, SIRPα, PD-L1 and ARG1 were the most expressed molecules although signal levels were significantly higher in moDC gMFI when compared to the M-MDSCs (figure 3.17). FasL, IDO and VISTA were expressed at lower levels in both populations.

This showed that both myeloid population frequencies and patterns of immunosuppressive molecules expression were similar in both *in vivo* and *in vitro* conditions, thus *in vitro* could be used to model events *in vivo*. It should be noted that only Fasl was different, which could be a consequence of the absence of other type of cells in the surroundings.

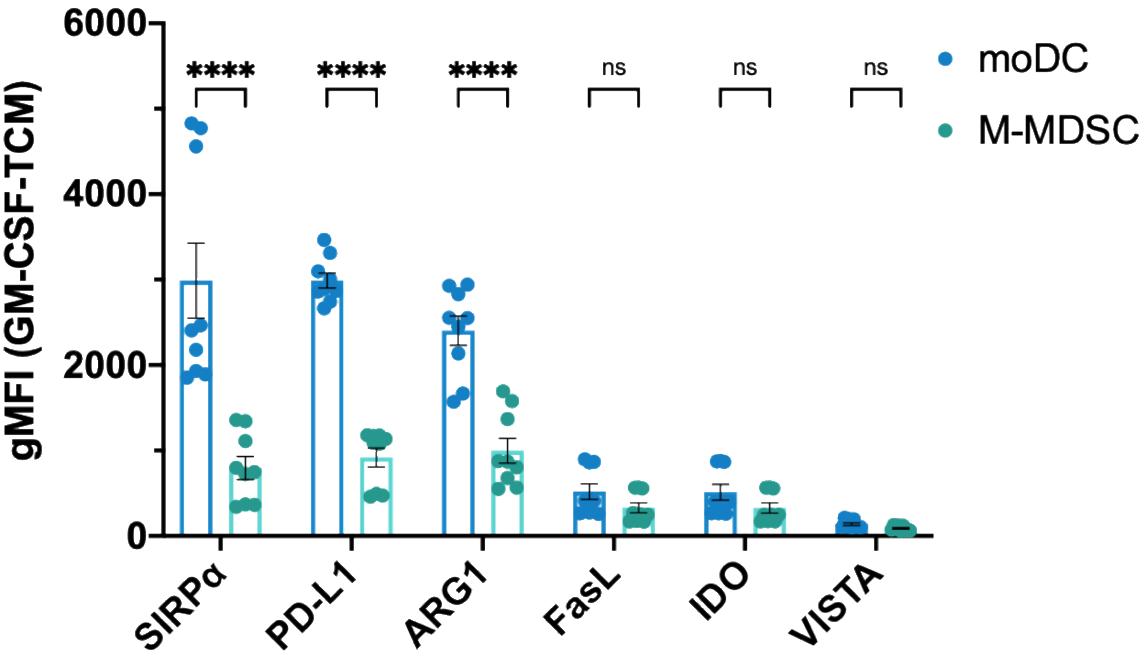

Figure 3.17. GM-CSF-TCM grown moDCs present higher level of expression of immune modulator molecules compared to M-MDSCs. (A) The moDC and M-MDSC cells grown for five days in contact with GM-CSF-TCM expressed SIRPα, PD-L1, FasL, VISTA, ARG1 and IDO. Data are mean ± SEM; * = $p < 0.05$, ** = $p < 0.01$, *** = $p < 0.001$, **** = $p<0.0001$ using 2-way ANOVA test with a Šidák's multiple comparison post hoc test. Experiments n=3 in triplicates.

When previously looking at the progression of immune modulator expression *in vivo* from day 5 to day 11, we assumed that a maturation of the M-MDSC towards moDCs was possible and hypothesised that tumour exudate could induce this progression.

We sought to verify if a similar pattern in the *in vitro* system following contact with GM-CSF-TCM. This was assessed by comparing the GM-CSF normalised expression profiles and percentage of marker positive between the two cell cultures. Interestingly, when comparing cells differentiated in presence of GM-CSF and GM-CSF-TCM, the latter showed an increasing trend of suppressive molecules expression as explained below.

Focusing first on moDC, SIRPα and PD-L1 expression were high (figure 3.17) and shared among all the cells (Appendix 8.3 A and B), but TCM treatment had no effect on the levels (figure 3.18 A and B). The T cell activator antagonist VISTA and FasL were significantly upregulated in the presence of the tumour condition media (figure 3.18 C and D) which increased also, both the percentage of positive cells of around 10% (appendix 8.3 C and D).

Other important MDSC suppressive mechanisms of the TME involve nutrient depletion, thus ARG1 and IDO were analysed. The latter is involved in the mechanism of tumour escape by reducing tryptophan and kynurenine production which effectively blocks T cell maturation in the TME. ARG1 instead reduces arginine that impairs T cells maturation. Contrary to expectation, IDO was reduced following exposure to TCM, whilst ARG1 showed a tendency to increase (figure 3.18 E and F), both didn't increase in percentage of positive cells which were respectively 50 and 60% (appendix 8.3 E and F).

Collectively, moDCs were characterised by a high expression of SIRPα and PD-L1, indicating they were prone to be affected by the "do not eat me signal" and that they would strongly engage PD1 to inhibit T cells inflammation. The TCM didn't seem to have a significant effect on the molecules involved in nutrient depletion but it did increase the expression of FasL and VISTA. That suggested the moDCs were already matured myeloid suppressive cells.

CD11c^{+}CD11b^{+}Ly6C^{+} (moDC)

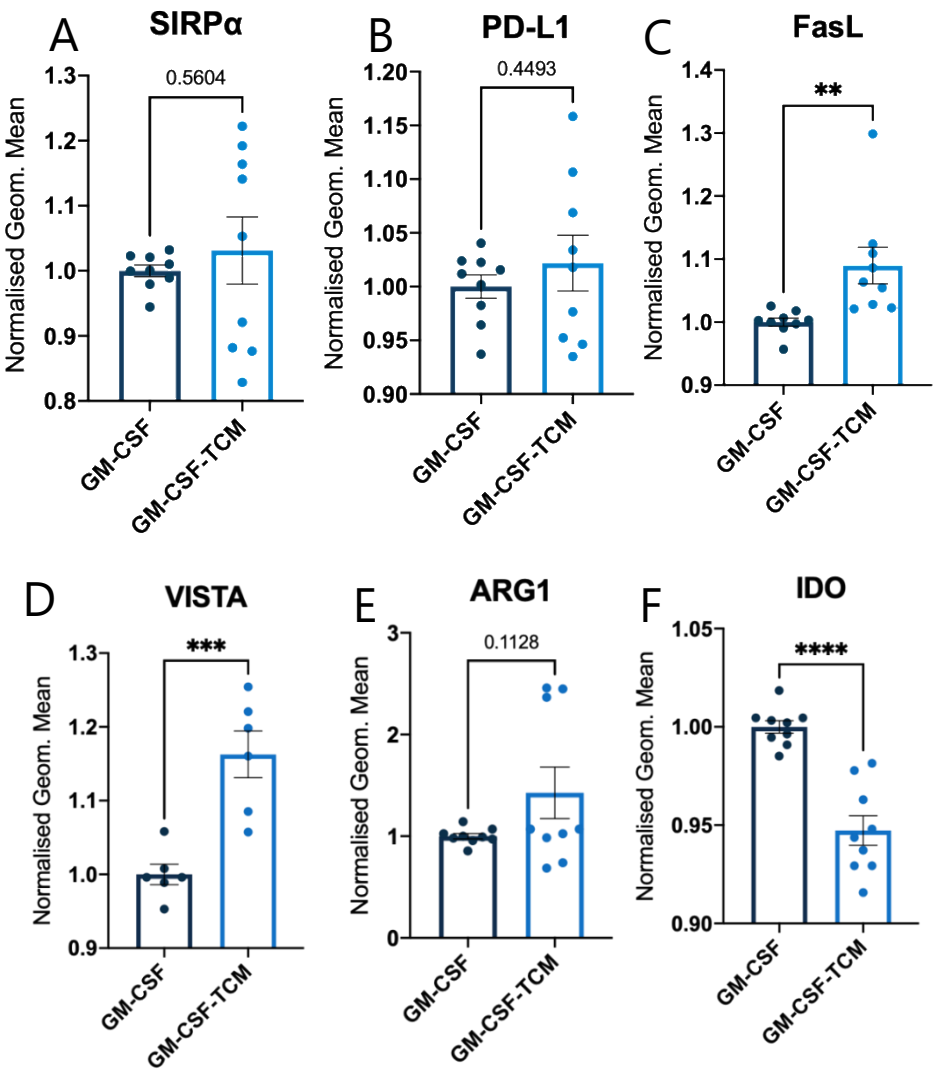

Figure 3.18. Modulation of suppressive molecules expression in moDCs ($CD11c^+CD11b^+Ly6C^+$) by GM-CSF-TCM. Flow cytometric quantification of the expression levels (geometric mean) of moDCs cultured in GM-CSF vs GM-CSF-TCM for **(A)** signal-regulatory protein alpha, SIRPα, **(B)** programmed death-ligand 1, PD-L1, **(C)** type-II transmembrane protein Fas Ligand, **(D)** V-domain Ig suppressor of T cell activation VISTA, **(E)** arginase 1, ARG1 and **(F)** indoleamine 2,3-dioxygenase, IDO. Data normalised by GM-CSF samples and are mean ± SEM; * = $p < 0.05$, ** = $p < 0.01$, *** = $p < 0.001$, **** = $p<0.0001$ using unpaired t test. Experiments n=3 in triplicates.

We then examined the suppressive repertoire on *in vitro* generated M-MDSC. *In vivo* data implied that the M-MDSCs were less differentiated than the moDCs cells because of lower levels of suppressive molecules expressed. *In vitro* following GM-CSF-TCM exposure, the M-MDSCs were 100% $SIRP\alpha^+$, $PD\text{-}L1^+$ and 35% $ARG1^+$ (appendix 8.4 A-B and E) however, the gMFI was lower than seen on moDCs (Figure 3.17), Consistent with this notion, when focusing on the effects of GM-CSF alone or with TCM on M-MDSCs, a significant increase in SIRPα and PD-L1 was detected (figure 3.19 A and B) when in presence of TCM unlike moDC, indicating a greater sensitivity of M-MDSC to TCM.

The increase in SIRPα and PD-L1 receptors has the potential to render them more suppressive by impairing phagocytic function and altered T cell signaling. VISTA, also a negative T cell regulatior, was upregulated by the TCM, it incresed the relative gMFI (figure 3.19 D) and percentage of positive (appendix 8.4 D), but its expression was far less than PDL1 (figure 3.17). FasL gMFI of M-MDSC wasn't presenting increase in contrast to moDC (figure 3.19 C), but the percentage of positive cells augmented in

presence of TCM (appendix 8.4 C) suggesting that *in vitro*, this axis may create a disadvantageous environemnt for the survival of T cells. ARG1 levels increased (figure 3.19 E) and the percentage of positive remained the same (appendix 8.4 E), no differences were detected in the case of IDO (figure 3.19 F).

While M-MDSCs expressed lower levels of suppressive molecules compared to the examined moDCs, they were influenced more by the contact with TCM, boosting the expression of suppressive mediators becoming effectively closer to the levels detected on the moDC. Together, these data suggest that although some of the immunosuppressive signatures in the moDCs and M-MDSCs (based on markers of suppression) vary slightly between the *in vitro* and *in vivo* situations, the in vitro model mimics the myeloid compartment in melanoma, and can be used to study the behaviour of myeloid cells. Moreover, data indicate that M-MDSCs could be a precursor of moDC cells.

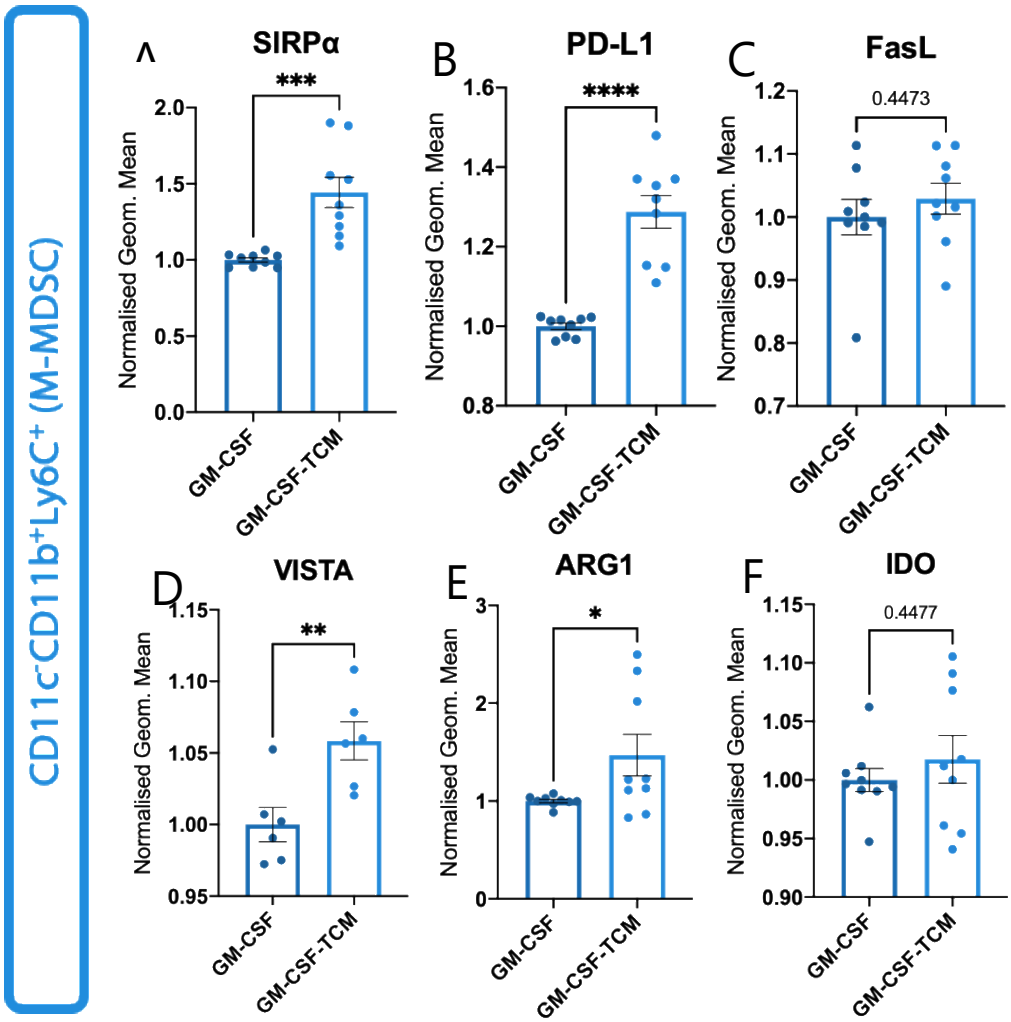

Figure 3.19. Modulation of suppressive molecules expression in M-MDSCs (CD11c$^-$CD11b$^+$Ly6C$^+$) by GM-CSF-TCM. Flow cytometric quantification of the expression levels (geometric mean) of M-MDSCs cultured in GM-CSF vs GM-CSF-TCM for **(A)** signal-regulatory protein alpha, SIRPα, **(B)** programmed death-ligand 1, PD-L1, **(C)** type-II transmembrane protein Fas Ligand, **(D)** V-domain Ig suppressor of T cell activation, VISTA, **(E)** arginase 1, ARG1 and **(F)** indoleamine 2,3-dioxygenase, IDO. Data are mean ± SEM; * = $p < 0.05$, ** = $p < 0.01$, *** = $p < 0.001$, **** = $p<0.0001$ using unpaired t test. Experiments n=3 in triplicates.

3.6 Summary

Here we performed an initial analysis of myeloid derived suppressor populations at different points of murine melanoma tumour growth. We observed a gradual increase in CD11b$^+$ cells as tumours established , and within this population Ly6C$^+$ cells were

the most represented, indicating the infiltration of monocytic myeloid cells, particularly moDCs and M-MDSCs[463]. Within the remodelling environment, SIRPα expression remained stable at the time points examined and thus used as a reliable marker to distinguish monocytic-DCs ($CD11c^+CD11b^+Ly6c^+SIRP\alpha^+$) from Monocytic-MDSCs ($CD11c^-CD11b^+Ly6C^+SIRP\alpha^+$) consistent with the nomenclature defined in the literature[699,405,322] . Ex vivo proliferation assays confirmed both M-MDSC and moDC suppressive capacity towards T cell proliferation, and function as myeloid derived suppressor cells. Examination of suppressive mediators supported the notion of a switch to immune suppression, and indicated that enhanced suppression observed in MDSC of established tumours may be mediated via PD-L1[684,700,433], FASL as previously reported[277, 701]. The presence of Arginase1 and IDO imply that the $Ly6C^+$ may also exert their suppressive actions via nutrient depletion and production of toxic molecules[702, 703, 469, 704].

It should be noted however, that we experinced diffculties with *in vivo* cells isolation, and after optimization, MACS technology resulted in the best viability but couldn't distinguish between the two populations. Neverthless, based on the immune modulator marker expression detected *in vivo*, the M-MDSC were less specialised moDCs. The latter expressed an higher concentration of the molecules involved in immunoescape compared to the M-MDSCs but by day 11, their numbers and expression levels increased to similar levels. As, M-MDSCs and moDCs may be part of the same family resulting[705,706,707] in the same TME effect, we must continue to study both.

Indeed, to better study MDSCs cells we created an *in vitro* system. Haematopoietic stem cells extracted from the bone marrow were matured to myeloid cells by contact with GM-CSF, as a first stimuli, and TCM to better simulate melanoma-derived cues. This cell culture generated mature myeloid cells, dominated by $Ly6C^+$ cells which expressed similar molecules, pattern of expression detected in the TME and T cell

suppressive functions. Exposure to TCM drove a decrease of $CD11c^{-}CD11b^{+}$ and an increase in $CD11c^{+}CD11b^{+}$ cells. However, while the proportion of $Ly6C^{+}$ subpopulations weren't significantly different, cells exposed to TCM exhibited more potent suppression of both CD4 and CD8 T cell proliferation, indicating an effect of TCM on functional rather than differentiation status. In line with this, baseline levels of suppressive mediators were lower in M-MDSC, but these cells were more highly responsive to TCM, upregulating PD-L1, SIRPα, VISTA and ARG1. Thus, our *in vitro* system, successfully and reliably generated functional MDSCs to be used in further studies, which resembled *in vivo* phenotypes and were plastic towards tumour derived cues.

Critically, SIRPα, which was used to identify moDC and M-MDSCs also plays a key role in their function. When activated by the CD47 ligand, SIRPα suppresses phagocytosis in the antigen presenting cells[476, 476]. Reports have suggested that once this path is triggered the reduction on phagocytosis is accompanied by inhibition of their inflammatory activities[708,638]. Thus, is it possible that this axis is key to the effects we have observed. Its role in MDSC function and potential as a therapeutic target will be investigated in the next chapters.

CHAPTER 4

CD47 INDUCES AN IMMUNOSUPPRESSIVE PHENOTYPE IN MYELOID CELLS

4.1 Introduction

In the previous chapter we saw that myeloid suppressor cells were present in the melanoma TME, and were enriched for Ly6C-expressing cells as tumour developed. Ly6C expression was spread between M-MDSC and moDCs, indicating that both may be part of the same family. This was supported by the fact that the expression of molecules involved in suppression was higher in moDCs than M-MDSC. This was recapitulated in vitro, where data showed that M-MDSC, when immersed in tumour condition media became more like moDCs. The difference between these two clusters resided in the level of CD11c which, as seen in HSC maturation, developed in response to molecular cues present in the media. Indeed, CD11b and Ly6C expressing cells were able to suppress the T cell proliferation, and contact with TCM induced a similar myeloid phenotype to indicate that both clusters were related. Similarly in human monocyte cultures, grown in the presence of GM-CSF, IL-4 and IL-10 for seven days generated a mix of moDCs and M-MDSC, and one affected the maturation and suppressive capacity of the other[709]. Thus, it is likely that depending on local cues, M-MDSC and moDC cell phenotype and functions would also interchange *in vivo*, based on their plastic nature.

Both moDCs and M-MDSC showed the expression of common immune modulators, PD-L1 and SIRPα. The SIRPα receptor has been associated with the regulation of dendritic cell homeostasis in lymphoid organs[710], the spleen and the bone marrow[711]. It is a common phenotypical denominator in several myeloid families and was demonstrated to be spread across our defined cDC2, moDC and M-MDSC. The ligand of SIRPα is the signal regulatory protein CD47, and their interaction was established to prevent phagocytosis of RBCs or platelets by macrophages[712,713,714]. Hence, it is part of the so called "do not eat me signal" repertoire that controls the clearance of old cells or non-self-antigen presenting cells[715]. The SIRPα-CD47 axes has been reported to

contribute to tumour development and drug resistance by inhibition of phagocyte-dependent clearance[716]. Therapeutic blockade of CD47 lead to an activation of an anti-tumour cytotoxic T lymphocyte (CTL) responses. This effect was dependent on DCs but not by macrophage in cross-priming T cell responses [717].

Thus, the SIRPα-CD47 interaction may serve as one of the 'persistent signals' underlying the regulation of myeloid development and function in the TME. Because of its implication in dendritic cell maintenance and impact on phagocytosis of antigen presenting cells we hypothesized that SIRPα-CD47 interactions represent an alternate immune modulatory signalling axis within the TME, regulating the suppressive phenotype that characterises M-MDSC and moDC cells. In the following chapter we sought to characterize CD47 expression in the TME and determine its functional impact on myeloid cells.

4.1.2 Widespread CD47 expression, but myeloid restricted SIRPα within the TME.

ScRNAseq data previously generated in our laboratory characterised cell populations composing the microenvironment and tumour draining lymph node (TDLN) of B16-F10 tumours[651] (figure 4.1 A). The analysis was made with the methods described in the just aforementioned paper. To give a brief explanation, the tSNE plot and Principal Component Analysis (PCA) are unsupervised non-linear dimensionality reduction and data visualization techniques which use different mathematical methods to graphically plot the overall relatedness of several data stores. The strongest signal is picked up and weighted by sets of probes which best separate the data in Principal Components (PCs). Those can be plot against each other to obtain a view of clusters that shares signal similarities between PCs. Also, the tSNE method is a dimensionally reduction technique to simplify the view of large data set. It differs from the PCA because it

produces a 2D separation reducing the number of components forming the clusters and it is also non-deterministic meaning that every time is run will create a probabilistic distribution, hence won't create always an equal output but similar. This is an advantage with non-linear signals like the one generated by mRNA sequencing, the outliers tend to have a smaller effect on the final analysis and separation between relevant groups is improved (https://www.bioinformatics.babraham.ac.uk).

Here, phagocytes and dendritic cells were identified by Itgam (CD11b) and Itgax (CD11c) markers respectively. Within these clusters, a complex myeloid landscape was evident, with adgre1 (F4/80)-expressing macrophage observed in concomitancy with Ly6G and Ly6C positive cells, possibly neutrophils and monocytes. Furthermore, the dendritic cells were clustered into cDC1 (Clec9a, Tlr3, Tlr11, Ly75, and XCR1), cDC2 (CD11b, Fcγr1 and SIRPα) and pDCs (Bst2 and SiglecH). This characterisation, based on mRNA expression strongly correlated observations at the protein level in the current project.

A great work using single cells sequencing indeed, depicted the complicated scenery of the myeloid composing the lung TME. An unbiased comparison between the human and mouse samples uncovered more than 25 states of the tumour-infiltrating myeloid cells (TIMs). These were reproducible between patients and across species identifying a near-complete congruence of population structures among dendritic cells and monocytes, conserved neutrophil subsets, and species differences among macrophages[718]. The pathological relevance of all these distinct subsets will certainly improve our understanding of the TIMs.

Thus, having shown that Ly6C expressing cells functionally suppressed T cells, we exploited the consistency between studies to interrogate the distribution of immune modulatory molecules across myeloid populations in more detail. With the observation that SIRPα was a common denominator between cDC2, moDC and M-MDSC and with roles in myeloid cell homeostasis and ability to exert phagocytic and

cross-presentation functions, we focused on the pattern of expression of the CD47-SIRPα axis. Single cell data was reanalysed for the presence of CD47 ligand and SIRPα receptor[474]. This highlighted the widespread expression of CD47 ligand across all cell types in the TME (figure 4.1 B and D). In contrast, the distribution of SIRPα was much more restricted, with expression limited to myeloid cells, and lymphatic and CAF subpopulations (also reported to scavenge and cross-present antigen[74,719]) (figure 4.1 C and E). With these patterns of expression, it indicates that CD47 presence isn't purely a mechanism by which tumour cells evade clearance, but a persistent anti-phagocytic, inhibitory signal from across the TME which could affect the homeostasis of the myeloid towards suppression.

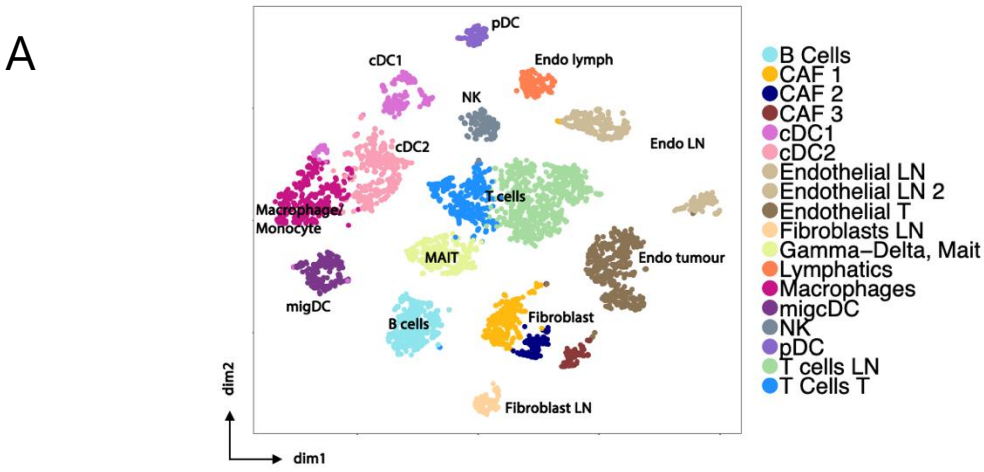
A
pDC
cDC1
Endo lymph
NK
Endo LN
cDC2
T cells
Macrophage/
Monocyte
MAIT
Endo tumour
migDC
B cells
Fibroblast
Fibroblast LN
dim2
dim1
B Cells
CAF 1
CAF 2
CAF 3
cDC1
cDC2
Endothelial LN
Endothelial LN 2
Endothelial T
Fibroblasts LN
Gamma–Delta, Mait
Lymphatics
Macrophages
migcDC
NK
pDC
T cells LN
T Cells T

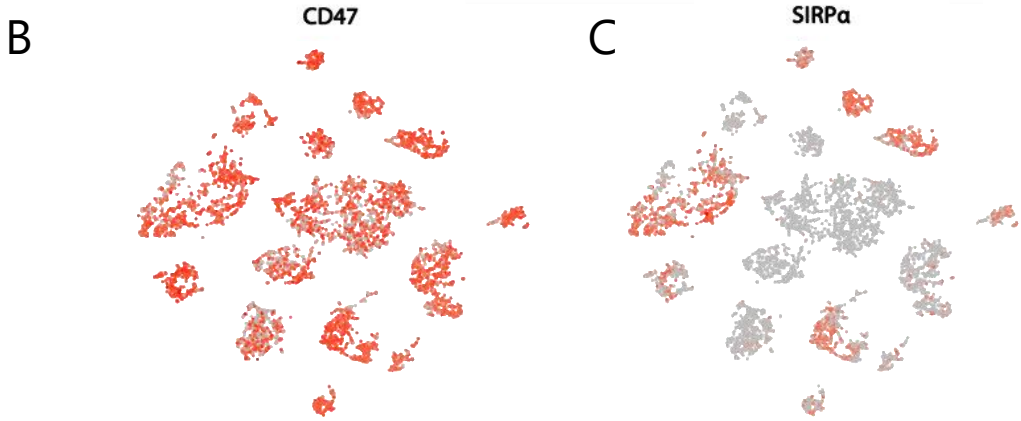
B
CD47
C
SIRPα

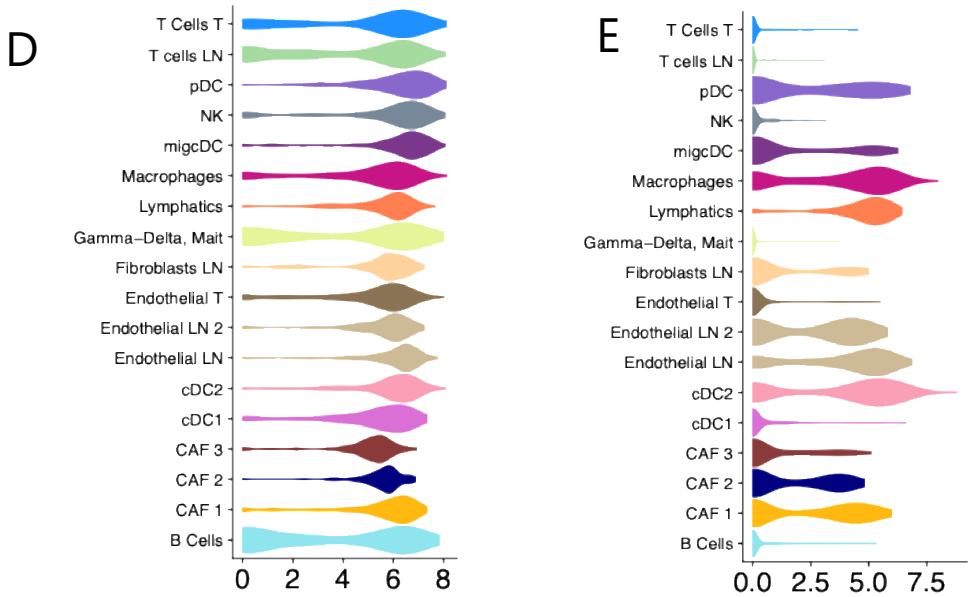
D
T Cells T
T cells LN
pDC
NK
migcDC
Macrophages
Lymphatics
Gamma–Delta, Mait
Fibroblasts LN
Endothelial T
Endothelial LN 2
Endothelial LN
cDC2
cDC1
CAF 3
CAF 2
CAF 1
B Cells
0 2 4 6 8
E
T Cells T
T cells LN
pDC
NK
migcDC
Macrophages
Lymphatics
Gamma–Delta, Mait
Fibroblasts LN
Endothelial T
Endothelial LN 2
Endothelial LN
cDC2
cDC1
CAF 3
CAF 2
CAF 1
B Cells
0.0 2.5 5.0 7.5

Figure 4.1. Opposing distribution of CD47 and SIRPα across components of the TME. (A) tSNE plots generated by Sarah Davidson, display all populations isolated from B16 melanoma (4627 cells) and lymph nodes (LN), coloured according to their cell type **(B-C)** tSNE plots showing the expression of CD47 and SIRPα. **(D-E)** Violin plots showing the expression of CD47 and SIRPα in each TME cell population.

We next confirmed CD47 expression patterns in day 11 tumours at the protein level using general markers to identify immune cells (CD45), endothelial (CD31) and fibroblast (Pdgfrα, Pdgfrβ and Thy1). The immune cells were also stained for CD11b, CD4 and CD8 with an antibody cocktail due to panel restrictions. However, as Thy1 is also expressed by T cells[720], this allowed us to distinguish lymphoid from CD11b positive myeloid cells.

To better visualise the distribution of the markers at the protein level, we utilized the tSNE analysis plugin in Flowjo, which applies the same principles used for single cell RNA sequencing to cluster cells based on gMFI. The software shows the median expression comparing the signal between each live cell and visualises by a range of colours, blue indicated low expression, green basal expression and yellow-red high expression. This type of visualisation gave a defined idea of how a protein was expressed between all the live cells in a sample without any gating. $CD45^+$ cells were dominant (figure 4.2 A); this was likely a consequence of tumour cell death after processing and staining. Within $CD45^+$ clusters, myeloid cells identified by CD11b were the major group while the other were T cells (figure 4.2 B and C), identified by the co-expression of Thy1 (figure 4.2 C). Consistent with RNA data, CD47 was widespread across clusters composing the TME (figure 4.2 D).

Levels of CD47 expression were then quantified in the different clusters as described above, with the addition of lineage negative cells considered as tumour cells. The CD45 positive cells were gated and $CD11b^+CD4^+CD8^+$ analysed by the expression of Thy1 to distinguish the T cells from the CD11b cells. This allowed to quantify CD47 expression on these two immune cells populations. The CD45 negative cells were separated by CD31 positive and negative expression. The $CD31^+$ were endothelial cells. Then $CD45^-$

CD31$^-$ double negative cells but positive for Pdgfrα, Pdgfrβ and Thy1 identified as two families of fibroblasts. Finally, the lineage negative cells were considered tumour cells. The gating made in this manner allowed us to quantify the CD47 expression by the single clusters. However, while RNA showed diffuse expression across populations, the protein levels expressed varied. CD47 wasn't expressed by endothelial and the fibroblast-Thy1$^-$ cells while tumour and myeloid cells expressed it lowly and fibroblast-Thy1$^+$ and T cells expressed it at higher level (figure 4.2 E).

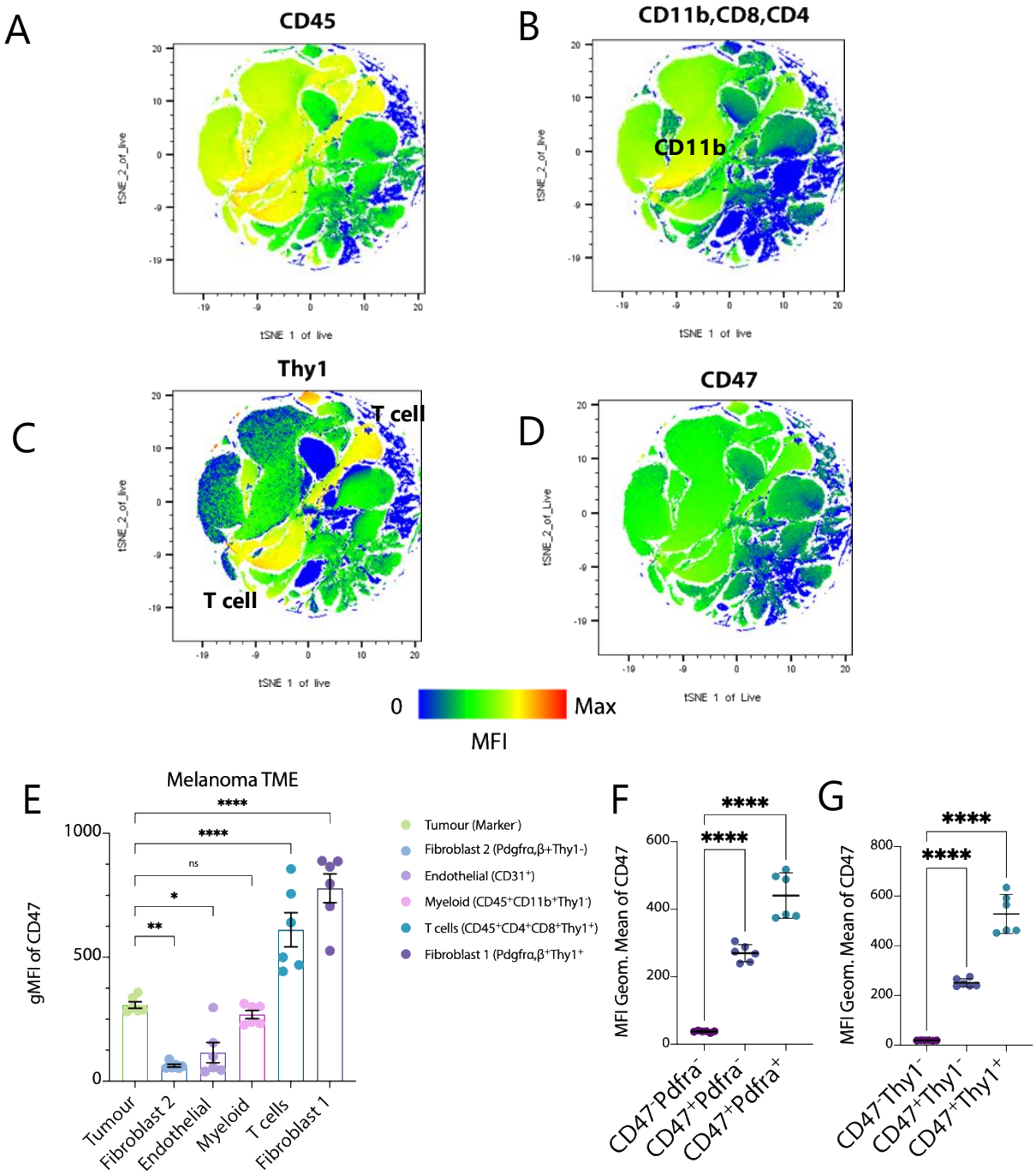

Figure 4.2. CD47 protein is widespread across constituents of the TME. Representative tSNE FACS plots obtained from B16-F10 melanoma TME populations highlighting **(A)** CD45, **(B)** CD11b, CD4, CD8 **(C)** Thy1 and **(D)** CD47. **(E)** Quantification of CD47 expression as MFI geometric mean of T ($CD45^+CD4^+CD8^+Thy1^+$), fibroblast 1 ($Pdgfr\alpha^+Pdgfr\beta^+Thy1^+$), fibroblast 2 ($Pdgfr\alpha^+Pdgfr\beta^+Thy1^-$), myeloid ($CD45^+CD11b^+Thy1^-$), endothelial ($CD31^+$) and tumour ($marker^-$) cells. **(F)**

Correlation between CD47 and Pdgfrα expression. **(G)** Correlation between CD47 and Thy1 expression. (E-G) Data are mean ± SEM; * = $p < 0.05$, ** = $p < 0.01$, *** = $p < 0.001$, **** = $p < 0.0001$ using ordinary one-way ANOVA with a Dunnett post hoc test. Assays mice=3 in two independent experiments.

Interestingly, CD47 expression levels correlated with Thy1 and Pdgfrα expression (figure 4.2 F and G) marking T cells and fibroblasts, and potentially, could be used as biomarkers to study the CD47 presence in the TME. Furthermore, CD47 expression by T cells in the TME was correlated with reduced type 1 immune responses and a suppressed phenotype[591]. The data may indicate that these populations have a key role in modulating myeloid phagocytic capacity and downstream immune function in remodelling the TME[721]. In this tumour set up, the lower expression by lin- tumour cells is important to note as could indicates that tumour cells may contribute less to the CD47-SIRPα engagement, with the major signals brought by CD47 instead coming from the tumour stromal cells, in particular T cells and fibroblasts. This indicates a potential role for stroma in immune modulation and function of SIRPα expressing myeloid populations, possibly via phagocytosis inhibition.

4.1.3 CD47 binding SIRPα enhances expression of immunosuppressive molecules in moDCs and M-MDSCs.

Looking at the inhibitory nature of the SIRPα-CD47 signalling and at the dynamic distribution in the TME we hypothesised that this signal persistency could further contribute in modulating the myeloid cells suppressive phenotype and function. Thus, to test if CD47 signalling indeed modulated myeloid cell function, we utilized our in vitro models described in chapter 3, which showed maturation of HSCs towards moDC and M-MDSC, and increased expression of suppressive molecules with TCM. We also used this approach to determine if the CD47 pathway further enhanced the suppressive effects of TCM.

After five days of HSC maturation towards myeloid cells in the presence of GM-CSF and GM-CSF-TCM, cells were then put in contact with a passively coated active CD47 plate and incubated two days. The CD47 active protein used was the ectodomain

fragment able to bind human SIRPα. Samples were then stained with the panel of markers used previously to characterise immunomodulators (SIRPα, PD-L1, VISTA, FasL, ARG1, IDO). Again, both the Ly6C positive moDC and M-MDSC populations were analysed.

In moDC, the 100% of cells expressed SIRPα (appendix 8.5 A) which wasn't affected by TCM, but addition of CD47 induced a slight increase (p value 0.05014) (figure 4.3 A). As discussed earlier, SIRPα was one of the molecules with the highest expression on the moDCs and it may have reached the highest possible expression on the cell surface, making impossible any further increase of the molecule and then, its detection.

T cells inhibitors PD-L1 and VISTA presented a clear increase upon CD47 stimuli. PD-L1, unaffected by TCM, was specifically upregulated following CD47 exposure (figure 4.3 B and C). But, being VISTA far less expressed, as we saw in figure 3.17, it may have a minor role in the regulation of T cells. Still, the gMFI levels further augmented in TCM-CD47 conditions compared to GM-CSF stimuli only (figure 4.3 C).

Similarly, FasL was increased upon CD47 stimulation compared with GM-CSF (figure 4.3 D) and passed from 30 to 50% of population expressing it (appendix 8.5 C). Interestingly, T cells expressing FasL have been reported to induce apoptosis in myeloid suppressive cells[687]. But our data suggested that possibly the moDCs could induce apoptosis of T cells presenting Fas.

In contrast to surface molecules, ARG1 expression was not significantly impacted by either TCM or TCM-CD47 (figure 4.3 E). This was not unexpected since moDCs had a subpopulation that constitutively expressed this molecule, thus to see further changes in ARG1 modulation different conditions may be required. IDO was less visible but while TCM did not impact its expression, an increase was observed in the presence of CD47 (figure 4.3 F) and the percentage of positive population passed from50 to 65%

(appendix 8.5 F). Like ARG1, its reliable detection may require different culture conditions with another type of cell to provide a substrate.

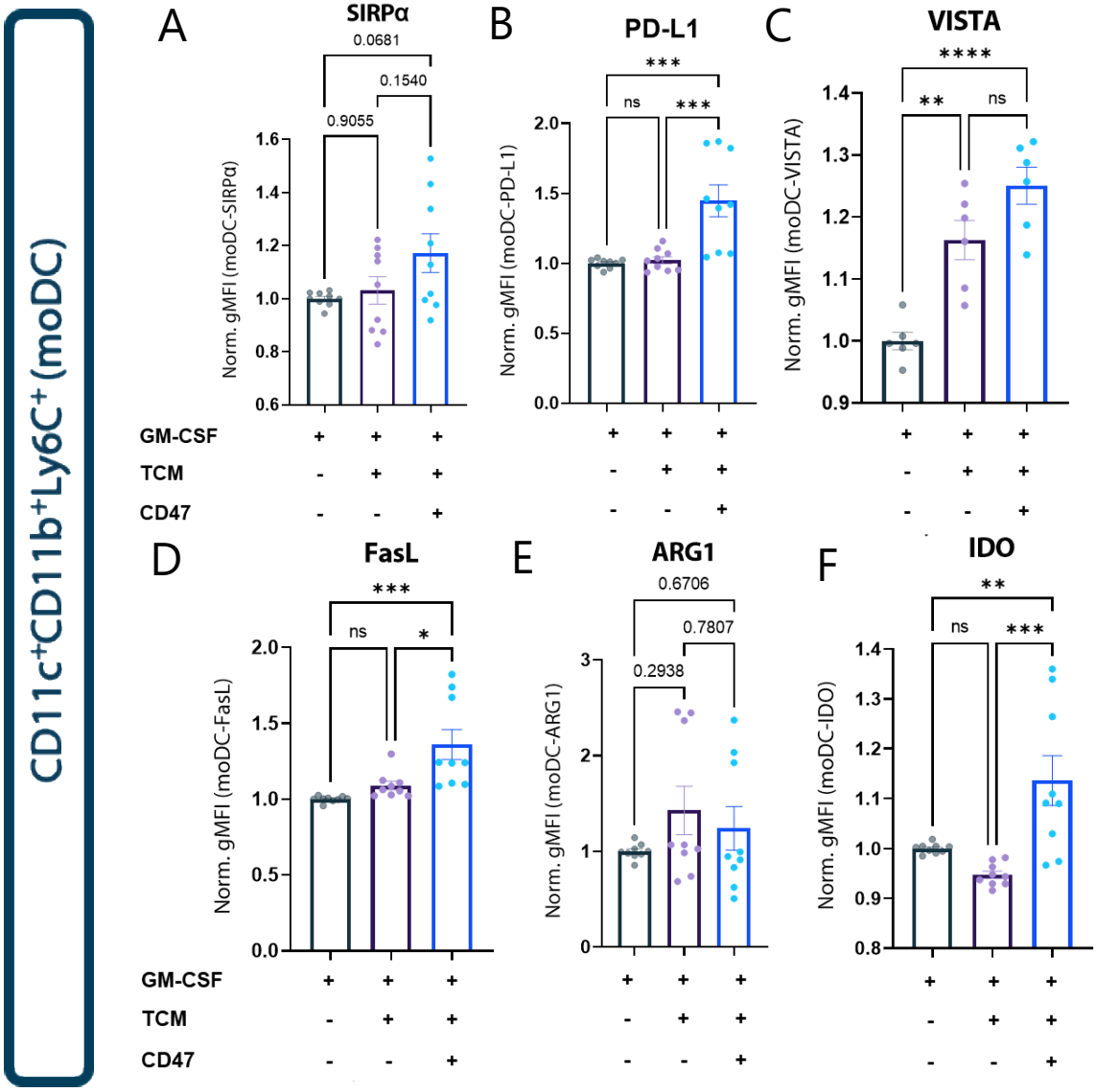

Figure 4.3. Expression of some immunosuppressive molecules by moDC increases or tend to increase in presence of the CD47 protein. The graphs show the effect of GM-CSF, GM-CSF-TCM and GM-CSF-TCM-CD47 on the moDC as MFI geometric mean of **(A)** SIRPα, **(B)** PD-L1, **(C)** VISTA, **(D)** FasL, **(E)** ARG1 and **(F)** IDO immune modulators. The data were normalised for the GM-CSF samples. (A to F) Data are mean ± SEM; * = $p < 0.05$, ** = $p < 0.01$, *** = $p < 0.001$, **** = $p<0.0001$ using ordinary one-way ANOVA with a Dunnett post hoc test. Assays n=3 in three independent experiments.

Thus, while TCM had limited impact on the moDC repertoires, engagement of these cells by CD47 active protein induced upregulation of specific molecules, consistent with an increasing suppressive phenotype. Interestingly, it is possible that engagement of SIRPα by CD47 increases its concentration, which may represent an autologous mechanism to block phagocytosis and inflammatory mechanisms associated with the myeloid cells.

In a similar manner, the M-MDSC were analysed. Previously, this population showed to express a lower level of the immune modulators tested when compared to moDCs (figure 3.17), but were also able to strongly suppress T cells. Despite the lesser baseline expression, they were susceptible to the influence of TCM, and increased immune modulator molecules when in its presence.

Addition of CD47 to the already strong effect of TCM further increased the expression of PD-L1, FasL and IDO. No further increases in SIRPα expression were detected (figure 4.4 A) in contrast to moDCs. As we saw in figure 3.17-chapter 3, the SIRPα level was lower in the M-MDSCs and we hypothesis that further suppressive engagement (for example CD47) could push their maturation towards moDCs, indicating that CD47-SIRPα may not regulate SIRPα expression in the M-MDSCs. The result wasn't in support, however, PD-L1, which was already greatly affected by the TCM and despite the entire population was positive (appendix 8.6 B), there was a clear tendency in further boost it by CD47 engagement, as reported for moDC which supports our hypothesis (figure 4.4 B). This indicates that for both cell types, PD-L1 could be principal interaction responsible for blockade of T cell proliferation.

FasL and IDO showed only a slight increase to CD47 engagement (figure 4.4 D and F) but the percentage of positive population was bigger, respectively from 20 to 30 and 40-50% (appendix 8.6 C and F) indicating the formation of more cells expressing those molecules. The 35% of positive cells expressed ARG1 (appendix 8.6 E), which showed

no further increase with TCM and CD47, likely as a consequence of the significant variability in detection (figure 4.4 E).

While VISTA significantly increased in moDC, changes for M-MDSC were marginal (figure 4.4 C). The ability to detect differences between conditions may be confounded firstly by the low level of expression found within myeloid populations (figure 3.17 – chapter 3), and secondly because VISTA is a pH-sensitive ligand[722] which could affect its conformation *in vitro*, where levels of acidity are counter balanced by the buffer present in the media.

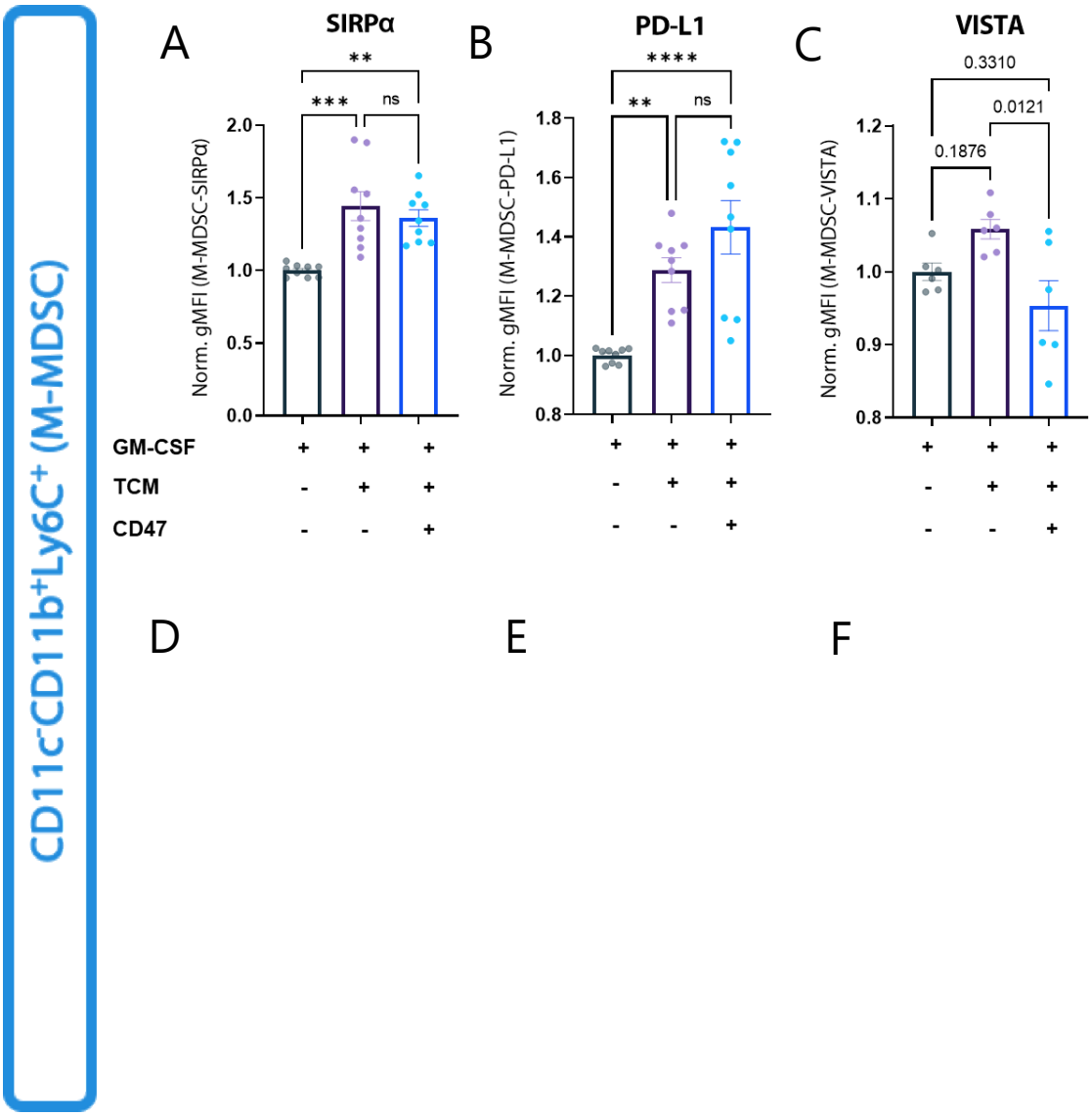

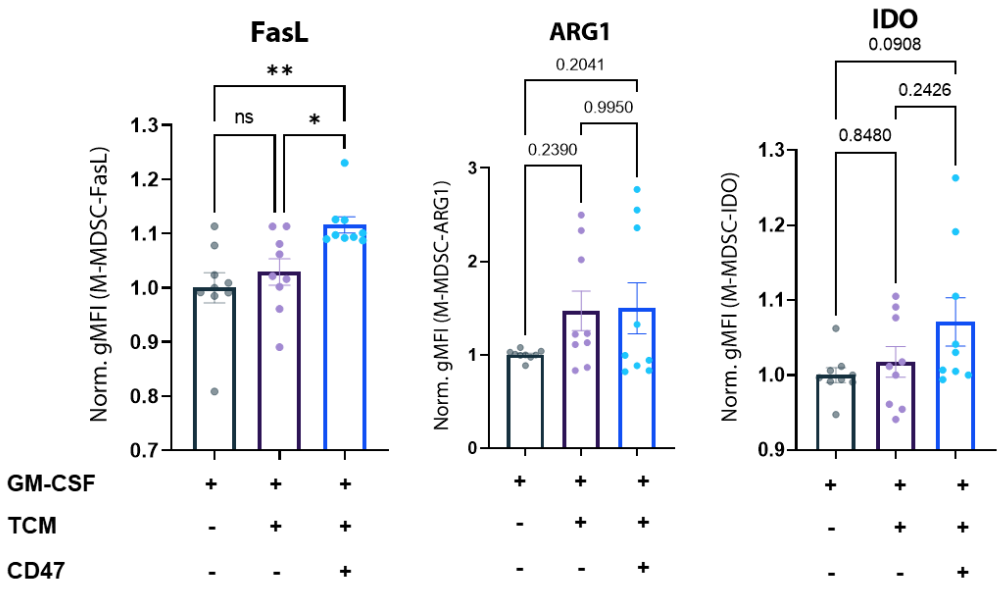

Figure 4.4. M-MDSC immunosuppressive molecules increase or tend to increase in response to CD47. The graphs show the effect of GM-CSF, GM-CSF-TCM and GM-CSF-TCM-CD47 on the M-MDSC cells as MFI geometric mean of **(A)** SIRPα, **(B)** PD-L1, **(C)** VISTA, **(D)** FasL, **(E)** ARG1 and **(F)** IDO immune modulators. The data were normalised for the GM-CSF samples. (A to F) Data are mean ± SEM; * = $p < 0.05$, ** = $p < 0.01$, *** = $p < 0.001$, **** = $p<0.0001$ using ordinary one-way ANOVA with a Dunnett post hoc test. Assays n=3 in three independent experiments.

Overall, the ly6C positive moDCs or M-MDSCs, matured a variety of molecules involved in mechanisms of immunosuppression. The addition of the persistent CD47 stimulus played a role in further increasing this expression. This depicted a possible role of CD47 in strengthening the suppressive molecular milieu of the myeloid derived suppressor cells. Thus, having verified how widespread the presence of CD47 in the TME was, and how this may impact the phenotype of stimulated cells, the question now was to determine if CD47-SIRPα engagement would translate in a stronger suppressive function.

4.4 Anti-SIRPα antibody blockade of CD47: A binding curve study.

We have seen that CD47 was able to induce an increase in molecules associated with immunosuppression, and that SIRPα expressing myeloids were in contact with a CD47-rich tumour microenvironment. Thus, we can think of them being mobilised from the bone marrow and arriving in the TME where they encounter this inhibitory "do not eat me signal". This interaction would engage the SIRPα expressing cells, reducing their activation and inducing an increase of the molecules involved in immunosuppression. This should translate in a stronger suppression of the T cells and failed immune clearance. However, if this axis indeed is in operation, how this would translate to impact their interaction with other cells and functional consequences needs to be assessed. To test this hypothesis, it would also be necessary to block the CD47-SIRPα.

CD47 has been a promising target for immunotherapy. Pre-clinical studies showed the efficacy of an anti-CD47 in combination with anti-HER2 antibody for the treatment of breast cancer[723], ovarian cancer[724] and on human non-Hodgkin lymphoma cells by the mechanism of antibody dependent cellular phagocytosis (ADPC) in vitro[627]. Based on these studies human clinical trials proceeded using CD47 antagonist antibodies. Those have been successful in affecting the tumour growth, however, gave severe side effects including anaemia. Functional RBCs tends to express high levels of CD47 to avoid opsonisation and recycling, but the antagonist antibodies affected this mechanism inducing an antibody-dependent cellular cytotoxicity (ADCC)[633]. In light of the off-target effects reported for CD47, and our observations of widespread distribution throughout the tumour we chose instead to disrupt the CD47-SIRPα interaction by targeting SIRPα.

To do this we utilized the Biolegend Ultra-LEAF™ anti-SIRPα (clone P84) antibody. As we mentioned in the introduction (section 1.7.4 in chapter 1) it had limited efficacy

with established tumours but was commercially available and accessible. Thus, we tried to optimise its concentration to obtain better results.

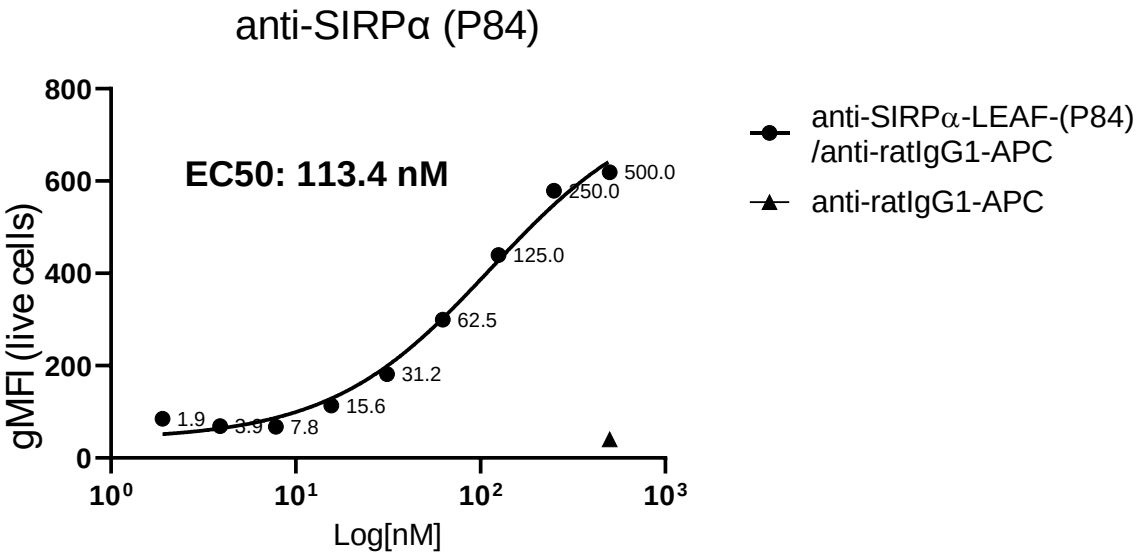

Figure 4.5. Anti-CD172a (SIRPα) P84 antibody binding curve. (A) Quantification of SIRPα binding to bone marrow extracted cells. The binding curve was used to calculate the half maximal effective concentration (EC50). Antibody concentration used was transformed logarithmic scale (X=Log(X)) and the EC50 was calculated with a nonlinear fitting of log(agonist) vs. response (three parameters) curve. Assays n=1 in triplicate.

We tested different antibody concentrations to determine the best concentration. We generated an antibody binding curve to calculate the half maximal effective concentration (EC50) which defines the drug concentration required to induce a 50% engagement of the binding site. For us it was important to have an estimate of the amount of antibody to use to have half of the receptors bound, hence translated to an effect on the cells. Extracted bone marrow cells, depleted of red blood cells, were seeded in equal number and the anti-SIRPα antibody was titrated starting from a 500nM concentration. Bound P84 antibody was then detected by the addition of a fluorescent anti-rat IgG1 which wasn't binding by itself. The MFI generated with each antibody concentration was transformed to a logarithmic scale and the non-linear fitting function was used to calculate the EC50. This reveal that the optimal starting

concentration of P84 antibody to use in experiments was around 113.4 nM (figure 4.5), although for each study assay optimisations were performed.

4.5 CD47 strengthens the M-MDSC and moDC cells suppression over the T cell proliferation.

Having observed the increased immunosuppressive repertoire induced by CD47 in vitro, and having determined the optimal concentration of P84 anti SIRPα antibody, we then added this to the *in vitro* culture system. Here we aimed to determine whether the changes in myeloid cell behaviour induced by CD47 could augment the suppression potency towards T cells and be reversed by blocking SIRPα.

The T cells only proliferation control was compared with the T cells in contact with $Ly6C^+$ myeloid cells grown respectively in GM-CSF, GM-CSF-TCM, GM-CSF-TCM with CD47 coating and GM-CSF-TCM CD47 coating but with myeloid pre-treatment with the anti-SIRPα antibody. This last condition was set in order to impede the CD47-SIRPα interaction and obtain an equal suppression to the GM-CSF-TCM myeloid condition. In other words, prove that by blocking SIRPα, the myeloid cells wouldn't be affected by the CD47 addictive stimulus and limit their suppressive ability to the TCM effect.

Consistent with earlier data, $Ly6C^+$ myeloid cells suppressed CD8 and CD4 proliferation, and this effect was enhanced in the presence of TCM (figure 4.6 A and B). The presence of CD47 further boosted the suppressive activity of moDCs and MDSCs, from 70% proliferation down to 40%, indicating the stimulation of additional or enhanced suppressive pathways in myeloid cells following its engagement.

To determine if this was in part modulated by SIRPα engagement, and whether disruption of CD47-SIRPα could reverse suppression, myeloid cells were pre-incubated with the anti-SIRPα antibody. This ensured SIRPα sites were occupied prior to exposure to CD47 and TCM effects. Importantly, the CD47 induced suppressive increment was ablated when the myeloid were pre-incubated with the anti-SIRPα returning CD4 and CD8 proliferation to levels equal to incubation with GM-CSF-TCM (figure 4.6 A and B).

While the anti-SIRPα antibody managed to revert the impact of CD47 presence, it was not sufficient to overcome the suppressive GM-CSF-TCM driven effect. To have an insight of which this may not be the sole effect, we monitored two immune modulators, PD-L1 protein and ARG1. For PD-L1, the samples containing CD47 showed a tendential increase of PD-L1 expression that was in accord with the data generated previously in the CD47 Ly6C^{+} cells cultures. It is possible that this wasn't as much as previously evident because the lower amount of myeloid on which the gMFI signals were calculated. However, in the case where anti-SIRPα was bound to the cell-surface SIRPα, preventing ligation by CD47 we appreciated a slight reduction that indirectly confirms that CD47 binding support PD-L1 expression (figure 4.6 C). The cytosolic arginase1 enzyme was checked to address a possible anti-SIRPα driven effect in reducing nutrient depletion. Consistent with the previous data, the addition of CD47 didn't augment its expression compared to TCM. However, a reduction in ARG1 levels were visible when anti-SIRPα was bound to the myeloid cells (figure 4.6 D).

Together, these data allow us to speculate that the CD47-SIRPα axis plays a role in inhibiting T cell proliferation, and it's blockade partly restores proliferative capacity. Although here, we examine just two candidates, disruption to CD47-SIRPα may exert its effects by rewiring internal cell signalling to induce a more inflammatory myeloid cell phenotype; In the case of ARG1, reducing enzyme thereby avoiding nutrient

depletion for T cells. It is likely that additional functional changes occur in myeloid cells in response to engagement of SIRPα.

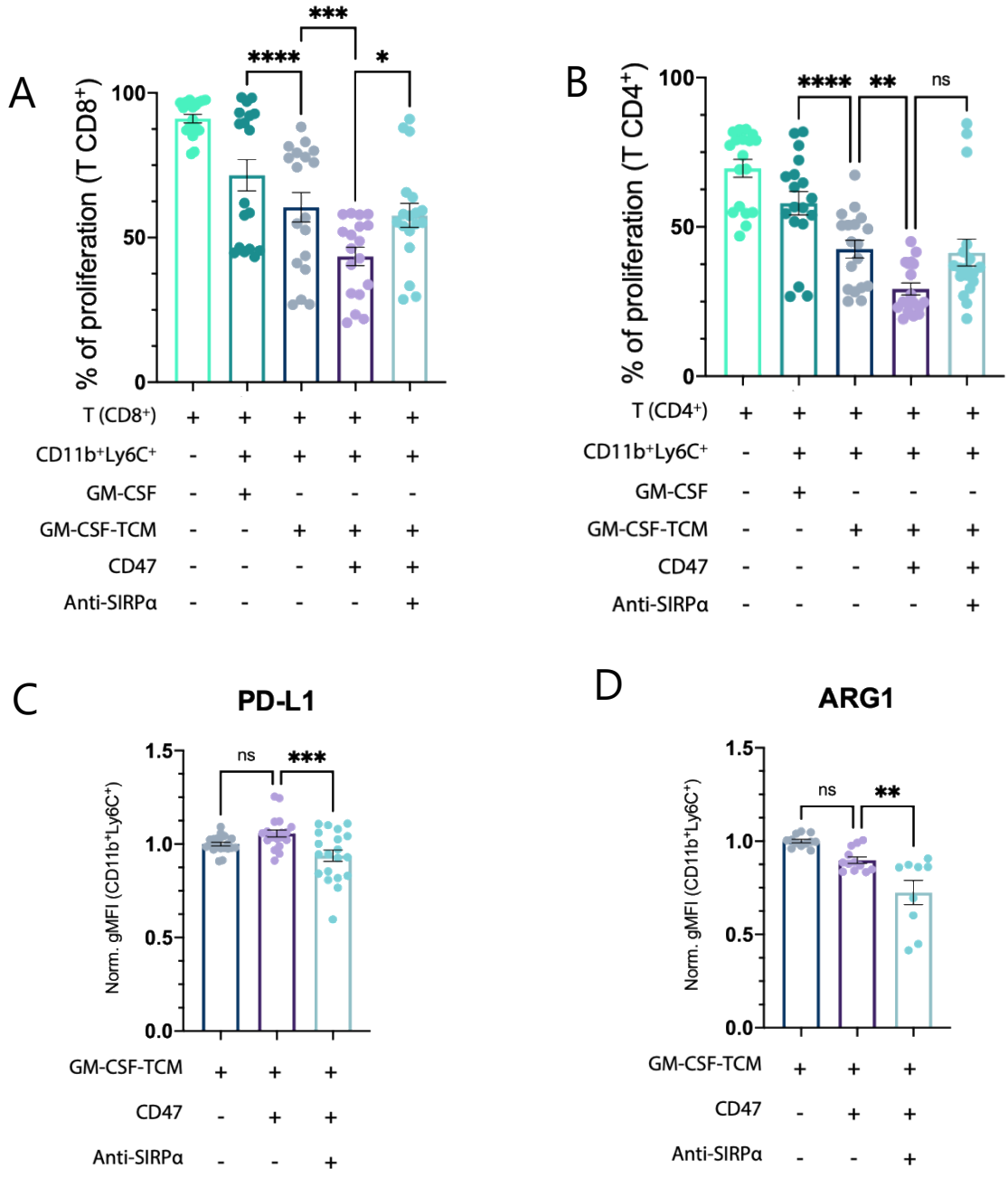

Figure 4.6. SIRPα blockade cancels the effect of CD47 induced suppressive potency. **(A** and **B)** Quantification of $CD8^+$ and $CD4^+$ T cell proliferation under the influence of $CD11b^+Ly6C^+$ cells grown in GM-CSF, GM-CSF-TCM, GM-CSF-TCM with CD47, and GM-CSF-TCM-CD47 with anti-SIRPα. **(C)** Quantification of MFI geometric mean of PD-L1 and **(D)** ARG1 expressed by $CD11b^+Ly6C^+$ cells present in the T cell proliferation assay. (A-D) Data are mean ± SEM; * = p <

0.05, ** = p < 0.01, *** = p < 0.001, **** = p<0.0001 using ordinary one-way ANOVA with a Dunnett post hoc test. (A-B-C) Assays n=6 in triplicate. (D) Assays n=3 in triplicate.

4.6 Phagocytosis is regulated by CD47 in moDC and M-MDSCs.

Having observed an impact on T cell behaviour we sought to examine in more detail how the myeloid cells may exert their effects. As a major role of myeloid populations is to sample and present material to tumours, and CD47-SIRPα is a modulator of "do not eat me" signals, we further explore functional changes brought via the CD47-SIRPα interaction, focusing on their phagocytosis.

Knowing that the CD47-SIRPα axes directly modulates phagocytic mechanisms, we measured if moDC and M-MDCSs were able to phagocytose, and secondly if this was modulated by CD47 expression levels on the other components of the TME. We then tested if SIRPα blockade had any capacity to reactivate this key feature of antigen presenting cells, reinstating and enhancing phagocytic function.

To do this, we modified our *in vitro* system (figure 4.7 A). moDCs and MDSCs were grown in GM-CSF-TCM for five days to induce suppressive states. These were co-cultured with different fluorescently labelled cell types expressing varying levels of CD47, highlighted in figure (figure B and C). Cell lines with low and high CD47 were used as natural modulators of the CD47-SIRPα interaction. In addition, cell debris to be phagocytosed, was obtained by killing a quarter of the CD47 expressing cells, then the degree of phagocytosis was measured. In place of live cell microscopy to track engulfment[725], we took a quantifiable flow cytometry based approach.

Based on the previous *in vivo* characterisations which showed tumour cells had low CD47 expression and tumour stroma were high, we first measured CD47 expression levels at the protein level across a panel cell lines. Flow cytometry confirmed that

indeed CD47 was lowly expressed on the B16-F10 melanoma and E0771 breast cancer cells, whilst the cancer associated fibroblasts showed the highest levels (figure 4.7 B and C). Therefore, B16-F10 melanoma cells and cancer associated fibroblast were chosen based on their differentially expressed CD47.

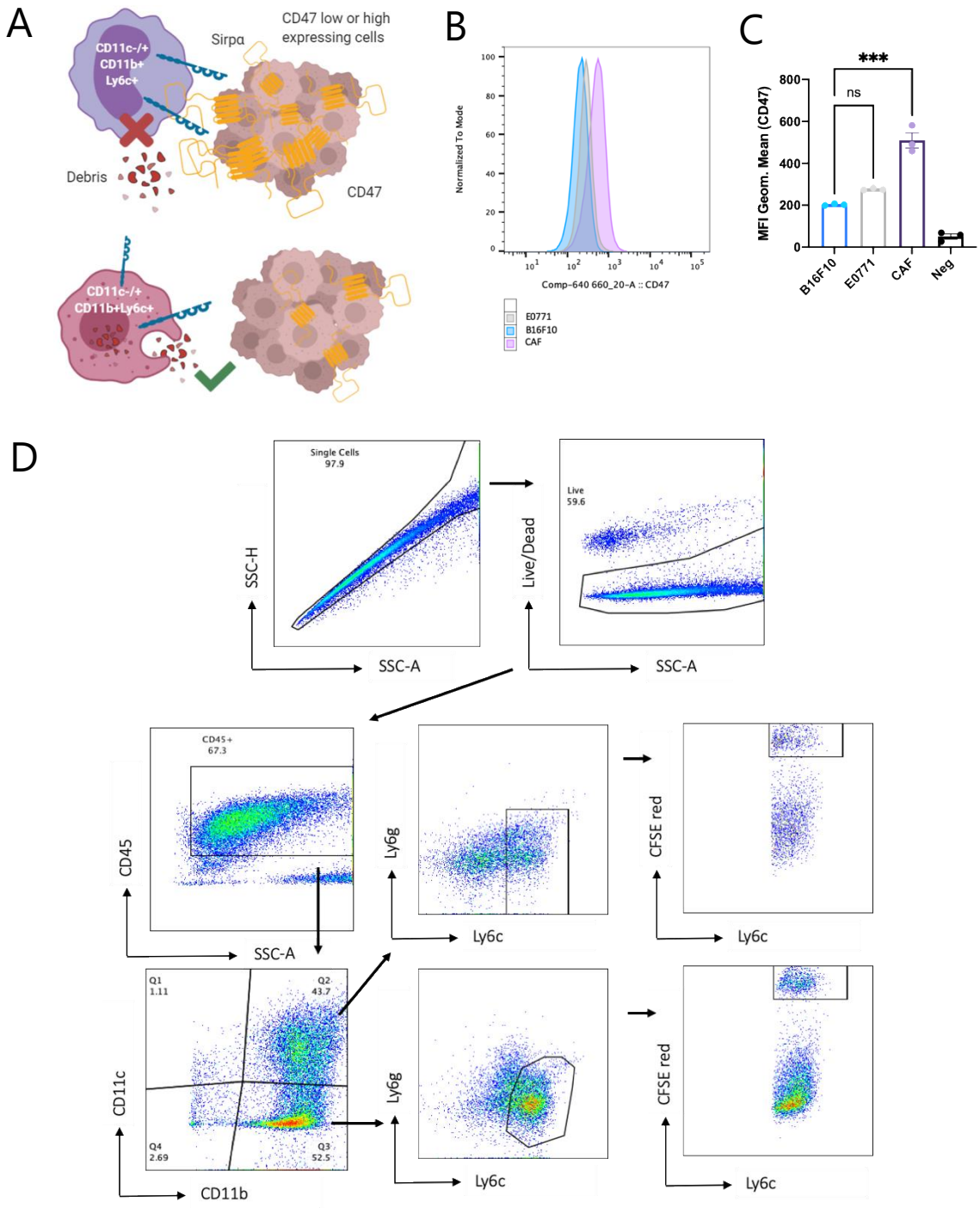

Figure 4.7. Development of an assay to evaluate CD47 modulation of moDC and M-MDSC phagocytosis. (A) Assay schematic: M-MDSC and moDC were mixed with fluorescently labelled high or low CD47 expressing cells. The high concentration of CD47 should prevent the phagocytosis of stained debris whilst a low concentration should allow it. **(B)** Representative

histogram of the CD47 signal detected on cell lines tested. **(C)** Quantification of CD47 level on B16-F10 melanoma, E0771 breast cancer and fibroblasts. **(D)** Gating strategy used to analyse uptake of red cell trace dye stained debris by moDC and M-MDSC cells. (C) Data are mean ± SD; * = $p < 0.05$, ** = $p < 0.01$, *** = $p < 0.001$, using ordinary one-way ANOVA with a Dunnett post hoc test. Assays n=1 in triplicate.

Because of the quick phagocytic response observed by phagocytes[726], the assay was performed for four hours. This time was a long enough window to detect differences in uptake. The samples were stained according to previous strategy and gated accordingly (figure 4.7 D). moDC and M-MDSC populations were then also analysed for red cell trace dye fluorescence, demonstrating engulfment of the fluorescent debris derived from labelled CD47-expressing cell lines. With this approach we expected to detect a higher level of phagocytosis in the presence of CD47 low B16-F10 cells than with CD47 high CAF cells, and an increase phagocytosis with anti-SIRPα following disruption of the CD47-SIRPα "do not eat me signal".

Indeed, phagocytosis by M-MDSC was modulated by CD47. When in presence of CD47 high CAF cells, uptake of red cell trace dye labelled debris was low (figure 4.8 A). In contrast, phagocytosis in the presence of CD47 low B16-F10 cells was approximately six times higher. Once the modulation by different amount of CD47 was verified, the same phagocytic signal was compared to the same condition but using anti- SIRPα block the CD47-SIRPα interaction on the myeloid. When focusing on cells expressing high levels of CD47, it was clear that the SIRPα blockade doubled the capacity to engulf particles by the M-MDSCs (figure 4.8 B). Furthermore, when the focus was moved on the samples containing low CD47-expressors we were still able to detect a similar increase in phagocytosis after SIRPα blockade, even though the baseline levels of debris uptake were significantly more (figure 4.8 C).

These data indicate that M-MDCS cells were regulating phagocytosis based on CD47 levels and that disruption of its interaction with SIRPα was able to partially re-instate this mechanism. It should be noted here however, that anti-SIRPα was utilised at a 1nM prior to titrations confirming its potency. Despite the low concentration used the anti-SIRPα still produced the expected result. Thus, a higher concentration may be required to overcome the "do not eat me signal" by saturating all the SIRPα molecules.

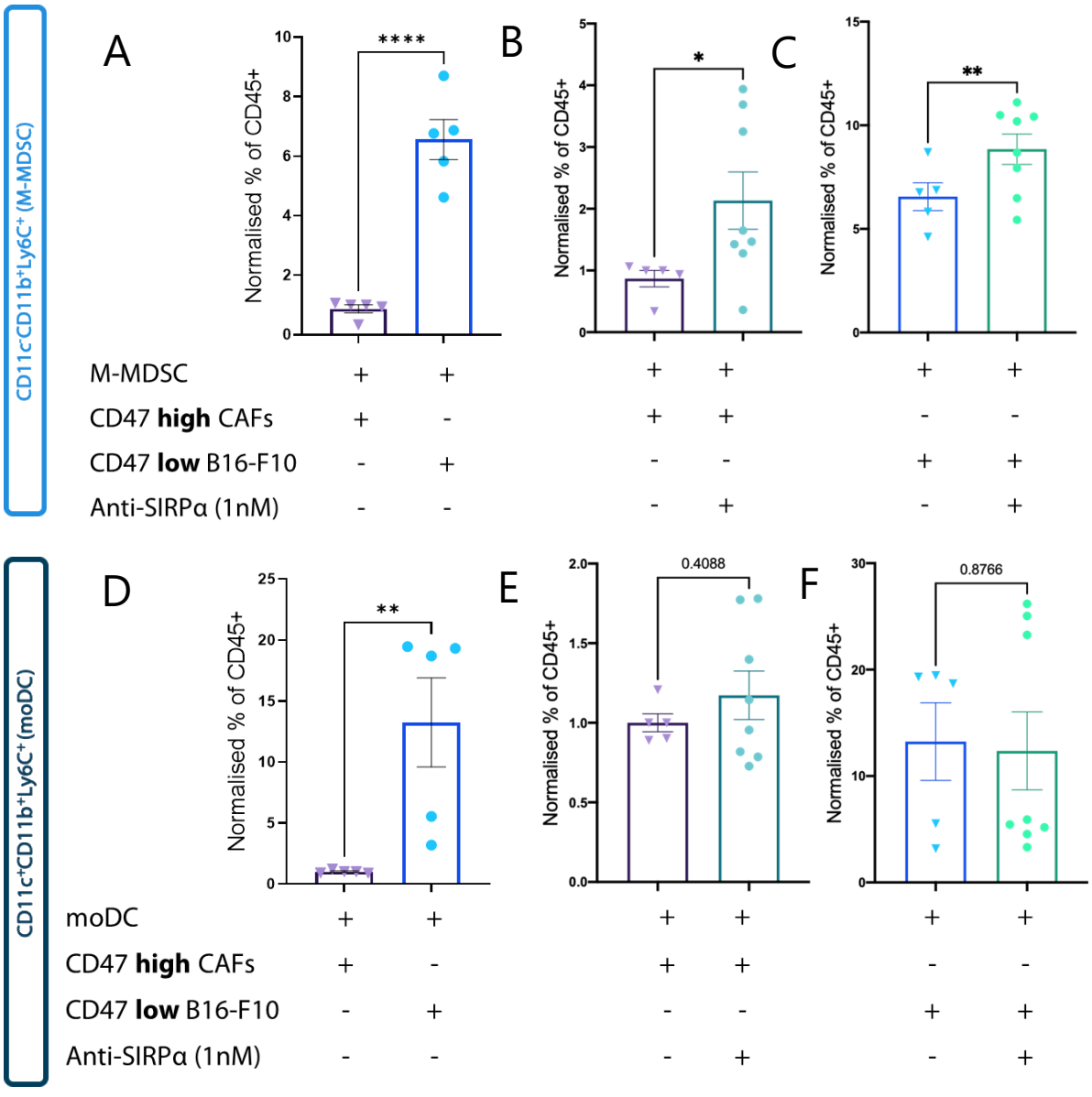

Figure 4.8. Phagocytosis by M-MDSC and moDC cells is regulated by the CD47-SIRPα interaction. (A) Flow cytometry quantification of uptake of labelled CD47-high-CAFs or CD47-low-B16-F10 cell debris by M-MDSCs. **(B)** Quantification of M-MDSCs phagocytosis in presence of CD47 high CAFs expressing cells. **(C)** Quantification of M-MDSCs phagocytosis in presence of CD47 low B16-F10 expressing cells with or without anti-SIRPα. **(D)** Flow cytometry quantification of uptake of labelled CD47-high-CAFs or CD47-low-B16-F10 cell debris by moDCs. **(E)** Quantification of moDC phagocytosis in presence of CD47 high expressing cells with or without anti-SIRPα. **(F)** Quantification of moDC phagocytosis in presence of CD47 low expressing B16-F10 cells with or without anti-SIRPα. The data are shown as percentage of CD45 normalised by the samples containing CD47 high expressing CAF cells. Data are mean ± SEM; * = $p < 0.05$, ** = $p < 0.01$, *** = $p < 0.001$, **** = $p<0.0001$ using (A and D) ordinary one-way ANOVA with Dunnett's post hoc test and (B-C and E-F) unpaired t test. Assays n=3 at least in duplicate.

The moDC cells were, similarly, affected by CD47 signalling (figure 4.8 D), where CD47-low B16-F10 cells induced significantly more engulfment of debris compared to the CD47 high expressing CAF cells; around ten times more material was taken up. In contrast to M-MDSCs however, anti- SIRPα addition had little impact on moDC phagocytosis for either CD47 high or low conditions (figure 4.8 E and F). This may be due to the fact that the moDC cells were presenting higher SIRPα surface density (shown in figure 3.17), resulting in an insufficient concentration of the antibody to prevent effective CD47-SIRPα signalling.

To notice, the gMFI signal just showed a tendential increase when CD47-SIRPα was blocked and no difference between samples (appendix 8.7). The potential reason was that after four hours of incubation the cells were reaching maximum engulfment, thus we analysed the data by % of CD45 cells positive to phagocytosis.

Together these data confirm that phagocytic activity of moDC and MDSC was modulated by the CD47-SIRPα interaction directed between myeloid cells and other components of the TME. Furthermore, even at low concentrations, likely without

saturating SIRPα sites, the antibody blockade was able to overcome the CD47 effect on this mechanism in accord with our hypothesis.

4.6.1 Anti-SIRPα induces an antibody dose dependent cellular phagocytosis (ADCP).

We observed that MDSCs and moDCs were able to engulf debris in a CD47-SIRPα regulated manner, but 1nM anti-SIRPα could only overcome the "do not eat me signal" and reinstate the phagocytic ability of M-MDSCs. The lack of response in moDCs to blockade may be a consequence of higher expression of SIRPα, and just a problem of receptor density rather a physical characteristic. To address this, and ascertain if this was indeed due to expression levels and antibody concentration, phagocytosis experiments were repeated titrating the anti-SIRPα. The experiments were set in the same manner described in the previous section. Once matured, the $Ly6C^+$ cells were incubated with a titration of the anti-SIRPα antibody (0.2, 2, 20 and 200nM) and co-cultured with labelled high and low CD47 cells and cell debris.

As before, M-MDSCs were responsive to SIRPα blockade. Cells showed a dose dependent increase in phagocytosis determined by the anti-SIRPα concentration used (figure 4.9 A). M-MDSCs cultured with CD47 low expressing B16-F10 cells, when phagocytosis was high, showed a clear increase in uptake, with two times more material engulfed between control and 20nM antibody (figure 4.9 A). The data matched the one where 1nM was used, the graphs showed the same trend at equal concentration. As expected, the CD47 high CAF cells diminished the ability of the anti-SIRPα to bring back the phagocytosis, however, a significant increase in uptake was apparent with higher concentrations (figure 4.9 B).

While moDCs didn't show an increase in phagocytic capacity when 1nM of anti-SIRPα was used, the titration showed a clear indication that phagocytic behaviour could be re-activated adjusting the antibody concentration. Now, with increasing concentration, responses mirrored those of M-MDSCs. Culture with CD47 low expressing B16-F10 cells showed a progressive increase in uptake with increasing antibody concentration (figure 4.9 C). This indicated that previous data was indeed due to a lack of efficient SIRPα blocking due to high levels of surface expression in moDCs. In a similar manner and even in the most difficult situation with high CD47 CAF cells and high SIRPα moDCs, the antibody proved to increase at higher concentrations (figure 4.9 D).

The CD47-SIRPα interaction resulted in strongly inhibiting phagocytosis and may be because of its crucial function in preventing self-cells engulfment and recycling. Thus, these data showed that to achieve an effective phagocytic boost, complete blockade of the SIRPα regulatory protein was needed.

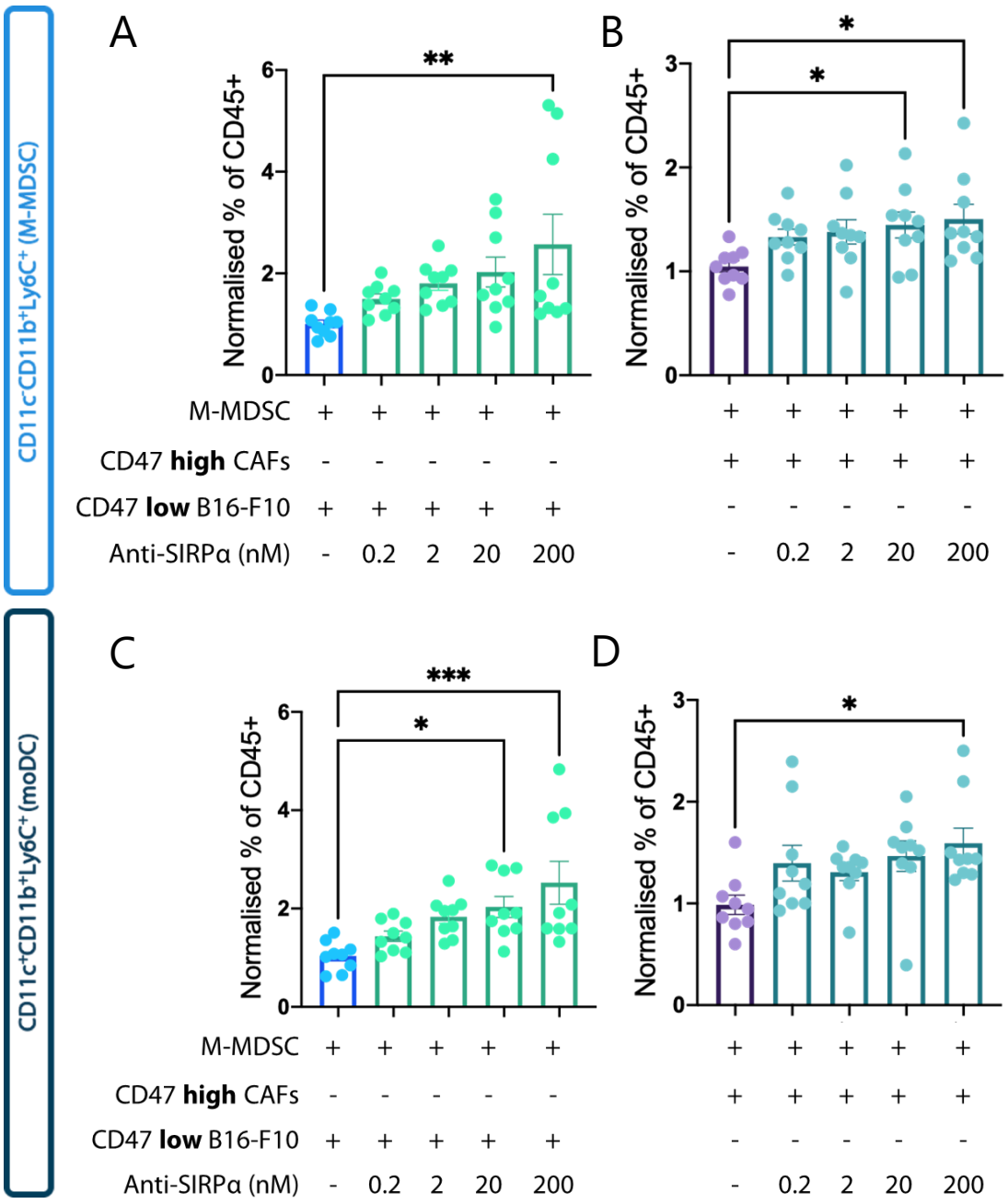

Figure 4.9. SIRPα blockade restores phagocytosis in a dose dependent manner. Quantification of labelled debris uptake by **(A and B)** M-MDCSs or **(C and D)** moDCs in the presence of **(A and C)** CD17-low-B16-F10 or **(B and D)** high-CD47-CAF expressing cells. Data are shown as percentage of CD45 cells normalised by the anti-SIRPα negative sample. Data are mean ± SEM; * = $p < 0.05$, ** = $p < 0.01$, *** = $p < 0.001$, **** = $p < 0.0001$ using ordinary one-way ANOVA with Dunnett's post hoc test. Assays n=3 from 3 independent experiments.

4.7 Anti- SIRPα reduces SHP2 and STAT3 phosphorylation status.

To date, these results suggest that CD47-SIRPα signalling is important for the suppressive phenotype and behaviour of myeloid cells towards T cells, and is potentially initiated by reduced uptake of cellular debris. Blockade of anti-SIRPα modulated phagocytosis by counteracting CD47 negative signals, and was proportional to the antibody concentration used. To then test if blocking SIRPα actually altered its downstream signalling, we examined the phosphorylation state of associated accessory proteins.

Here, we focused on the phosphorylation state of the (SH2)-containing protein tyrosine phosphatase-2 (SHP2) at the initiation of the phagocytosis inhibition signal cascade. When CD47 and SIRPα engage, the SIRPα cytosolic portion that contains tyrosine residues conform loosely to inhibitory immunoreceptor tyrosine-based inhibition motifs (ITIMs)[618,727], which mediate its association with the phosphatase SH2-domain-containing protein tyrosine phosphatase 2 (SHP2)[728,617]. This initiates a dephosphorylation cascade directed in part at phosphotyrosine in myosin, as well as F-actin recruitment[622] and further, inhibits integrin activation in the macrophage, reducing macrophage-target contact and suppressing phagocytosis[729].

Downstream of SHP2, the signal transducer and activator of transcription 3 (STAT3) was examined. It has been reported that activate, phosphorylated STAT3 was constitutively present in cells of the TME, and was responsible for modulation of immune mediator's towards promoting tumour escape[730]. Indeed, in M-MDSCs, a STAT3 activated gene signature was correlated with monocyte reprogramming towards immunosuppresision[731] and in impairment of maturation and antigen presentation in dendritic cells [732,733].

The Ly6C^{+} cells were matured in GM-CSF-TCM media, then incubated for four hours in presence of CD47 or CD47-anti-SIRPα before protein was collected for western blot analysis. Following a basic time course optimization, four hours incubation was chosen to reflect the best signal detected in a time course experiment that defined a window of sensitivity reflective of signalling post phagocytosis (appendix 8.8 A-B). Bands generated were normalized to alpha-tubulin enabling us to calculate phosphorylated/dephosphorylated SHP2 and STAT3 ratios. The presence of CD47, did not induce a significant increase in the ratio of SHP2-P/SHP2 compared to TCM alone. However, when SIRPα was blocked, the ratio halved indicating the antibody impaired SIRPα signalling activity (figure 4.10 A, C and E) and consequently diminished the phagocytosis inhibition signal.

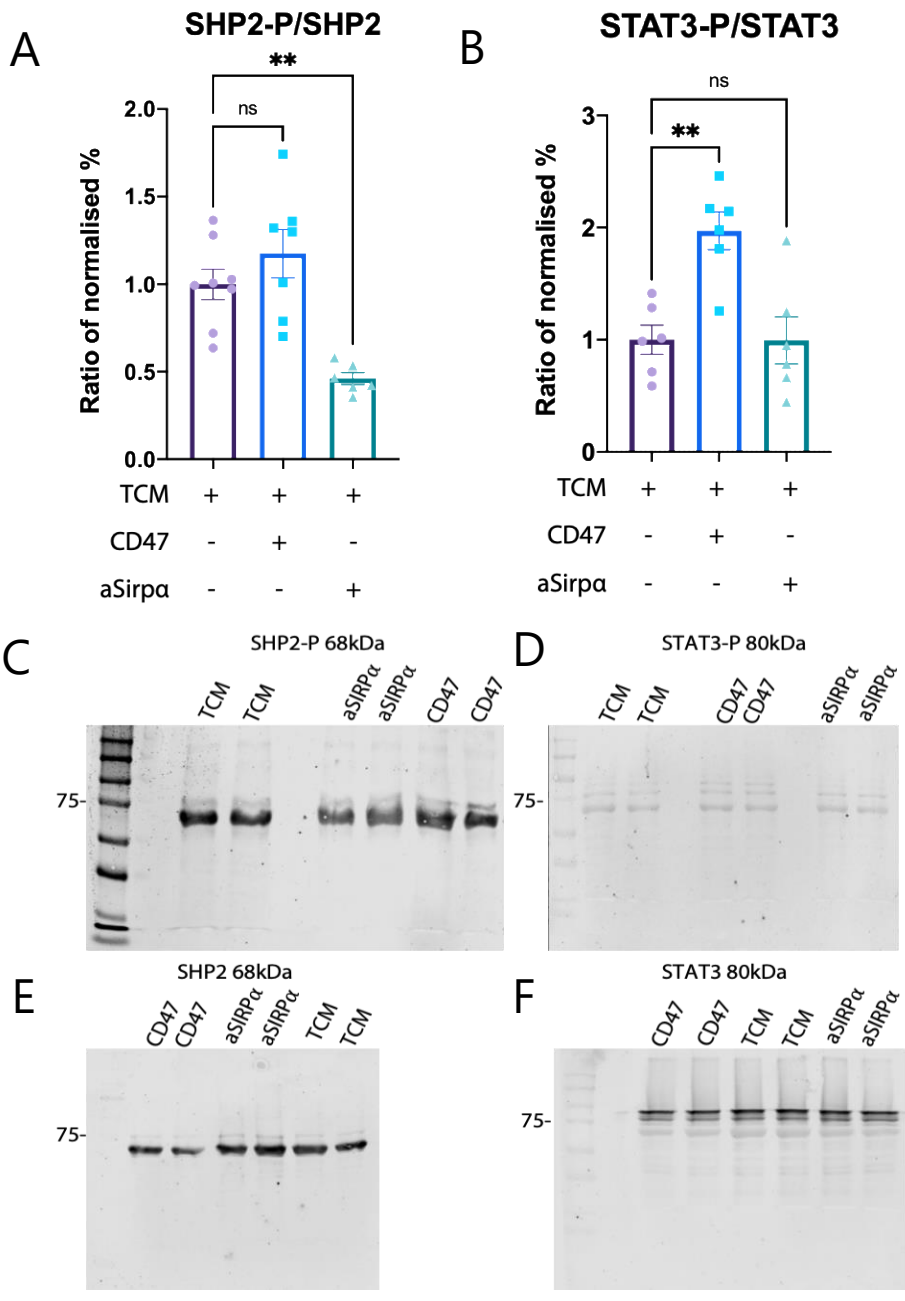

Figure 4.10. CD47 and anti-SIRPα modulate the phosphorylation state of SHP2 and STAT3. Quantification of the ratio of **(A)** SHP2-P/SHP2 and **(B)** STAT3-P/STAT3 proteins expressed in the CD11b^{+}Ly6C^{+} (moDC and M-MDSC) cells grown in GM-CSF-TCM, GM-CSF-TCM-CD47 and GM-CSF-TCM with anti-SIRPα. Representative western blots for **(C)** SHP2-P **(D)** STAT3-P **(E)** SHP2 and **(F)** STAT3 for CD11b^{+}Ly6C^{+} cells in presence of GM-CSF-TCM, GM-CSF-TCM-CD47 and GM-CSF-TCM-aSIRPα. (A-B) Data are mean ± SEM; * = $p < 0.05$, ** = $p < 0.01$ using ordinary one-way ANOVA with a Dunnett post hoc test. Assays n=6.

Different results were observed regarding the STAT3 state of phosphorylation. It was evident that the persistent stimulation by the CD47-SIRPα engagement was correlated with an increase of STAT3 phosphorylation, doubling compared to the baseline. When SIRPα was blocked by the anti-SIRPα antibody, STAT3 phosphorylation was remained at base line level. Hence, "do not eat me signal" signalling also utilized STAT3 activation (figure 4.10 B, D and F).

Thus, western blotting revealed that there was a cell signalling change following CD47-SIRPα interaction. Consistent with the onset of changing cell behaviours following anti SIRPα treatment, phosphorylation of these intracellular signalling molecules decreased by 4 hours. This indicates that SHP2 and STAT3 phosphorylation may be an early response to SIRPα engagement operating by transmitting the "do not eat me" signals within the cell, contributing to the development of the myeloid suppressive state.

4.8 CD47-SIRPα boost ROS production in CD11b^{+}ly6C^{+} (moDC and M-MDSC)

STAT3 signalling in the MDSC cells has been associated with high production of ROS via upregulation of NADPH oxidase (NOX2) and implicated in MDSC-mediated T cell suppression and tumour escape[448]. Within the TME, changing ROS levels have been implicated in reduced capacity to induce nitric oxide signalling and angiogenesis[734]. Furthermore, ROS increases the general oxidative stress reducing enzymatic functions that in cancer, leads to a state of chronic inflammation which unbalance the immune cells homeostasis allowing tumour escape and metastasization[735].

Thus, having observed changes in signalling and behaviour of myeloid populations, we next measured ROS production and the effects which CD47-SIRPα interaction and disruption could have on the moDCs and M-MDSCs. Intracellular ROS was detected using the cell-permeant 2',7'-dichlorodihydrofluorescein diacetate (H2DCFDA). The compound is reduced upon cleavage of the acetate groups by intracellular esterases and oxidation. This induces conversion of nonfluorescent H2DCFDA into the highly fluorescent 2',7'-dichlorofluorescein (DCFDA), making it detectable by flow cytometry.

After maturation in TCM, the Ly6C$^+$ population was purified and re-plated and recovered in the media for four hours, prior to DCFDA addition. This step was taken as the reaction is fast and needs to be stopped promptly meaning that discrimination of populations by staining wasn't possible after the DCFDA incubation without impacting the reliability of readouts. After ten minutes in DCFDA, Ly6C$^+$ cells were stained with the live cell dye immediately prior to analysis, gating on live cells and the DCFDA signal (figure 4.11 A).

Initially, we assessed if the Ly6C$^+$ myeloids grown in GM-CSF vs. GM-CSF-TCM presented with differences in ROS production, however while ROS production was high in both populations, a clear difference wasn't observable. This indicates that these cells are both producing high quantities of ROS which may contribute to their suppressive capacity (figure 4.11B).

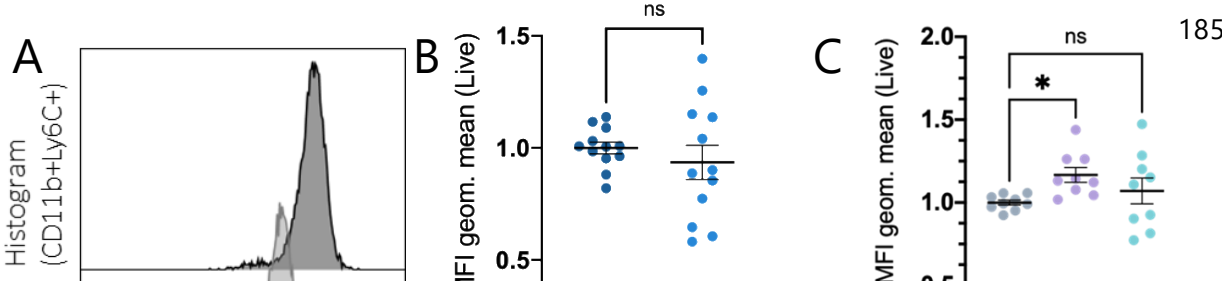

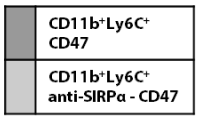

Figure 4.11. CD47-SIRPα modulates ROS production by CD11b$^+$Ly6C$^+$ cells. (A) Representative flow cytometry histogram showing DCFDA signal in live cells. **(B)** Quantification of the DCFDA gMFI signal detected for the CD11b$^+$Ly6C$^+$ cells grown in GM-CSF vs. GM-CSF-TCM. **(C)** Quantification of the DCFDA gMFI signal detected for the CD11b$^+$Ly6C$^+$ cells grown in GM-CSF-TCM, GM-CSF-TCM-CD47 and GM-CSF-TCM-CD47 where CD11b$^+$Ly6C$^+$ cells were pre-incubated with anti-SIRPα. (B) Data were normalised by the GM-CSF samples. Data are mean ± SEM; ns = $p > 0.05$ using paired t test. Assays n=4 in triplicate. (C) data were normalised by GM-CSF-TCM samples. Data are mean ± SEM; * = $p < 0.05$, using matched data one-way ANOVA with a Dunnett's post hoc test. Assays n=3 in triplicate.

We then sought to determine if contact with CD47 or CD47-SIRPα blockade altered this production. CD47 induced a small, but significant increase in ROS levels compared with GM-CSF-TCM grown cells, and SIRPα blockade cancelled this effect (figure 4.11C). Together, these data suggested that the *in vitro* cultured Ly6C$^+$ myeloid were presenting phenotypical characteristics described for suppressive MDSCs, consistent with the established literature. Moreover, already high levels of ROS production were increased by a CD47 rich environment, which could be reduced by blocking SIRPα.

4.9 The CD47-SIRPα interaction affects the metabolism of the moDC and M-MDSCs.

Recent work by Baumann and colleagues identified that human MDSCs displayed strongly reduced metabolism that led to the accumulation, transfer of the metabolite methylglyoxal and paralysis of T cells[736]. Thus, with evidence to suggest that the CD47-SIRPα interaction was contributing to the suppressive behaviour of the myeloid cells, we then examined if this change was accompanied by a modification of metabolic state.

We first tested molecules involved in the glycolysis function by using 2-NBDG, a fluorescent analogue to monitor glucose uptake in live cells. GM-CSF-TCM induced moDC and M-MDSCs of all treatment groups were incubated for four hours in glucose depleted media prior to 2-NBDG. After 20 minutes exposure to 2-NBDG to allow the uptake, cells were kept in ice and stained to distinguish the different populations.

The presence of active CD47 presence in the well induced a tendential reduction in glucose uptake relative to untreated for both moDC (figure 4.12 A) and M-MDSCs (figure 4.12 B). Importantly, this effect was reversed with SIRPα blockade, and glucose uptake recovered.

GLUT-1, the main transporter mediating glucose uptake, also changed on both moDC and M-MDSCs following perturbation of CD47-SIRPα interactions. Interestingly, and opposite of what we expected CD47 induced an increase in expression levels of the transporter in opposition to glucose uptake. This was augmented further following SIRPα blockade, coincident with restoration of inflammatory functions including phagocytosis and antigen processing (figure 4.12 C and D).

The discrepancy between uptake and glucose transporter, following CD47 stimulation was suggesting that the glucose was utilised differently.

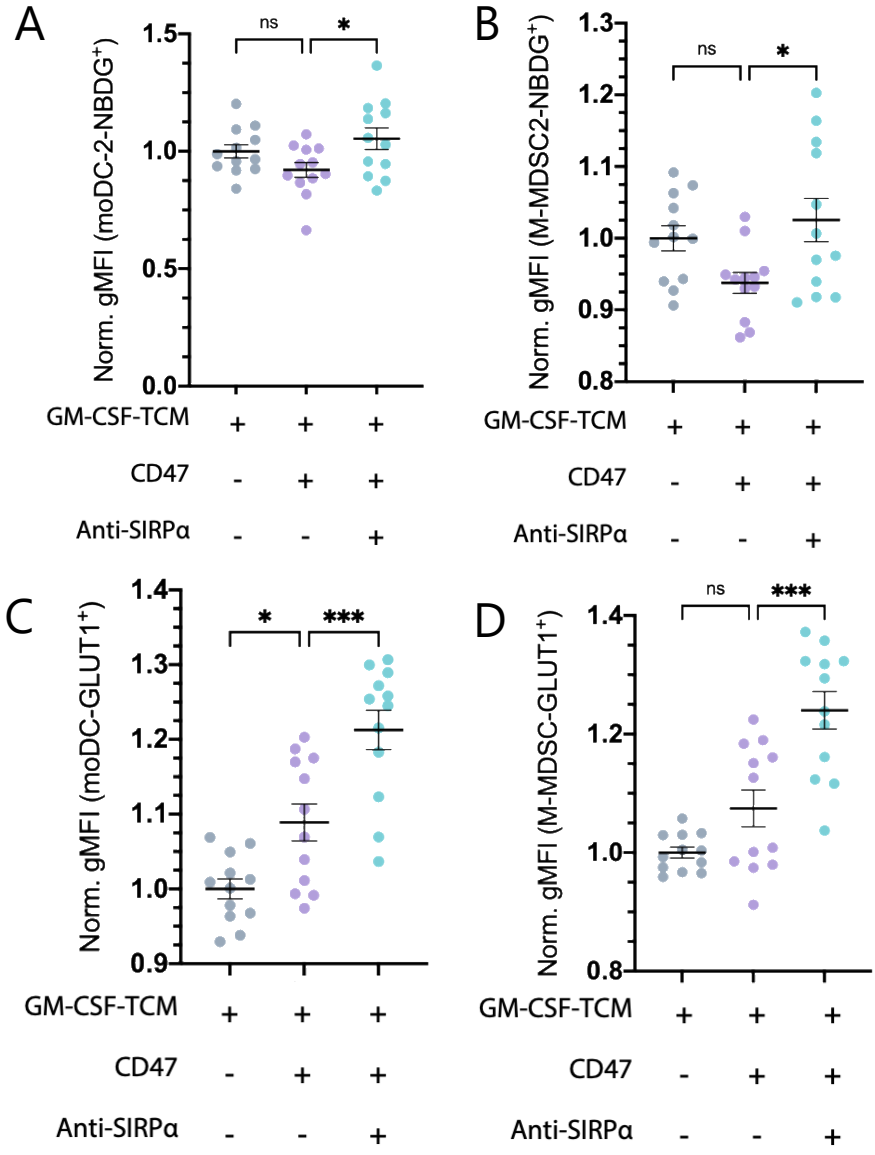

Figure 4.12. CD47-SIRPα interactions modulate glucose uptake and GLUT-1 expression in moDC and M-MDSCs. Quantification of uptake of the glucose analogue 2-NBDG by **(A)** M-MDSC and **(B)** moDC cells generated by GM-CSF-TCM cell culture. Quantification of glucose transporter GLUT-1 cell surface expression levels by the **(C)** M-MDSC and **(D)** moDC cells obtained by GM-CSF-TCM cell culture. (A to D) The data were normalised by the signal detected in the GM-CSF-TCM samples. Data are mean ± SEM; * = $p < 0.05$, ** = $p < 0.01$, **** = $p<0.0001$ using the ordinary one-way ANOVA with a Dunnett's post hoc test. Assays n=4 in triplicate.

To understand if the glucose was entering the glycolysis cycle, we then investigated the enzyme hexokinase. This enzyme converts the glucose in glucose-6-phospate entering in the glycolysis cycle, and its activity can be measured by the total amount of NADH produced. The $CD11b^{+}Ly6C^{+}$ cells were deprived of glucose before receiving a short pulse before cell lysis. The total NADH was measured and normalised by the concentration detected in the GM-CSF or GM-CSF-TCM control. We detected the NADH in both GM-CSF and GM-CSF-TCM grown myeloid cells. Although a slight increase was observed with CD47 stimulation in GM-CSF grown moDC and M-MDSC (figure 4.13 A), changes were not significant, and we detected no significant cancellation upon SIRPα blockade. Likewise, For the GM-CSF-TCM grown myeloids we detected no significant variance with treatment (figure 4.13 B). Thus, although NADH was produced in both cases wasn't possible to correlate with the increase or decrease of glucose uptake.

Reports have suggested that in cancer, myeloid populations modulate their activation state by increasing the synthesis and secretion of ATP in the tumour microenvironment where is rapidly catabolised into adenosine[737,738]. Its accumulation in solid tumours then impairs antitumor T-cell responses[739]. We therefore looked further down the line to a general metabolic energetic marker, measuring the total ATP production is an indicator of the energetic state of cells.

Initially, we compared the ATP levels in CD11b+Ly6C+ cells grown in GM-CSF and GM-CSF-TCM. Even though most ATP is produced by the electron transport chain and not by glycolysis, deprivation of glucose was done to keep equal conditions between experiments. Ly6C+ cells matured in GM-CSF grown produced ATP, but levels were significantly lower than those from GM-CSF-TCM (figure 4.13 C) indicating the presence of a shift in energetic state induced by TCM.

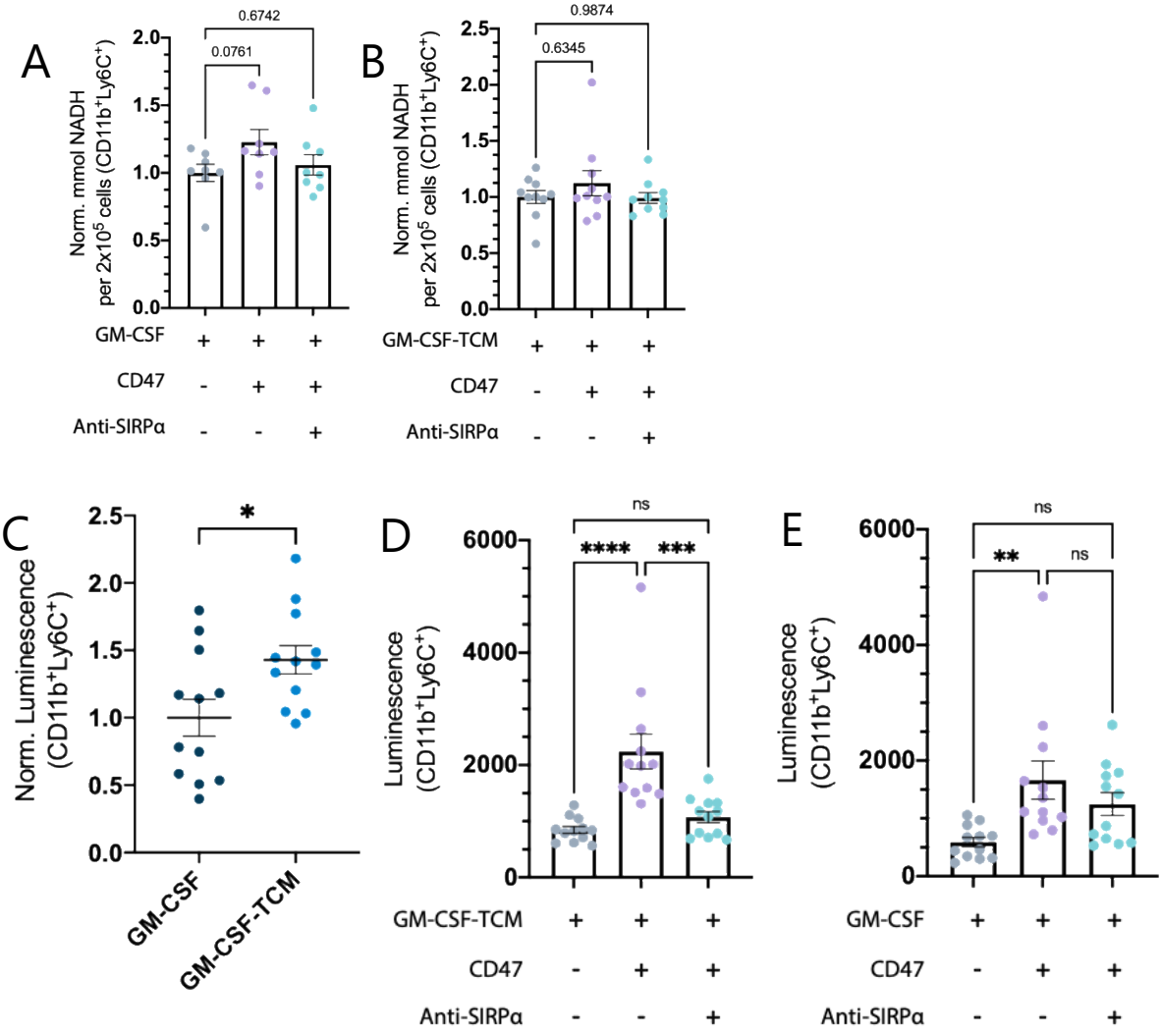

Figure 4.13. CD47-SIRPα induced hexokinase activity and ATP in CD11b⁺Ly6C⁺ cells. Quantification of hexokinase activity in CD11b⁺Ly6C⁺ cells grown in **(A)** GM-CSF and **(B)** GM-CSF-TCM measured as total NADH production. **(C)** Luminescence detected for the ATP levels in CD11b⁺Ly6C⁺ cells grown in GM-CSF or GM-CSF-TCM. Quantification of ATP luminescence driven by the CD47-SIRPα interactions for CD11b⁺Ly6C⁺ cells grown in **(D)** GM-CSF-TCM and **(E)** GM-CSF. (A and B) The data were normalised by the signal detected in the GM-CSF or GM-CSF-TCM samples. Data are mean ± SEM; using the ordinary one-way ANOVA test with Dunnett's post hoc test. Assays with GM-CSF n=4 in duplicate. (C) Data are mean ± SEM; * = $p < 0.05$, using t test. Assays n=6 at least in duplicate. (D and E) Data are mean ± SEM; * = $p < 0.05$, ** = $p < 0.01$, *** = $p < 0.001$, using the one-way ANOVA test with Tukey's post hoc test. n=6 in duplicate.

We then tested how the presence of CD47 and CD47/ anti-SIRPα may change these baselines energetics. CD47 stimulation of GM-CSF grown cells induced a significant increase in ATP, but the blockade failed to diminish effect (figure 4.13 E). Cells grown in GM-CSF-TCM started with higher energetic levels, and they exhibited a greater response to the CD47 protein to increase the ATP production. In contrast these cells grown in TCM were highly responsive to the SIRPα blockade, and ATP levels returned to baseline (figure 4.13 D). These data showed that the TCM grown moDC and M-MDSC were more energetically active. The production of ATP was higher in the TCM myeloid and the CD47-SIRPα interaction increased it.

Upon CD47 stimulus the cells were storing more ATP and the anti-SIRPα was preventing it maybe indicating a different energy usage. We saw how the moDC and M-MDSC upon anti-SIRPα blockade were more actively phagocyting and suppressing less the T cells. This biological activity could correlate with ATP consumption and maybe a possibility to interpret the lower level detected upon SIRPα blockade.

4.10 Summary

We previously saw that moDCs and M-MDSCs cells were implicated in T cell suppression, and this was enhanced by TCM. In this chapter we examined this suppressive function in the wider context of the TME focusing on the CD47-SIRPα interaction; While SIRPα was a common denominator shared by moDCs and M-MDSCs, and restricted largely to the myeloid compartment, we confirmed that CD47 was widely distribute throughout the TME at both the RNA and protein level. SIRPα stimulation by CD47 sparks the "do not eat me signal" physically impeding phagocytosis. Interestingly, we observed that tumour cells expressed only low levels

of CD47 indicating that the myeloid would encounter this negative phagocytic cue principally from stromal components of the TME.

Taking advantage of the in vitro system that closely resembled the myeloid cells present in the TME we showed that addition of CD47 enhanced suppression of T cells proliferation and resulted in increased expression of immunosuppressive molecules by myeloid cells, especially PD-L1. Disruption of CD47-SIRPα signalling by an anti-SIRPα antibody removed this suppression by the Ly6C^{+} myeloid towards the T cells. Moreover, it contributed in damping down PD-L1 and ARG1 expression. CD47-SIRPα axis has been shown to play a key role in avoiding unwanted chronic tissue inflammation. Mouse models of autoimmunity displayed accelerated disease development if SIRPα was knocked out[740]. This is consistent with our results where CD47-SIRPα signals may contribute chronic immunosuppressive signals within the TME, and where its blockade may support active T cell function.

Besides impacting T cell proliferation, we observed a direct effect on myeloid function. CD47 levels regulated their capacity to engulf material, consistent with engagement of the "do not eat me signal"[741,742,743,717]. When the CD47-SIRPα axes was disrupted using the anti-SIRPα (P84) antibody, intracellular signalling was altered [623,744,745] and lead to a perturbation of the "do not eat me signal" and an augmentation of phagocytosis in M-MDSCs. However, based on these data, SIRPα blockade only reduced the additional impact of CD47 stimulation rather than completely inhibiting suppressive functions. As discussed in the results section, this could be a consequence of insufficient antibody concentration and high levels of SIRPα on moDCs and to a lesser extent M-MDSC. This, it is likely that to fully overcome suppression, complete blockade of SIRPα will be required, or combination[746,747] with other immune-oncology

drugs targeting addition T cell functions will be needed to uplift the anti-tumour immune response.

In summary we showed that CD47-SIRPα signalling modulated phagocytosis in myeloid population, with reduced uptake in a TME rich in CD47 stromal cells. This reduced capacity to sample debris was correlated with the acquisition of a suppressive phenotype, in which immune checkpoints contributed to impaired T cell proliferation. As innate immune cells are required to present antigen to T cells to stimulate or suppress T cell activity[748,749,750,] it remains to be determined if CD47-SIRPα modulation of phagocytosis translates to less antigen presentation and poorer T cell stimulation as an additional suppressive mechanism.

These observations could have implications for therapeutically targeting myeloid populations phagocytosis via the CD47-SIRPα in vivo. Due to the breadth of distribution, approaches to block CD47 induce unwanted side-effects[650,751,752], however, targeting SIRPα instead would more specifically impact myeloid population, avoiding off-target effects while still reprogramming them towards more phagocytic inflammatory phenotype. We will investigate the mechanisms by which anti-SIRPα contribute loss of immune suppression, and therapeutic potential in the next chapter.

CHAPTER 5

THE REMODELLING OF THE MYELOID CELLS COMPARTMENT IN THE TME DRIVEN BY THE ANTI-SIRPα ANTIBODY

5.1 Introduction

In the previous chapters we characterised how the tumour exudate was able to induce a suppressive phenotype in the myeloid cells. CD47 expression by cells of the TME dictated the phagocytic capacity of myeloid cells, and its presence enhanced suppressive phenotypes with coincident inhibition of T cell proliferation. This was modulated via SIRPα engagement on moDC and M-MDSCs, downstream SHP2-STAT3 activation, and changes in cellular energetics. Preventing this interaction using a SIRPα antibody reduced the suppressive effects against T cells, phagocytosis was enhanced in a dose dependent manner and supported by increases in glucose uptake.

Having observed the potential therapeutic role of the SIRPα blockade by reduction of suppression and phagocytosis activation in vitro, in this fifth chapter, we will explore the effects of such a therapy in melanoma tumour bearing mice. Moreover, we will elucidate the potential mechanism of action by which the therapy would work.

5.1.1 The potential of the SIRPα blockade.

Having observed the widespread distribution of CD47, and reported side effects of its inhibition, our data indicate that disruption of SIRPα, which displays a more restricted expression pattern, may prove a better approach offering less off target effects.

Studies have shown a potent effect on tumour growth by blocking SIRPα using a clone called MY-1[643,644] (Section 1.7.4 Chapter 1). However, while we were able to obtain the MY-1 hybridoma, and show it had the same response as P84 *in vitro* (data not shown), we were unable to purify it for use in vivo. Thus, as in the previous chapter, we utilized the Ultra-LEAF™ purified CD172a (clone P84) from Biolegend which has also been shown to block SIRPα and have impact on tumour growth in vivo[638,644]. We first, developed a control that could help determine if anti-SIRPα reaches the tumour and thus, be bioavailable to the myeloid cells in the TME.

Here, the Ultra-LEAF™ purified CD172a (clone P84) and its fluorophore conjugated twin were used. Both antibodies bind the same epitope, thereby blocking the other interacting with the antigen. In the *in vivo* context, delivery of the Ultra-LEAF™ P84 anti-SIRPα to the tumour and effective binding to SIRPα would mean that, the epitope already be occupied. As a consequence, SIRPα would be undetectable to the fluorophore-conjugated twin upon FACS analysis.

GM-CSF-TCM induced Ly6C$^+$ cells were incubated with the Ultra-LEAF™ anti-SIRPα antibody that had a rat IgG1 backbone. Cells were then divided and incubated with either the fluorophore conjugated anti-SIRPα or with an anti-ratIgG1 that should bind to the IgG of the Ultra-LEAF™ version. As expected, the fluorophore conjugated anti-SIRPα was unable to bind the SIRPα antigen already occupied by the Ultra-LEAF™ antibody. The antigen was completely undetectable apart from the positive control where the LEAF antibody wasn't initially added (figure 5.1 A). Instead, the fluorescent anti-rat-IgG1clearly bound to the rat antibody backbone proving that the LEAF anti-SIRPα antibody reached its target avoiding internalisation (figure 5.1 B).

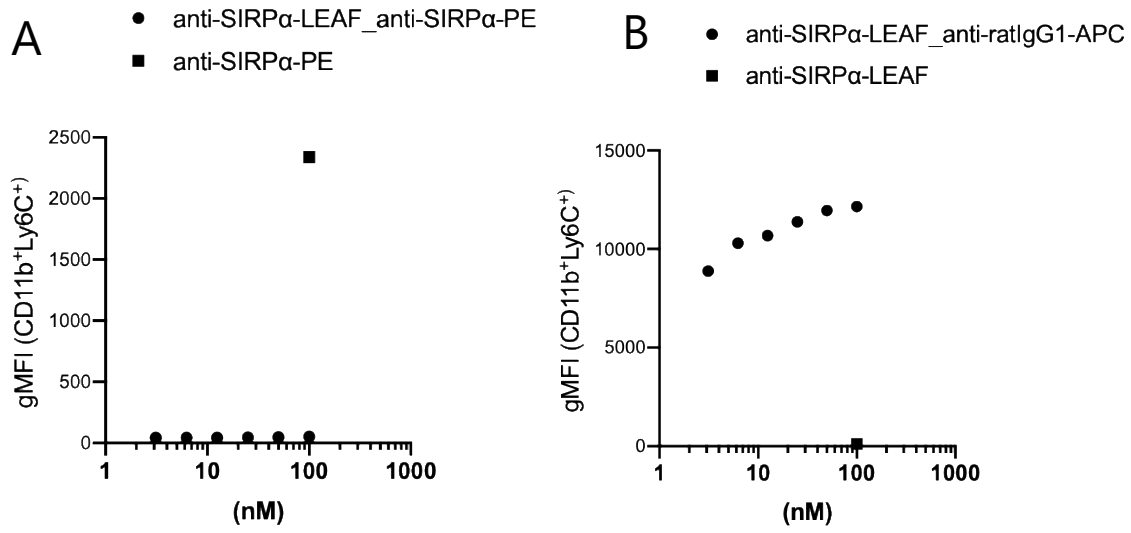

Figure 5.1. Ultra-LEAF™ P84 blocks the SIRPα epitope to detection of fluorophore conjugated P84 on Ly6C⁺ GM-CSF-TCM cells. (A) Quantification of the gMFI signal detected for fluorophore conjugated anti-SIRPα (P84) antibody after epitope blockade by Ultra-LEAF anti-SIRPα (P84) antibody on isolated Ly6C⁺ cells grown in GM-CSF-TCM. **(B)** Quantification of the gMFI signal detected after incubation with the Ultra-LEAF anti-SIRPα (P84) antibody, and detected by a fluorophore conjugated anti-ratIgG1 antibody. (A and B) The X axes with the concentration of the antibody used were transformed in logarithmic scale (X=Log(X)). Assay n=1 in triplicate.

This confirmed that this method could be used to determine the *in-situ* bioavailability of the anti-SIRPα antibody thus connecting the potential therapeutic effects to successful delivery to the tumour site. Moreover, this should give indication that the antibody concentration dose and the length of the *in vivo* experiments were functional to allow tumour localisation and potential therapeutic effect.

5.2 CD47-SIRPα blockade slows tumour growth in vivo

B16-F10 melanoma bearing mice received the first dose of anti-SIRPα at day 5, when tumours were palpable, followed second dose on day 8 at the concentration of 5mg/kg (figure 5.2 A). Alongside mice receiving the therapy, one group of mice was injected with PBS and the other with a rat-IgG1 control.

By day 11, we appreciated a significant reduction in tumour volume for the mice dosed with anti-SIRPα (figure 5.2 B). We noted first that in this time frame the tumours growth was stalling but were not regressing yet. It is possible, that we are at the peak immune response and would see a greater regression if we take the experiment out further as noted for other ICIs used in the lab. Second, the rat-IgG1 was potentially inducing a partial immune response highlighting the importance of comparing it to the therapy group.

Examining individual tumours for each cohort provided further evidence supporting the anti-SIRPα therapeutic effect (figure5.2 C-E). While the tumours in the mice injected with PBS and IgG showed exponential increase of their size, the mice receiving therapy showed slower growth already after the first dose, which was strengthened by the second injection to either maintain or support initial stages of shrinkage. We can speculate that the dosage and the time between injections were capable of inducing an inflammatory state and remodelling of the microenvironment sufficient to support a tumour growth reduction.

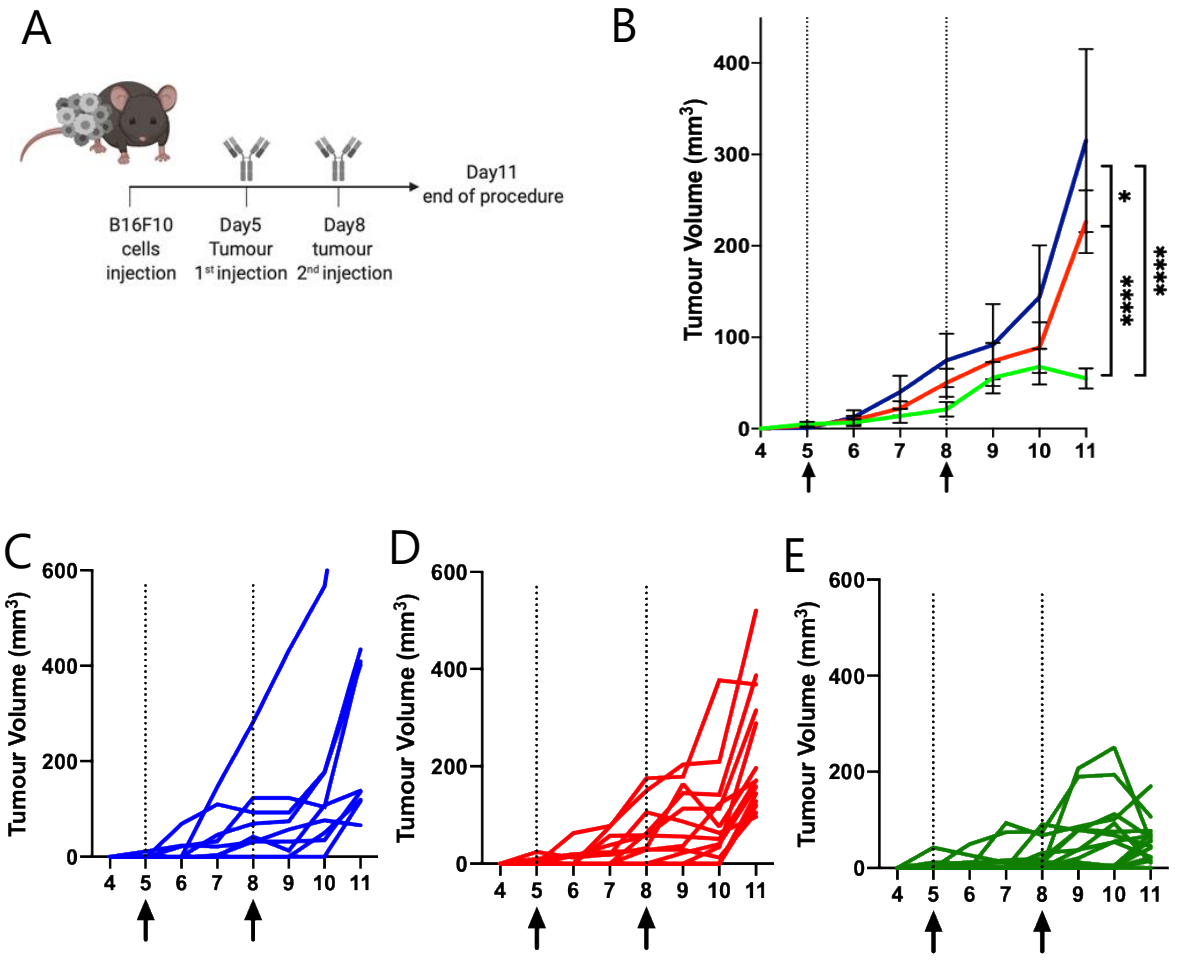

Figure 5.2. SIRPα blockade slows growth of established tumours in vivo. (A) Schematic representation of the experiment treatment strategy in palpable tumours. **(B)** Tumour volume growth curves (mm3) for mice injected with PBS (blue), rat-IgG1 (red) and anti-SIRPα-P84 (green). **(C)** Tumour growth for each animal injected with **(C)** PBS, (**D)** rat-IgG1 or **(E)** anti-SIRPα-P84 antibody). (B) Data are mean ± SEM; * = p < 0.05, = p < 0.001, **** = p<0.0001 using the ordinary 2way ANOVA with a Tukey's post hoc test. Total mice n=9 from 3 independent experiments (PBS) and n=14 (rat-IgG1) and n=15 (anti-SIRPα-P84) from 5 independent experiments.

5.2.1 Myeloid cells remodelling by SIRPα blockade in the TME.

Having observed that monoclonal anti-SIRPα therapy diminished tumour grow rate, we then examined changes in the myeloid cells given the big role they play in remodelling of the tumour microenvironment. Using the same marker panels as for the initial characterisation of the melanoma, we obtained an overview of the myeloid modification state related to the therapy. One of the main effects of blockade was on the percentage of cDC1. After receiving anti-SIRPα their abundance almost doubled compared to the PBS control, and was significantly higher compared to the rat-IgG1 injected mice (figure 5.3 A). This suggested that this population, which is correlated to inflammation and positive patient outcome was increased upon therapy and could play a role in delaying the tumour growth.

In chapter three, the cDC2 and monocytes derived myeloid cells showed an increase in immunosuppressive markers between day 5 to day 11. In this period, the cDC2 decreased their presence whilst the monocytic myeloid cells increased and expressed more PD-L1, FasL and ARG1.

Anti-SIRPα therapy showed a clear trend to reduce the frequency of cDC2 cells when comparing with IgG1 control whilst no difference was visible when compared with the PBS treated mice (figure 5.3 B). moDCs also showed a reduction compared to the IgG control and a reduction tendency compared to PBS (figure 5.3 C). In concomitance the M-MDSCs tended to be lower when compared to PBS control but higher when comparing to the IgG1 control (figure 5.3 D). In the previous chapters we noticed that the M-MDSCs expressed less immunosuppressive molecules than the moDC, thus it was possible that the moDCs number reduced because couldn't develop from the less mature M-MDSCs which, indeed tended to increase their number.

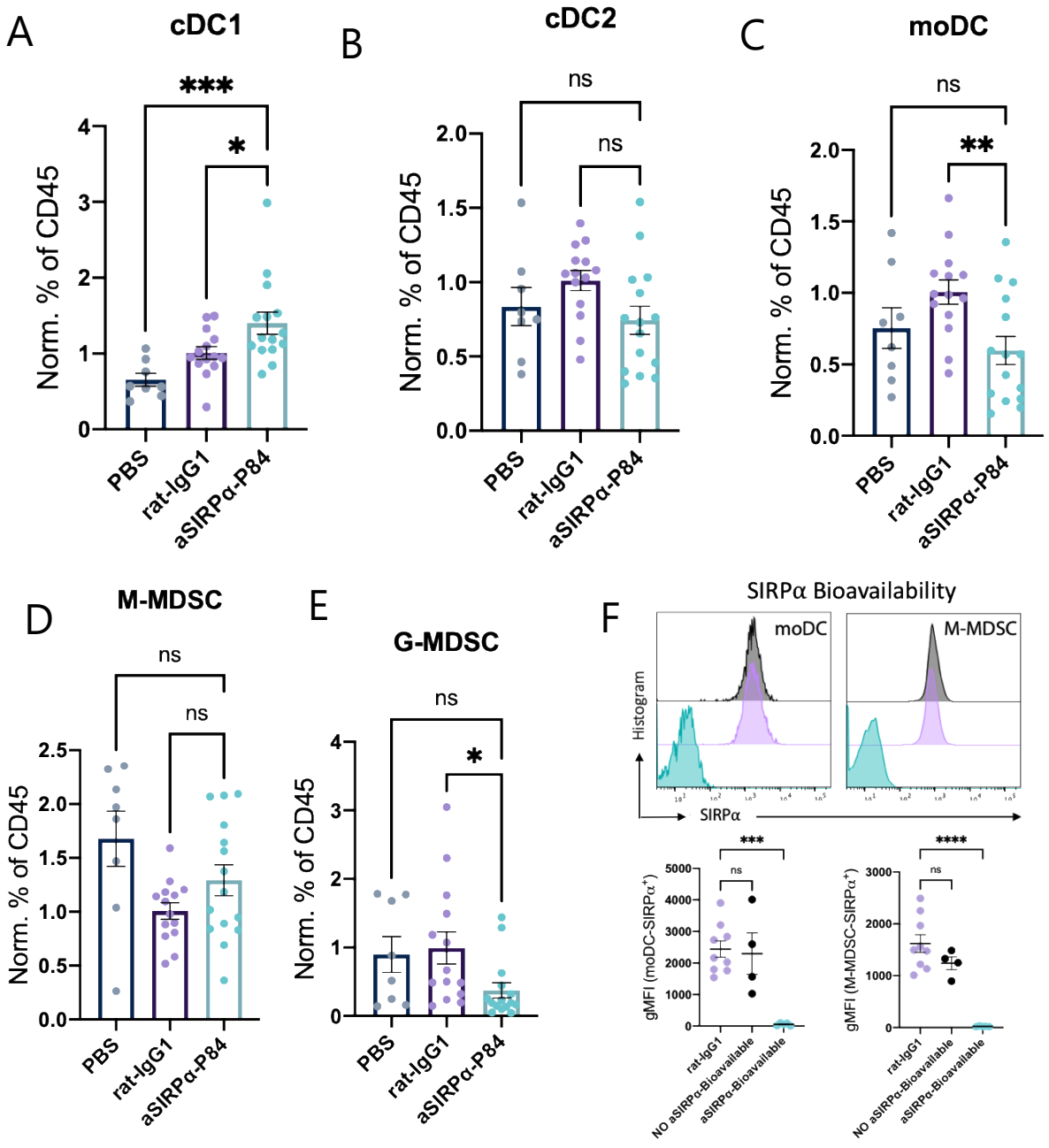

Figure 5.3. SIRPα blockade induced remodelling of the myeloid compartment. Quantification of **(A)** cDC1 ($CD11c^+XCR1^+$), **(B)** cDC2 ($CD11c^+CD11b^+Ly6C^-$), **(C)** moDC ($CD11c^+CD11b^+Ly6C^+$), **(D)** M-MDSC ($CD11c^-CD11b^+Ly6C^+$) and **(E)** G-MDSC ($CD11c^-CD11b^+Ly6G^+$) cells calculated as percentage of total $CD45^+$ cells for PBS and rat-IgG1 controls, and anti-SIRPα-P84 antibody. **(F)** SIRPα bioavailability at the tumour site. In black are represented excluded mice from the analysis injected with anti-SIRPα. Violet describes mice injected with the rat-IgG1 control. In light blue are represented mice included in the analysis injected with anti-SIRPα. (A to F) The data were normalised by the signal detected for the rat-IgG1 injected mice samples. Data are mean ± SEM; * = $p < 0.05$, ** = $p < 0.01$, *** = $p < 0.001$ using the ordinary one-way ANOVA with a Dunnett's post

hoc test. (A-E) Total mice n=8 from 3 independent experiments (PBS) and n=14 (rat-IgG1) and n=15 (anti-SIRPα-P84) from 5 independent experiments.

Another thing to notice was the amount of G-MDSCs. Even though they were underrepresented in the tumour, they are also associated with immunosuppression. Their quantity was generally low in our characterisation, but their number was sharply increasing if new blood vessels were forming around the tumour (data not shown). Indeed, G-MDSCs are associated with a systemic expansion in later stages of the disease[753,754] , thus are brought to the tumour site preferentially via the blood stream[755]. Even though our system looked at the primary tumour lesion, the G-MDSC were constantly present and importantly were more than halved when the anti-SIRPα therapy was given (figure 5.3 E). As specified, this could be just an effect due to the smaller tumour size, hence less blood vessels and then less G-MDSCs. Despite that, SIRPα was expressed in a G-MDSCs subset, thus potentially making them sensitive to the therapy. As we mentioned before, the anti-SIRPα bioavailability at the tumour site was checked by the lack of staining and, the tumours where SIRPα was still detectable were removed from the analysis (figure 5.3 F).

In summary, the anti-SIRPα therapy induced myeloid remodelling in the TME. While the suppressive species generally were reduced, the cDC1 that are associated with T cells activation augmented. This double action could contribute to the growth deceleration observed in the tumours.

5.2.3 Analysis of the CX3CR1 (monocyte) and F4/80 (macrophage) markers expression in the myeloid clusters.

The remodelling observed after anti-SIRPα therapy indicated that suppressive cDC2, moDC and G-MDSC cells tended to, or diminished and the M-MDSC which presented lower expression of immunosuppressive molecules compared to moDCs, were less than the PBS control but more than the rat-IgG1 control. This indicated that SIRPα

blockade would stop M-MDSCs maturation towards moDCs while the inflammatory cDC1, which correlate with good prognosis, increased.

In initial analyses, the abundance of F4/80^{+}-cDC2 decreased although expression levels augmented, while CX3CR1 remained constant over tumour evolution. This might indicate a selective pressure towards a smaller but more M1-like population. In general, there was a reduction of the specialised populations expressing those markers. We now sought to determine if SIRPα blockade altered this.

cDC2, moDC and M-MDSC were positive for CX3CR1 at 60, 70 and 30% respectively. However, the monocyte marker didn't show any change in abundance between the anti-SIRPα therapy to the IgG control. While the G-MDSCs seemed to increase this could be a consequence of the low number of these cells detected in presence of the therapy (figure 5.4 A). The gMFI geometric mean was also analysed but didn't show any meaningful difference either (appendix 8.9 A).

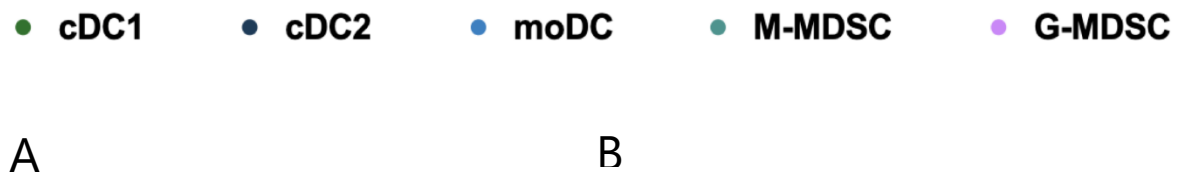

A B

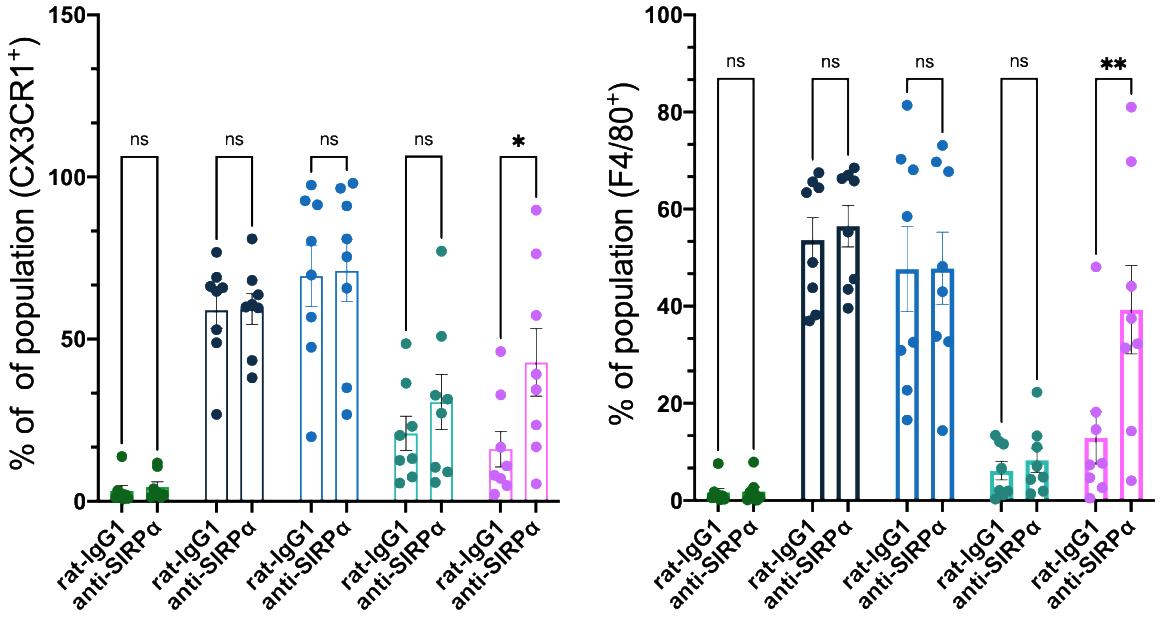

Figure 5.4. Myeloid remodelling as for CX3CR1⁺ monocyte and F4/80⁺ macrophage markers of melanoma tumour bearing mice induced by the therapeutic effect of CD47-SIRPα blockade. The graphs show the percentage of cDC1, cDC2, moDC, M-MDSC and G-MDSC positive for **(A)** CX3CR1and **(B)** F4/80 in mice groups injected with rat-IgG1 (control) and anti-SIRPα-P84 antibody. (A and B) Data are mean ± SEM; * = p < 0.05, ** = p < 0.01, *** = p < 0.001, **** = p<0.0001 using the 2way ANOVA with a Šidák's post hoc test. Assays n=4 in duplicate.

Measurement of F4/80 was very similar to the CX3CR1. The abundance of cells expressing this macrophage marker associated with an M1 inflammatory phenotype didn't alter between conditions, although, we could observe a distribution between clusters. G-MDSC again showed to increase F4/80 frequency but this could depend by the low number of cells present in the samples. In this case too, the gMFI geometric mean associated with each myeloid population didn't reveal significant changes when comparing therapy and control (appendix 8.9 B).

From this analysis we couldn't conclude that the anti-SIRPα was remodelling the cells expressing the markers associated with macrophage M1 and monocytes. The therapy remodelled the entire landscape of myeloid cells in the TME, but this wasn't reflected by these last two markers.

5.2.4 Analysis of immune suppression associated markers expression in the myeloid clusters.

We next profiled immune modulatory molecules expressed following treatment, first focusing on PD-L1 and ARG1 because of diminished expression upon SIRPα blockade in *vitro*. It was very difficult to detect significant shifts between treatment groups. Regarding PD-L1, cDC2 cells showed a decreasing tendency of expression upon SIRPα blockade (figure 5.5 A) as did moDCs (figure 5.5 B). However, the M-MDSC didn't show any difference between the anti-SIRPα and rat-IgG1 samples but a decrease when comparing with PBS (figure 5.5 C). As PD-L1 is one of the most represented molecules expressed by myeloids it is possible that slight, but functionally significant variations in expression would not be detected by flow cytometry.

Having previously observed increasing ARG1 expression during tumour evolution we also measured expression upon SIRPα blockade. Expression across the populations barely changed, although cDC2 cells showed some sensitivity in this regard, with a decreasing trend of ARG1 after anti-SIRPα injection (figure 5.5 D). moDC cells showed a very slight decrease (figure 5.5 E), but no differences were detected for M-MDSCs (figure 5.5 F).

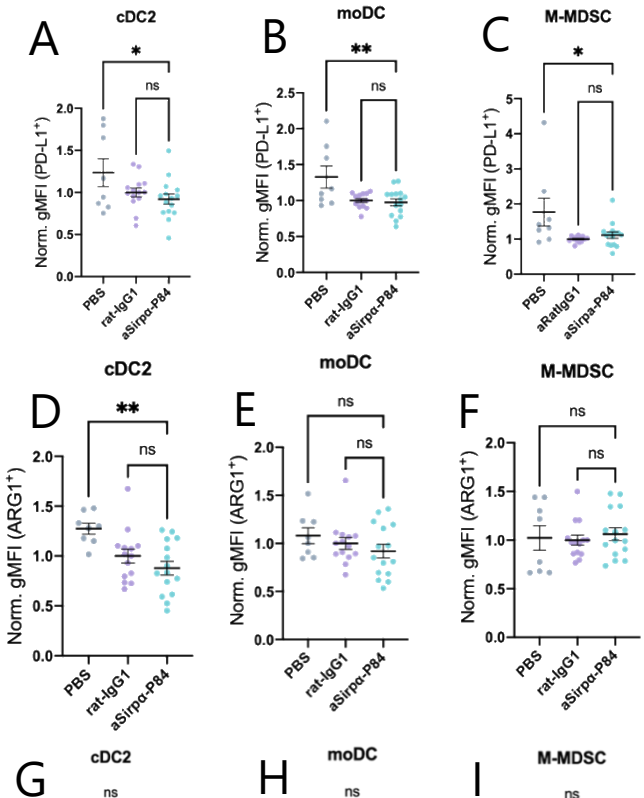

Figure 5.5. Myeloid function-associated-markers remodelling in melanoma tumour bearing mice induced by the therapeutic effect of CD47-SIRPα blockade. The graphs show **(A to C)** PD-L1, **(D to F)** ARG1, **(G to I)** FasL and **(L to N)** NOS2 gMFI variation associated to cDC2, moDC and M-MDSC cells in mice groups injected with PBS (control), rat-IgG1 (control) and anti-SIRPα-P84 antibody. (A to I) The data were normalised by the signal detected in the rat-IgG1 injected mice samples. Data are mean ± SEM; * = $p < 0.05$, ** = $p < 0.01$, using the ordinary ANOVA with a Dunnett's post hoc test. Total mice n=8 from 3 independent experiments (PBS) and n=14 (rat-IgG1) and n=15 (anti-SIRPα-P84) from 5 independent experiments. The data were normalised by the signal detected in the rat-IgG1 injected mice samples. (L to N) Data are mean ± SEM; ns = $p > 0.05$, using the unpaired t test. Mice n=4 for each group from two independent experiments.

In chapter three we characterised other markers associated with potential immunosuppressive mechanisms, the FasL and NOS2 which were also analysed in the SIRPα blockade contest. As we characterised the expression of FasL by the myeloid before, which was upregulated upon GM-CSF-TCM-CD47 contact, we sought to analyse it in the context of SIRPα blockade.

FasL expression did not change in either cDC2 and moDC following treatment (figure 5.5 G and H) but, the M-MDSC were showing a tendential increase when SIRPα was blocked (figure 5.5 I). Since it was reported that in cancer MDSCs induce T cells apoptosis by FasL-Fas[686], this would be in contradiction with the observed tumour reduction if MDSCs were to induce apoptosis in T cells using this mechanism. This would need further investigation and might be associated with the regulation of the immune response or killing of tumour Fas expressing cells.

We also analysed NOS2, which we previously showed to be expressed by moDC at day 11 of tumour development. Although its expression was observed in the three myeloid populations, we were unable to detect any significative changes after anti-SIRPα therapy (figure 5.5 L to N).

The suppressive molecules showed tendencies in being modulated, then we sought to analyse MHCII to correlate the myeloid with activation of T cells.

5.2.5 The myeloid cells MHCII expression with SIRPα blockade.

Another interesting molecule that was expressed throughout the myeloid groups was the major histocompatibility complex II (MHCII). The latter loads extracellular peptides previously engulfed and processed onto the complex which migrates on the cells surface exposing the antigen to activate lymphocytes immune responses[756]. Because of the action of CD47-SIRPα blockade we thought possible that the myeloid cells

would increase the engulfed antigens coming from the tumour and consequently increase their expression via MHCII.

The cDC2 showed a slight increase in the level of MHCII expression when comparing the rat-IgG1 control with the anti-SIRPα therapy in accord with our hypothesis, but much variability was detected in PBS injected mice (figure 5.6 A). For moDCs, a trending increase was noted in comparison with the PBS samples but, the signal of the rat-IgG1 control were higher than the therapy (figure 5.6 B), while the levels of MHCII remained constant in M-MDSC irrespective of condition (figure 5.6 C). We then also examined the abundance of MHCII-expressing cells as a percentage of infiltrating $CD45^+$ cells. cDC2 cells upregulating MHCII were more frequent in rat-IgG1 and the therapy cohorts, however there was no significant difference between rat IgG and anti-SIRPα (figure 5.6 D). moDC showed a lower MHCII prevalence with therapy provided (figure 5.6 E) while the M-MDSC in contrast, showed to present more MHCII (figure 5.6 F).

Thus, when comparing rat-IgG1 and the therapy, the cDC2 and moDC showed less expression of MHCII whilst M-MDSC a tendential increase. This could be explained by the overall remodelling of the CD45 myeloid compartment upon SIRPα blockade which earlier showed a decrease in cDC2 and moDC clusters while M-MDSCs increased.

To resume, we saw reshuffle of myeloid composition and indications of a possible less suppressive environment upon SIRPα blockade *in vivo*. This wasn't as clear as we thought but, it may also be the case that at the current doses, in vivo treatment may impact localisation of infiltrating myeloid populations to modulate T cell proliferation. Therefore, the T cells status will be analysed in the next section.

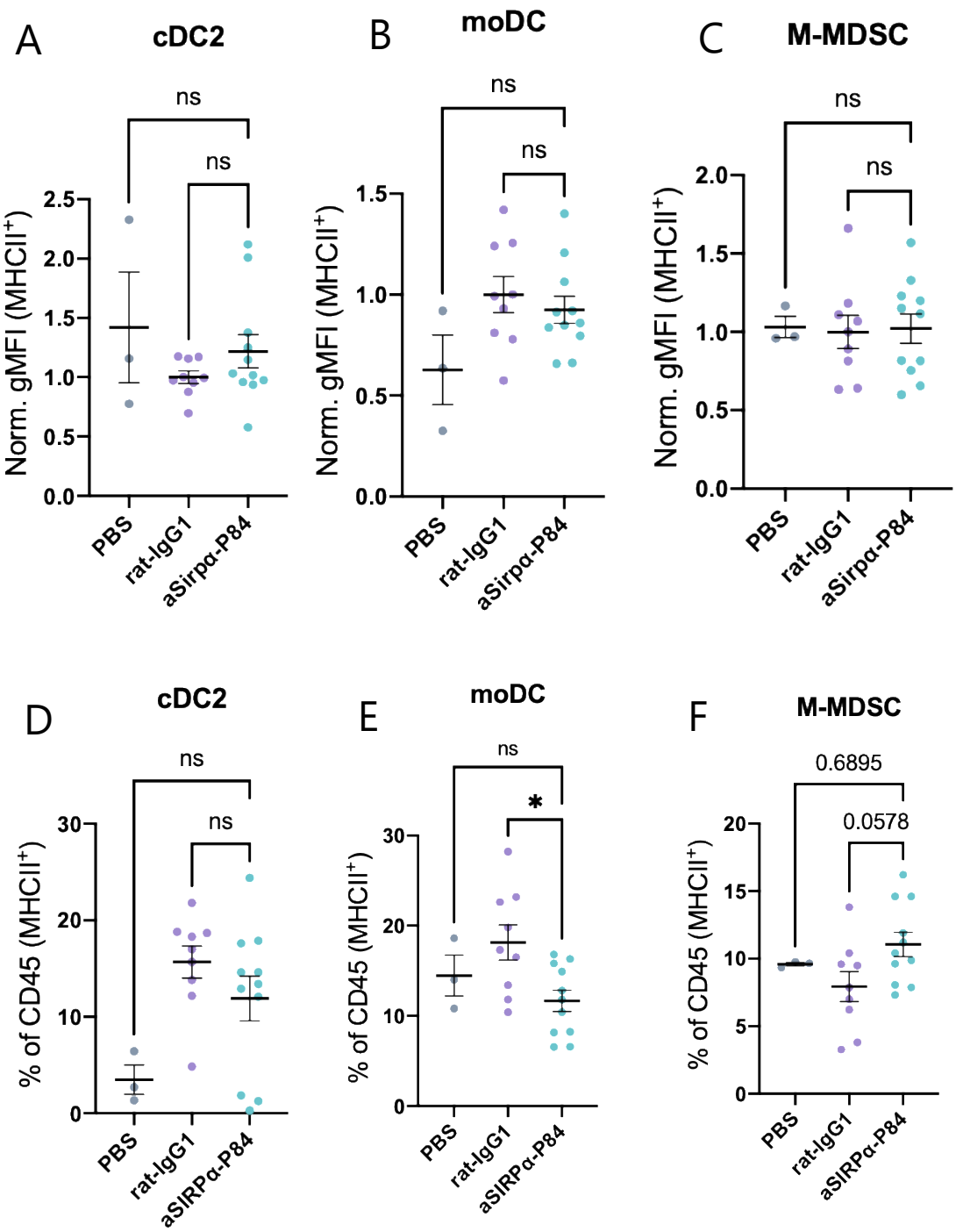

Figure 5.7. Myeloid MHCII-associated-marker remodelling in melanoma tumour bearing mice induced by the therapeutic effect of CD47-SIRPα blockade. The graphs show MHCII **(A to C)** gMFI variation and **(D to F)** percentage of total CD45$^+$ cells variation associated to cDC2, moDC and M-MDSC cells in mice groups injected with PBS (control), rat-IgG1 (control) and anti-SIRPα-P84 antibody. (A to C) The data were normalised by the signal detected in the rat-IgG1 injected mice samples. (A-F) Data are mean ± SEM; * = $p < 0.05$, using the ordinary one-way

ANOVA with a Dunnett's post hoc test. Total mice n=3 from one experiment (PBS), n=9 (rat-IgG1) and n=11 (anti-SIRPα-P84) from 3 independent experiments.

5.2.6 Therapy effect on the CD8$^+$T and Treg cells in the TCM.

With anti-SIRPα treatments reducing tumour growth, remodelling the myeloid compartment via the reduction of moDC, cDC2 and increasing inflammatory cDC1 cells, we next measured T cells. Here we focussed on the CD8$^+$ T cells and Tregs associated with patient prognosis[250,757,758]. Melanoma infiltration by CD8$^+$ T cells strongly correlated with an increased survival, while Tregs were associated with the suppression of tumour-specific T cell immunity[759,760,761]. Thus, the ratio of CD8-positive T cells versus Treg in the tumour microenvironment is predictive for survival of patients with melanoma[142].

Following SIRPα blockade, samples were stained CD8 and CD4 positive lymphocytes. The CD4$^+$ T cells were further stained for the expression of the protein forkhead box P3 (FOXP3) which is a master regulator of the regulatory pathway in the development and function of regulatory T cells[762,763]. Hence, we distinguished CD45$^+$CD8$^+$ T cells and CD45$^+$CD4$^+$FOXP3$^+$ T regulatory cells (figure 5.7 A). SIRPα blockade resulted in a 1.5-fold increase in CD8 T cell infiltration (figure 5.7 B), but there was no significant difference in Treg infiltration between the anti-SIRPα therapy and the rat-IgG1 control (figure 5.7 C). Calculation of the ratio between the count of CD8$^+$ T cells and Tregs enabled us to determine if the T cell balance would be in favour of clearance. Indeed, SIRPα blockade shifted the ratio in favour of CD8 positive infiltrating lymphocytes, which were approximately 1.5-fold more abundant than the T regulatory cells (figure 5.7 D).

Overall, these data indicate changes in T cells infiltration related to the anti-SIRPα therapy towards more infiltration and more potent T cell response. Together with

earlier data on myeloid cells, it is possible that these observations are interconnected by the phagocytosis boost effect reported *in vitro*. Here SIRPα blockade and disruption of the "do not eat me" signal would support the moDC and M-MDSC cells to engulf more debris, more antigen processing and presentation and a greater immune response activation. This will be clarified in the coming sections.

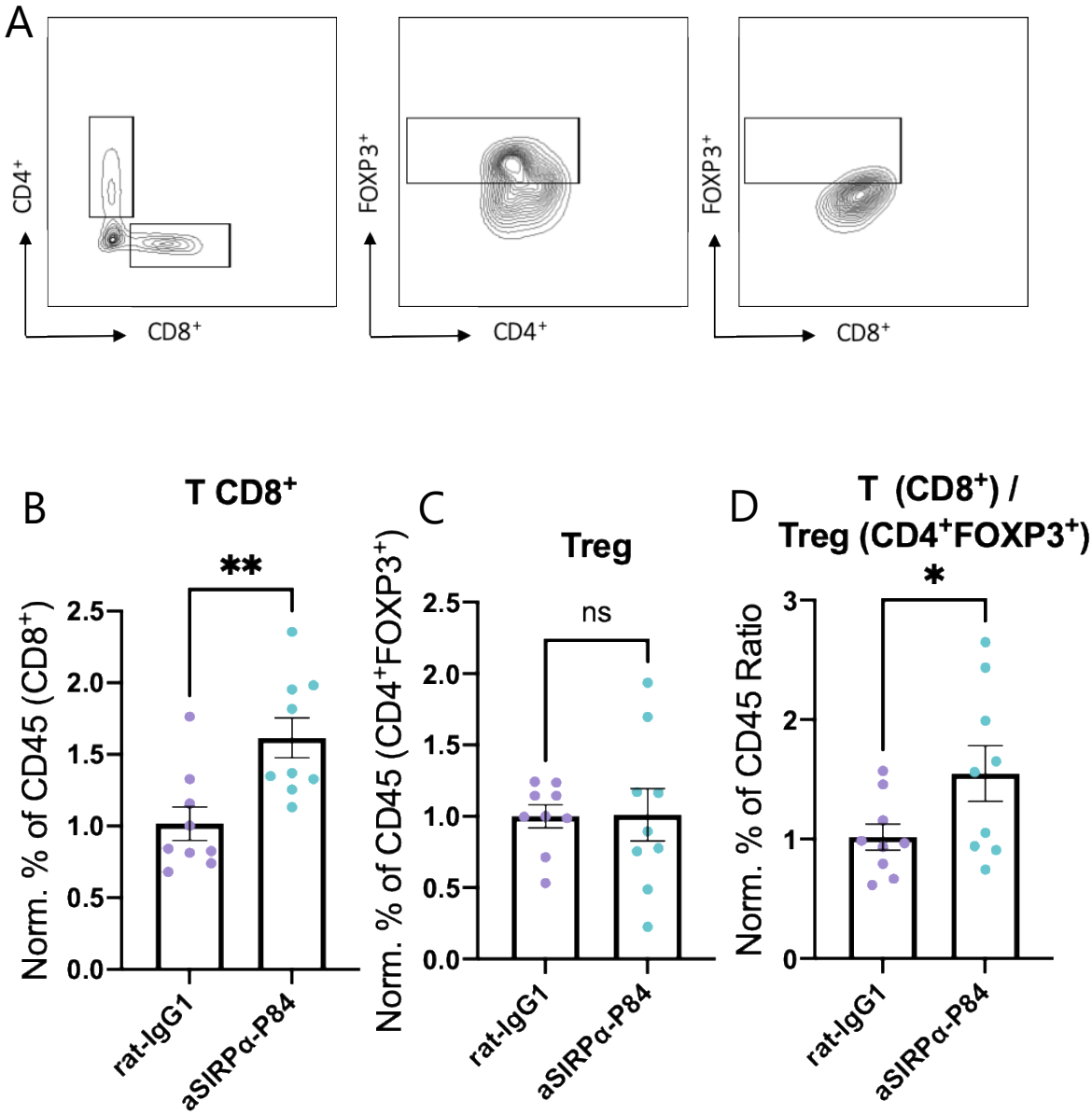

Figure 5.7. SIRPα blockade supports T cell infiltration towards immune clearance. (A) Representative FACS plots of the gating strategy used to calculate $CD8^+$ T and $CD4^+FOXP3^+$ T cells. Quantification of **(B)** $CD8^+$ T cells calculated as percentage of the total $CD45^+$ cells, **(C)** $CD4^+FOXP3^+$ T cells calculated as percentage of the total $CD45^+$ cells, **(D)** ratio of $CD8^+$/ $CD4^+FOXP3^+$ T cells. The data were obtained by mice groups injected with rat-IgG1 (control) and anti-SIRPα-P84 antibody. (B to D) The data were normalised by the signal detected in the rat-IgG1 injected mice samples. Data are mean ± SEM; * = $p < 0.05$, ** = $p < 0.01$, using the unpaired t test. Assays n=3 for each group from 3 independent experiments.

Together, these trends suggest that the anti-SIRPα treatment may be influencing the whole process of antigen presentation. Hence, the main mechanism to explain the reduction in tumour growth could be found in the SIRPα blockade enhancement of phagocytosis, antigen processing and presentation.

5.3. Phagocytosis increase due to anti-SIRPα therapy in tumour bearing mice.

Having determined that remodelling of the myeloid cell clusters in the TME followed anti-SIRPα therapy which coincided with an increase of T $CD8^+$ cells infiltration and reduced tumour volume, we then sought to determine the underlying mechanism of action. *In vitro*, we earlier saw how anti-SIRPα was able to boost the ability of moDCs and M-MDSCs to engulf cellular debris overcoming the CD47 activated "do not eat me" signal. This mechanism could be responsible of the effects seen on the myeloid cells remodelling to explain the tumour reduction by anti-SIRPα therapy. However, we demonstrated this in a setting where half of the cells to engulf were killed to artificially generate debris to simulate the death cells coming from the tumour. Thus, it was necessary to determine if the same mechanisms also occurred in an *in vivo* setting.

Using GFP-labelled B16-F10 to generate tumours (figure 5.8 A), we would be able to detect if the fluorescent tumour cells were phagocytosed by myeloids to a greater extent in an anti-SIRPα therapeutic setting. Tumour-bearing mice received two doses of anti-SIRPα antibody at day 5 and day 8 as previously described. However, this time, mice were culled twenty-four hours later (figure 5.8 B) to provide a window in which we could detect enough engulfed dead green tumour cells in the myeloid populations.

As before, there wasn't much difference between therapy and control until the second injection, and by day 9 we started to observe a deceleration of growth in treated animals (figure 5.8 C).

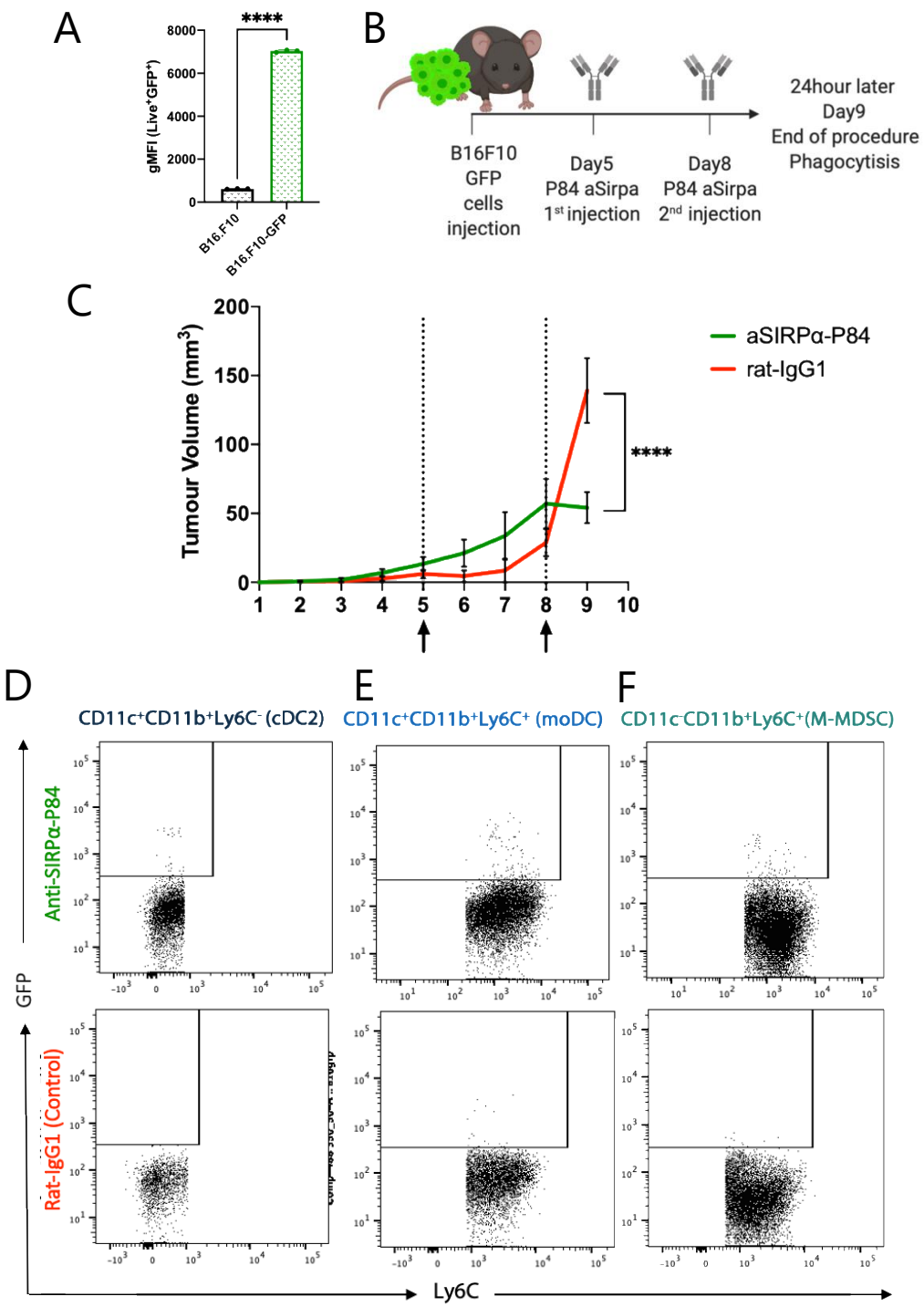

Figure 5.8. Phagocytosis of myeloid cells in GFP-melanoma tumour bearing mice was induced by CD47-SIRPα blockade. (A) Quantification of gMFI of the GFP fluorescent protein in a stably transduced B16-F10 melanoma cell line. **(B)** Schematic representation of the therapeutic strategy. **(C)** Tumour volume growth curves (mm3) for GFP-tumour bearing mice groups injected

with rat-IgG1 (red) and anti-SIRPα-P84 antibody (green). **(D-F)** Representative FACS plots of the gating strategy used to compare GFP^+ cDC2, moDC and M-MDSC cells between anti-SIRPα injected mice and control. (A) Data are mean ± SD; **** = $p<0.0001$ using the unpaired t test, Assays n=1 in triplicate and (C) 2way ANOVA with a Šidák's post hoc test. Mice n=4, two independent experiments.

The mice were culled, and the tumours extracted to be analysed using flow cytometry. Using the previous gating strategy, we selected cDC2, moDC and M-MDSC from the pool of $CD45^+$ live cells. Examination of tumours by flow cytometry confirmed that we were indeed able to detect GFP^+ signal within myeloid populations. Despite the monocyte/ macrophage fast turnover[764,765,766], we showed that *in vivo* we can detect phagocytosis of tumour material as we did *in vitro* (figure 5.8 D-F). This provides a direct readout of myeloid functionality in response to therapy.

We determined the phagocytic capacity of tumour infiltrating cDC2, moDCs and M-MDSC. First, we used gMFI to measure the amount of ingested material by each of the populations (figure 5.9 A-C). We detected a tendential increase in the level of uptake by moDC following anti-SIRPα therapy, and the cDC2 and M-MDSC showed a significant increase of phagocytosis amount (figure 5.9 A-C). We then examined if more cells were becoming green following treatment as percentage of the total $CD45^+$ cells.

This showed a clear and significant increase in the frequency cDC2, moDC and M-MDCS phagocytosing the GFP tumour cells when the anti-SIRPα therapy was administered. Compared to rat-IgG1 control, cells phagocyted almost two times more for moDCs and M-MDSCs and one and a half times for cDC2, demonstrating a certain grade of sensitivity to the CD47-SIRPα blockade (figure 5.9 D to F).

Such an increase of the phagocytosis rates confirmed how interrupting the CD47 "do not eat me signal" in vivo was able to boost the uptake of tumour-derived material as a first step towards inflammatory function. Phagocytosis is then followed by digestion and antigen processing in order to present the antigen on the surface of the

membrane and activate innate and adaptive immunity against a pathogenic insult. Hence, it was necessary to next demonstrate how the anti-SIRPα disruption, aside increasing phagocytosis would also boost antigen processing and presentation.

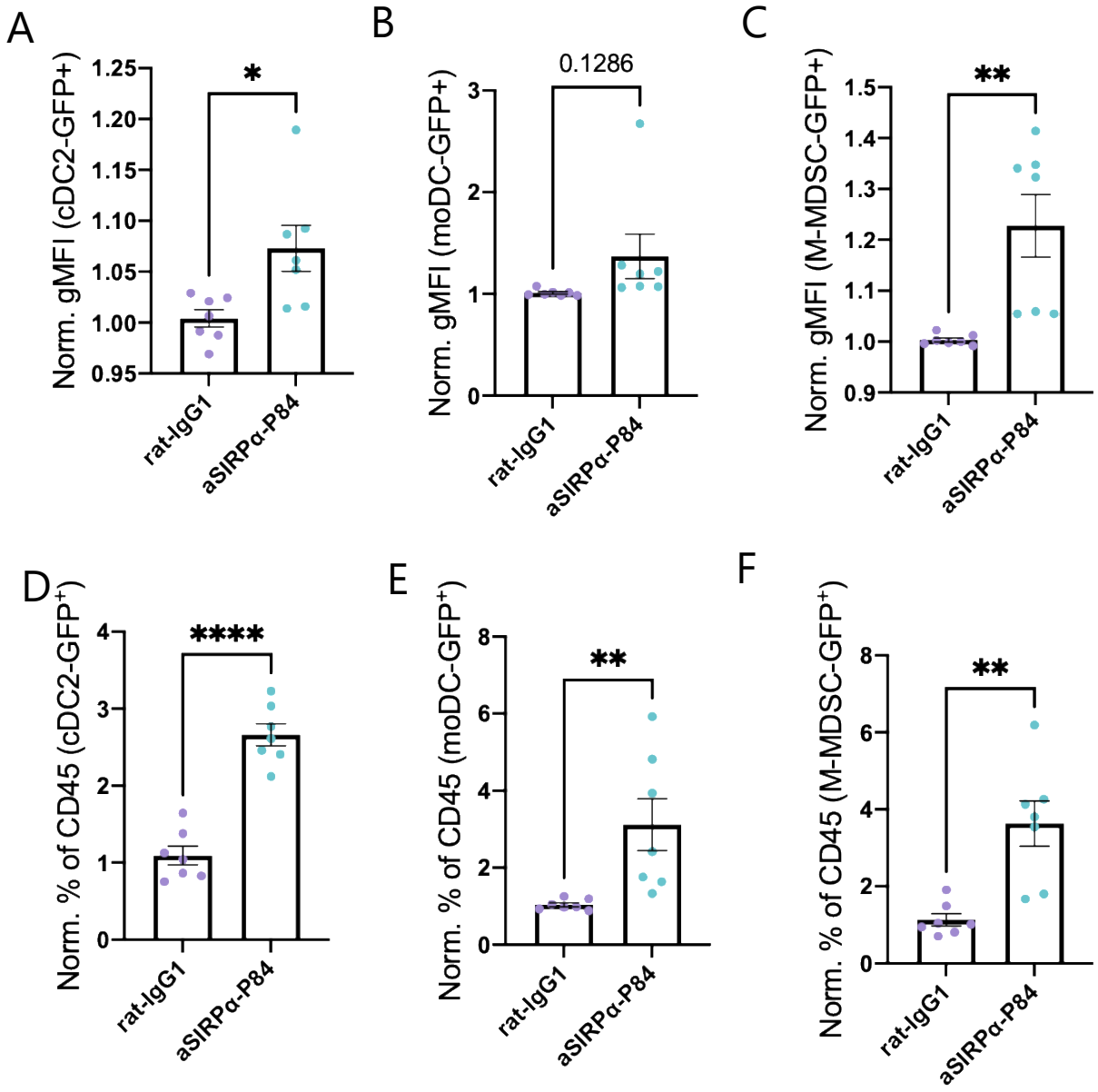

Figure 5.9. Myeloid cells phagocytosis of GFP⁺-melanoma cells from GFP⁺-tumour bearing mice induced by the therapeutic effect of CD47-SIRPα blockade. The graphs show the cDC2, moDC and M-MDSC that phagocyted the GFP⁺-tumour cells as **(A to C)** gMFI of GFP⁺ myeloid cells, **(D to F)** percentage of CD45⁺GFP⁺ cells for each population, in mice groups injected with rat-IgG1 (control) and anti-SIRPα-P84 antibody. (A to F) The data were normalised by the signal detected in the rat-IgG1 injected mice samples. Data are mean ± SEM; * = $p < 0.05$, ** = $p < 0.01$, *** = $p < 0.001$, **** = $p<0.0001$ using the unpaired t test. Mice n=4 in two independent experiments.

5.3.1 The antigen processing modulation of the cDC2, moDC and M-MDSC cells by the CD47-SIRPα interaction.

Antigen processing is composed by protein internalization, denaturation, reduction, and proteolysis, followed by association of the resulting peptides with MHC molecules and surface expression. To determine if the myeloid cells were also able to increase antigen proteolysis upon anti-SIRPα CD47 blockade we utilized DQ ovalbumin. This is a model to study processing of soluble antigen and a suitable model to understand if the suppressive myeloid we generated were able firstly, to utilise this mechanism and secondly, if this could be modulated removing the CD47-SIRPα interaction. If an increase would be confirmed, it may be an indicator that tumour debris would be processed in a similar manner. More antigen proteolysis and accumulation in cellular organelles may be associated with increased antigen presentation by APCs. Thus, we looked at this intermediate step expecting that upon SIRPα blockade the myeloid cells would process more antigen due to the higher phagocytosis. Ovalbumin (OVA) is one of the major constituents of the egg white. This allergen is recognised as a non-self-antigen and induces an immune response; hence it was widely utilized as a model antigen to evaluate immune activation in experimental vaccine delivery or as a pseudo-tumour antigen in transgenic cancer cell lines. While OVA has been successively coupled to a fluorescent protein for studying the real-time kinetics of antigen uptake in live cells, a drawback is its sensitivity to pH. Thus, we utilized DQ-OVA, which is a self-quenched BODIPY conjugated form of OVA, emitting green fluorescence upon proteolytic degradation. This substrate is designed especially for the study of antigen

uptake[767] and processing[768]. DQ-OVA is non-fluorescent until is cleaved by proteases inside, at which point fluorescence is proportional to the degree of processing.

Myeloid cells generated in GM-CSF-TCM *in vitro* were treated with CD47 active protein, anti- SIRPα, or both as previously described. Samples were let recover for three hours and then pulsed 10 minutes with with DQ-OVA, washed and incubated 35 minutes to allow processing, and then stained for myeloid markers and flow cytometric analysis of DQ-OVA processing.

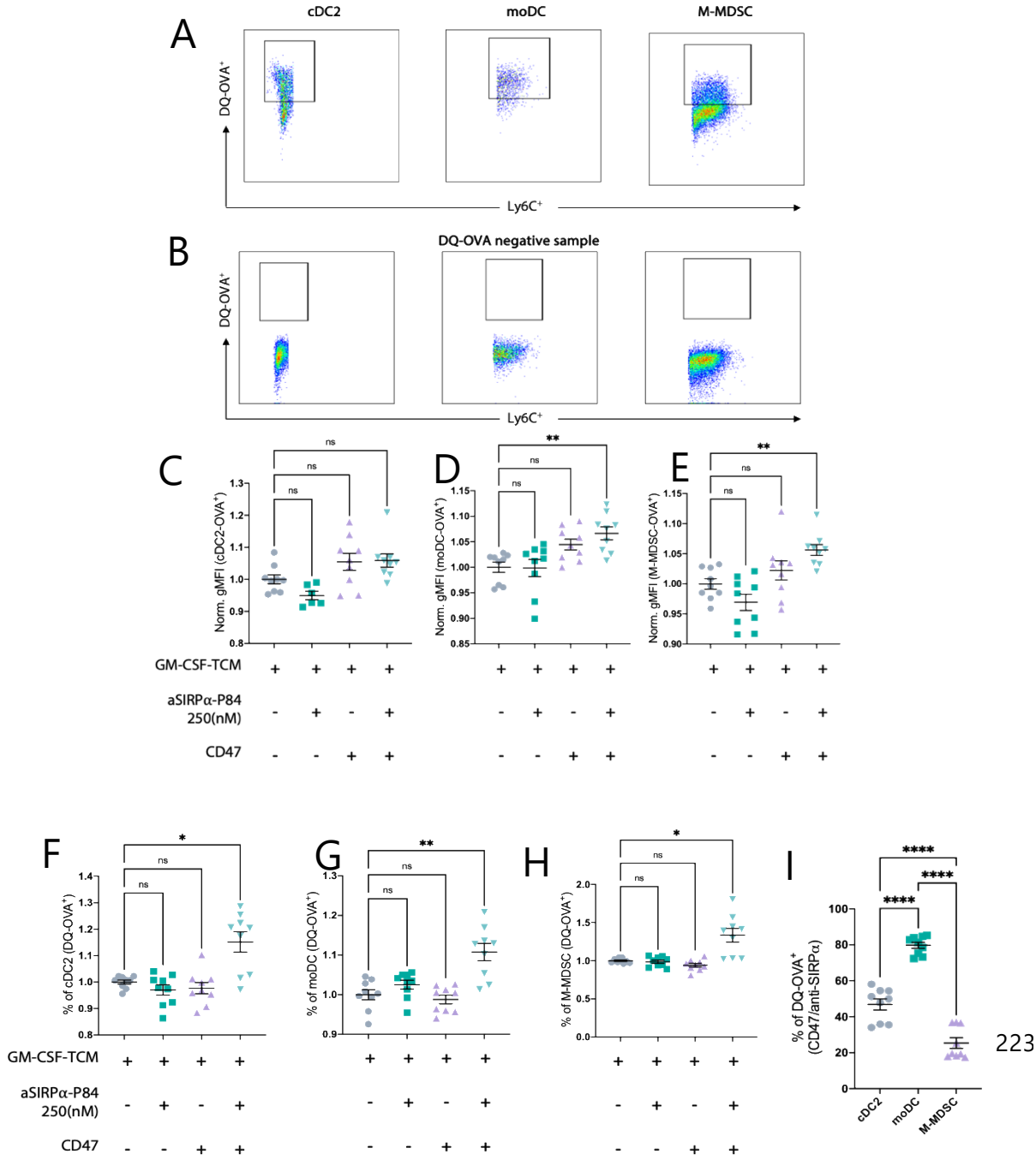

Figure 5.10. GM-CSF-TCM grown cDC2, moDC and M-MDSC cells DQ-OVA antigen processing induced by anti-SIRPα antibody. (A) Representative cytofluorimeter plots of the gating strategy used to calculate DQ-OVA positive cells. **(B)** Representative cytofluorimeter plots of DQ-OVA negative cells. **(C to E)** DQ-OVA$^+$ cells calculated as gMFI of cDC2, moDC and M-MDSC cells. **(F to H)** DQ-OVA$^+$ cells calculated as percentage of cDC2, moDC and M-MDSC cells. The GM-CSF-TCM grown myeloid cells were incubated with DQ-OVA in presence of GM-CSF-TCM media (control), GM-CSF-TCM and anti-SIRPα-P84 antibody, GM-CSF-TCM-CD47, GM-CSF-TCM-CD47 and anti-SIRPα-P84 antibody. **(I)** Percentage of DQ-OVA positive cDC2, moDC and M-MDSC upon SIRPα blockade. (C to H) The data were normalised by the signal detected in the GM-CSF-TCM (control) samples. Data are mean ± SEM; * = $p < 0.05$, ** = $p < 0.01$, using the ordinary one-way ANOVA with a Dunnett's post hoc test. (I) Data are mean ± SEM; **** = $p<0.0001$ using the ordinary one-way ANOVA with a Tukey's post hoc test. Assays n=3 in triplicate.

The cDC2, moDCs and M-MDSC were clearly able to internalise and proteolyze DQ-OVA as indicated by the green signal (figure 5.10 A and B), however cDCs and moDCs were more efficient than M-MDSC.

Across treatments, the degree of antigen processing was quantified. cDC2 didn't show a significant change in the amount of processing with any of the treatments (figure 5.10 C), but moDCs did show a significant shift when the anti- SIRPα was blocking the interaction with the CD47 active protein which was coating the wells (figure 5.10 D).

A similar behaviour was observed for the M-MDSCs, the presence of the antibody produced a slight decrease in antigen processing while there was any difference between baseline and CD47 only. The increase was detected again when both proteins were in the solution with the myeloid cells (figure 5.10 E). Examining an earlier time point may have shown a greater difference in the rate of processing between treatments.

We then measured, if the variation of the percentage of positive cells able to process antigen was impacted by the treatments. Here, cDC2 cells showed a slight (10%)

increase when the CD47 signal was disrupted by the anti-SIRPα antibody (figure 5.10 F). The moDCs variation was also effective upon SIRPα blockade but smaller when compared to cDC2 (figure 5.10 G). The M-MDSCs enhanced the most in processing DQ-OVA with CD47-SIRPα disruption (figure 5.10 H). To notice the percentage of population positive for DQ-OVA varied between the myeloid populations. With disrupted CD47-SIRPα the cDC2, moDC and M-MDSC were respectively positive at 50%, 80% and 25% (figure 5.10 I), thus the variation is related to the percentage of cells capable of increasing processing.

Together, these data begin to show that the wider antigen processing pathway is impacted by SIRPα blockade. However, whether this extended to impact the level of antigen presentation in the surface of myeloid populations, thereby modulating T cell responses remained to be determined.

5.3.2 The antigen presentation modulation due to anti-SIRPα therapy in tumour bearing mice.

Now, having seen that cDC2, moDCs and M-MDSCs were modulated by the disruption of the CD47-SIRPα interaction in terms of phagocytosis and antigen processing, we wanted to determine if the phagocytised processed antigen was then also presented on the surface of the myeloid cells. This is a crucial aspect of the activation of the adaptive immune response by $CD8^+$ and $CD4^+$ T cells[769].

We utilized an OVA transfected B16-F10 cell which expresses OVA as pseudo-tumour antigen that is processed and presented to OVA- specific T cells[74]. This was used to verify if the SIRPα blockade would increase the antigen presentation by myeloid

populations within the TME. Antigen presentation was detected using and antibody recognizing the ovalbumin Kb-binding peptide, SIINFEKL, when complex with MHCI [770].

As before, B16-OVA cells were injected in C57BL/6 syngeneic mice and tumours were treated with anti-SIRPα injected on the fifth and eighth day (figure 5.11 A). Mice were culled twenty-four hours later. Consistent with earlier experiments, effect of SIRPα blockade on growth could be seen after the second dose (figure 5.11 B).

Single cell suspensions were analysed by FACS, and an antibody recognising SIINFEKL was used to quantify if OVA was presented on the surface of cDC2, moDC and M-MDSC. moDCs were the more prone to present the OVA, but the peptide could be detected in each population (figure 5.11 C). This signal was actually very close to what we saw when the SIRPα was measured on the surface of the myeloid groups. As a positive control we checked the binding of the SIINFEKL antibody on CD45 negative cells representing the tumour formed by injecting B16-F10-OVA^{+} cells (figure 5.11 D).

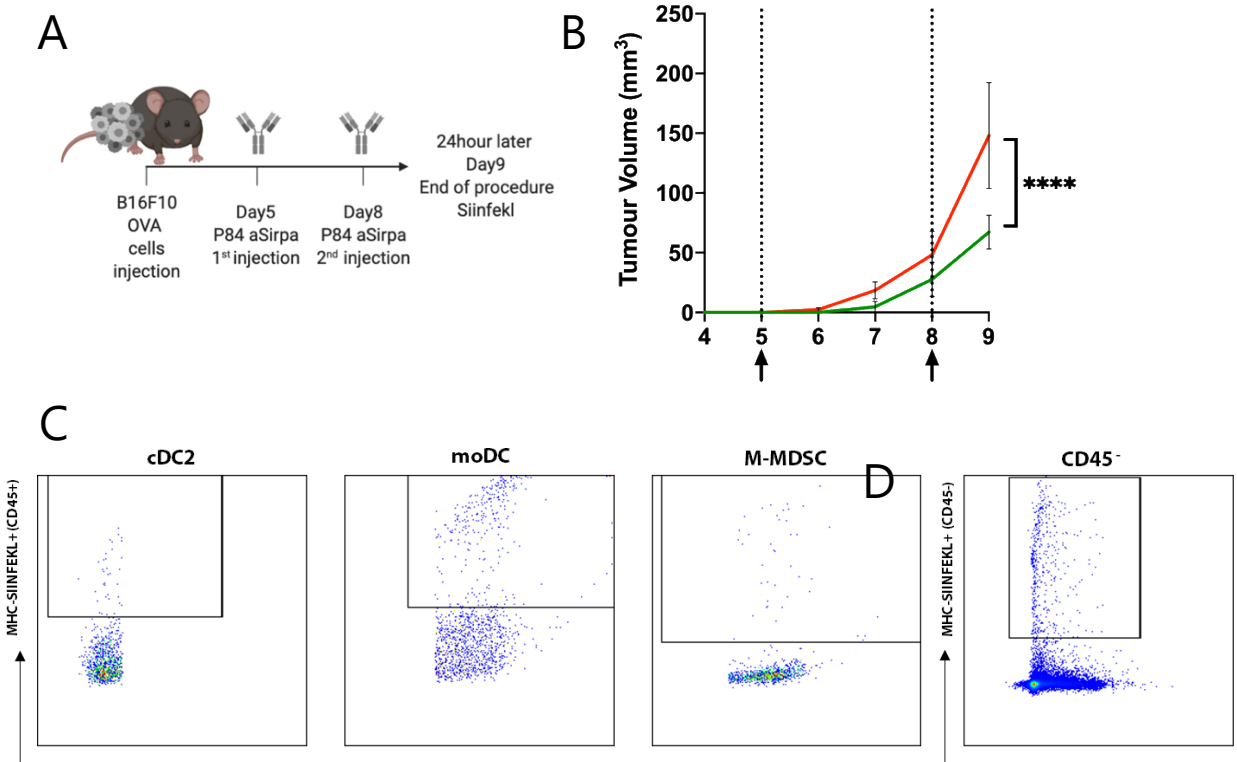

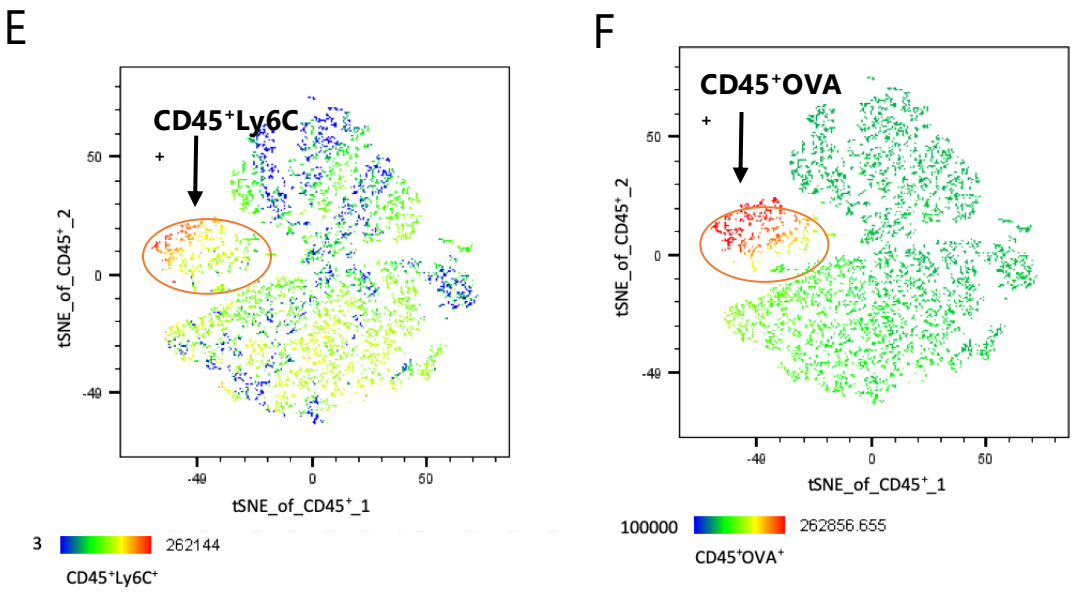

Figure 5.11. OVA presentation by myeloid cells can be detected in myeloid populations in vivo. (A) Schematic representation of the therapeutic strategy. **(B)** Tumour volume growth curve (mm3) for OVA-expressing-tumours with rat-IgG1 (red) and anti-SIRPα-P84 antibody (green). **(C)** Representative flow cytometry plots showing MHC-SIIFEKL positive cDC2, moDC and M-MDSC cells. (D) Representative flow cytometry plot showing MHC-SIIFEKL positive on CD45 negative cells (tumour cells). **(E and F)** tSNE plots showing the expression of Ly6C and OVA positive cells of $CD45^+$ cells. (B) Data are mean ± SEM; **** = $p<0.0001$ using the 2way ANOVA with a Šidák's post hoc test. Mice n=4 for each group from 2 independent experiments.

To help confirm that the Ly6C positive myeloids were the population presenting the majority of the OVA peptide, tSNE visualisation was used (figure 5.11 E and F). Indeed, of all immune cells within the TME, the Ly6C expressing cluster was the one to also show a prominent SIINFEKL signal. The representative plots demonstrated a clear

overlapping of the two signals, confirming that the Ly6C$^+$ cells were also the one presenting the majority of the OVA peptide complexed with the MHCI evidenced by the fluorophore conjugated anti-SIINFEKL specific binding.

Initially, the gMFI geometric mean of anti-SIINFEKL signal was quantified for each myeloid population to determine the level of presentation and normalised by the rat-IgG1 injected mice control. The moDCs demonstrated a significant increase in expression levels whilst cDC2 and M-MDSCs showed little change (figure 5.12 A to C). We then measured the frequency of SIINFEKL-expressing cells within each myeloid group. cDC2 and moDC exhibited a significant increase in OVA-peptide expressing cells (doubling the signal) following SIRPα blockade and M-MDSC cells showed a tendency to increase (figure 5.12 D to F). This result meant that while cells were not presenting more, the frequency of cells presenting OVA-MHCI complex to incoming T cells was enhanced.

In summary, these data confirmed that following SIRPα blockade therapy, antigen uptake, processing and eventual presentation on the myeloid cell surface was enhanced. This was correlated with increased CD8 infiltration and a reduction in tumour size.

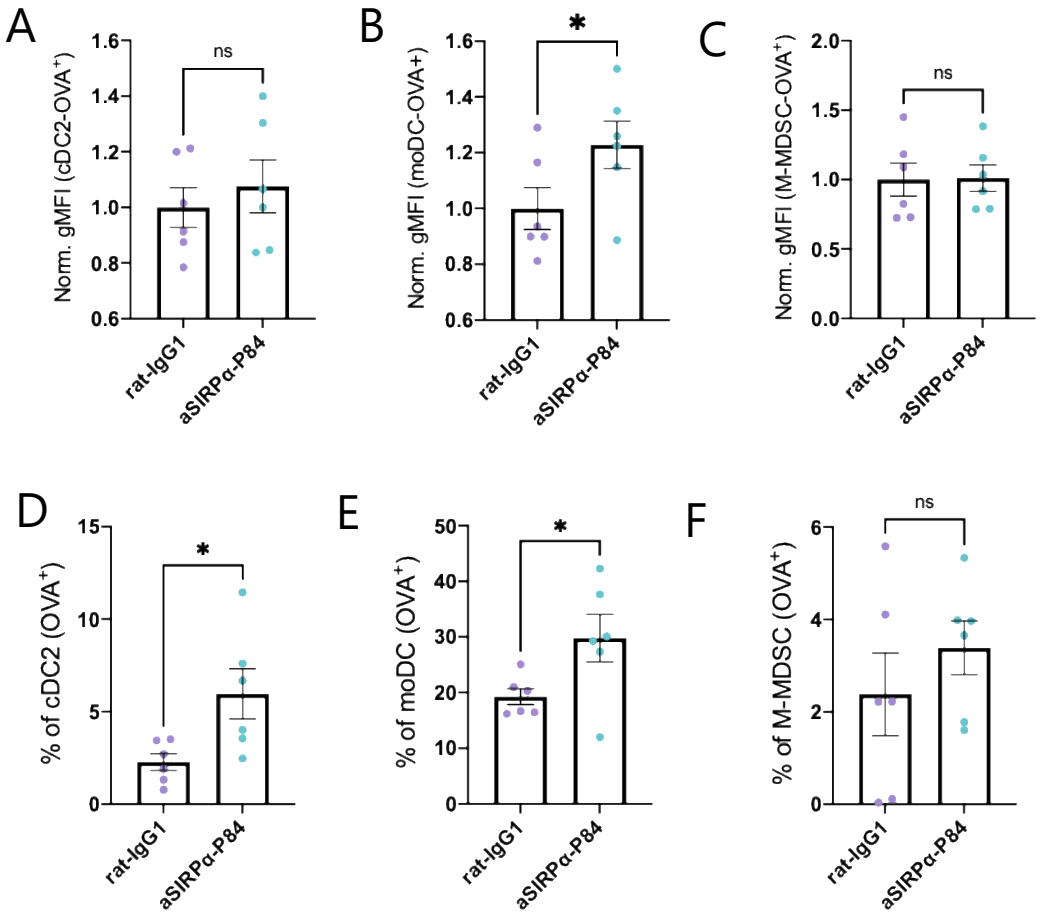

Figure 5.12. Presentation of the OVA peptide acquired from uptake of OVA-expressing-melanoma cells was enhanced after CD47-SIRPα blockade. The graphs show the cDC2, moDC and M-MDSC presenting OVA peptide acquired phagocyting OVA-expressing-tumour cells as **(A to C)** gMFI of OVA^+ cells, **(D to F)** percentage of myeloid population OVA^+ in mice groups injected with rat-IgG1 (control) and anti-SIRPα-P84 antibody. Data were normalised by the signal detected in the rat-IgG1 control. Data are mean ± SEM; * = $p < 0.05$, ** = $p < 0.01$, using the unpaired t test. Mice n=4 for each group from 2 independent experiments.

5.4 Summary

In this chapter we explored the changes occurring upon therapeutic SIRPα blockade utilizing a protocol based on Matozaki et al.[644] and showed that it's disruption was

sufficient to slow growth, coincident antigen uptake, processing and presentation, and improved T and cDC1 cell infiltration.

We developed a control method to check the bioavailability of the antibody at the tumour site and confirmed if the antibody was reaching its target thereby associating the therapeutic effects to SIRPα blockade. Consistent with Matozaki' MY-1 antibody clone[644], treatment with SIRPα, induced a reduction in tumours growth compared to PBS and IgG controls. However, we noticed that the rat-IgG1 control was inducing a small immune response, so, it was important to compare the data from the therapy with the rat-IgG1 control to be certain that the therapeutic effects were induced by SIRPα blockade. As tumours weren't going in complete remission, we were able to study the response at the cellular level. Myeloid cell composition remodelled towards inflammatory phenotypes following treatment[771,328]; antigen presenting cDC1 augmented the infiltration of the tumour while the cDC2 and moDC which expressed immunosuppressive molecules decreased.

Based on our previous observations, the M-MDSCs present seemed to be less specialised, and less suppressive. From this observation when combined with therapy data, we speculate that the SIRPα blockade impairs M-MDSCs developing a moDC phenotype, thus the moDCs reduced and the M-MDSCs increased [705,706,707]. This myeloid remodelling could partially explain the tumour reduction.

Expression of immune modulatory molecules PD-L1 and ARG1, modulated by CD47-SIRPα interaction were reduced by blockade *in vitro*, and slightly *in vivo*. However, the reduced immune suppression may instead depend more on the decrease of suppressive myeloid populations. The cDC1 associated with antigen presentation and inflammation increased while the cDC2 expressing suppressive molecules tended to reduce. Furthermore, we assisted to a reduction of moDCs that were intended as mature highly suppressive M-MDSCs, the latter were tended to reduce when compared to PBS control but increased when comparing with rat-IgG1 injected mice.

This different myeloid landscape reflected in that is associated with good prognosis in melanoma cancer patients[772]. However, we also unexpectedly observed changes in percentage of moDC and M-MDSC expressing MHCII where moDCs decreased but M-MDSCs increased. Together, these conflicting trends suggest that rather than changing specific molecules, anti-SIRPα treatment may influence the whole process of antigen presentation. Hence, the main mechanism to explain the reduction in tumour growth could be mediated by an enhancement of phagocytosis, antigen processing and presentation. Supporting this idea, we proved *in vivo* that mice treated with anti-SIRPα overrode the inhibitory CD47 signal to induce an increase in phagocytic activity, and antigen processing which resulted in an increase of antigen presentation on the surface of the myeloid cells.

In these experiments though, the gMFI detection as measure of signal intensity may be limited in revealing an increase for these experiments. It could have been that the presence of the anti-SIRPα would not increase much the intensity but the proportion of cells becoming positive. Because of it the second parameter to be analysed was the positive percentage of cells expressing fluorescence within each myeloid population.

In chapter 3 we saw how the myeloid were characterised by the SIRPα expression, this was the highest in the moDCs followed by the cDC2 to close with the M-MDSCs. This correlates with the sensitivity in phagocytosis and processing and presenting OVA antigen when the CD47-SIRPα axes was disrupted. Indeed, the antigen processing baseline was different for the three groups analysed. The 40, 70 and 20% of cDC2, moDC and M-MDSC cells respectively were able to elaborate the antigenic molecule. Similarly, the ability to present antigen also, seemed proportional to SIRPα level of expression and blockade directly causing a proportional phagocytic increase, antigen processing and then, OVA presentation.

These results associated shed light on the differential thresholds that those cells need to overcome to internalise and process the antigen. The sensitivity was associated with

the amount of SIRPα expression but also may reflect the different states of maturation in which those cells were. In fact, we detected very different concentrations of immune modulator molecules that may be responsible of the responsiveness to antigen phagocytosis and processing. The whole myeloid cluster though was affected by modulating the CD47 interaction with SIRPα inducing us to conclude that this process is strongly associated with the TME remodelling towards more inflammatory phenotypes.

Importantly while some changes were subtle, our data indicated that following therapy, the number of cells changing phenotype, rather than expression level by individual cells was a driver in the anti-tumour effect.

To strengthen this conclusion, we analysed the $CD8^+$ T and Tregs cells composition upon SIRPα blockade. Consistent with immune checkpoint inhibitor studies[773,774,775], the $CD8^+$ T cells were increasing the tumour infiltration while the suppressive Tregs remained constant. This may indicate that anti SIRPα myeloid remodelling also changes the cytokine milieu to impact either recruitment or differentiation of T cell within the TME. Importantly, the ratio between the two species was in favour of the $CD8^+$ T cells. This result associated with the increase of cDC1 showed how the immune balance was tending towards inflammation associated with favourable outcome[326,776].

In summary, we have provided evidence that indicates a viable anti-tumour response following SIRPα blockade. It would be interesting to determine if effects were enhanced by combining this approach, which targets myeloid populations with platforms that target adaptive immune populations.

CHAPTER 6

DISCUSSION

6.1 Project rationale and overview

Malignant melanoma is characterized by the development of chronic inflammation in the tumour microenvironment. Chronic inflammation ultimately leads to strong immunosuppression associated with rapid tumour progression[777]. This tolerogenic environment and T cell suppression can in part be attributed to the presence of myeloid cells in the tumour microenvironment. Tumours recruit and modulate endogenous myeloid cells, maturing them into tumour associated macrophages (TAM), dendritic cells (DC), myeloid-derived suppressor cells (MDSC) and tumour associated neutrophils (TAN), thus sustaining an immunosuppressive environment. However, despite advances in determining specific phenotypes, functional experiments remain a benchmark to define these populations as suppressive[413,405].

The TME directly augments MDSC function. The acquisition of suppressive phenotypes is dictated by the tumour, other immune and stromal cells indicating the inherent plasticity of MDSCs and therefore offers a biological niche which may be exploited. Platforms to revert these tumour-induced changes are sought to achieve tumour rejection. But to do this, and utilise these cells as a therapeutic target, it is critical to understand which molecules contribute to the myeloid suppressive behaviour.

To elucidate the mechanisms behind MDSC development, we initially investigated the changes caused by melanoma evolution in the myeloid compartment and established their suppressive behaviour. Moreover, we recapitulated these changes and investigated whether the CD47-SIRPα 'do not eat me signal' was involved in sustaining the myeloid suppressive function. Finally, we studied the impact of SIRPα blockade on the remodelling of the TME. With this approach we provided evidence that CD47-SIRPα engagement increases the MDSCs suppressive potency which can be reverted by blockade inducing increase in phagocytosis, antigen processing and presentation.

6.2 MDSCs and moDCs develop a suppressive phenotype in the melanoma TME

To assess changes in the myeloid composition in melanoma, we used a well-established injectable murine melanoma model. Melanoma is a potentially fatal form of skin cancer characterised by rapid progression and metastasis to regional lymph nodes and distant organs. Moreover, melanoma is often associated with therapeutic resistance[778,779]. Melanoma and other progressive cancers establish the need to further understand the interplay between mechanisms of immunosuppression and tumour immunity. Researchers have described a strong correlation between the development of chronic inflammatory conditions in the TME and the recruitment, enrichment and activation of MDSCs[780,781,782,783,784].

Accordingly, we initially analysed the presence of MDSCs in the melanoma TME. We noted an accumulation of $CD11b^{+}Ly6C^{+}$ cells representing a quarter of the total $CD45^{+}$ population. This increase over time, selected for two main populations; $CD11c^{+}CD11b^{+}Ly6C^{+}$ (moDC) and $CD11c^{-}CD11b^{+}Ly6C^{+}$ (M-MDSC), while $CD11c^{-}CD11b^{+}Ly6G^{+}$ (G-MDSC) were represented to a lesser extent. This result contrasted in comparison to a model of spontaneous melanoma in transgenic (Grm1)EPv mice which showed preferential accumulation of G-MDSCs over M-MDSCs. However, both models confirmed that the MDSCs suppressed melanoma antigen-specific T cells via ARG1, NO, and TGF-β production[785]. Similar results were obtained by Raber *et al*. who found that in lung cancer and melanoma models more G-MDSCs were present compared to M-MDSCs but found the opposite to be true in colon carcinoma[786]. However, this data was obtained by positive magnetic isolation of Ly6G cells and the proportions were calculated by comparing the fractions of the two cells types. Our work differed by assessing the proportions of represented cell types through directly staining the tumour cells and ensuring that the entire tumour was assessed. Our work defines the

early evolution of a melanoma tumour before the maximum growth reaches 12mm. Hence, we described the conditions observed within this parameter.

Between day 5 and day 11 of tumour growth, a gradual increase in $CD11b^+$ cells, enriched for $Ly6C^+$ and indicated a switch from inflammatory cDC-type towards a more immunosuppressive environment containing less mature myeloid infiltrates but increasing moDCs and M-MDSCs. The gradual increase in $CD11b^+$ expression has also been documented in sarcoma, mammary carcinoma and melanoma cancers, and is attributed to the increased expression of CCL2, a monocyte chemoattractant[787,788,781]. These works corroborated the expansion we observed. However, our work was further characterised by the TME myeloid populations expression of SIRPα which remained consistent over time. This allowed the identification of monocytic-DCs ($CD11c^+CD11b^+Ly6c^+SIRP\alpha^+$) from monocytic-MDSCs ($CD11c^-CD11b^+Ly6C^+SIRP\alpha^+$)[699,405,322]. These populations also expressed subsets of $CX3CR1^+$ (monocytes) and $F4/80^+$ (macrophages) indicating the high complexity and plasticity of myeloid cells, which remains under debate. In a mammary adenocarcinoma tumour model, it was demonstrated that $Ly6C^+CX3CR1^{low}$ monocytes were the primary precursors of all subsets of TAM. These cells can differentiate into an M2-like suppressive phenotype which can also express F4/80[789,790]. The presence of these two markers in our analysis depicted a complex interplay between monocytes, macrophages and dendritic cells.

After demonstrating the presence of myeloid cells in the melanoma model, it became important to correlate their presence with tumour remodelling. The hypothesis being that with an increased myeloid population, there would be an increase in molecules associated with immunosuppression, supporting tumour progression. Indeed, we observed an increase in PD-L1 and ARG1 expression in both moDC and M-MDSC. The M-MDSCs were associated with an increase in PD-L1 expression due to the tumour

hypoxic environment, as facilitated by hypoxia-inducible factor 1-alpha (HIF-1-alpha)[700]. Moreover, myeloid expression of PD-L1 was required to activate the immune checkpoint PD-1 to establish an immunosuppressive environment[684]. In the TME of colon cancer it was found that PD-L1 was highly expressed by tumour-infiltrating M-MDSCs[433]. ARG1 has also been associated with M-MDSCs immunosuppressive function[413,689]. An increase in our analysis confirmed that the myeloid cells were contributing to both increased ARG1 and PD-L1 in the TME during tumour evolution. Interestingly, it was also reported that ARG1 expression wasn't inducing the critical MDSC-mediated inhibition toward T cells. On the contrary, inhibition was dependent on direct cell contact[791]. Based on this, we utilised transwell plates in a T cell proliferation assay to keep the M-MDSC separate from the T cells and found that no suppression was obtained (appendix 8.10 A-B) regardless of ARG1 concentration when the cells were physically separated (appendix 8.10 C). However, a caveat of this data was that this study was preliminary, and the assay was affected because the media was refreshed. Regardless, the overexpression of ARG1 correlates with poor prognosis in colorectal[792], ovarian[793], hepatic[794] and melanoma cancers[795]. Overall, our analysis of PD-L1and ARG1 could be associated with their mediation of T cell suppression through both direct and indirect cell contact, respectively.

In addition to PD-L1 and ARG1, we also observed an increase in the expression of Fas ligand (CD178). Fas-mediated apoptosis of T cells is a well-studied mechanism to regulate T cell homeostasis and to prevent immunopathology. Triggering the induction of Fas ligand (FasL) expression on T cells causes activation-induced cell death (AICD) [796], and qualifies the Fas-FasL interaction as an immune checkpoint mechanism[686]. C57BL/6 FasL−/− mice showed an increased accumulation of potent M-MDSCs that correlated with reduced survival of the tumour-bearing mice[797]. Recent research indicated that other cells types in the tumour microenvironment can also express FasL and trigger the apoptosis of tumour-infiltrating lymphocytes (TIL),

including endothelial cells[277], CAFs[74] and myeloid-derived suppressor cells (MDSC) [686]. We identified that the myeloid cells in the melanoma TME were expressing FasL, and this gradually increased with tumour progression. This indicates that myeloid cells could be regulating the homeostasis of the T cells using FasL[701]. However, it is not the only mechanism used by myeloid cells and it is unlikely that these cells are solely responsible for T cell suppression through this mechanism.

Lastly, we observed specific expression of inducible NOS2 by the moDC. It was proved that the production of nitric oxide by MDSCs impaired the Fc receptor-mediated cytotoxicity of NK cells[798] and that the $CD11b^+$ cells producing NO suppressed T-cell-mediated antitumor immunity[458]. moDCs expressing NOS2 produced NO which is required to control both bacterial and viral infections in vivo. However, in vitro GM-CSF and IL-4 differentiated monocyte-derived human DCs (moDCs) don't readily express NOS2[799]. This is in contrast to observation by Thwe and Amiel, suggesting that the right environmental conditions in vitro are critical for NOS2 expression[800]. Whilst we didn't detect NOS2 in the M-MDSCs at the time points we examined, work by Raber *et al.*, M-MDSC NO production strongly correlated with the impairment of T cell response [786]. This is not necessarily in contrast to what we found because in this work CD11c wasn't used to distinguish moDC and M-MDSC which were instead identified by $CD11b^+Ly6C^+Ly6G^-$.

6.2.1 moDCs and M-MDSCs are highly suppressive towards T cells

In the TME of melanoma tumour bearing mice, there was a selection for moDC and M-MDSC cells as characterised by molecules associated with T cell suppression. Those clues indicated that the myeloid cells were involved in creating a permissive environment for cancer development. We confirmed that extracted myeloid could effectively suppress activated T cells. Two methods of myeloid extraction were tested but difficulties were encountered, and we opted for the methodology which allowed

us to demonstrate that $CD11b^+Ly6C^+$ myeloid cells were suppressive, but accepting the limitation that this method can't distinguish between moDC and M-MDSC populations.

The fact that MDSCs can inhibit different types of T cell response is widely accepted[466,801,802]. In accordance with this work, Lesokhin *et al*. demonstrated that $CCR2^+CD11b^+$ M-MDSCs extracted from B16-F10 tumours, were able to suppress the proliferation of CD3/CD28 activated $CD8^+$ T cells[803]. It was also described that moDC from the TME, were often skewed towards tolerance. This is observed in several cancer models where the moDCs are sensitive to phagocytosis but poor at antigen presentation[804]. In our findings, $CD11b^+Ly6C^+$ moDC and M-MDSCs extracted from the TME of melanoma tumour bearing mice were able to suppress T cells and, based on the immune modulator marker expression detected in vivo, our data indicated that the M-MDSCs were less specialised moDCs and may be part of the same family. In humans, it has been observed that monocytes extracted from peripheral blood and cultured with interleukin (IL)-10 differentiated into moDCs and M-MDSCs ($CD14+HLA\text{-}DR^{low}$) with reduced stimulatory capacity. A similarity shared with mouse MDSC[705]. Activation of the transcription factor IRF4 was responsible for differentiating the $Ly6C^+$ monocytes into moDC[706,707].

6.3.1 The in vitro model recapitulates MDSCs suppressive phenotype

Due to the difficulties in obtaining moDC and M-MDSC *in vivo*, we developed an alternative *in vitro* system. Melanoma cells are reported to be able to produce a variety of inflammatory mediators including GM-CSF, VEGF, TGF-β, TNF-α, IL-1β, IL-6, IL-10 and multiple chemokines (CCL2, CCL5, CXCL1, CXCL2, CXCL8, CXCL10)[780,781,782,783,784]. Several papers matured M-MDSCs from bone marrow utilising cocktails of GM-CSF, one of the main protagonists of 'emergency' myelopoiesis[375], interleukin 6 (IL-6)[376] or alternatively, tumour conditioned media (TCM)[377]. Others reported maturation of

MDSCs from HSCs using bone marrow hematopoietic progenitor cells[805]. In our system we wanted to generate myeloid cells as comparable as possible to those present in *in vivo*. Therefore, we extracted HSCs and stimulated maturation utilising a combination of GM-CSF and condition media obtained from a B16-F10 cell culture. As the cells progressively matured, we noticed that the stem cells developed first into MDSCs which later expressed the $CD11c^+$ marker, thus becoming moDCs.

At this point it wasn't clear whether our in vitro matured cells resembled those present in vivo. In terms of percentages and myeloid markers the cell populations matched but in comparison to cells grown only in GM-CSF media they couldn't be distinguished as different populations. However, multiple reports have demonstrated the effects of TCM in inducing suppressive MDSC phenotypes. Condition media from a renal carcinoma cell line induced monocytes to acquire a monocytic MDSC phenotype which was characterised by a stronger suppression of T cells compared to the control[806]. Moreover, TCM obtained from an oropharyngeal squamous cell carcinoma was used to generate MDSCs which acquired suppression[807], and HNSCC cell line–derived conditioned media was used to differentiate human PBMCs into suppressive cells[808]. Further studies demonstrated how the stimulation of myeloid cells with GM-CSF induced a suppressive phenotype[809], and associated the accumulation of MDSC in the progression of colitis to cancer[810]. With this in mind we treated in vitro cultures with TCM. We expected that growing our cells in GM-CSF would cause them to develop a certain grade of suppression, but this would be enhanced by TCM. Consistent with these reports, $Ly6C^+$ myeloid cells grown in melanoma GM-CSF-TCM were more suppressive towards T cell proliferation and survival than the control cells, and so, a direct effect of the B16-F10 exudate stimulating MDSC maturation was proven. So, we decided to use GM-CSF grown cells as the control to evaluate the potency of TCM as a stimulator of MDSC maturation.

6.3.2 *In vitro* generated moDCs and M-MDSCs express similar suppressive mediators to tumours

We characterised the moDC and M-MDSC generated in TCM for suppressive molecules. This was to corroborate functional data and to allow comparison to the data obtained *in vivo*. The moDCs and M-MDSCs expressed molecules such as SIRPα, PD-L1, ARG1 and FasL with similar levels to those detected *in vivo*. Again, we observed that moDCs were expressing a higher concentration of these molecules, indicating a possible common maturation from the MDSCs[705,706,707]. Supporting this hypothesis, peripheral blood monocytes were differentiated in moDCs within 7 days using IL- 4 and GM-CSF, however, the addition of IL-10 resulted in the generation of a MDSC ($CD14^{+}HLA\text{-}DR^{low}$) phenotype[705]. This showed the intimate relation between these two populations and highlights that their fundamental plasticity depends on their external stimuli.

SIRPα expression confirmed the identity of moDCs and M-MDSCs and may indicate a regulatory role in myeloid homeostasis. Indeed, SIRPα mutant mice manifested a marked reduction in the number of splenic DCs compared to the wild type indicating an important role in myeloid cell survival[596]. We showed that CD47-SIRPα interaction had profound effects on the function exerted by moDC and M-MDSC in the melanoma TME. PD-L1 has also been reported several times to be upregulated in MDSCs dependent upon different stimuli[705,811] and in different tumour types, including breast[812], to support our findings in melanoma . The third molecule we detected both in vivo and in myeloid cell culture was ARG1, the inhibition of which blocks myeloid cell-mediated immune suppression in the tumour microenvironment in multiple mouse models[702]. Another molecule we observed *in vivo* was FasL. When comparing the expression levels, the concentration *in vitro* was most comparable to day 5 of the *in vivo* melanoma evolution. FasL expression in T cells was reported to be enhanced by IL-2 expression however its upregulation didn't correlate directly with increased

activation of induced cell death (AICD)[813] which may associate a low level of expression with a potent Fas-FasL activation. It is now widely accepted that once cancer cells acquire resistance to Fas-mediated apoptosis, further stimulation of Fas is tumorigenic[814]. For instance, overexpression of Fas by lung cancer tumour cells was correlated with the accumulation of MDSC through an increase in PGE(2) expression[815]. We speculate that MDSCs could upregulate FasL under the influence of the TME stimuli, and from one perspective induce T cells killing and the other stimulating the self-recruitment of more myeloid suppressive cells to the tumour site.

Comparable to the level of FasL expression and IDO were detected in the myeloid cell cultures. IDO exerts its suppressive effects via the reduction of local tryptophan availability and the generation of kynurenine which blocks the initiation of an Ag-specific immune response. IDO also reduces the antitumor cytotoxicity of activated T cells, and increases Treg recruitment and infiltration[816,817,818]. Moreover, IDO was found significantly upregulated in MDSCs isolated from fresh breast cancer tissues[469] and PGE2 has been shown to induce the upregulation of IDO in *ex vivo*-generated MDSCs[485]. The suppressive effect of IDO is just one of the mechanisms that MDSCs use to create an environment of tumour tolerance[704]. Its detection in our culture system strengthened the association of our moDC and MDSCs with a suppressive phenotype.

Another molecule of the B7 family which includes the immunosuppressive PD-L1, is V-domain Ig suppressor of T-cell activation (VISTA). VISTA, like PD-L1, is associated with the inhibition of T cells and mediation of immune evasion in cancer[819]. In our in vitro cell culture system for moDCs and MDSCs, VISTA was detected but at a low level. However, MDSCs have been reported to be responsible for T cell proliferation blockade through VISTA which, if blocked, allowed for the restoration of a protective anti-tumour response[820,821]. Hypoxia (HIF)-1α binding promoted VISTA upregulation on myeloid cells[822] and its immune co-receptor engagement to the adhesion and co-

inhibitory receptor P-selectin glycoprotein ligand-1 (PSGL-1) is dependent on an acidic pH [823]. This makes it difficult to simulate optimum conditions for VISTA expression in our cell culture system thus a difficult molecule to investigate in an in vitro context. However, TCM grown myeloid cells showed to induce a partial upregulation of VISTA which correlated with possible T cells inhibition.

The presence of these molecules, all associated with immunosuppressive mechanisms used by MDSCs, confirm that our cell culture system was maturing MDSCs and moDCs reflecting the phenotype observed *in vivo*. When compared against the same cells grown in GM-CSF only media it was clear that TCM addition facilitated an increase in the expression of these suppressive mediators. This may explain the major immunosuppressive potency found in these cells. It was also the confirmation required to show that we could use the cultured cells to further understand their cancer biology.

6.4.1 CD47 expressed in the TME cells engage SIRPα on the myeloid

The discussion in the previous section delineated the reduction of cDC and the increase of moDCs and M-MDSCs in tandem with tumour progression. Both cell types were expressing an array of immune modulator molecules associated with immune suppression. Using TCM to provide an equivalent in vivo stimulus, we obtained the same composition of myeloid cells found in the melanoma TME from bone marrow derived HSCs. The myeloid cells shared similar patterns of modulators which exerted their immunosuppressive function over activated T cells by reducing their proliferation. The molecule which was consistently expressed and conserved was SIRPα. In the work of Chauhan *et al.*, mass spectrometry was used to characterise MDSCs ($CD11b^{+}GR1^{+}$) harvested from mammary tumour bearing mice. The surface glycoproteins expressed molecules typical of the "don't eat me" signal, such as CD47, and its binding partners thrombospondin-1 (TSP1) and SIRPα[474]. The SIRPα expression they described matched our observations, however, the role of the SIRPα-CD47 axis on MDSC function

remained unclear. In 2019, Pengam *et al*. used a model of long-term kidney allograft tolerance which was sustained by MDSCs. They observed that SIRPα or CD47 blockade with monoclonal antibodies induced the MDSC differentiation towards a myeloid cell overexpressing MHCII, with CD86 costimulatory molecule expression and increased secretion of macrophage-recruiting chemokines (e.g. MCP-1). This blockade resulted in an inflammatory environment which induced graft dysfunction and rejection[631]. We can speculate that a SIRPα agonist could be used in transplant patients to obtain immune tolerance. Our work was partially based on these publications, if MDSC SIRPα blockade induced transplant rejection it meant that the SIRPα-CD47 axis was regulating MDSC homeostasis, and could be exploited to "reject" tumours.

Based on our initial SIRPα rich myeloid characterization, we explored the expression of its binder, CD47. CD47 was widely expressed by cells of the TME, both at the single cell RNA and protein level. However, B16-F10 melanoma cells didn't show a high expression of CD47 indicating that they may contribute less to the SIRPα engagement. Despite this, B16-F10 cells with a CD47 knock out were targeted with a melanoma specific antibody resulting in an increased amount of phagocytosis[712]. Furthermore, patients with ovarian, breast, colon, bladder, glioblastoma, hepatocellular carcinoma, and prostate tumours expressed CD47[349]. Regardless of the cells expressing this molecule, myeloid cells encounter a CD47-rich TME which contributes to SIRPα-CD47 engagement. We speculate that independently from tumour CD47 expression, this molecule could always characterise the TME, thus having implications for therapy efficacy and stratifying therapeutic intervention when based exclusively on the CD47 expression. Endogenous expression of CD47 on a variety of cell types, including erythrocytes, creates a formidable antigen sink that may limit the efficacy of CD47-targeting therapies[824]. Conversely, SIRPα has a more restricted histological distribution compared to CD47, which could lead to less toxicity and greater blockade when therapeutically targeted[825].

6.4.2 CD47-SIRPα engagement enhances the suppressive immune molecules

For these reasons, we used CD47 expression to assess functional changes in the moDCs and M-MDSCs and blocked their SIRPα protein in order to understand myeloid reactivation in the TME. Through this we established the contribution of CD47-SIRPα engagement in the development of moDCs and M-MDSCs and their suppressive phenotypes. PD-L1 slightly increased upon CD47 engagement. This correlates with data found in mice vaccinated with CD47-/- or CD47+/+ melanoma cell line. Here, suppressor cells, including the G and M-MDSCs, were highly downregulated in the TME of CD47−/− vaccinated tumours. This was accompanied by reduced numbers of NK cells, elevated levels regulatory T cells and 'M2-like' macrophages which were expressing high levels of PD-L1 indicating a link between CD47 and PD-L1 expression[826].

We also observed an increase of FasL matching with the general suppressive enhancement driven by CD47-SIRPα engagement. It was also demonstrated that Fas (CD95) was identified as a lateral binding partner of CD47 in T cells. Activation of the Fas receptor on T cells by an antibody or by Fas ligand binding induced death only in cells that expressed CD47[827,828]. This may be associated with the FasL increase we observed on moDCs and M-MDSCs, which could induce CD47-expressing T-cell death through Fas-FasL engagement[686]. These findings made us consider that combinations with the SIRPα in combination with Fas αand FasL blockade maybe beneficial in increasing T cell survival and tumour regression.

The suppressive potency towards activated T cells of moDCs and M-MDSCs upon CD47-SIRPα engagement was stronger than with myeloid cells in GM-CSF-TCM only. This correlates with the increased expression of PD-L1 and FasL detected in the cell culture phenotyping. We associated the anti-SIRPα treatment with the reduction of

ARG1 which could result in the availability of L-arginine for maturation of the T cell receptor [829]. L-arginine supplementation to mammary tumour bearing mice demonstrated an increase in their survival by inhibiting the tumour growth associated with reduction of suppressive MDSCs[703]. Therefore, it would be a promising strategy to combine SIRPα blockade with supplements of amino acids in order to strengthen the T cell response.

6.4.3 CD47-SIRPα engagement and blockade modulate the phagocytosis of moDCs and M-MDSC in the TME

Besides the regulation of CD47 expression in cancer cells, it is also responsible for the regulation of other cell types. As we saw in our phagocytosis assays, moDCs and M-MDSC uptake was inhibited by CAFs which expressed more CD47 than the melanoma cells. Indeed, the ability of the myeloid cells to engulf debris directly correlated with levels of CD47 expression. It has been speculated that CD47 up-regulation in fibroblasts may be a consequence of exposure to the inflammatory cytokines TNF-α, CXCL10, and IFN-α[830]. In particular, fibrotic associated fibroblasts were found to upregulate CD47 and PD-L1. The expression drove lung fibrosis development, which was abrogated by the administration of anti-CD47[831]. Research has also proved that CD47 up-regulation on vascular smooth muscle cells was caused by TNF-α, which could also explain the impairment in macrophage phagocytosis within human atherosclerotic plaques[832]. Furthermore, CD47 expression by T cells in the TME was correlated with reduced type 1 immune responses and a suppressed phenotype[591]. We speculate that the chronic inflammation in the melanoma tumour could promote CD47 expression through the fibroblasts and T cells, promoting the engagement of SIRPα expressing myeloid cells and contributing to their suppressive development. For instance, it was found that in hepatocellular carcinoma the associated fibroblast derived IL6 was responsible for the STAT3 activation of neutrophils, which resulted in

up-regulation of PD-L1 expression and a subsequent increase in suppression[833]. This suggests that fibroblasts may contribute to the regulation of phagocytic ability in MDSCs in addition to their suppressive development. Also, we saw a correlation with PDFRα, Thy1 and CD47 expression. PDGFRα and PDGF signalling has long been associated with activation of fibroblasts[834] while Thy1 identifies active T cells[720], we wonder if CD47-SIRPα signalling could be involved in regulating the functions of these cells and may be involved in pathologies progression.

The myeloid cells were inhibited by CD47 expressing cells in the TME. Using SIRPα blockade we abrogated this inhibition and increased the levels of phagocytosis, showing a dose dependency between SIRPα blockade, its abrogation of CD47 engagement and increased phagocytosis. Therefore, when using an anti-SIRPα therapy, the bioavailability of CD47 at the tumour site should be considered for an informed dosage strategy which can overcome CD47 mediated inhibition. Research by Hayes *et al*. determined that soluble SIRPα binding to human CD47 displayed on Chinese hamster ovary (CHO) cells was blocked by SIRPα membrane surface co-display. This means that SIRPα expressing cells can also express CD47, thus their engagement could happen in *cis* [712]. This research group presented a poster in 2021 with preliminary data which implied that full disruption of CD47 binding is necessary to obtain a curative effect. This would be achieved through pro-phagocytic and tumour-opsonizing IgG, therefore facilitating a 'phagocytic feedback'. This could affect the efficacy of SIRPα blockers and should be considered in drug development if elimination of CD47-"self" inhibition added to an "eat me" signal wants to be achieved[835].

Several clinical trials encouraged by positive pre-clinical data using SIRPα targeting are currently taking place[836]. The design of these studies has started to consider combination therapies using tumour-specific opsonizing antibodies. It has been noticed that SIRPα blockade was lowering the threshold of phagocytosis activation but

in addition to this, a positive 'eat me signal' may also be required. Nan Guo Ring *et al.*, developed the monoclonal antibody, KWAR23, which binds human SIRPα and disrupts its binding to CD47. This antibody administered alone only had a small effect on the tumour. However, when used in combination with tumour-opsonizing monoclonal antibodies, it increased the myeloid-mediated killing towards human tumour-derived cell lines[632].

Indeed, combinatorial approaches are being used in clinical trials involving the CD47 and SIRPα blockade. Examples include Hu5F9-G4 with rituximab (anti-CD20), cetuximab (anti-EGFR) and Avelumab (anti-PD-L1), CC-90002 with rituximab, and ALX148 with trastuzumab (anti-HER2) and rituximab. All these trials aim to combine the advantages of the CD47-SIRPα blockade and simultaneously harness the mechanisms targeting other pathways. A similar approach is used in the clinical trial of BI-765063 which is an antagonist monoclonal antibody of SIRPα. This molecule is being evaluated alone and in combination with anti-PD-1 which is also involved in the "do not eat me signal" and of course, T cell activation (Section 7 of chapter 1).

6.4.4 CD47-SIRPα modulates intracellular signalling

Profound downstream changes were detected in the myeloid in their cell signalling. SIRPα blockade reduced SHP2 while CD47-SIRPα engagement activated STAT3, this could be associated with decrease in suppressive molecule expression and downstream inhibition of T cell proliferation. The observation was corroborated by work of Toledano *et al.* who reported that CD47-SIRPα triggers STAT3. In addition to the formation of the ITIM-SHP-1-2 complex which transmits an anti-phagocytotic signal It was also linked to the development of an immature APC phenotype and peripheral tolerance. This phenotype was overcome by CD47 suppression using specific siRNAs and shRNAs[623]. We also observed that CD47 induced STAT3 activation may play a role in ROS production. In hypoxia driven STAT3 activation, increased ROS

production was facilitated by Nox4 and positively correlated with tumour angiogenesis and progression[837]. This implies that the induction of STAT3 and subsequent ROS production induced by CD47-SIRPα stimulation may be direct effects of tumour progression and T cell suppression.

In addition to changing ROS production, disruption of CD47-SIRPα changed cellular energetics, likely needed to support functional adaptations in the moDCs and MDSC. CD47-SIRPα engagement caused an ATP accumulation and a glucose uptake reduction, indicating that M-MDSCs and moDCs were energetically less active. Indeed, MDSCs isolated from patients with hepatocellular carcinoma were characterised by low levels of glucose and ATP when compared to monocytes from healthy patients[736]. This weak energetic state was associated with the production of an intermediate metabolite of glycolysis, metilglyoxal, which was passed and inhibited the T cell by depleting L-arginine and lysine, both important for maturation and activation. This inhibition was mediated by cell-to-cell contact between MDSCs and T cells causing T cell paralysis. High CD47 expression in hepatocellular carcinoma correlates with poor prognosis[838] and we speculate that the SIRPα-CD47 interaction may be involved in ATP related metabolic disruption.

In contrast, SIRPα blockade induced a faster uptake of glucose, which was associated with an increase in the expression of surface glucose transporter GLUT1, while ATP was being consumed. We speculate that the energy was being used to reactivate phagocytosis or contribute to a metabolic reprogramming of the cells, back towards an activated inflammatory state. The ATP consumption we observed could be associated with the paracrine signalling utilised by myeloid cells to induce Ca^{++} signalling for efficient phagocytosis. Extracellular ATP is a signalling molecule exploited by the immune cells for both autocrine regulation and paracrine communication[839]. This research was based on live calcium imaging experiments showing that macrophages were able to activate phagocytosis in resting cells through calcium

signalling which required the release of extracellular ATP. We observed that the CD47-SIRPα interaction induced an intracellular accumulation of ATP and we speculate that the interaction could be preventing its release. As implied above, this could be another mechanism by which the SIRPa-CD47 interaction mediates inhibition of phagocytosis.

However, it is unknown whether the ATP accumulated in CD47 stimulated moDCs and M-MDSCs could be released into the extracellular space. In the introduction we explained that one of the possible therapies targeting myeloid derived suppression involved targeting CD73, which when coupled with CD39 is responsible for ATP hydrolysis into adenosine[840]. Adenosine is absorbed by the T cells which, in turn reduces IFN-γ production and impairs membrane-proximal T-cell receptor signalling. Differentiation of naïve $CD8^+$ T cells into cytotoxic T cells is also affected by adenosine as a consequence of IFNγ availability[841]. CD73/CD39 molecules were found to be upregulated on MDSCs via TGF-β-mTOR-HIF-1 signalling in patients with non-small cell lung cancer[842]. It is unknown whether the CD47-SIRPα interaction could have a role in providing ATP to these membrane enzymes. If so, it is possible that the interaction could enrich the TME in adenosine, and perhaps SIRPα blockade could reduce this via activation of inflammatory pathways and increased ATP consumption.

6.5.1 SIRPα blockade increases cDC1 (CD11c+XCR1+) and T (CD8+) inflammatory cells

Having established that the CD47-SIRPα interaction is partially responsible for the suppressive function of moDC and M-MDSCs towards T cells, we sought to explore the potential of SIRPα blockade in melanoma bearing mice. Our *in vitro* data elucidated the connection between a CD47 rich TME and inhibition of $SIRP\alpha^+$ myeloid cells which reduced their phagocytic ability. In general, we also observed the expression of molecules involved in suppressive mechanisms, such as PD-L1, FasL, ROS and STAT3. Using an anti-SIRPα antibody we prevented the suppressive effects

mediated by CD47 and recovered the phagocytic ability of both moDCs and M-MDSCs. This recovery was concentration dependent with the increase in phagocytosis being directly proportional to the blockade of SIRPα. In this discussion we have highlighted the importance of achieving a total blockade of SIRPα and how the use of an antibody may not prevent CD47 *cis* binding therefore a full blockade of this pathway may require a second stimulatory molecule to achieve tumour remission.

We sought to block SIRPα rather than CD47 to reduce any off-target effects and antigen sink. The CD47 expression in normal tissues may create an 'antigen sink' that could minimize the therapeutic efficacy of blocking CD47 by limiting its localisation in solid tumours. We speculate that a valid approach should be the creation of bispecific antibodies which combines the SIRPα blockade, activation of T cells and retain Fc induced immune response. Indeed, bispecific antibodies are now being developed to create therapies which should improve the bioavailability of anti-CD47 within the tumour. One example is a bispecific antibody which targets both CD47 and CD20. It is designed as a therapeutic target against non-Hodgkin lymphoma (NHL), and whilst the molecule has a reduced affinity for CD47 (relative to the parental antibody), it retains strong binding to CD20[843]. Using this approach, they synergistically induced selective phagocytosis of tumour cells using a bispecific. Another study coupled anti-CD47 to a tumour associated antigen (TAA) called glypcan-3 (GPC3) which is expressed by hepatocellular carcinoma cells. The therapy specifically induced the phagocytosis of these cells and it also caused an enhancement of Fc-mediated effector functions[844]. As demonstrated, there are efforts being made in this field to improve the tumour bioavailability for anti-CD47 drugs. This approach aims to flag the tumour cells in situ to the myeloid cells whilst removing the CD47 'do not eat me signal'.

The use of antibodies targeting SIRPα reduces the sink effect because its expression is more limited in healthy tissues in comparison to CD47. The restriction in the histological distribution of SIRPα offers the possibility for reduced toxicity and greater

blockade when targeted therapeutically and makes SIRPα a more attractive therapeutic target than CD47. However, in addition to myeloid immune cells, SIRPα is also highly expressed on cells of the central and peripheral nervous systems[845]. Whilst this is a clear therapeutic risk, large protein-based therapeutics typically struggle to penetrate the blood brain barrier[846].

In our research we observed that within the TME, SIRPα expression was restricted to myeloid and endothelial cells. Moreover, we showed that the dosage of drug which we injected was bioavailable at the tumour site, and was sufficient to translate to delayed tumour growth. Yanagita *et al.*,[644] reported that anti-SIRPα therapy using the same monoclonal antibody, produced tumour reduction when simultaneously injected with renal adenocarcinoma cells. However, its administration didn't show any effect in the established tumour. In contrast, we observed effects in small, but established tumours using a lower dosage and number of injections. We also observed a good immune response. This differing outcome may be a consequence of tumour type and the different dynamics of tumour development, or treatment regime. Unfortunately, we also observed a partial immune response using the rat-IgG1 backbone control for the anti-SIRPα antibody but there was a clear difference in tumour reduction between these groups.

Depending on the controls used we saw different patterns of remodelling in the myeloid compartment. We clearly observed an increase in cDC1 ($CD11c^+XCR1^+$) cells upon SIRPα blockade. A cell type which plays a critical role in T cell priming and is associated with patient survival in addition to rejection of immunogenic cancers[326]. The cDC1 cells stimulate de novo T cell responses and prime antigen-specific cytotoxic T cells by presenting tumour antigens. They can also activate natural killer (NK) and natural killer T (NKT) cells and secrete inflammatory cytokines, enhancing local cytotoxic T cell function[776]. To our knowledge, the detection of an increased presence of cDC1 cells in melanoma has not been associated with SIRPα blockade previously. It

would be beneficial to understand why the blockade induced the development of the cDC1 cells.

In comparison to the mice injected with the control antibody, we observed a decrease in the cells we defined cDC2 ($Ly6C^-$) and moDCs ($Ly6C^+$). These cells were expressing immunosuppressive molecules indicating that the SIRPα blockade either favoured a phenotypic switch or promoted the accumulation of inflammatory cDC1 cells. Three-dimensional, organotypic cultures proved how melanoma could induce cDC2s to become $CD14^+$ expressing DCs, a marker typically associated with monocytes in humans[847]. This may contrast with what we observed *in vitro*, where M-MDSC ($CD11c^-$) were becoming moDC ($CD11c^+$). More characterisation may be required for this system but importantly, we defined their depletion upon SIRPα blockade reduced immunosuppressive pressure and allowed increased $CD8^+$ T cell infiltration. Strangely, the M-MDSC ($CD11c^-Ly6C^+$) showed a tendential increased accumulation compared to rat-IgG1 injected mice but a reduction in comparison to mice injected with PBS. It would be interesting to use mass spectrometry to deeply profile the activation of inflammatory pathways and changes in metabolism. This could provide cues on potential therapies to associate at SIRPα blockade.

Similarly, in research by Yanagita *et al.*[644], a more potent anti-SIRPα monoclonal antibody (MY-1) was injected. Here, the MDSCs ($CD11b^+Gr\text{-}1^+$) population didn't vary, but an increase in T cells and NK was seen. They also showed an increase in Tregs but didn't calculate the ratio in comparison to $CD8^+$ cells which may have been more informative. They also depleted $CD8^+$T cells from tumours showing a markedly reduced antitumor effect when using an anti-SIRPα mAb. Therefore, they suggested $CD8^+$T cells, but not $CD4^+$ T cells, participate in the effects of SIRPα blockade on tumour formation and growth, that macrophages tended to favour an M1 ($F4/80^+Ly6C^-MHCII^{hi}CD206^{lo}$) inflammatory phenotype. While we didn't detect any variation of the $F4/80^+$ expression in the myeloid populations, there was a slight

increase in M-MDSCs however this data was inconclusive. Furthermore, the moDCs were largely characterised by the expression of the monocytic marker CX3CR1 which didn't vary upon SIRPα blockade. One publication reported that moDC defined as $CX3CR1^{+}CD103^{-}$ had a poor T cell stimulatory capacity, however, these DC effectively took up OVA peptide *in vivo*[848,849]. We made a similar observation that moDC were processing OVA and their efficiency was boosted upon SIRPα blockade as was their capacity to present antigen making them more able to support T cell activation. Another aspect that may be worth investigation was the reduction of G-MDSC. These cells decreased upon SIRPα blockade which may indicate that SIRPα plays a novel role in regulation of G-MDSCs.

We aimed to correlate tumour regression with the fluctuations of immunosuppressive molecules as we had seen *in vitro*. We detected a tendency towards decreasing PD-L1 and ARG1 expression, however this wasn't significant. Increasing the number of mice tested could have clarified this result. As we saw, CD47-SIRPα engagement potentially increased PD-L1 expression which was reduced upon SIRPα blockade. Indeed, clinical trials are exploiting the blockade of PD-1 and SIRPα in an attempt to synergise the benefits of blocking these two connected molecules. In the BI 765063 clinical trial, a monoclonal antibody directed against SIRPα is being tested in combination with anti-PD-1. In another study, blockade of PD-1/PD-L1 in vivo increased macrophage phagocytosis and reduced tumour growth[587]. Despite this PD-L1 remained largely expressed and using a combination (like the BI 765063 clinical trial) to block both pathways could provide a dual effect of removing suppression of the myeloid cells and activating the T cells to induce phagocytosis.

Regarding ARG1, the slight general decrease observed following therapy could be associated with an increase in nutrient availability for T cells maturation. We also need to consider that ARG1 may be secreted in small extracellular vesicles capable of affecting T cell function[793]. This could be also the case in melanoma and may be at the

base of the difficulty encountered in assessing the ARG1 intensity. We also observed a reduction in the MHCII expressing moDC population. This was unexpected given the important role of MHCII for activation of $CD4^+$ T cell responses, and at the contrary, we found that moDCs expressing MHCII were suppressive. In support of our findings, Nagaraj *et al.*, found that MDSCs had the ability to induce antigen-specific $CD4^+$ T-cell tolerance *in vivo* which was dependent on the expression of MHC class II. They used $IAb^{-/-}$ MC38 tumour-bearing mice which in contrast to their wild type counterpart, showed reduction of MDSCs suppressive activity towards T cells. Their data indicated that MDSCs in tumour bearing mice can induce antigen-specific $CD4^+$ T-cell suppression, provided that the MDSCs express a sufficient level of MHCII. The cell-to-cell contact formed upon MHCII engagement also led to upregulation of cox2 and PGE2 both of which are implicated in MDSC-mediated immune suppression[850]. We speculate that the MHCII modulation observed upon SIRPα blockade could be in accordance with a reduction in the suppression mediated by MDSCs and this relationship should be further elucidated to establish the effects on $CD4^+$ T cells.

Our data demonstrated that CD47-SIRPα engagement was inducing a more suppressive phenotype in the MDSCs. As expected, its blockade induced a reduction in suppressive myeloid species and increased the proportion of cDC1 and $CD8^+$ T over Treg cells homing to the TME, resulting in tumour reduction. The $CD8^+$ T cells were associated with inflammation and with a good clinical outcome whilst the Tregs were associated with worse prognosis[250]. Melanoma infiltration by $CD8^+$ T cells strongly correlated with an increased survival. The latter directly correlates to the tumour infiltrating lymphocytes (TILs): the greater the density of lymphocytes within the tumour, the higher was the survival probability[757,758]. On Tregs there is still some uncertainty. Their presence was related to tumour regression in patients with head and neck cancers[851], whereas in melanoma their infiltration was described to predict local recurrence[760] and serve as an independent prognostic marker of poor survival[761].

However, the study of the suppressive molecules expressed on the cell surface of moDC and M-MDSC did not explain the reduction in suppression. *In vitro* it was clear that SIRPα blockade induced a dose dependent increase in phagocytosis. From this, we correlated tumour reduction with reactivation of phagocytosis, antigen processing and presentation. To our knowledge, we were the first to observe and document this mechanism of action in melanoma tumour bearing mice upon SIRPα blockade. In a mirrored way, it was shown that CD47 regulated antigen uptake by SIRPα^{+} dendritic cells[852]. Mice immunised with CD47(-/-) RBCs-OVA were presenting proliferation of T cells at the contrary of immunisation with WT RBCs-OVA demonstrating that DCs were phagocyting and presenting antigen when the CD47 was removed. Moreover, It was shown that the dendritic cells contributed to the in vivo efficacy of CD47-blocking therapies in immunocompetent tumour models[717] as driven by the stimulation of antigen presentation by either macrophages or dendritic cells[825]. Therefore, therapies targeting the CD47-SIRPα axis may promote adaptive immune responses against tumours. We observed similar results by blocking SIRPα as opposed to CD47. We clearly show an enhancement of phagocytosis *in vivo*, indicating that the threshold to activate phagocytosis was lowered. Furthermore, the increased phagocytosis correlated with antigen processing, which was differential between the cDC2, moDC and M-MDSCs cells. The moDCs appeared to be the most sensitive to SIRPα blockade and the sensitivity was dependent on the amount of SIRPα protein expressed. An alternative explanation is that their switch to inflammation was easier to obtain as their threshold barrier was lower than the other cell types tested. In accordance with this, the antigen presentation of engulfed antigen from OVA-expressing melanoma cells was increased predominantly by the moDC population but in fact by all the SIRPα^{+} myeloid cells.

At this stage, we had all the elements to hypothesize that the changes observed were dependent on the modification of antigen phagocytosis, processing and presentation

on the myeloid cell surface. This mechanism of action was confirmed in vitro and *in vivo*, and explained how the SIRPα blockade was reactivating the myeloid cells by circumventing the "do not eat me signal". This was very important because it was overcoming the persistent CD47 signal in the TME. The CD47 positive cells were partially responsible for the suppressive behaviour of moDC and M-MDSC cells. Thus, we reactivated one of the fundamental mechanisms of innate immunity associated with inflammation.

6.6.1 The complement pathway and its potential as therapeutic target

The activated complement system recognizes and eliminates invading microorganisms. However, it also contributes towards cellular homeostasis by facilitating the elimination of dead or modified self-cells, including apoptotic particles and cellular debris. The complement system has more than sixty components and has multiple activation products. C3a is generated by the C3 convertase and is involved in inflammation. It binds to the cell surface receptors for complement components, C3aR, which is expressed on neutrophils, monocytes and in general APCs. Newly released C3a recruits immune effector cells, whilst C3b or C3 activation fragments become deposited on the foreign surfaces acting to flag cells and promote phagocytosis through opsonization[853].

In cancer, clinical studies report a negative correlation between complement activation and patients survival in various human cancers[854]. C3 and C3a were found to be elevated in cancer patients at either the primary lesion or the serum, and their presence was associated with poor prognosis in ovarian cancer[855]. In tumour bearing C3-/- mice it was indicated that C3 was produced by the host cells in melanoma, breast and cervical cancer models and produced by the tumour itself in ovarian cancer[856,857]. Similar to C3a, interaction between C5a and its receptor increased migration of MDSCs into the tumour and enhanced the suppressive capacity of tumour-associated

MDSCs[855]. Both the C3aR and theC5aR engagement is implicated the regulation of immune checkpoints molecules which affects T cell function and maturation of myeloid populations[858,859,860]. C3a-C3aR interaction promoted melanoma growth which was delayed in mice lacking C3aR[861]. In this scenario, the TME was depleted of suppressive macrophages and enriched in neutrophils which upregulated inflammatory response genes[861]. Thus, Reducing C3a engagement may reduce this suppressive population which in turn could be activated by SIRPα blockade.

6.6.2 *In vivo* SIRPα and C3a combination blockade doesn't synergise

In our work we observed that SIRPα blockade reduced the moDCs which were expressing more immunosuppressive molecules, and Ly6C. The phagocytic activation threshold was also lowered resulting in an increase of antigen engulfment, processing and presentation. Additionally, SIRPα blockade also favoured $CD8^+$ T cell and cDC1 accumulation indicating a more inflammatory environment. Despite this immunological response we did not observe complete remission but instead a decrease in tumour growth.

Previous work from our lab showed that an immune regulating CAF subset ($CD34^{high}$) produced the complement molecule C3 across a variety of cancer types[64]. Furthermore, the interaction between this CAF population and the receptor, C3aR, expressing macrophages was also conserved. It was demonstrated that blockade of the C3 cleavage product C3a, reduced tumour macrophage populations while boosting Ly6C expressing myeloid cells, in turn this may boost the number of $CD8^+$ T-cells and decrease malignant growth. This suggests that C3a may represent a therapeutic target in a range of cancers. Similar to C3a, C5a also acts on immune populations, increasing MDSC accumulation in the tumour and promoting their suppressive activity[855,862]. Blocking C5a in combination with PD1 inhibitors was more

effective than either monotherapy alone, suggesting that a combined approach may improve clinical efficacy[863].

With this knowledge we saw an opportunity to combine the anti-C3a therapy with the anti- SIRPα blockade. Both therapies produced a decrease of tumour growth but not total remission. We hypothesised that the accumulation of Ly6C$^+$ myeloid cells produced by the C3a therapy was preventing a full response of the immune cells against the cancer. Whereas the SIRPα blockade produced activation of innate immunity in terms of phagocytosis and antigen presentation. We hoped that combining the therapies would reduce myeloid driven suppression and drive the cells towards creating an inflammatory environment thus reducing cancer tolerance.

In an attempt to combine the anti-C3a therapy with the SIRPα blockade, we merged the therapeutic strategies so tumour-bearing mice received either the rat-IgG1/mouse-IgG2a control, anti-SIRPα, anti-C3a[64] or a combination (figure 6.1 A). Whilst it was clear that the monotherapies and the combination reduced tumour growth compared to the control, in these preliminary experiments, an additive effect of the combination was difficult to spot (figure 6.1 B-G). The combination showed mixed results, appearing that the therapy dynamics failed to synergise (figure 6.1 D to G) indicating that other pathways may enter in conflict.

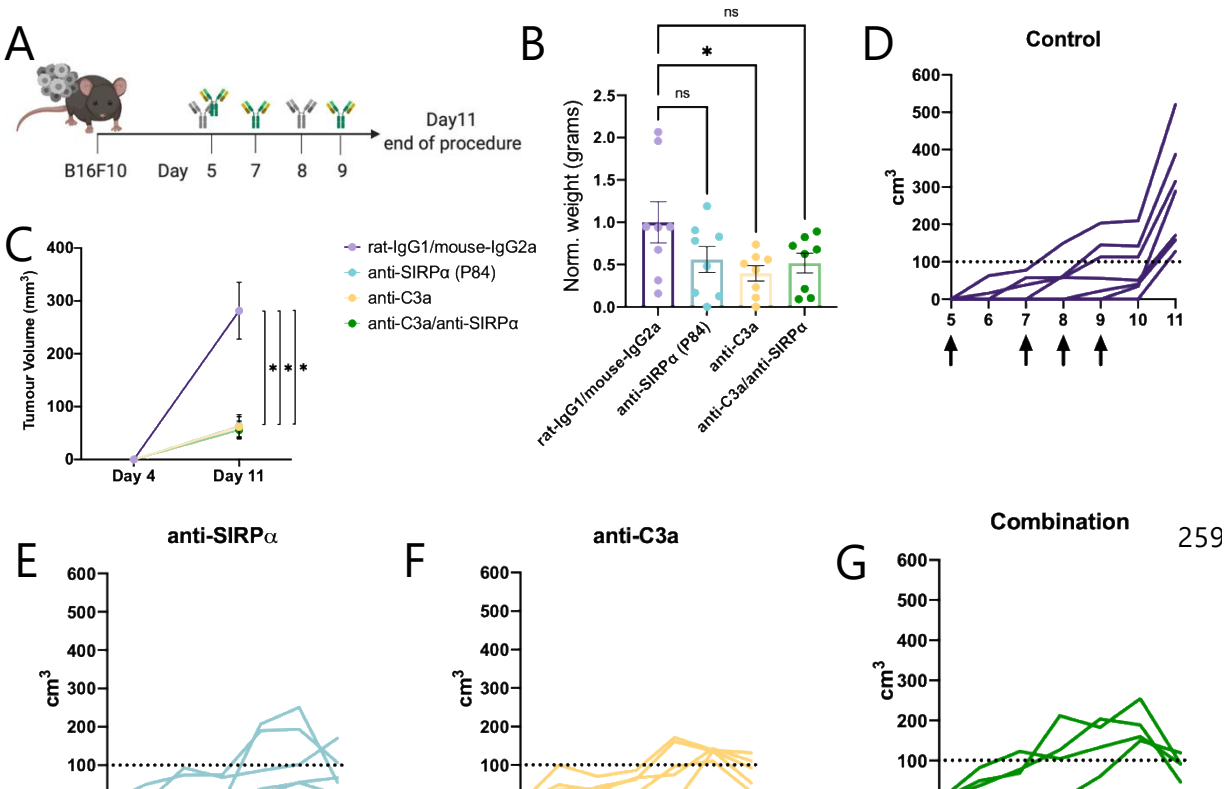

Figure 6.1. Double blockade of SIRPα and C3a reduces tumour growth but doesn't synergize. **(A)** Schematic representation of the therapeutic strategy. **(B)** Quantification of tumour weight normalised to control (grams) and **(C)** the tumour growth at day 4 and final day, for each mouse receiving **(D)** rat-IgG1 and mouse-IgG2a), **(E)** anti-SIRPα-P84 antibody, **(F)** anti-C3a antibody and **(G)** with the combination of the two. Data are mean ± SEM; * = $p < 0.05$, using the (B) ordinary one-way ANOVA with a Dunnett's post hoc test and (C) ordinary 2way ANOVA with a Tukey's post hoc test. Mice n=4 for each group in two independent experiments.

We speculate that removing the persistent C3a inflammation was beneficial in terms of reducing suppressive macrophages but the moDCs and MDSCs stimulated by SIRPα blockade didn't synergise. C3-/- IL-10 reporter mice, showed that $CD8^+$ TILs were increasing the expression of IL-10[859]. This interleukin was correlated with direct activation and expansion of tumour-resident $CD8^+$ T cells and tumour regression[860]. Based on this we can justify the regression observed in the anti-C3a however, depletion of the late components of complement (C3-9) was associated with the loss of ability to clear IgM-sensitized cells and a marked macrophage deficit to clear IgG-coated cells[864]. This could be the reason why the double therapy didn't synergise. Moreover, the macrophage phagocytic response is controlled by an integration of the inhibitory SIRPα signal with prophagocytic signals derived from Fcγ and complement receptor activation. A significant signal from Fcγ and/or complement receptors is required to overcome the normal SIRPα signal[713]. It may be that the SIRPα blockade reduces the phagocytic threshold which is not supported by a correct complement

activation if C3a is inhibited. Therefore, the therapies singularly reduce tumour growth, but they may conflict when used in combination.

Despite the failing to produce a synergistic effect we analysed the myeloid cell clusters comparing cDC1, cDC2, moDC, M-MDSC and G-MDSCs in order to explain the decrease in tumour growth. The SIRPα blockade produced similar tendencies to those described in chapter 5 which didn't reach significance due to the lower number of mice (appendix 8.11 A to E). No significant changes in the composition of these populations within the tumour was observed, nor were there significant changes in the expression of suppressive modulators (appendix 8.12 A to F). If any change was seen in these suppressive populations, it tended towards an increase of cDC2 and decrease of M-MDSCs upon treatment, and may indicate a switch from suppression to inflammation as we know that C3a/C3aR interaction was described in impairing dendritic cell maturation and favoured an M2-like phenotype in macrophages[865,866, 867,868]. Moreover, mice lacking C3aR were having myeloid cells with activated inflammatory genes profile[861]. In a breast cancer study, cells which expressed C3a induced an accumulation of immature low-density neutrophils in liver metastatic sites and its perturbation favoured anti-metastatic mature high-density neutrophils[869]. Therefore, indicating that C3a blockade was reducing cancer growth by favouring inflammatory neutrophils which may happened also in our case.

Interestingly, the M-MDSCs in the blood stream of the mice with combination therapy reduced PD-L1 expression perhaps indicating a less suppressive systemic effect (appendix 8.11 F).

Since changes in the myeloid compartment were not clear, $CD8^+$ T cell and the Treg cell populations were also examined. Small changes in the number of infiltrating $CD8^+$ and Tregs were noted (figure 6.2 A-B). On their own, these were not significant, but when ratio of CD8:Treg was calculated, the double therapy skewed the T cells in favour of CD8 phenotype (figure 6.2 C). These results were partially in contrast to the effects

seen with tumour growth. The anti-C3a was the most effective therapy in reducing tumour weight but the possible association with inflammatory myeloid or lymphoid cells wasn't clear. A deep analysis should be carried out to assess the inflammatory changes in specific populations.

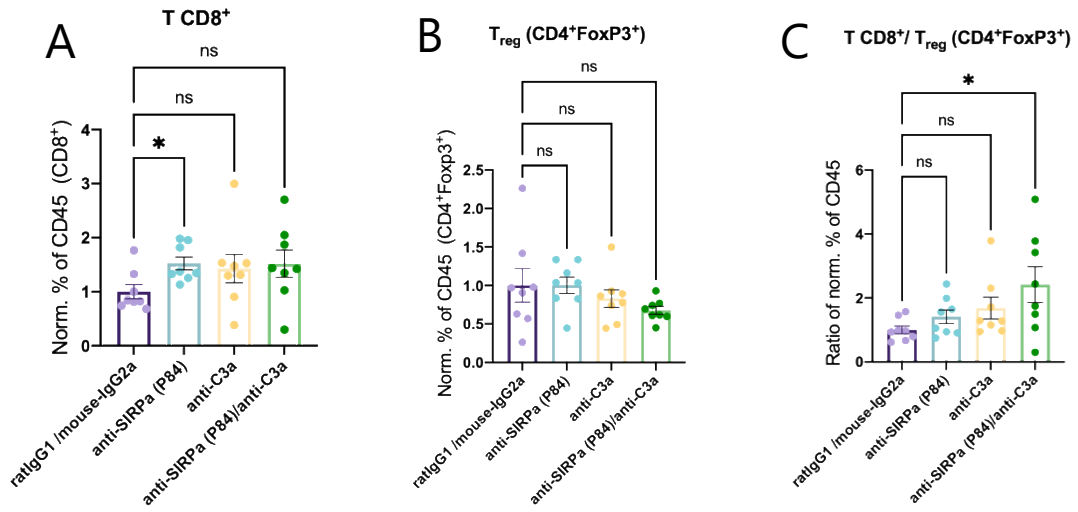

Figure 6.2. The C3a and SIRPα combination blockade favour the presence of T CD8⁺ over the Treg cells in the TME. (A) CD8⁺ T cells calculated as percentage of the total CD45⁺ cells. **(C)** CD4⁺FOXP3⁺ T cells calculated as percentage of the total CD45⁺ cells. **(C)** Ratio of CD8⁺/ CD4⁺FoxP3⁺ T cells. The data were obtained by mice groups injected with rat-IgG1 (control) and anti-SIRPα-P84 antibody. (A to C) The data were normalised by the signal detected in the rat-IgG1 injected mice. Data are mean ± SEM; * = $p < 0.05$, using the one-way ANOVA with a Dunnett's post hoc test. Assays mice n=4 for each group in two independent experiments.

It was recently reported that SIRPα expressed on CD8⁺ T cells which were sorted from chronically infected mice had greater *in vitro* cytotoxicity than the SIRPα⁻ cells extracted from the same mice[870]. Even though this work didn't show any SIRPα-CD47 dependent regulation of the T cells, the blockade might contribute in combination with the C3a removal to favour CD8⁺ T cells as opposed to Tregs. Unfortunately, in the panel used to identify the T cells we didn't include SIRPα, but it might be interesting in the future to assess the presence and modulation of these SIRPα⁺CD8⁺ T cells.

The double therapy produced contrasting effects but it certainly didn't synergise against tumour growth. C3a stimulation in cancer remains controversial but its blockade appears to confer T cell stimulation which is characterised by an antagonistic function towards tumour growth. Regarding SIRPα blockade which removes a break to the myeloid activation, it may require an agonist of T cell activation to exploit its full therapeutic potential.

6.7.1 Conclusions and future directions

In summary we have presented data to suggest that CD47-SIRPα axis contributes in the development of suppressive moDCs and M-MDSCs in melanoma. This may be perturbed by SIRPα blockade. SIRPα has a more restricted histological distribution and is highly expressed on the myeloid cells[650] which makes it a more favourable target, and thereby may bypass potential side effects seen with approaches blocking CD47. From these data we propose that SIRPα signalling mediates suppression via SHP-STAT dependent changes in phagocytosis, antigen processing and presentation. This is accompanied by changes in surface and soluble suppressive mediators, and is supported by changes in cellular metabolism. Blockade of this pathways reactivates antigen processing machinery and effective antigen presentation to T cells, which together with less suppressive intermediates enables T cell mediated anti-tumour effects (figure 6.3 A and B).

We have shown the potential of blocking CD47-SIRPα axis in a murine model of melanoma. SIRPα blockade is a valid strategy to achieve tumour remission by (re)-activating the phagocytic cornerstone between innate and adaptive immunity. Going forwards, examining archived human tumour samples for SIRPα infiltration and location would provide us with an indication of the prognostic/stratification potential. It would also be necessary to determine if similar effects can be observed in other tumour types rich in MDSC infiltration, and whether it functions by a similar

mechanism to promote a therapeutic effect. We have models of breast and pancreas in the lab that could be tested and also, we could acquire SIRPα deficient mice[600] to strengthen our findings. Approaches such as scRNAseq and mass spectrometry on treated tumours would provide greater insight into the biological changes happening with therapy.

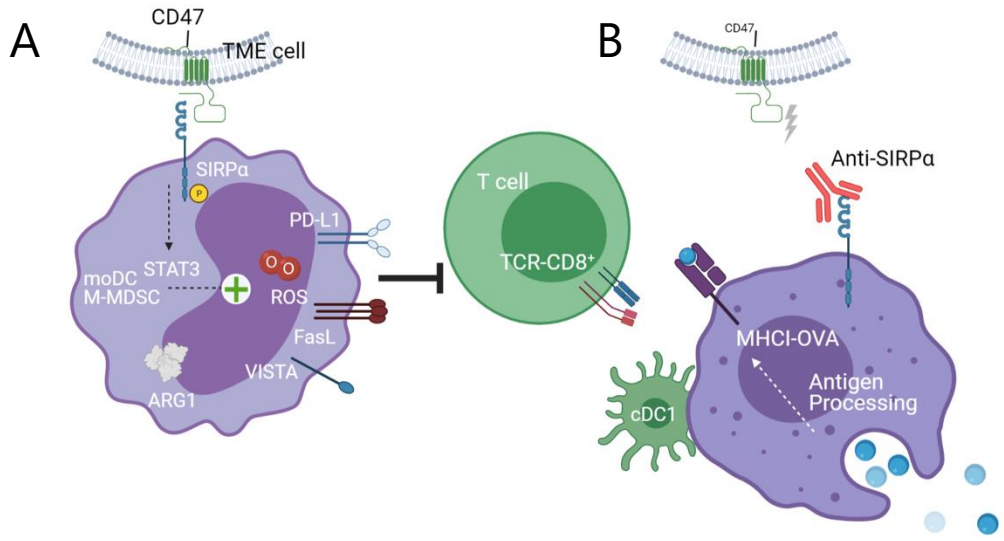

Figure 6.3. The CD47-SIRPα interaction and disruption effects over the functionality of myeloid cells in the TME. Myeloid cells develop an immunosuppressive phenotype due to contact with protein and cytokine rich tumour exudate. **(A)** In the TME, they enter in a CD47-rich environment which, when binding with SIRPα, enhances STAT3 signalling and is involved in ROS production and upregulation of suppressive molecules, such as PD-L1, FasL and VISTA. These contribute to increased suppressive potency causing inhibition of T cell proliferation. **(B)** The disruption of CD47-SIRPα interaction by blocking SIRPα on myeloid cells causes remodelling of the myeloid compartment by decreasing suppressive species and increasing inflammatory cDC1. Furthermore, it lowers the threshold of phagocytosis activation and consequently, antigen processing and presentation via MHCI. Those changes results in an increase of T $CD8^+$ cells and slows the tumour growth.

Having observed changes on myeloid phenotype and suppressive function in response to tumour derived stimulus, we need to determine what in the TME supports these

changes. This could be examined by mass spectrometry. We generated preliminary data to compare the M-MDSCs obtained in the presence of GM-CSF and GM-CSF-TCM (Supplementary 8.13 A). This process highlighted that lactoferrin may play a role in promoting suppressive development. This molecule has been associated with suppressive MDSCs transitory presence in neonates to control inflammation and allow gut microbial formation[871]. Moreover, Lactoferrin-/- mice infused with melanoma cells intravenously developed more metastasis in the lung which was associated with a suppressive state of the MDSCs[872]. Our preliminary data suggested that MDSCs grown in presence of lactoferrin (appendix 8.13 B) were more suppressive towards T cells (appendix 8.13 C). This may be investigated in the future using Lactoferrin-/- mice[873] to understand whether it drives the development of suppressive characteristics in MDSCs in the TME.

We also started to elucidate potential metabolic changes involving glycolysis and ATP consumption. Further studies would be required to assess these findings. This would require further characterisation using sea horse technology to understand changes in respiration to be associated with metabolic intermediates accumulation explored using mass spectrometry. The ATP accumulation observed in the CD47 stimulated cells may play a role in adenosine accumulation in the TME. In this sense, regulation of CD73/CD39 may be connected to the CD47-SIRPα axis and we would like to explore the possibility. In general, metabolic changes due to SIRPα blockade may reveal another potential adjuvant to increase the therapeutic efficacy.

Moreover, having seen a significant impact of monotherapy on tumour growth albeit without complete regression, it would be worth investigating different treatment regimens in tumour bearing mice; dosing schedule, concentration and examining local vs. systemic delivery. A recent study demonstrated that local delivery of anti PD-1 improved therapy responses in mice compared to systemic dosage via i.p delivery[874]. We would then also examine potential combination therapies. Targeting both innate

and adaptive arms, it may be possible to reduce doses of T cell ICI's to reduce associated toxicity, while still improving T cell infiltration in the face of augmented antigen processing, presentation, and stimulatory cues. In a very long term, one interesting approach would be to create a bispecific antibody to merge SIRPα blockade and T cells agonist retaining Fc functionality to induce opsonisation. This could fully embrace the therapeutic potential of the CD47-SIRPα disruption.

7 REFERENCES

1. Hanahan, D. & Coussens, L. M. Accessories to the Crime: Functions of Cells Recruited to the Tumor Microenvironment. *Cancer Cell* **21**, 309–322 (2012).
2. Maman, S. & Witz, I. P. A history of exploring cancer in context. *Nat. Rev. Cancer* **18**, 359–376 (2018).
3. DuPage, M. *et al.* Endogenous T cell responses to antigens expressed in lung adenocarcinomas delay malignant tumor progression. *Cancer Cell* **19**, 72–85 (2011).
4. Koebel, C. M. *et al.* Adaptive immunity maintains occult cancer in an equilibrium state. *Nature* **450**, 903–907 (2007).
5. Loeser, S. *et al.* Spontaneous tumor rejection by cbl-b-deficient CD8+ T cells. *J. Exp. Med.* **204**, 879–891 (2007).
6. Suzanne Ostrand-Rosenberg. Immune Surveillance: A Balance Between Pro- and Anti-tumor Immunity. *NIH Public Access* **23**, 1–7 (2008).
7. Berendt, M. J. & North, R. J. T-cell-mediated suppression of anti-tumor immunity. An explanation for progressive growth of an immunogenic tumor. *J. Exp. Med.* **151**, 69–80 (1980).
8. Li, A. *et al.* IL-33 Signaling Alters Regulatory T Cell Diversity in Support of Tumor Development. *Cell Rep.* **29**, 2998-3008.e8 (2019).
9. Degnim, A. C. *et al.* Alterations in the immune cell composition in premalignant breast tissue that precede breast cancer development. *Clin. Cancer Res.* **23**, 3945–3952 (2017).
10. Deeb, G. *et al.* Hypoxia-inducible factor-1α protein expression is associated with poor survival in normal karyotype adult acute myeloid leukemia. *Leuk. Res.* **35**, 579–584 (2011).
11. Du, R. *et al.* HIF1α Induces the Recruitment of Bone Marrow-Derived Vascular Modulatory Cells to Regulate Tumor Angiogenesis and Invasion. *Cancer Cell* **13**, 206–220 (2008).
12. Schito, L. & Semenza, G. L. Hypoxia-Inducible Factors: Master Regulators of Cancer Progression. *Trends in Cancer* **2**, 758–770 (2016).
13. Damaghi, M. *et al.* Chronic acidosis in the tumour microenvironment selects for overexpression of LAMP2 in the plasma membrane. *Nat. Commun.* **6**, (2015).
14. Boedtkjer, E. *et al.* Contribution of Na+,HCO3--cotransport to cellular pH control in human breast cancer: A role for the breast cancer susceptibility locus NBCn1 (SLC4A7). *Int. J. Cancer* **132**, 1288–1299 (2013).
15. Gerweck, L. E. & Seetharaman, K. Cellular pH gradient in tumor versus normal tissue: Potential exploitation for the treatment of cancer. *Cancer Res.* **56**, 1194–1198 (1996).
16. Rotin, D., Steele-Norwood, D., Grinstein, S. & Tannock, I. Requirement of the Na+/H+ Exchanger for Tumor Growth. *Cancer Res.* **49**, 205–211 (1989).
17. Jain, R. K., Martin, J. D. & Stylianopoulos, T. The role of mechanical forces in tumor growth and therapy. *Annu. Rev. Biomed. Eng.* **16**, 321–346 (2014).
18. Rofstad, E. K., Galappathi, K. & Mathiesen, B. S. Tumor Interstitial Fluid Pressure-A Link between Tumor Hypoxia, Microvascular Density, and Lymph Node Metastasis. *Neoplasia (United States)* **16**, 586–594 (2014).

19. Bergers, G. *et al.* Matrix metalloproteinase-9 triggers the angiogenic switch during carcinogenesis. *Nat. Cell Biol.* **2**, 737–744 (2000).

20. Shojaei, F. *et al.* Bv8 regulates myeloid-cell-dependent tumour angiogenesis. *Nature* **450**, 825–831 (2007).

21. De Palma, M., Biziato, D. & Petrova, T. V. Microenvironmental regulation of tumour angiogenesis. *Nat. Rev. Cancer* **17**, 457–474 (2017).

22. Ucuzian, A. A., Gassman, A. A., East, A. T. & Greisler, H. P. Molecular mediators of angiogenesis. *J. Burn Care Res.* **31**, 158–175 (2010).

23. Bremnes, R. M. *et al.* The role of tumor stroma in cancer progression and prognosis: Emphasis on carcinoma-associated fibroblasts and non-small cell lung cancer. *J. Thorac. Oncol.* **6**, 209–217 (2011).

24. Walker, C., Mojares, E. & Del Río Hernández, A. *Role of extracellular matrix in development and cancer progression*. *International Journal of Molecular Sciences* vol. 19 (2018).

25. Ondeck, M. G. *et al.* Dynamically stiffened matrix promotes malignant transformation of mammary epithelial cells via collective mechanical signaling. *Proc. Natl. Acad. Sci. U. S. A.* **116**, 3502–3507 (2019).

26. DeFilippis, R. A. *et al.* CD36 repression activates a multicellular stromal program shared by high mammographic density and tumor tissues. *Cancer Discov.* **2**, 826–839 (2012).

27. DeFilippis, R. A. *et al.* Stress signaling from human mammary epithelial cells contributes to phenotypes of mammographic density. *Cancer Res.* **74**, 5032–5044 (2014).

28. Öhlund, D. *et al.* Distinct populations of inflammatory fibroblasts and myofibroblasts in pancreatic cancer. *J. Exp. Med.* jem.20162024 (2017) doi:10.1084/jem.20162024.

29. Frantz, C., Stewart, K. M. & Weaver, V. M. The extracellular matrix at a glance. *J. Cell Sci.* **123**, 4195–4200 (2010).

30. Afik, R. *et al.* Tumor macrophages are pivotal constructors of tumor collagenous matrix. *J. Exp. Med.* **213**, 2315–2331 (2016).

31. Liguori, M., Solinas, G., Germano, G., Mantovani, A. & Allavena, P. Tumor-associated macrophages as incessant builders and destroyers of the cancer stroma. *Cancers (Basel).* **3**, 3740–3761 (2011).

32. Faouzi, S. *et al.* Myofibroblasts are responsible for collagen synthesis in the stroma of human hepatocellular carcinoma: An in vivo and in vitro study. *J. Hepatol.* **30**, 275–284 (1999).

33. Erdogan, B. *et al.* Cancer-associated fibroblasts promote directional cancer cell migration by aligning fibronectin. *J. Cell Biol.* **216**, 3799–3816 (2017).

34. Yoshimura, H. *et al.* Cellular Sources of Tenascin-C in Canine Mammary Carcinomas. *Vet. Pathol.* **52**, 92–96 (2015).

35. Wei, S. C. *et al.* Matrix stiffness drives epithelial-mesenchymal transition and tumour metastasis through a TWIST1-G3BP2 mechanotransduction pathway. *Nat. Cell Biol.* **17**, 678–688 (2015).

36. Hanley, C. J. *et al.* A subset of myofibroblastic cancer-associated fibroblasts regulate collagen fiber elongation, which is prognostic in multiple cancers. *Oncotarget* **7**, 6159–6174 (2016).

37. Pankova, D. *et al.* Cancer-associated fibroblasts induce a collagen cross-link switch in tumor stroma. *Mol. Cancer Res.* **14**, 287–295 (2016).

38. Kharaishvili, G. *et al.* The role of cancer-associated fibroblasts, solid stress and other microenvironmental factors in tumor progression and therapy resistance. *Cancer Cell Int.* **14**, 41 (2014).

39. Paszek, M. J. *et al.* Tensional homeostasis and the malignant phenotype. *Cancer Cell* **8**, 241–254 (2005).

40. Venning, F. A., Wullkopf, L. & Erler, J. T. Targeting ECM disrupts cancer progression. *Front. Oncol.* **5**, 1–15 (2015).

41. Huang, Y. *et al.* Pulmonary Vascular Destabilization in the Premetastatic Phase Facilitates Lung Metastasis. *Cancer Res.* **69**, 7529 LP – 7537 (2009).

42. Jacob, A. & Prekeris, R. The regulation of MMP targeting to invadopodia during cancer metastasis. *Front. Cell Dev. Biol.* **3**, 1–9 (2015).

43. Baniyash, M. Myeloid-derived suppressor cells as intruders and targets: clinical implications in cancer therapy. *Cancer Immunol. Immunother.* **65**, 857–867 (2016).

44. Kessenbrock, K., Plaks, V. & Werb, Z. Matrix Metalloproteinases: Regulators of the Tumor Microenvironment. *Cell* **141**, 52–67 (2010).

45. Houck, K. A., Leung, D. W., Rowland, A. M., Winer, J. & Ferrara, N. Dual regulation of vascular endothelial growth factor bioavailability by genetic and proteolytic mechanisms. *J. Biol. Chem.* **267**, 26031–26037 (1992).

46. Belotti, D. *et al.* Matrix metalloproteinases (MMP9 and MMP2) induce the release of vascular endothelial growth factor (VEGF) by ovarian carcinoma cells: implications for ascites formation. *Cancer Res.* **63**, 5224–5229 (2003).

47. Fridlender, Z. G. *et al.* Polarization of Tumor-Associated Neutrophil Phenotype by TGF-b: 'N1' versus 'N2' TAN. *Cancer Cell* **16**, 183–194 (2009).

48. Ohshio, Y. *et al.* Cancer-associated fibroblast-targeted strategy enhances antitumor immune responses in dendritic cell-based vaccine. *Cancer Sci.* **106**, 134–142 (2015).

49. Weathington, N. M. *et al.* A novel peptide CXCR ligand derived from extracellular matrix degradation during airway inflammation. *Nat. Med.* **12**, 317–323 (2006).

50. Houghton, A. M. *et al.* Elastin fragments drive disease progression in a murine model of emphysema. *J. Clin. Invest.* **116**, 753–759 (2006).

51. Midwood, K. *et al.* Tenascin-C is an endogenous activator of Toll-like receptor 4 that is essential for maintaining inflammation in arthritic joint disease. *Nat. Med.* **15**, 774–780 (2009).

52. Johnson, G. B., Brunn, G. J., Kodaira, Y. & Platt, J. L. Receptor-Mediated Monitoring of Tissue Well-Being Via Detection of Soluble Heparan Sulfate by Toll-Like Receptor 4. *J. Immunol.* **168**, 5233–5239 (2002).

53. Hartmann, N. *et al.* Prevailing Role of Contact Guidance in Intrastromal T-cell Trapping in Human Pancreatic Cancer. *Clin. Cancer Res.* **20**, 3422 LP – 3433 (2014).

54. Kuczek, D. E. *et al.* Collagen density regulates the activity of tumor-infiltrating T cells. *bioRxiv* **6**, 1–15 (2018).

55. Li, B. & Wang, J. H. C. Fibroblasts and myofibroblasts in wound healing: Force generation and measurement. *J. Tissue Viability* **20**, 108–120 (2011).

56. Cirri, P. & Chiarugi, P. Cancer-associated-fibroblasts and tumour cells: A diabolic liaison driving cancer progression. *Cancer Metastasis Rev.* **31**, 195–208 (2012).

57. Calvo, F. *et al.* Mechanotransduction and YAP-dependent matrix remodelling is required for the generation and maintenance of cancer-associated fibroblasts. *Nat. Cell Biol.* **15**, 637–646 (2013).

58. De Wever, O. *et al.* Tenascin-C and SF/HGF produced by myofibroblasts in vitro provide convergent pro-invasive signals to human colon cancer cells through RhoA and Rac. *FASEB J. Off. Publ. Fed. Am. Soc. Exp. Biol.* **18**, 1016–1018 (2004).

59. Foster, C. T., Gualdrini, F. & Treisman, R. Mutual dependence of the MRTF-SRF and YAP-TEAD pathways in cancer-associated fibroblasts is indirect and mediated by cytoskeletal dynamics. *Genes Dev.* **31**, 2361–2375 (2017).

60. Erez, N., Truitt, M., Olson, P., Arron, S. T. & Hanahan, D. Cancer-Associated Fibroblasts Are Activated in Incipient Neoplasia to Orchestrate Tumor-Promoting Inflammation in an NF-kappaB-Dependent Manner. *Cancer Cell* **17**, 135–147 (2010).

61. Sanz-Moreno, V. *et al.* ROCK and JAK1 signaling cooperate to control actomyosin contractility in tumor cells and stroma. *Cancer Cell* **20**, 229–245 (2011).

62. Cortez, E., Roswall, P. & Pietras, K. Functional subsets of mesenchymal cell types in the tumor microenvironment. *Semin. Cancer Biol.* **25**, 3–9 (2014).

63. Augsten, M. Cancer-associated fibroblasts as another polarized cell type of the tumor microenvironment. *Front. Oncol.* **4 MAR**, 1–8 (2014).

64. Davidson, S. *et al.* Single-Cell RNA Sequencing Reveals a Dynamic Stromal Niche That Supports Tumor Growth. *Cell Rep.* **31**, 107628 (2020).

65. Elyada, E. *et al.* Cross-species single-cell analysis of pancreatic ductal adenocarcinoma reveals antigen-presenting cancer-associated fibroblasts. *Cancer Discov.* **9**, 1102–1123 (2019).

66. Costa, A. *et al.* Fibroblast Heterogeneity and Immunosuppressive Environment in Human Breast Cancer. *Cancer Cell* **33**, 463-479.e10 (2018).

67. Jia, C. C. *et al.* Cancer-Associated Fibroblasts from Hepatocellular Carcinoma Promote Malignant Cell Proliferation by HGF Secretion. *PLoS One* **8**, 1–9 (2013).

68. Kalluri, R. & Zeisberg, M. Fibroblasts in cancer. *Nat. Rev. Cancer* **6**, 392–401 (2006).

69. Zhang, R. *et al.* Cancer-associated fibroblasts enhance tumor-associated macrophages enrichment and suppress NK cells function in colorectal cancer. *Cell Death Dis.* **10**, (2019).

70. Ren, G. *et al.* CCR2-dependent recruitment of macrophages by tumor-educated mesenchymal stromal cells promotes tumor development and is mimicked by TNFα. *Cell Stem Cell* **11**, 812–824 (2012).

71. Deng, Y. *et al.* Hepatic carcinoma-associated fibroblasts enhance immune suppression by facilitating the generation of myeloid-derived suppressor cells. *Oncogene* **36**, 1090–1101 (2017).

72. Comito, G. *et al.* Cancer-associated fibroblasts and M2-polarized macrophages synergize during prostate carcinoma progression. *Oncogene* **33**, 2423–2431 (2014).

73. Harper, J. & Sainson, R. C. A. Regulation of the anti-tumour immune response by cancer-associated fibroblasts. *Semin. Cancer Biol.* **25**, 69–77 (2014).

74. Lakins, M. A., Ghorani, E., Munir, H., Martins, C. P. & Shields, J. D. Cancer-associated fibroblasts induce antigen-specific deletion of CD8+T Cells to protect tumour cells. *Nat. Commun.* **9**, 1–9 (2018).

75. Inoue, K. ichi *et al.* Cancer-associated fibroblasts show heterogeneous gene expression and induce vascular endothelial growth factor A (VEGFA) in response to environmental stimuli. *Ann. Gastroenterol. Surg.* **3**, 416–425 (2019).

76. Singer, C. F. *et al.* MMP-2 and MMP-9 expression in breast cancer-derived human fibroblasts is differentially regulated by stromal-epithelial interactions. *Breast Cancer Res. Treat.* **72**, 69–77 (2002).

77. Wandel, E., Grasshoff, A., Mittag, M., Haustein, U. F. & Saalbach, A. Fibroblasts surrounding melanoma express elevated levels of matrix metalloproteinase-1 (MMP-1) and intercellular adhesion molecule-1 (ICAM-1) in vitro. *Exp. Dermatol.* **9**, 34–41 (2000).

78. Geiger, B., Bershadsky, A., Pankov, R. & Yamada, K. M. Transmembrane extracellular matrix-cytoskeleton crosstalk. *Nat. Rev. Mol. Cell Biol.* **2**, 793–805 (2001).

79. Liao, S. & Padera, T. P. Lymphatic function and immune regulation in health and disease. *Lymphat. Res. Biol.* **11**, 136–143 (2013).

80. Shayan, R., Achen, M. G. & Stacker, S. A. Lymphatic vessels in cancer metastasis: Bridging the gaps. *Carcinogenesis* **27**, 1729–1738 (2006).

81. Hirschi, K. K. & D'Amore, P. A. Pericytes in the microvasculature. *Cardiovasc. Res.* **32**, 687–698 (1996).

82. Hellström, M. *et al.* Lack of pericytes leads to endothelial hyperplasia and abnormal vascular morphogenesis. *J. Cell Biol.* **152**, 543–553 (2001).

83. Hynes, R. O. The extracellular matrix: Not just pretty fibrils. *Science (80-.).* **326**, 1216–1219 (2009).

84. Tilki, D. *et al.* Zone-specific remodeling of tumor blood vessels affects tumor growth. *Cancer* **110**, 2347–2362 (2007).

85. Dudley, A. C. Tumor endothelial cells. *Cold Spring Harb. Perspect. Med.* **2**, (2012).

86. Nagy, J. A., Chang, S. H., Dvorak, A. M. & Dvorak, H. F. Why are tumour blood vessels abnormal and why is it important to know? *Br. J. Cancer* **100**, 865–869 (2009).

87. Lee, S., Jilan, S. M., Nikolova, G. V., Carpizo, D. & Luisa Iruela-Arispe, M. Processing of VEGF-A by matrix metalloproteinases regulates bioavailability and vascular patterning in tumors. *J. Cell Biol.* **169**, 681–691 (2005).

88. Hida, K., Maishi, N., Annan, D. A. & Hida, Y. Contribution of tumor endothelial cells in cancer progression. *Int. J. Mol. Sci.* **19**, 1–12 (2018).

89. Yang, J. *et al.* Guidelines and definitions for research on epithelial–mesenchymal transition. *Nat. Rev. Mol. Cell Biol.* **21**, 341–352 (2020).

90. Zeisberg, E. M., Potenta, S., Xie, L., Zeisberg, M. & Kalluri, R. Discovery of endothelial to mesenchymal transition as a source for carcinoma-associated fibroblasts. *Cancer Res.* **67**, 10123–10128 (2007).

91. Hida, K. *et al.* Tumor-associated endothelial cells with cytogenetic abnormalities. *Cancer Res.* **64**, 8249–8255 (2004).

92. Dudley, A. C., Shih, S.-C., Cliffe, A. R., Hida, K. & Klagsbrun, M. Attenuated p53 activation in tumour-associated stromal cells accompanies decreased sensitivity to etoposide and vincristine. *Br. J. Cancer* **99**, 118–125 (2008).

93. St Croix, B. *et al.* Genes expressed in human tumor endothelium. *Science* **289**, 1197–1202

(2000).

94. Seaman, S. *et al.* Genes that Distinguish Physiological and Pathological Angiogenesis. *Cancer Cell* **11**, 539–554 (2007).

95. Van Beijnum, J. R. *et al.* Tumor angiogenesis is enforced by autocrine regulation of high-mobility group box 1. *Oncogene* **32**, 363–374 (2013).

96. Chae, Y. K. *et al.* Overexpression of adhesion molecules and barrier molecules is associated with differential infiltration of immune cells in non-small cell lung cancer. *Sci. Rep.* **8**, 1–10 (2018).

97. Langley, R. R. *et al.* Quantification of murine endothelial cell adhesion molecules in solid tumors. *Am. J. Physiol. - Hear. Circ. Physiol.* **277**, (1999).

98. Piali, L., Fichtel, A., Terpe, H. J., Imhof, B. A. & Gisler, R. H. Endothelial vascular cell adhesion molecule 1 expression is suppressed by melanoma and carcinoma. *J. Exp. Med.* **181**, 811–816 (1995).

99. Griffioen, A. W., Damen, C. A., Blijham, G. H. & Groenewegen, G. Tumor angiogenesis is accompanied by a decreased inflammatory response of tumor-associated endothelium. *Blood* **88**, 667–673 (1996).

100. Griffioen, A. W., Damen, C. A., Martinotti, S., Blijham, G. H. & Groenewegen, G. Endothelial intercellular adhesion molecule-1 expression is suppressed in human malignancies: the role of angiogenic factors. *Cancer Res.* **56**, 1111–1117 (1996).

101. Griffioen, A. W. *et al.* Angiogenesis inhibitors overcome tumor induced endothelial cell anergy. *Int. J. cancer* **80**, 315–319 (1999).

102. Pober, J. S. *et al.* Activation of cultured human endothelial cells by recombinant lymphotoxin: comparison with tumor necrosis factor and interleukin 1 species. *J. Immunol.* **138**, 3319–3324 (1987).

103. Pober, J. S. Cytokine-mediated activation of vascular endothelium. Physiology and pathology. *Am. J. Pathol.* **133**, 426–433 (1988).

104. Boucher, Y., Baxter, L. T. & Jain, R. K. Interstitial pressure gradients in tissue-isolated and subcutaneous tumors: implications for therapy. *Cancer Res.* **50**, 4478–4484 (1990).

105. Rodig, N. *et al.* Endothelial expression of PD-L1 and PD-L2 down-regulates CD8+ T cell activation and cytolysis. *Eur. J. Immunol.* **33**, 3117–3126 (2003).

106. Farnsworth, R. H., Achen, M. G. & Stacker, S. A. The evolving role of lymphatics in cancer metastasis. *Curr. Opin. Immunol.* **53**, 64–73 (2018).

107. Swartz, M. A. & Lund, A. W. Lymphatic and interstitial flow in the tumour microenvironment: Linking mechanobiology with immunity. *Nat. Rev. Cancer* **12**, 210–219 (2012).

108. Tewalt, E. F. *et al.* Lymphatic endothelial cells induce tolerance via PD-L1 and lack of costimulation leading to high-level PD-1 expression on CD8 T cells. *Blood* **120**, 4772–4782 (2012).

109. Johnson, L. A. *et al.* Dendritic cells enter lymph vessels by hyaluronan-mediated docking to the endothelial receptor LYVE-1. *Nat. Immunol.* **18**, 762–770 (2017).

110. Seyfizadeh, N., Muthuswamy, R., Mitchell, D. A., Nierkens, S. & Seyfizadeh, N. Migration of dendritic cells to the lymph nodes and its enhancement to drive anti-tumor responses. *Crit. Rev. Oncol. Hematol.* **107**, 100–110 (2016).

111. Society, A. C. Melanoma Skin Cancer Guide. 2–3 (2015).

112. Villanueva, J. & Herlyn, M. Melanoma and the tumor microenvironment. *Curr. Oncol. Rep.* **10**, 439–446 (2008).

113. Krapcho M, et al. H. N. N. A. SEER Cancer Statistics Review 1975-2013 National Cancer Institute SEER Cancer Statistics Review 1975-2013 National Cancer Institute. *SEER Cancer Stat. Rev. 1975-2013, Natl. Cancer Institute. Bethesda, MD, http//seer.cancer.gov/csr/1975_2013/, based Novemb. 2015 SEER data submission, posted to SEER web site, April 2016*. 1992–2013 (2016).

114. Filippi, A. R. *et al.* Radiotherapy and immune checkpoints inhibitors for advanced melanoma. *Radiother. Oncol. J. Eur. Soc. Ther. Radiol. Oncol.* **120**, 1–12 (2016).

115. Klemen, N. D. *et al.* Survival after checkpoint inhibitors for metastatic acral , mucosal and uveal melanoma. 1–6 (2020) doi:10.1136/jitc-2019-000341.

116. Brenner, M. & Hearing, V. J. The protective role of melanin against UV damage in human skin. *Photochem. Photobiol.* **84**, 539–549 (2008).

117. Califano, J. & Nance, M. Malignant Melanoma. *Facial Plast. Surg. Clin. North Am.* **17**, 337–348 (2009).

118. Larue, L. & Beermann, F. Cutaneous melanoma in genetically modified animals. *Pigment Cell Res.* **20**, 485–497 (2007).

119. Domingues, B., Lopes, J., Soares, P. & Populo, H. Melanoma treatment in review. *ImmunoTargets Ther.* **Volume 7**, 35–49 (2018).

120. Wilson, M. A. & Schuchter, L. M. Chemotherapy for Melanoma. *Cancer Treat. Res.* **167**, 209–229 (2016).

121. Soengas, M. S. & Lowe, S. W. Apoptosis and melanoma chemoresistance. *Oncogene* **22**, 3138–3151 (2003).

122. Brose, M. S. *et al.* BRAF and RAS mutations in human lung cancer and melanoma. *Cancer Res.* **62**, 6997–7000 (2002).

123. Batus, M. *et al.* Optimal management of metastatic melanoma: current strategies and future directions. *Am. J. Clin. Dermatol.* **14**, 179–194 (2013).

124. Livingstone, E., Zimmer, L., Vaubel, J. & Schadendorf, D. BRAF, MEK and KIT inhibitors for melanoma: adverse events and their management. *Chinese Clin. Oncol.* **3**, 29 (2014).

125. Flaherty, K. T. *et al.* Improved survival with MEK inhibition in BRAF-mutated melanoma. *N. Engl. J. Med.* **367**, 107–114 (2012).

126. Robert, C. *et al.* Ipilimumab plus Dacarbazine for Previously Untreated Metastatic Melanoma. *N. Engl. J. Med.* **364**, 2517–2526 (2011).

127. Hamid, O. *et al.* Five-year survival outcomes for patients with advanced melanoma treated with pembrolizumab in KEYNOTE-001. *Ann. Oncol.* **30**, 582–588 (2019).

128. Chen, D. S. & Mellman, I. Elements of cancer immunity and the cancer-immune set point. *Nature* **541**, 321–330 (2017).

129. Hodi, F. S. *et al.* Nivolumab plus ipilimumab or nivolumab alone versus ipilimumab alone in advanced melanoma (CheckMate 067): 4-year outcomes of a multicentre, randomised, phase 3 trial. *Lancet. Oncol.* **19**, 1480–1492 (2018).

130. Boon, T., Coulie, P. G., Van den Eynde, B. J. & van der Bruggen, P. Human T cell responses

against melanoma. *Annu. Rev. Immunol.* **24**, 175–208 (2006).

131. Merimsky, O., Shoenfeld, Y., Chaitchik, S., Yecheskel, G. & Fishman, P. Antigens and antibodies in malignant melanoma. *Tumour Biol. J. Int. Soc. Oncodevelopmental Biol. Med.* **15**, 188–202 (1994).

132. Seliger, B. Novel insights into the molecular mechanisms of HLA class I abnormalities. *Cancer Immunol. Immunother.* **61**, 249–254 (2012).

133. Benitez, R. *et al.* Mutations of the beta2-microglobulin gene result in a lack of HLA class I molecules on melanoma cells of two patients immunized with MAGE peptides. *Tissue Antigens* **52**, 520–529 (1998).

134. Maleno, I., López-Nevot, M. A., Cabrera, T., Salinero, J. & Garrido, F. Multiple mechanisms generate HLA class I altered phenotypes in laryngeal carcinomas: high frequency of HLA haplotype loss associated with loss of heterozygosity in chromosome region 6p21. *Cancer Immunol. Immunother.* **51**, 389–396 (2002).

135. Romero, J. M. *et al.* Coordinated downregulation of the antigen presentation machinery and HLA class I/beta2-microglobulin complex is responsible for HLA-ABC loss in bladder cancer. *Int. J. cancer* **113**, 605–610 (2005).

136. Speeckaert, R. *et al.* Immune reactions in benign and malignant melanocytic lesions: Lessons for immunotherapy. *Pigment Cell Melanoma Res.* **24**, 334–344 (2011).

137. Hino, R. *et al.* Tumor cell expression of programmed cell death-1 ligand 1 is a prognostic factor for malignant melanoma. *Cancer* **116**, 1757–1766 (2010).

138. Wang, P., Zhang, X., Sun, N., Zhao, Z. & He, J. Comprehensive Analysis of the Tumor Microenvironment in Cutaneous Melanoma associated with Immune Infiltration. *J. Cancer* **11**, 3858–3870 (2020).

139. Croci, D. O. *et al.* Dynamic cross-talk between tumor and immune cells in orchestrating the immunosuppressive network at the tumor microenvironment. *Cancer Immunol. Immunother.* **56**, 1687–1700 (2007).

140. Fujimura, T., Kambayashi, Y. & Aiba, S. Crosstalk between regulatory T cells (Tregs) and myeloid derived suppressor cells (MDSCs) during melanoma growth. *Oncoimmunology* **1**, 1433–1434 (2012).

141. Fujimura, T., Ring, S., Umansky, V., Mahnke, K. & Enk, A. H. Regulatory T cells stimulate B7-H1 expression in myeloid-derived suppressor cells in ret melanomas. *J. Invest. Dermatol.* **132**, 1239–1246 (2012).

142. Jacobs, J. F. M., Nierkens, S., Figdor, C. G., de Vries, I. J. M. & Adema, G. J. Regulatory T cells in melanoma: The final hurdle towards effective immunotherapy? *Lancet Oncol.* **13**, 32–42 (2012).

143. Kimpfler, S. *et al.* Skin melanoma development in ret transgenic mice despite the depletion of CD25+Foxp3+ regulatory T cells in lymphoid organs. *J. Immunol.* **183**, 6330–6337 (2009).

144. Fantini, M. C. *et al.* Cutting Edge: TGF-β Induces a Regulatory Phenotype in CD4 + CD25 − T Cells through Foxp3 Induction and Down-Regulation of Smad7. *J. Immunol.* **172**, 5149–5153 (2004).

145. Nizar, S., Meyer, B., Galustian, C., Kumar, D. & Dalgleish, A. T regulatory cells, the evolution of targeted immunotherapy. *Biochim. Biophys. Acta* **1806**, 7–17 (2010).

146. Lim, S. Y., Yuzhalin, A. E., Gordon-Weeks, A. N. & Muschel, R. J. Targeting the CCL2-CCR2

signaling axis in cancer metastasis. *Oncotarget* **7**, 28697–28710 (2016).

147. Obermajer, N., Muthuswamy, R., Odunsi, K., Edwards, R. P. & Kalinski, P. PGE 2-induced CXCL 12 production and CXCR4 expression controls the accumulation of human MDSCs in ovarian cancer environment. *Cancer Res.* **71**, 7463–7470 (2011).

148. Gargett, T. *et al.* GM-CSF signalling blockade and chemotherapeutic agents act in concert to inhibit the function of myeloid-derived suppressor cells in vitro. *Clin. Transl. Immunol.* **5**, e119 (2016).

149. Waight, J. D., Hu, Q., Miller, A., Liu, S. & Abrams, S. I. Tumor-derived G-CSF facilitates neoplastic growth through a granulocytic myeloid-derived suppressor cell-dependent mechanism. *PLoS One* **6**, 70–80 (2011).

150. Elkabets, M. *et al.* IL-1β regulates a novel myeloid-derived suppressor cell subset that impairs NK cell development and function. *Eur J Immunol* **40**, 3347–3357 (2010).

151. Tobin, R. P. *et al.* IL-6 and IL-8 Are Linked With Myeloid-Derived Suppressor Cell Accumulation and Correlate With Poor Clinical Outcomes in Melanoma Patients. *Front. Oncol.* **9**, 1–12 (2019).

152. Mao, Y. *et al.* Inhibition of tumor-derived prostaglandin-E2 blocks the induction of myeloid-derived suppressor cells and recovers natural killer cell activity. *Clin. Cancer Res.* **20**, 4096–4106 (2014).

153. Wang, J. & Chen, L. Myeloid Cells' Evasion of Melanoma Immunity. *J. Invest. Dermatol.* **134**, 2675–2677 (2014).

154. Filipazzi, P. *et al.* Identification of a new subset of myeloid suppressor cells in peripheral blood of melanoma patients with modulation by a granulocyte-macrophage colony-stimulation factor-based antitumor vaccine. *J. Clin. Oncol.* **25**, 2546–2553 (2007).

155. Gazzaniga, S. *et al.* Targeting tumor-associated macrophages and inhibition of MCP-1 reduce angiogenesis and tumor growth in a human melanoma xenograft. *J. Invest. Dermatol.* **127**, 2031–2041 (2007).

156. Varney, M. L. *et al.* Monocyte/macrophage recruitment, activation and differentiation modulate interleukin-8 production: a paracrine role of tumor-associated macrophages in tumor angiogenesis. *In Vivo* **16**, 471–477 (2002).

157. Varney, M. L., Olsen, K. J., Mosley, R. L. & Singh, R. K. Paracrine regulation of vascular endothelial growth factor--a expression during macrophage-melanoma cell interaction: role of monocyte chemotactic protein-1 and macrophage colony-stimulating factor. *J. Interf. cytokine Res. Off. J. Int. Soc. Interf. Cytokine Res.* **25**, 674–683 (2005).

158. Ntayi, C., Hornebeck, W. & Bernard, P. Influence of cultured dermal fibroblasts on human melanoma cell proliferation, matrix metalloproteinase-2 (MMP-2) expression and invasion in vitro. *Arch. Dermatol. Res.* **295**, 236–241 (2003).

159. Meierjohann, S. *et al.* MMP13 mediates cell cycle progression in melanocytes and melanoma cells: in vitro studies of migration and proliferation. *Mol. Cancer* **9**, 201 (2010).

160. Kääriäinen, E. *et al.* Switch to an invasive growth phase in melanoma is associated with tenascin-C, fibronectin, and procollagen-I forming specific channel structures for invasion. *J. Pathol.* **210**, 181–191 (2006).

161. Zhou, Y. *et al.* Osteopontin expression correlates with melanoma invasion. *J. Invest. Dermatol.* **124**, 1044–1052 (2005).

162. Harrell, M. I., Iritani, B. M. & Ruddell, A. Tumor-induced sentinel lymph node lymphangiogenesis and increased lymph flow precede melanoma metastasis. *Am. J. Pathol.* **170**, 774–786 (2007).

163. Hirakawa, S. *et al.* VEGF-A induces tumor and sentinel lymph node lymphangiogenesis and promotes lymphatic metastasis. *J. Exp. Med.* **201**, 1089–1099 (2005).

164. FIDLER, I. J. Selection of Successive Tumour Lines for Metastasis. *Nat. New Biol.* **242**, 148–149 (1973).

165. Nakamura, K. *et al.* Characterization of mouse melanoma cell lines by their mortal malignancy using an experimental metastatic model. *Life Sci.* **70**, 791–798 (2002).

166. van Elsas, A., Hurwitz, a a & Allison, J. P. Combination immunotherapy of B16 melanoma using anti-cytotoxic T lymphocyte-associated antigen 4 (CTLA-4) and granulocyte/macrophage colony-stimulating factor (GM-CSF)-producing vaccines induces rejection of subcutaneous and metastatic tumors accompanied . *J. Exp. Med.* **190**, 355–366 (1999).

167. Curran, M. A., Montalvo, W., Yagita, H. & Allison, J. P. PD-1 and CTLA-4 combination blockade expands infiltrating T cells and reduces regulatory T and myeloid cells within B16 melanoma tumors. *Proc. Natl. Acad. Sci. U. S. A.* **107**, 4275–4280 (2010).

168. Merritt, R. E., Yamada, R. E., Crystal, R. G. & Korst, R. J. Augmenting major histocompatibility complex class I expression by murine tumors in vivo enhances antitumor immunity induced by an active immunotherapy strategy. *J. Thorac. Cardiovasc. Surg.* **127**, 355–364 (2004).

169. Lim, Y. S. *et al.* Augmentation of therapeutic antitumor immunity by B16F10 melanoma cells transfected by interferon-gamma and allogeneic MHC class I cDNAs. *Mol. Cells* **8**, 629–636 (1998).

170. Steitz, J. *et al.* Genetic immunization of mice with human tyrosinase-related protein 2: implications for the immunotherapy of melanoma. *Int. J. cancer* **86**, 89–94 (2000).

171. Umansky, V., Sevko, A., Gebhardt, C. & Utikal, J. Myeloide Suppressorzellen (MDSC) beim malignen Melanom. *JDDG - J. Ger. Soc. Dermatology* **12**, 1021–1027 (2014).

172. Jiang, H. *et al.* Elevated chronic inflammatory factors and myeloid-derived suppressor cells indicate poor prognosis in advanced melanoma patients. *Int. J. Cancer* **136**, 2352–2360 (2015).

173. Sanmamed, M. F., Chester, C., Melero, I. & Kohrt, H. Defining the optimal murine models to investigate immune checkpoint blockers and their combination with other immunotherapies. *Ann. Oncol.* **27**, 1190–1198 (2016).

174. Melnikova, V. O., Bolshakov, S. V, Walker, C. & Ananthaswamy, H. N. Genomic alterations in spontaneous and carcinogen-induced murine melanoma cell lines. *Oncogene* **23**, 2347–2356 (2004).

175. Dankort, D. *et al.* BrafV600E cooperates with Pten loss to induce metastatic melanoma. *Nat. Genet.* **41**, 544–552 (2009).

176. Richards, V. Cancer immunology--an overview. *Prog. Exp. Tumor Res.* **25**, 1–60 (1980).

177. Dobosz, P. & Dzieciątkowski, T. The Intriguing History of Cancer Immunotherapy. *Front. Immunol.* **10**, (2019).

178. Onkologie, C. 11 Prinzipien der Immuntherapie Immuntherapie. *Kleintieronkologie* 1–2 (2016) doi:10.1055/b-0036-130815.

179. Oelschlaeger, T. A. Bacteria as tumor therapeutics? *Bioeng. Bugs* **1**, 146–147 (2010).

180. Merien, F. A Journey with Elie Metchnikoff: From Innate Cell Mechanisms in Infectious Diseases to Quantum Biology. *Front. Public Heal.* **4**, (2016).

181. Behring, E. & Kitasato, S. Ueber das Zustandekommen der Diphtherie-Immunität und der Tetanus-Immunität bei Thieren. *Dtsch. Med. Wschr* doi:https://doi.org/10.17192/eb2013.0164.

182. Behring, E. Untersuchungen über das Zustandekommen der Diphtherie-Immunität bei Thieren. *Dtsch. Med. Wschr*.

183. Kaufmann, S. H. E. Immunology's coming of age. *Front. Immunol.* **10**, 1–13 (2019).

184. McCarthy, E. F. The toxins of William B. Coley and the treatment of bone and soft-tissue sarcomas. *Iowa Orthop. J.* **26**, 154–158 (2006).

185. Decker, W. K. & Safdar, A. Bioimmunoadjuvants for the treatment of neoplastic and infectious disease: Coley's legacy revisited. *Cytokine Growth Factor Rev.* **20**, 271–281 (2009).

186. Virus interference. I. The interferon. *Proc. R. Soc. London. Ser. B - Biol. Sci.* **147**, 258–267 (1957).

187. GRAHAM, J. B. & GRAHAM, R. M. The effect of vaccine on cancer patients. *Surg. Gynecol. Obstet.* **109**, 131–138 (1959).

188. Burnet, M. Cancer-A Biological Approach I. The Processes Of Control. *Br. Med. J.* **1**, 779–786 (1957).

189. Thomas, L. On immunosurveillance in human cancer. *Yale J. Biol. Med.* **55**, 329–333 (1982).

190. Burnet, S. I. R. M. Immunological factors in the process of carcinogenesis. 1959–1963 (1959).

191. Miller, J. F. A. P., Mitchell, G. F. & Weiss, N. S. Cellular basis of the immunological defects in thymectomized mice. *Nature* **214**, 992–997 (1967).

192. Steinman, R. M. & Cohn, Z. A. Identification of a novel cell type in peripheral lymphoid organs of mice: I. Morphology, quantitation, tissue distribution. *J. Exp. Med.* **137**, 1142–1162 (1973).

193. Zinkernagel, R. M. & Doherty, P. C. Restriction of in vitro T cell-mediated cytotoxicity in lymphocytic choriomeningitis within a syngeneic or semiallogeneic system. *Nature* **248**, 701–702 (1974).

194. Kiessling, R., Klein, E., Pross, H. & Wigzell, H. 'Natural' killer cells in the mouse. II. Cytotoxic cells with specificity for mouse Moloney leukemia cells. Characteristics of the killer cell. *Eur. J. Immunol.* **5**, 117–121 (1975).

195. Shankaran, V. *et al.* IFNgamma and lympohcytes prevent primary tomour development and shape tomour immunogenicity. *Nature* **410**, 1107–1111 (2001).

196. Kim, R., Emi, M. & Tanabe, K. Cancer immunoediting from immune surveillance to immune escape. *Immunology* **121**, 1–14 (2007).

197. Teng, M. W. L., Kershaw, M. H. & Smyth, M. J. Cancer Immunoediting: From Surveillance to Escape. *Cancer Immunother. Immune Suppr. Tumor Growth Second Ed.* **3**, 85–99 (2013).

198. Dunn, G. P., Old, L. J. & Schreiber, R. D. The three Es of cancer immunoediting. *Annu. Rev. Immunol.* **22**, 329–360 (2004).

199. Ehrlich, P. Ueber den jetzigen Stand der Karzinomforschung. *Ned. Tijdschr. Geneeskd.* vol. 5 273–290 (1909).

200. Möller, G. & Möller, E. The Concept of Immunological Surveillance against Neoplasia. *Immunol. Rev.* **28**, 3–17 (1976).

201. Macleod, K. Tumor suppressor genes. *Curr. Opin. Genet. Dev.* **10**, 81–93 (2000).

202. Carmeliet, P. & Jain, R. K. Angiogenesis in cancer and other diseases. *Nature* **407**, 249–257 (2000).

203. Sternlicht, M. D. & Werb, Z. How matrix metalloproteinases regulate cell behavior. *Annu. Rev. Cell Dev. Biol.* **17**, 463–516 (2001).

204. Vicari, A. P. & Caux, C. Chemokines in cancer. *Cytokine Growth Factor Rev.* **13**, 143–154 (2002).

205. Zingoni, A. *et al.* NKG2D and its ligands: 'One for all, all for one'. *Front. Immunol.* **9**, (2018).

206. Galli, G. *et al.* CD1d-restricted help to B cells by human invariant natural killer T lymphocytes. *J. Exp. Med.* **197**, 1051–1057 (2003).

207. Sims, G. P., Rowe, D. C., Rietdijk, S. T., Herbst, R. & Coyle, A. J. HMGB1 and RAGE in inflammation and cancer. *Annu. Rev. Immunol.* **28**, 367–388 (2010).

208. Palmieri, E. M., McGinity, C., Wink, D. A. & McVicar, D. W. Nitric oxide in macrophage immunometabolism: Hiding in plain sight. *Metabolites* **10**, 1–34 (2020).

209. Schreiber, R. D., Pace, J. L., Russell, S. W., Altman, A. & Katz, D. H. Macrophage-activating factor produced by a T cell hybridoma: physiochemical and biosynthetic resemblance to gamma-interferon. *J. Immunol.* **131**, 826–832 (1983).

210. Takeda, K. *et al.* Involvement of tumor necrosis factor-related apoptosis-inducing ligand in surveillance of tumor metastasis by liver natural killer cells. *Nat. Med.* **7**, 94–100 (2001).

211. Hayakawa, Y. *et al.* Cutting edge: tumor rejection mediated by NKG2D receptor-ligand interaction is dependent upon perforin. *J. Immunol.* **169**, 5377–5381 (2002).

212. Sallusto, F., Mackay, C. R. & Lanzavecchia, A. The role of chemokine receptors in primary, effector, and memory immune responses. *Annu. Rev. Immunol.* **18**, 593–620 (2000).

213. Huang, A. Y. *et al.* Role of bone marrow-derived cells in presenting MHC class I-restricted tumor antigens. *Science* **264**, 961–965 (1994).

214. Albert, M. L., Sauter, B. & Bhardwaj, N. Dendritic cells acquire antigen from apoptotic cells and induce class I-restricted CTLs. *Nature* **392**, 86–89 (1998).

215. Schoenberger, S. P., Toes, R. E., van der Voort, E. I., Offringa, R. & Melief, C. J. T-cell help for cytotoxic T lymphocytes is mediated by CD40-CD40L interactions. *Nature* **393**, 480–483 (1998).

216. Loeb, L. A., Loeb, K. R. & Anderson, J. P. Multiple mutations and cancer. *Proc. Natl. Acad. Sci. U. S. A.* **100**, 776–781 (2003).

217. Lengauer, C., Kinzler, K. W. & Vogelstein, B. Genetic instabilities in human cancers. *Nature* **396**, 643–649 (1998).

218. Schreiber, R. D., Old, L. J. & Smyth, M. J. Cancer immunoediting: Integrating immunity's roles in cancer suppression and promotion. *Science (80-.).* **331**, 1565–1570 (2011).

219. Konkel, J. E. *et al.* Transforming Growth Factor-β Signaling in Regulatory T Cells Controls T Helper-17 Cells and Tissue-Specific Immune Responses. *Immunity* **46**, 660–674 (2017).

220. Bierie, B. & Moses, H. L. Transforming growth factor beta (TGF-β) and inflammation in cancer. *Cytokine Growth Factor Rev.* **21**, 49–59 (2010).

221. Liu, C. Y. *et al.* M2-polarized tumor-associated macrophages promoted epithelial-mesenchymal transition in pancreatic cancer cells, partially through TLR4/IL-10 signaling pathway. *Lab. Investig.* **93**, 844–854 (2013).

222. Khong, H. T. & Restifo, N. P. Natural selection of tumor variants in the generation of 'tumor escape' phenotypes. *Nat. Immunol.* **3**, 999–1005 (2002).

223. Chen, D. S. & Mellman, I. Oncology meets immunology: The cancer-immunity cycle. *Immunity* **39**, 1–10 (2013).

224. Ferguson, T. A., Choi, J. & Green, D. R. Armed response: How dying cells influence T-cell functions. *Immunol. Rev.* **241**, 77–88 (2011).

225. Kroemer, G., Galluzzi, L., Kepp, O. & Zitvogel, L. Immunogenic cell death in cancer therapy. *Annu. Rev. Immunol.* **31**, 51–72 (2013).

226. Gunn, M. D. *et al.* A chemokine expressed in lymphoid high endothelial venules promotes the adhesion and chemotaxis of naive T lymphocytes. *Proc. Natl. Acad. Sci. U. S. A.* **95**, 258–263 (1998).

227. Moser, B. & Loetscher, P. Lymphocyte traffic control by chemokines. *Nat. Immunol.* **2**, 123–128 (2001).

228. Moran, C. J. *et al.* Rantes expression is a predictor of survival in stage I lung adenocarcinoma. *Clin. Cancer Res.* **8**, 3803–3812 (2002).

229. Gudowska-Sawczuk, M., Kudelski, J. & Mroczko, B. The role of chemokine receptor cxcr3 and its ligands in renal cell carcinoma. *Int. J. Mol. Sci.* **21**, 1–11 (2020).

230. Jöhrer, K. *et al.* Tumour-immune cell interactions modulated by chemokines. *Expert Opin. Biol. Ther.* **8**, 269–290 (2008).

231. Mullins, I. M. *et al.* CXC chemokine receptor 3 expression by activated CD8+ T cells is associated with survival in melanoma patients with stage III disease. *Cancer Res.* **64**, 7697–7701 (2004).

232. Laudanna, C., Kim, J. Y., Constantin, G. & Butcher, E. Rapid leukocyte integrin activation by chemokines. *Immunol. Rev.* **186**, 37–46 (2002).

233. Comrie, W. A., Li, S., Boyle, S. & Burkhardt, J. K. The dendritic cell cytoskeleton promotes T cell adhesion and activation by constraining ICAM-1 mobility. *J. Cell Biol.* **208**, 457–473 (2015).

234. Grakoui, A. *et al.* The immunological synapse: A molecular machine controlling T cell activation. *Science (80-.).* **285**, 221–227 (1999).

235. Jaime-Sanchez, P. *et al.* Cell death induced by cytotoxic CD8 + T cells is immunogenic and primes caspase-3-dependent spread immunity against endogenous tumor antigens. *J. Immunother. Cancer* **8**, 1–14 (2020).

236. Mellman, I., Coukos, G. & Dranoff, G. Cancer immunotherapy comes of age. *Nature* **480**, 480–489 (2011).

237. Bousso, P. T-cell activation by dendritic cells in the lymph node: Lessons from the movies. *Nat. Rev. Immunol.* **8**, 675–684 (2008).

238. Gallimore, A. *et al.* Induction and exhaustion of lymphocytic choriomeningitis virus-specific cytotoxic T lymphocytes visualized using soluble tetrameric major histocompatibility complex class I-peptide complexes. *J. Exp. Med.* **187**, 1383–1393 (1998).

239. Mead, K. I. *et al.* Exocytosis of CTLA-4 is dependent on phospholipase D and ADP ribosylation factor-1 and stimulated during activation of regulatory T cells. *J. Immunol.* **174**, 4803–4811 (2005).

240. Takahashi, T. *et al.* Immunologic self-tolerance maintained by CD25(+)CD4(+) regulatory T cells

constitutively expressing cytotoxic T lymphocyte-associated antigen 4. *J. Exp. Med.* **192**, 303–310 (2000).

241. Krummel, M. F. & Allison, J. P. CD28 and CTLA-4 have opposing effects on the response of T cells to stimulation. *J. Exp. Med.* **182**, 459–465 (1995).

242. Francisco, L. M., Sage, P. T. & Sharpe, A. H. The PD-1 pathway in tolerance and autoimmunity. *Immunol. Rev.* **236**, 219–242 (2010).

243. Wang, H. Bin *et al.* Rise of PD-L1 expression during metastasis of colorectal cancer: Implications for immunotherapy. *J. Dig. Dis.* **18**, 574–581 (2017).

244. Katsuya, Y. *et al.* Immunohistochemical status of PD-L1 in thymoma and thymic carcinoma. *Lung Cancer* **88**, 154–159 (2015).

245. Ritprajak, P. & Azuma, M. Intrinsic and extrinsic control of expression of the immunoregulatory molecule PD-L1 in epithelial cells and squamous cell carcinoma. *Oral Oncol.* **51**, 221–228 (2015).

246. Yearley, J. H. *et al.* PD-L2 Expression in Human Tumors: Relevance to Anti-PD-1 Therapy in Cancer. *Clin. cancer Res. an Off. J. Am. Assoc. Cancer Res.* **23**, 3158–3167 (2017).

247. Chen, L. & Flies, D. B. Molecular mechanisms of T cell co-stimulation and co-inhibition. *Nat. Rev. Immunol.* **13**, 227–242 (2013).

248. Maruhashi, T. *et al.* LAG-3 inhibits the activation of CD4 + T cells that recognize stable pMHCII through its conformation-dependent recognition of pMHCII. *Nat. Immunol.* **19**, 1415–1426 (2018).

249. Hashimoto, M. *et al.* CD8 T Cell Exhaustion in Chronic Infection and Cancer: Opportunities for Interventions. *Annu. Rev. Med.* **69**, 301–318 (2018).

250. Fridman, W. H., Pagès, F., Saùts-Fridman, C. & Galon, J. The immune contexture in human tumours: Impact on clinical outcome. *Nat. Rev. Cancer* **12**, 298–306 (2012).

251. De Monte, L. *et al.* Intratumor T helper type 2 cell infiltrate correlates with cancer-associated fibroblast thymic stromal lymphopoietin production and reduced survival in pancreatic cancer. *J. Exp. Med.* **208**, 469–478 (2011).

252. Yoon, N. K. *et al.* Higher levels of GATA3 predict better survival in women with breast cancer. *Hum. Pathol.* **41**, 1794–1801 (2010).

253. Lv, L. *et al.* The Accumulation and Prognosis Value of Tumor Infiltrating IL-17 Producing Cells in Esophageal Squamous Cell Carcinoma. *PLoS One* **6**, e18219 (2011).

254. Hsieh, C.-S., Lee, H.-M. & Lio, C.-W. J. Selection of regulatory T cells in the thymus. *Nat. Rev. Immunol.* **12**, 157–167 (2012).

255. Ellis, J. S., Wan, X. & Braley-Mullen, H. Transient depletion of CD4+ CD25+ regulatory T cells results in multiple autoimmune diseases in wild-type and B-cell-deficient NOD mice. *Immunology* **139**, 179–186 (2013).

256. Sato, E. *et al.* Intraepithelial CD8+ tumor-infiltrating lymphocytes and a high CD8+/regulatory T cell ratio are associated with favorable prognosis in ovarian cancer. *Proc. Natl. Acad. Sci. U. S. A.* **102**, 18538–18543 (2005).

257. Bates, G. J. *et al.* Quantification of regulatory T cells enables the identification of high-risk breast cancer patients and those at risk of late relapse. *J. Clin. Oncol.* **24**, 5373–5380 (2006).

258. Han, S. J., Toker, A., Liu, Z. Q. & Ohashi, P. S. Turning the tide against regulatory T cells. *Front.*

Oncol. **9**, 1–16 (2019).

259. Qureshi, O. S. *et al.* Trans-endocytosis of CD80 and CD86: a molecular basis for the cell-extrinsic function of CTLA-4. *Science* **332**, 600–603 (2011).

260. Chen, M. L. *et al.* Regulatory T cells suppress tumor-specific CD8 T cell cytotoxicity through TGF-β signals in vivo. *Proc. Natl. Acad. Sci. U. S. A.* **102**, 419–424 (2005).

261. Hart, K., Byrne, K., Molloy, M., Usherwood, E. & Berwin, B. IL-10 Immunomodulation of Myeloid Cells Regulates a Murine Model of Ovarian Cancer . *Frontiers in Immunology* vol. 2 29 (2011).

262. Wang, S., He, Z., Wang, X., Li, H. & Liu, X. S. Antigen presentation and tumor immunogenicity in cancer immunotherapy response prediction. *Elife* **8**, 1–20 (2019).

263. Kitamura, H. *et al.* Interleukin-6/STAT3 signaling as a promising target to improve the efficacy of cancer immunotherapy. *Cancer Sci.* **108**, 1947–1952 (2017).

264. Mittal, S. K. & Roche, P. A. Suppression of antigen presentation by IL-10. *Curr. Opin. Immunol.* **34**, 22–27 (2015).

265. Veglia, F. *et al.* Lipid bodies containing oxidatively truncated lipids block antigen cross-presentation by dendritic cells in cancer. *Nat. Commun.* **8**, (2017).

266. Ning, Y. *et al.* Tumor exosomes block dendritic cells maturation to decrease the T cell immune response. *Immunol. Lett.* **199**, 36–43 (2018).

267. Ohno, Y. *et al.* IL-6 down-regulates HLA class II expression and IL-12 production of human dendritic cells to impair activation of antigen-specific CD4+ T cells. *Cancer Immunol. Immunother.* **65**, 193–204 (2016).

268. Veglia, F. & Gabrilovich, D. I. Dendritic cells in cancer: the role revisited. *Curr. Opin. Immunol.* **45**, 43–51 (2017).

269. Guirnalda, P., Wood, L., Goenka, R., Crespo, J. & Paterson, Y. Interferon γ-induced intratumoral expression of CXCL9 alters the local distribution of T cells following immunotherapy with Listeria monocytogenes. *Oncoimmunology* **2**, (2013).

270. Harlin, H. *et al.* Chemokine expression in melanoma metastases associated with CD8 + T-Cell recruitment. *Cancer Res.* **69**, 3077–3085 (2009).

271. Joyce, J. A. & Fearon, D. T. T cell exclusion, immune privilege, and the tumor microenvironment. *Science (80-.).* **348**, 74 LP – 80 (2015).

272. Galon, J. *et al.* Type, Density, and Location of Immune Cells Within Human Colorectal Tumors Predict Clinical Outcome. *Science (80-.).* **313**, 1960 LP – 1964 (2006).

273. Molon, B. *et al.* Chemokine nitration prevents intratumoral infiltration of antigen-specific T cells. *J. Exp. Med.* **208**, 1949–1962 (2011).

274. Apte, R. S., Chen, D. S. & Ferrara, N. VEGF in Signaling and Disease: Beyond Discovery and Development. *Cell* **176**, 1248–1264 (2019).

275. Bellone, M. & Calcinotto, A. Ways to enhance lymphocyte trafficking into tumors and fitness of tumor infiltrating lymphocytes. *Front. Oncol.* **3 SEP**, 1–15 (2013).

276. Slaney, C. Y., Kershaw, M. H. & Darcy, P. K. Trafficking of T cells into tumors. *Cancer Res.* **74**, 7168–7174 (2014).

277. Motz, G. T. *et al.* Tumor endothelium FasL establishes a selective immune barrier promoting tolerance in tumors. *Nat. Med.* **20**, 607–615 (2014).

278. Rigamonti, N. *et al.* Role of angiopoietin-2 in adaptive tumor resistance to VEGF signaling blockade. *Cell Rep.* **8**, 696–706 (2014).

279. Anderson, K. G., Stromnes, I. M. & Greenberg, P. D. Obstacles Posed by the Tumor Microenvironment to T cell Activity: A Case for Synergistic Therapies. *Cancer Cell* **31**, 311–325 (2017).

280. Teixeira, H. C. & Kaufmann, S. H. Role of NK1.1+ cells in experimental listeriosis. NK1+ cells are early IFN-gamma producers but impair resistance to Listeria monocytogenes infection. *J. Immunol.* **152**, 1873–1882 (1994).

281. Poli, A. *et al.* CD56bright natural killer (NK) cells: An important NK cell subset. *Immunology* **126**, 458–465 (2009).

282. Abel, A. M., Yang, C., Thakar, M. S. & Malarkannan, S. Natural killer cells: Development, maturation, and clinical utilization. *Front. Immunol.* **9**, 1–23 (2018).

283. Colonna, M. Innate Lymphoid Cells: Diversity, Plasticity, and Unique Functions in Immunity. *Immunity* **48**, 1104–1117 (2018).

284. Boudreau, J. E. & Hsu, K. C. Natural Killer Cell Education and the Response to Infection and Cancer Therapy: Stay Tuned. *Trends Immunol.* **39**, 222–239 (2018).

285. Paul, S. & Lal, G. The molecular mechanism of natural killer cells function and its importance in cancer immunotherapy. *Front. Immunol.* **8**, (2017).

286. Gasser, S., Orsulic, S., Brown, E. J. & Raulet, D. H. The DNA damage pathway regulates innate immune system ligands of the NKG2D receptor. *Nature* **436**, 1186–1190 (2005).

287. Morvan, M. G. & Lanier, L. L. NK cells and cancer: You can teach innate cells new tricks. *Nat. Rev. Cancer* **16**, 7–19 (2016).

288. Habif, G., Crinier, A., André, P., Vivier, E. & Narni-Mancinelli, E. Targeting natural killer cells in solid tumors. *Cell. Mol. Immunol.* **16**, 415–422 (2019).

289. Paul, P. *et al.* HLA-G expression in melanoma: a way for tumor cells to escape from immunosurveillance. *Proc. Natl. Acad. Sci. U. S. A.* **95**, 4510–4515 (1998).

290. Ashiru, O. *et al.* Natural killer cell cytotoxicity is suppressed by exposure to the human NKG2D ligand MICA*008 that is shed by tumor cells in exosomes. *Cancer Res.* **70**, 481–489 (2010).

291. Xiao, G. *et al.* Soluble NKG2D ligand promotes MDSC expansion and skews macrophage to the alternatively activated phenotype. *J. Hematol. Oncol.* **8**, 13 (2015).

292. Oppenheim, D. E. *et al.* Sustained localized expression of ligand for the activating NKG2D receptor impairs natural cytotoxicity in vivo and reduces tumor immunosurveillance. *Nat. Immunol.* **6**, 928–937 (2005).

293. Lazarova, M. & Steinle, A. Impairment of NKG2D-Mediated Tumor Immunity by TGF-β. *Front. Immunol.* **10**, 2689 (2019).

294. Liu, B. *et al.* Glucocorticoid-induced tumor necrosis factor receptor negatively regulates activation of human primary natural killer (NK) cells by blocking proliferative signals and increasing NK cell apoptosis. *J. Biol. Chem.* **283**, 8202–8210 (2008).

295. Cools-Lartigue, J., Spicer, J., Najmeh, S. & Ferri, L. Neutrophil extracellular traps in cancer progression. *Cell. Mol. Life Sci.* **71**, 4179–4194 (2014).

296. Lee, W. L., Harrison, R. E. & Grinstein, S. Phagocytosis by neutrophils. *Microbes Infect.* **5**, 1299–1306 (2003).

297. Borregaard, N. & Cowland, J. B. Granules of the human neutrophilic polymorphonuclear leukocyte. *Blood* **89**, 3503–3521 (1997).

298. Shaul, M. E. *et al.* Tumor-associated neutrophils display a distinct N1 profile following TGFβ modulation: A transcriptomics analysis of pro- vs. antitumor TANs. *Oncoimmunology* **5**, 1–14 (2016).

299. Casbon, A.-J. *et al.* Invasive breast cancer reprograms early myeloid differentiation in the bone marrow to generate immunosuppressive neutrophils. *Proc. Natl. Acad. Sci.* **112**, E566–E575 (2015).

300. Jaillon, S. *et al.* Neutrophil diversity and plasticity in tumour progression and therapy. *Nat. Rev. Cancer* **20**, 485–503 (2020).

301. McCourt, M., Wang, J. H., Sookhai, S. & Redmond, H. P. Proinflammatory mediators stimulate neutrophil-directed angiogenesis. *Arch. Surg.* **134**, 1325–1332 (1999).

302. Deryugina, E. I. & Quigley, J. P. Tumor angiogenesis: MMP-mediated induction of intravasation- and metastasis-sustaining neovasculature. *Matrix Biol.* **44–46**, 94–112 (2015).

303. Gabrilovich, D. I. & Nagaraj, S. Myeloid-derived suppressor cells as regulators of the immune system. *Nat. Rev. Immunol.* **9**, 162–174 (2009).

304. Ardi, V. C., Kupriyanova, T. A., Deryugina, E. I. & Quigley, J. P. Human neutrophils uniquely release TIMP-free MMP-9 to provide a potent catalytic stimulator of angiogenesis. *Proc. Natl. Acad. Sci. U. S. A.* **104**, 20262–20267 (2007).

305. Gong, L. *et al.* Promoting effect of neutrophils on lung tumorigenesis is mediated by CXCR2 and neutrophil elastase. *Mol. Cancer* **12**, 154 (2013).

306. Houghton, A. M. *et al.* Neutrophil elastase-mediated degradation of IRS-1 accelerates lung tumor growth. *Nat. Med.* **16**, 219–223 (2010).

307. Wang, T.-T. *et al.* Tumour-activated neutrophils in gastric cancer foster immune suppression and disease progression through GM-CSF-PD-L1 pathway. *Gut* **66**, 1900–1911 (2017).

308. Coffelt, S. B., Wellenstein, M. D. & de Visser, K. E. Neutrophils in cancer: neutral no more. *Nat. Rev. Cancer* **16**, 431–446 (2016).

309. Nagaraj, S. *et al.* Altered recognition of antigen is a mechanism of CD8+ T cell tolerance in cancer. *Nat. Med.* **13**, 828–835 (2007).

310. Jensen, T. O. *et al.* Intratumoral neutrophils and plasmacytoid dendritic cells indicate poor prognosis and are associated with pSTAT3 expression in AJCC stage I/II melanoma. *Cancer* **118**, 2476–2485 (2012).

311. Rao, H.-L. *et al.* Increased intratumoral neutrophil in colorectal carcinomas correlates closely with malignant phenotype and predicts patients' adverse prognosis. *PLoS One* **7**, e30806 (2012).

312. Li, Y.-W. *et al.* Intratumoral neutrophils: a poor prognostic factor for hepatocellular carcinoma following resection. *J. Hepatol.* **54**, 497–505 (2011).

313. Ilie, M. *et al.* Predictive clinical outcome of the intratumoral CD66b-positive neutrophil-to-CD8-positive T-cell ratio in patients with resectable nonsmall cell lung cancer. *Cancer* **118**, 1726–1737 (2012).

314. Cools-Lartigue, J. *et al.* Neutrophil extracellular traps sequester circulating tumor cells and promote metastasis. *J. Clin. Invest.* **123**, 3446–3458 (2013).

315. Demers, M. *et al.* Cancers predispose neutrophils to release extracellular DNA traps that contribute to cancer-associated thrombosis. *Proc. Natl. Acad. Sci. U. S. A.* **109**, 13076–13081 (2012).

316. Park, J. *et al.* Cancer cells induce metastasis-supporting neutrophil extracellular DNA traps. *Sci. Transl. Med.* **8**, (2016).

317. Munir, H. *et al.* Stromal-driven and Amyloid β-dependent induction of neutrophil extracellular traps modulates tumor growth. *Nat. Commun.* **12**, 1–16 (2021).

318. Schlitzer, A., McGovern, N. & Ginhoux, F. Dendritic cells and monocyte-derived cells: Two complementary and integrated functional systems. *Semin. Cell Dev. Biol.* **41**, 9–22 (2015).

319. Cella, M. *et al.* Plasmacytoid monocytes migrate to inflamed lymph nodes and produce large amounts of type I interferon. *Nat. Med.* **5**, 919–923 (1999).

320. Karsunky, H., Merad, M., Cozzio, A., Weissman, I. L. & Manz, M. G. Flt3 ligand regulates dendritic cell development from Flt3+ lymphoid and myeloid-committed progenitors to Flt3+ dendritic cells in vivo. *J. Exp. Med.* **198**, 305–313 (2003).

321. Greter, M. *et al.* GM-CSF Controls Nonlymphoid Tissue Dendritic Cell Homeostasis but Is Dispensable for the Differentiation of Inflammatory Dendritic Cells. *Immunity* **36**, 1031–1046 (2012).

322. Wculek, S. K. *et al.* Dendritic cells in cancer immunology and immunotherapy. *Nat. Rev. Immunol.* **20**, 7–24 (2020).

323. Hildner, K. *et al.* Batf3 deficiency reveals a critical role for CD8α+ dendritic cells in cytotoxic T cell immunity. *Science (80-.).* **322**, 1097–1100 (2008).

324. Dorner, B. G. *et al.* Selective Expression of the Chemokine Receptor XCR1 on Cross-presenting Dendritic Cells Determines Cooperation with CD8+ T Cells. *Immunity* **31**, 823–833 (2009).

325. Huysamen, C., Willment, J. A., Dennehy, K. M. & Brown, G. D. CLEC9A Is a Novel Activation C-type Lectin-like Receptor Expressed on BDCA3+ Dendritic Cells and a Subset of Monocytes*. *J. Biol. Chem.* **283**, 16693–16701 (2008).

326. Böttcher, J. P. & Reis e Sousa, C. The Role of Type 1 Conventional Dendritic Cells in Cancer Immunity. *Trends in Cancer* **4**, 784–792 (2018).

327. Chiang, M. C. *et al.* Differential uptake and cross-presentation of soluble and necrotic cell antigen by human DC subsets. *Eur. J. Immunol.* **46**, 329–339 (2016).

328. Wculek, S. K. *et al.* Effective cancer immunotherapy by natural mouse conventional type-1 dendritic cells bearing dead tumor antigen. *J. Immunother. cancer* **7**, 100 (2019).

329. Collin, M. & Haniffa, M. Dendritic Cells and Dendritic Cell Subsets. in *Encyclopedia of Immunobiology* 345–352 (Elsevier, 2016). doi:10.1016/B978-0-12-374279-7.03008-3.

330. Binnewies, M. *et al.* Unleashing Type-2 Dendritic Cells to Drive Protective Antitumor CD4 + T Cell Immunity. *Cell* **177**, 556-571.e16 (2019).

331. Schlitzer, A. *et al.* IRF4 transcription factor-dependent CD11b+ dendritic cells in human and mouse control mucosal IL-17 cytokine responses. *Immunity* **38**, 970–983 (2013).

332. Villani, A.-C. *et al.* Single-cell RNA-seq reveals new types of human blood dendritic cells, monocytes, and progenitors. *Science (80-.).* **356**, eaah4573 (2017).

333. Sittig, S. P. *et al.* A Comparative Study of the T Cell Stimulatory and Polarizing Capacity of Human Primary Blood Dendritic Cell Subsets. *Mediators Inflamm.* **2016**, 3605643 (2016).

334. Guilliams, M. & van de Laar, L. A hitchhiker's guide to myeloid cell subsets: Practical implementation of a novel mononuclear phagocyte classification system. *Front. Immunol.* **6**, 1–12 (2015).

335. Segura, E. *et al.* Human Inflammatory Dendritic Cells Induce Th17 Cell Differentiation. *Immunity* **38**, 336–348 (2013).

336. Plantinga, M. *et al.* Conventional and Monocyte-Derived CD11b+ Dendritic Cells Initiate and Maintain T Helper 2 Cell-Mediated Immunity to House Dust Mite Allergen. *Immunity* **38**, 322–335 (2013).

337. Collin, M. & Bigley, V. Human dendritic cell subsets: an update. *Immunology* **154**, 3–20 (2018).

338. Scarlett, U. K. *et al.* Ovarian cancer progression is controlled by phenotypic changes in dendritic cells. *J. Exp. Med.* **209**, 495–506 (2012).

339. Lutz, M. B. & Schuler, G. Immature, semi-mature and fully mature dendritic cells: Which signals induce tolerance or immunity? *Trends Immunol.* **23**, 445–449 (2002).

340. Hasegawa, H. & Matsumoto, T. Mechanisms of tolerance induction by dendritic cells in vivo. *Front. Immunol.* **9**, (2018).

341. Kuipers, H. *et al.* Contribution of the PD-1 ligands/PD-1 signaling pathway to dendritic cell-mediated CD4+ T cell activation. *Eur. J. Immunol.* **36**, 2472–2482 (2006).

342. Wang, L. *et al.* VISTA, a novel mouse Ig superfamily ligand that negatively regulates T cell responses. *J. Exp. Med.* **208**, 577–592 (2011).

343. Clement, M. *et al.* CD31 is a key coinhibitory receptor in the development of immunogenic dendritic cells. *Proc. Natl. Acad. Sci. U. S. A.* **111**, (2014).

344. Spranger, S., Bao, R. & Gajewski, T. F. Melanoma-intrinsic β-catenin signalling prevents anti-tumour immunity. *Nature* **523**, 231–235 (2015).

345. Kumari, N., Dwarakanath, B. S., Das, A. & Bhatt, A. N. Role of interleukin-6 in cancer progression and therapeutic resistance. *Tumour Biol. J. Int. Soc. Oncodevelopmental Biol. Med.* **37**, 11553–11572 (2016).

346. Zong, J., Keskinov, A. A., Shurin, G. V. & Shurin, M. R. Tumor-derived factors modulating dendritic cell function. *Cancer Immunol. Immunother.* **65**, 821–833 (2016).

347. Tang, M. *et al.* Toll-like Receptor 2 Activation Promotes Tumor Dendritic Cell Dysfunction by Regulating IL-6 and IL-10 Receptor Signaling. *Cell Rep.* **13**, 2851–2864 (2015).

348. Chiba, S. *et al.* Tumor-infiltrating DCs suppress nucleic acid-mediated innate immune responses through interactions between the receptor TIM-3 and the alarmin HMGB1. *Nat. Immunol.* **13**, 832–842 (2012).

349. Willingham, S. B. *et al.* The CD47-signal regulatory protein alpha (SIRPa) interaction is a therapeutic target for human solid tumors. *Proc. Natl. Acad. Sci.* **109**, 6662 LP – 6667 (2012).

350. Martinez, F. O. & Gordon, S. The M1 and M2 paradigm of macrophage activation: Time for reassessment. *F1000Prime Rep.* **6**, 1–13 (2014).

351. Balkwill, F., Charles, K. A. & Mantovani, A. Smoldering and polarized inflammation in the initiation and promotion of malignant disease. *Cancer Cell* **7**, 211–217 (2005).

352. Canè, S. *et al.* The endless saga of monocyte diversity. *Front. Immunol.* **10**, 1–18 (2019).

353. Genard, G. *et al.* Proton irradiation orchestrates macrophage reprogramming through NFκB

signaling. *Cell Death Dis.* **9**, (2018).

354. Hu, H. *et al.* The combination of PKM2 overexpression and M2 macrophages infiltration confers a poor prognosis for PDAC patients. *J. Cancer* **11**, 2022–2031 (2020).

355. Nardin, A. & Abastado, J.-P. Macrophages and cancer. *Front. Biosci.* **13**, 3494–3505 (2008).

356. Varga, T. *et al.* Highly Dynamic Transcriptional Signature of Distinct Macrophage Subsets during Sterile Inflammation, Resolution, and Tissue Repair. *J. Immunol.* **196**, 4771–4782 (2016).

357. Yao, Y., Xu, X. H. & Jin, L. Macrophage polarization in physiological and pathological pregnancy. *Front. Immunol.* **10**, 1–13 (2019).

358. Mantovani, A. *et al.* The chemokine system in diverse forms of macrophage activation and polarization. *Trends Immunol.* **25**, 677–686 (2004).

359. Murray, P. J. *et al.* Macrophage activation and polarization: nomenclature and experimental guidelines. *Immunity* **41**, 14–20 (2014).

360. Chen, W., Wang, J., Jia, L., Liu, J. & Tian, Y. Attenuation of the programmed cell death-1 pathway increases the M1 polarization of macrophages induced by zymosan. *Cell Death Dis.* **7**, 1–10 (2016).

361. Hagemann, T. *et al.* 'Re-educating' tumor-associated macrophages by targeting NF-κB. *J. Exp. Med.* **205**, 1261–1268 (2008).

362. Wang, N., Liang, H. & Zen, K. Molecular Mechanisms That Influence the Macrophage M1–M2 Polarization Balance . *Frontiers in Immunology* vol. 5 614 (2014).

363. Porta, C., Riboldi, E., Ippolito, A. & Sica, A. Molecular and epigenetic basis of macrophage polarized activation. *Semin. Immunol.* **27**, 237–248 (2015).

364. Gordon, S. & Martinez, F. O. Alternative Activation of Macrophages: Mechanism and Functions. *Immunity* **32**, 593–604 (2010).

365. Hanakawa, S. & Kitoh, A. *Macrophages*. *Immunology of the Skin: Basic and Clinical Sciences in Skin Immune Responses* (2016). doi:10.1007/978-4-431-55855-2_10.

366. Lewis, J. S., Landers, R. J., Underwood, J. C. E., Harris, A. L. & Lewis, C. E. Expression of vascular endothelial growth factor by macrophages is up-regulated in poorly vascularized areas of breast carcinomas. *J. Pathol.* **192**, 150–158 (2000).

367. Coffelt, S. B. *et al.* Angiopoietin-2 regulates gene expression in TIE2-expressing monocytes and augments their inherent proangiogenic functions. *Cancer Res.* **70**, 5270–5280 (2010).

368. Castriconi, R. *et al.* Transforming growth factor β1 inhibits expression of NKP30 and NKG2d receptors: Consequences for the NK-mediated killing of dendritic cells. *Proc. Natl. Acad. Sci. U. S. A.* **100**, 4120–4125 (2003).

369. Mantovani, A. & Sica, A. Macrophages, innate immunity and cancer: balance, tolerance, and diversity. *Curr. Opin. Immunol.* **22**, 231–237 (2010).

370. Bak, S. P., Alonso, A., Turk, M. J. & Berwin, B. Murine ovarian cancer vascular leukocytes require arginase-1 activity for T cell suppression. *Mol. Immunol.* **46**, 258–268 (2008).

371. Marigo, I., Dolcetti, L., Serafini, P., Zanovello, P. & Bronte, V. Tumor-induced tolerance and immune suppression by myeloid derived suppressor cells. *Immunol. Rev.* **222**, 162–179 (2008).

372. Lin, H. *et al.* Host expression of PD-L1 determines efficacy of PD-L1 pathway blockade-mediated tumor regression. *J. Clin. Invest.* **128**, 805–815 (2018).

373. Wertel, I. *et al.* Macrophage-derived chemokine CCL22 and regulatory T cells in ovarian cancer patients. *Tumour Biol. J. Int. Soc. Oncodevelopmental Biol. Med.* **36**, 4811–4817 (2015).

374. Hao, N. B. *et al.* Macrophages in tumor microenvironments and the progression of tumors. *Clin. Dev. Immunol.* **2012**, (2012).

375. Becher, B., Tugues, S. & Greter, M. GM-CSF: From Growth Factor to Central Mediator of Tissue Inflammation. *Immunity* **45**, 963–973 (2016).

376. Lechner, M. G., Liebertz, D. J. & Epstein, A. L. Correction: Characterization of Cytokine-Induced Myeloid-Derived Suppressor Cells from Normal Human Peripheral Blood Mononuclear Cells. *J. Immunol.* **185**, 5668–5668 (2010).

377. Dufait, I. *et al.* Ex vivo generation of myeloid-derived suppressor cells that model the tumor immunosuppressive environment in colorectal cancer. *Oncotarget* **6**, 12369–82 (2015).

378. Xue, J. *et al.* Transcriptome-Based Network Analysis Reveals a Spectrum Model of Human Macrophage Activation. *Immunity* **40**, 274–288 (2014).

379. Guilliams, M., Mildner, A. & Yona, S. Developmental and Functional Heterogeneity of Monocytes. *Immunity* **49**, 595–613 (2018).

380. Swirski, F. K. *et al.* Identification of splenic reservoir monocytes and their deployment to inflammatory sites. *Science* **325**, 612–616 (2009).

381. Sprangers, S., Vries, T. J. D. & Everts, V. Monocyte Heterogeneity: Consequences for Monocyte-Derived Immune Cells. *J. Immunol. Res.* **2016**, (2016).

382. Kurotaki, D. *et al.* Essential role of the IRF8-KLF4 transcription factor cascade in murine monocyte differentiation. *Blood* **121**, 1839–1849 (2013).

383. Carlin, L. M. *et al.* Nr4a1-dependent Ly6Clow monocytes monitor endothelial cells and orchestrate their disposal. *Cell* **153**, 362–375 (2013).

384. Al Sayed, M. F. *et al.* T-cell-Secreted TNFα Induces Emergency Myelopoiesis and Myeloid-Derived Suppressor Cell Differentiation in Cancer. *Cancer Res.* **79**, 346–359 (2019).

385. Tacke, F. & Randolph, G. J. Migratory fate and differentiation of blood monocyte subsets. *Immunobiology* **211**, 609–618 (2006).

386. Nutt, S. L., Metcalf, D., D'Amico, A., Polli, M. & Wu, L. Dynamic regulation of PU.1 expression in multipotent hematopoietic progenitors . *J. Exp. Med.* **201**, 221–231 (2005).

387. McKercher, S. R. *et al.* Targeted disruption of the PU.1 gene results in multiple hematopoietic abnormalities. *EMBO J.* **15**, 5647–5658 (1996).

388. Glass, C. K. & Natoli, G. Molecular control of activation and priming in macrophages. *Nat. Immunol.* **17**, 26–33 (2016).

389. Nagulapalli, S., Pongubala, J. M. & Atchison, M. L. Multiple proteins physically interact with PU.1. Transcriptional synergy with NF-IL6 beta (C/EBP delta, CRP3). *J. Immunol.* **155**, 4330–8 (1995).

390. Feng, R. *et al.* PU.1 and C/EBPα/β convert fibroblasts into macrophage-like cells. *Proc. Natl. Acad. Sci. U. S. A.* **105**, 6057–6062 (2008).

391. Marigo, I. *et al.* Tumor-induced tolerance and immune suppression depend on the C/EBPβ transcription factor. *Immunity* **32**, 790–802 (2010).

392. Qian, B. Z. *et al.* CCL2 recruits inflammatory monocytes to facilitate breast-tumour metastasis.

Nature **475**, 222–225 (2011).

393. Nagarsheth, N., Wicha, M. S. & Zou, W. Chemokines in the cancer microenvironment and their relevance in cancer immunotherapy. *Nat. Rev. Immunol.* **17**, 559–572 (2017).

394. Van Overmeire, E. *et al.* M-CSF and GM-CSF receptor signaling differentially regulate monocyte maturation and macrophage polarization in the tumor microenvironment. *Cancer Res.* **76**, 35–42 (2016).

395. Priceman, S. J. *et al.* Targeting distinct tumor-infiltrating myeloid cells by inhibiting CSF-1 receptor: Combating tumor evasion of antiangiogenic therapy. *Blood* **115**, 1461–1471 (2010).

396. Zhu, Y. *et al.* CSF1/CSF1R blockade reprograms tumor-infiltrating macrophages and improves response to T-cell checkpoint immunotherapy in pancreatic cancer models. *Cancer Res.* **74**, 5057–5069 (2014).

397. Eubank, T. D., Galloway, M., Montague, C. M., Waldman, W. J. & Marsh, C. B. M-CSF Induces Vascular Endothelial Growth Factor Production and Angiogenic Activity From Human Monocytes. *J. Immunol.* **171**, 2637–2643 (2003).

398. Avraham-Davidi, I. *et al.* On-site education of VEGF-recruited monocytes improves their performance as angiogenic and arteriogenic accessory cells. *J. Exp. Med.* **210**, 2611–2625 (2013).

399. Gabrilovich, D. I. Myeloid-derived suppressor cells. *Cancer Immunol. Res.* **5**, 3–8 (2017).

400. Yáñez, A. *et al.* Granulocyte-Monocyte Progenitors and Monocyte-Dendritic Cell Progenitors Independently Produce Functionally Distinct Monocytes. *Immunity* **47**, 890-902.e4 (2017).

401. Robinson, W. A. > 20,000).

402. Talmadge, J. E. & Gabrilovich, D. I. History of myeloid-derived suppressor cells. *Nat. Rev. Cancer* **13**, 739–752 (2013).

403. Bennett, J. A., Rao, V. S. & Mitchell, M. S. Systemic bacillus Calmette-Guérin (BCG) activates natural suppressor cells. *Proc. Natl. Acad. Sci. U. S. A.* **75**, 5142–4 (1978).

404. Ben-Meir, K., Twaik, N. & Baniyash, M. Plasticity and biological diversity of myeloid derived suppressor cells. *Curr. Opin. Immunol.* **51**, 154–161 (2018).

405. Bronte, V. *et al.* Recommendations for myeloid-derived suppressor cell nomenclature and characterization standards. *Nat. Commun.* **7**, 1–10 (2016).

406. Bergenfelz, C. & Leandersson, K. The Generation and Identity of Human Myeloid-Derived Suppressor Cells. *Front. Oncol.* **10**, 17–19 (2020).

407. Rose, S., Misharin, A. & Perlman, H. HHS Public Access. **81**, 343–350 (2014).

408. Youn, J.-I., Nagaraj, S., Collazo, M. & Gabrilovich, D. I. Subsets of Myeloid-Derived Suppressor Cells in Tumor-Bearing Mice. *J. Immunol.* **181**, 5791–5802 (2008).

409. Hey, Y. Y., Tan, J. K. H. & O'Neill, H. C. Redefining myeloid cell subsets in murine spleen. *Front. Immunol.* **6**, 1–12 (2016).

410. Dumitru, C. A., Moses, K., Trellakis, S., Lang, S. & Brandau, S. Neutrophils and granulocytic myeloid-derived suppressor cells: Immunophenotyping, cell biology and clinical relevance in human oncology. *Cancer Immunol. Immunother.* **61**, 1155–1167 (2012).

411. Dolcetti, L. *et al.* Hierarchy of immunosuppressive strength among myeloid-derived suppressor cell subsets is determined by GM-CSF. *Eur. J. Immunol.* **40**, 22–35 (2010).

412. Kowanetz, M. *et al.* Granulocyte-colony stimulating factor promotes lung metastasis through mobilization of Ly6G+ Ly6C+ granulocytes. *Proc. Natl. Acad. Sci.* **107**, 21248–21255 (2010).

413. Kumar, V., Patel, S., Tcyganov, E. & Gabrilovich, D. I. The Nature of Myeloid-Derived Suppressor Cells in the Tumor Microenvironment. *Trends Immunol.* **37**, 208–220 (2016).

414. Poschke, I. & Kiessling, R. On the armament and appearances of human myeloid-derived suppressor cells. *Clin. Immunol.* **144**, 250–268 (2012).

415. Condamine, T., Mastio, J. & Gabrilovich, D. I. Transcriptional regulation of myeloid-derived suppressor cells. *J. Leukoc. Biol.* **98**, 913–922 (2015).

416. Almand, B. *et al.* Increased Production of Immature Myeloid Cells in Cancer Patients: A Mechanism of Immunosuppression in Cancer. *J. Immunol.* **166**, 678–689 (2001).

417. Jiang, M. *et al.* Interleukin-6 trans-signaling pathway promotes immunosuppressive myeloid-derived suppressor cells via suppression of suppressor of cytokine signaling 3 in breast cancer. *Front. Immunol.* **8**, (2017).

418. Condamine, T., Mastio, J. & Gabrilovich, D. I. Transcriptional regulation of myeloid-derived suppressor cells. *J. Leukoc. Biol.* **98**, 913–922 (2015).

419. Song, X. *et al.* CD11b+/Gr-1+ Immature Myeloid Cells Mediate Suppression of T Cells in Mice Bearing Tumors of IL-1 -Secreting Cells. *J. Immunol.* **175**, 8200–8208 (2005).

420. Strauss, L. *et al.* RORC1 Regulates Tumor-Promoting 'Emergency' Granulo-Monocytopoiesis. *Cancer Cell* **28**, 253–269 (2015).

421. Young, M. R., Newby, M. & Wepsic, H. T. Hematopoiesis and Suppressor Bone Marrow Cells in Mice Bearing Large Metastatic Lewis Lung Carcinoma Tumors Hematopoiesis and Suppressor Bone Marrow Cells in Mice Bearing Large Metastatic Lewis Lung Carcinoma Tumors1. *Cancer Res.* 100–105 (1987).

422. Immunol, E. J. & Piemonti, L. Allavena , P . et al . IL-10 prevents the differentiation of monocytes to dendritic cells but promotes their maturation to. 359–369 (1998) doi:10.1002/(SICI)1521-4141(199801)28.

423. Cheng, P. *et al.* Inhibition of dendritic cell differentiation and accumulation of myeloid-derived suppressor cells in cancer is regulated by S100A9 protein. *J. Exp. Med.* **205**, 2235–2249 (2008).

424. Kalinski, P., Hilkens, C. M., Snijders, A., Snijdewint, F. G. & Kapsenberg, M. L. IL-12-deficient dendritic cells, generated in the presence of prostaglandin E_2, promote type 2 cytokine production in maturing human naive T helper cells. *J. Immunol.* **159**, 28–35 (1997).

425. Obermajer, N. & Kalinski, P. Key role of the positive feedback between PGE 2 and COX2 in the biology of myeloid-derived suppressor cells. *Oncoimmunology* **1**, 762–764 (2014).

426. Bianchi, M. E. DAMPs, PAMPs and alarmins: all we need to know about danger. *J. Leukoc. Biol.* **81**, 1–5 (2006).

427. Umansky, V., Blattner, C., Gebhardt, C. & Utikal, J. The Role of Myeloid-Derived Suppressor Cells (MDSC) in Cancer Progression. *Vaccines* **4**, 36 (2016).

428. Umansky, V. *et al.* Myeloid-derived suppressor cells and tumor escape from immune surveillance. *Semin. Immunopathol.* **39**, 295–305 (2017).

429. Gabrilovich, D. I., Ostrand-Rosenberg, S. & Bronte, V. Coordinated regulation of myeloid cells by tumours. *Nat. Rev. Immunol.* **12**, 253–268 (2012).

430. Parker, K. H., Beury, D. W. & Ostrand-Rosenberg, S. Myeloid-Derived Suppressor Cells: Critical

Cells Driving Immune Suppression in the Tumor Microenvironment. *Adv. Cancer Res.* **128**, 95–139 (2015).

431. Meirow, Y., Kanterman, J. & Baniyash, M. Paving the road to tumor development and spreading: Myeloid-derived suppressor cells are ruling the fate. *Front. Immunol.* **6**, (2015).

432. Elliott, L. A., Doherty, G. A., Sheahan, K. & Ryan, E. J. Human tumor-infiltrating myeloid cells: Phenotypic and functional diversity. *Front. Immunol.* **8**, (2017).

433. Lu, C., Redd, P. S., Lee, J. R., Savage, N. & Liu, K. The expression profiles and regulation of PD-L1 in tumor-induced myeloid-derived suppressor cells. *Oncoimmunology* **5**, 1–13 (2016).

434. Yamauchi, Y. *et al.* Circulating and tumor myeloid-derived suppressor cells in resectable non-small cell lung cancer. *Am. J. Respir. Crit. Care Med.* **198**, 777–787 (2018).

435. Gebhardt, C. *et al.* Myeloid Cells and Related Chronic Inflammatory Factors as Novel Predictive Markers in Melanoma Treatment with Ipilimumab. *Clin. cancer Res. an Off. J. Am. Assoc. Cancer Res.* **21**, 5453–5459 (2015).

436. Rodriguez, P. C. *et al.* Arginase I Production in the Tumor Microenvironment by Mature Myeloid Cells Inhibits T-Cell Receptor Expression and Antigen-Specific T-Cell Responses Arginase I Production in the Tumor Microenvironment by Mature Myeloid Cells Inhibits T-Cell Receptor Expr. *Cancer Res.* **64**, 5839–5849 (2004).

437. Srivastava, M. K., Sinha, P., Clements, V. K., Rodriguez, P. & Ostrand-Rosenberg, S. Myeloid-derived suppressor cells inhibit T-cell activation by depleting cystine and cysteine. *Cancer Res.* **70**, 68–77 (2010).

438. Rodriguez, P. C. *et al.* Regulation of T cell receptor CD3zeta chain expression by L-arginine. *J. Biol. Chem.* **277**, 21123–21129 (2002).

439. Rodríguez, P. C. & Ochoa, A. C. Arginine regulation by myeloid derived suppressor cells and tolerance in cancer: mechanisms and therapeutic perspectives. *Immunol. Rev.* **222**, 180–191 (2008).

440. Levring, T. B. *et al.* Human CD4+ T cells require exogenous cystine for glutathione and DNA synthesis. *Oncotarget* **6**, 21853–21864 (2015).

441. Levring, T. B. *et al.* Activated human CD4 + T cells express transporters for both cysteine and cystine. *Sci. Rep.* **2**, 2–7 (2012).

442. Srivastava, M. K., Sinha, P., Clements, V. K., Rodriguez, P. & Ostrand-Rosenberg, S. Myeloid-derived suppressor cells inhibit T-cell activation by depleting cystine and cysteine. *Cancer Res.* **70**, 68–77 (2010).

443. Bannai, S. Transport of cystine and cysteine in mammalian cells. *Biochim. Biophys. Acta* **779**, 289–306 (1984).

444. Gmünder, H., Eck, H. P. & Dröge, W. Low membrane transport activity for cystine in resting and mitogenically stimulated human lymphocyte preparations and human T cell clones. *Eur. J. Biochem.* **201**, 113–117 (1991).

445. Hayes, J. D., Dinkova-Kostova, A. T. & Tew, K. D. Oxidative Stress in Cancer. *Cancer Cell* **38**, 167–197 (2020).

446. Kusmartsev, S., Nefedova, Y., Yoder, D. & Gabrilovich, D. I. Antigen-Specific Inhibition of CD8+ T Cell Response by Immature Myeloid Cells in Cancer Is Mediated by Reactive Oxygen Species. *J. Immunol.* **172**, 989 LP – 999 (2004).

447. Liu, Y., Wei, J., Guo, G. & Zhou, J. Norepinephrine-induced myeloid-derived suppressor cells block T-cell responses via generation of reactive oxygen species. *Immunopharmacol. Immunotoxicol.* **37**, 359–365 (2015).

448. Corzo, C. A. *et al.* Mechanism Regulating Reactive Oxygen Species in Tumor-Induced Myeloid-Derived Suppressor Cells. *J. Immunol.* **182**, 5693–5701 (2009).

449. Wanders, R. J. A., Waterham, H. R. & Ferdinandusse, S. Metabolic interplay between peroxisomes and other subcellular organelles including mitochondria and the endoplasmic reticulum. *Front. Cell Dev. Biol.* **3**, 1–15 (2016).

450. Beury, D. W. *et al.* Myeloid-Derived Suppressor Cell Survival and Function Are Regulated by the Transcription Factor Nrf2. *J. Immunol.* **196**, 3470–3478 (2016).

451. Schmielau, J. & Finn, O. J. Activated granulocytes and granulocyte-derived hydrogen peroxide are the underlying mechanism of suppression of t-cell function in advanced cancer patients. *Cancer Res.* **61**, 4756–4760 (2001).

452. Schmielau, J. & Finn, O. J. Activated Granulocytes and Granulocyte-derived Hydrogen Peroxide Are the Underlying Mechanism of Suppression of T-Cell Function in Advanced Cancer Patients Activated Granulocytes and Granulocyte-derived Hydrogen Peroxide Are the Underlying Mechanism of Su. 4756–4760 (2001).

453. Mazzoni, A. *et al.* Myeloid Suppressor Lines Inhibit T Cell Responses by an NO-Dependent Mechanism. *J. Immunol.* **168**, 689–695 (2002).

454. Nagaraj, S. *et al.* Tolerance in Cancer. *Nat Med.* **13**, 828–835 (2008).

455. Jayaraman, P. *et al.* Tumor-Expressed Inducible Nitric Oxide Synthase Controls Induction of Functional Myeloid-Derived Suppressor Cells through Modulation of Vascular Endothelial Growth Factor Release. *J. Immunol.* **188**, 5365 LP – 5376 (2012).

456. Markowitz, J. *et al.* Nitric oxide mediated inhibition of antigen presentation from DCs to CD4+ T cells in cancer and measurement of STAT1 nitration. *Sci. Rep.* **7**, 15424 (2017).

457. Bingisser, R. M., Tilbrook, P. A., Holt, P. G. & Kees, U. R. Macrophage-Derived Nitric Oxide Regulates T Cell Activation via Reversible Disruption of the Jak3/STAT5 Signaling Pathway. *J. Immunol.* **160**, 5729 LP – 5734 (1998).

458. Wang, Z. *et al.* A myeloid cell population induced by freund adjuvant suppresses T-cell-mediated antitumor immunity. *J. Immunother.* **33**, 167–177 (2010).

459. Ostrand-Rosenberg, S. & Sinha, P. Myeloid-derived suppressor cells: linking inflammation and cancer. *J. Immunol.* **182**, 4499–4506 (2009).

460. Obermajer, N. & Kalinski, P. Generation of myeloid-derived suppressor cells using prostaglandin E2. *Transplant. Res.* **1**, 15 (2012).

461. Zhao, F., Korangy, F. & Greten, T. F. Cellular immune suppressor mechanisms in patients with hepatocellular carcinoma. *Dig. Dis.* **30**, 477–482 (2012).

462. Hoechst, B. *et al.* A new population of myeloid-derived suppressor cells in hepatocellular carcinoma patients induces CD4(+)CD25(+)Foxp3(+) T cells. *Gastroenterology* **135**, 234–243 (2008).

463. Schlecker, E. *et al.* Tumor-Infiltrating Monocytic Myeloid-Derived Suppressor Cells Mediate CCR5-Dependent Recruitment of Regulatory T Cells Favoring Tumor Growth. *J. Immunol.* **189**, 5602 LP – 5611 (2012).

464. Lee, C. R., Lee, W., Cho, S. K. & Park, S. G. Characterization of multiple cytokine combinations and TGF-β on differentiation and functions of myeloid-derived suppressor cells. *Int. J. Mol. Sci.* **19**, 1–12 (2018).

465. Pan, P. Y. *et al.* Immune stimulatory receptor CD40 is required for T-cell suppression and T regulatory cell activation mediated by myeloid-derived suppressor cells in cancer. *Cancer Res.* **70**, 99–108 (2010).

466. Huang, B. *et al.* Gr-1+CD115+ immature myeloid suppressor cells mediate the development of tumor-induced T regulatory cells and T-cell anergy in tumor-bearing host. *Cancer Res.* **66**, 1123–1131 (2006).

467. Serafini, P., Mgebroff, S., Noonan, K. & Borrello, I. cell lymphoma by expanding regulatory T cells. **68**, 5439–5449 (2010).

468. Holmgaard, R. B. *et al.* Tumor-Expressed IDO Recruits and Activates MDSCs in a Treg-Dependent Manner. *Cell Rep.* **13**, 412–424 (2015).

469. Yu, J. *et al.* Myeloid-derived suppressor cells suppress antitumor immune responses through IDO expression and correlate with lymph node metastasis in patients with breast cancer. *J. Immunol.* **190**, 3783–3797 (2013).

470. Ku, A. W. *et al.* Tumor-induced MDSC act via remote control to inhibit L-selectin-dependent adaptive immunity in lymph nodes. *Elife* **5**, 1–29 (2016).

471. Hanson, E. M., Clements, V. K., Sinha, P., Ilkovitch, D. & Ostrand-Rosenberg, S. Myeloid-Derived Suppressor Cells Down-Regulate L-Selectin Expression on CD4+ and CD8+ T Cells. *J. Immunol.* **183**, 937–944 (2009).

472. Schouppe, E. *et al.* Tumor-induced myeloid-derived suppressor cell subsets exert either inhibitory or stimulatory effects on distinct CD8+ T-cell activation events. *Eur. J. Immunol.* **43**, 2930–2942 (2013).

473. Li, H., Han, Y., Guo, Q., Zhang, M. & Cao, X. Cancer-expanded myeloid-derived suppressor cells induce anergy of NK cells through membrane-bound TGF-beta 1. *J. Immunol.* **182**, 240–249 (2009).

474. Chauhan, S. *et al.* Surface Glycoproteins of Exosomes Shed by Myeloid-Derived Suppressor Cells Contribute to Function. *J. Proteome Res.* **16**, 238–246 (2017).

475. Isenberg, J. S. *et al.* Differential interactions of thrombospondin-1, -2, and -4 with CD47 and effects on cGMP signaling and ischemic injury responses. *J. Biol. Chem.* **284**, 1116–1125 (2009).

476. Oldenborg, P. A. *et al.* Role of CD47 as a marker of self on red blood cells. *Science (80-.).* **288**, 2051–2054 (2000).

477. Soto-Pantoja, D. R., Kaur, S. & Roberts, D. D. CD47 signaling pathways controlling cellular differentiation and responses to stress. *Crit. Rev. Biochem. Mol. Biol.* **50**, 212–230 (2015).

478. Pinton, L. *et al.* Activated T cells sustain myeloid-derived suppressor cell-mediated immune suppression. *Oncotarget* **7**, 1168–1184 (2016).

479. Ren, J. P. *et al.* Hepatitis C virus-induced myeloid-derived suppressor cells regulate T-cell differentiation and function via the signal transducer and activator of transcription 3 pathway. *Immunology* **148**, 377–386 (2016).

480. Zhao, D. *et al.* VEGF drives cancer-initiating stem cells through VEGFR-2/Stat3 signaling to upregulate Myc and Sox2. *Oncogene* **34**, 3107–3119 (2015).

481. Trikha, P. & Carson, W. E. 3rd. Signaling pathways involved in MDSC regulation. *Biochim. Biophys. Acta* **1846**, 55–65 (2014).

482. Sinha, P. *et al.* Proinflammatory S100 Proteins Regulate the Accumulation of Myeloid-Derived Suppressor Cells. *J. Immunol.* **181**, 4666–4675 (2008).

483. Lim, J. W., Kim, H. & Kim, K. H. Nuclear factor-kappaB regulates cyclooxygenase-2 expression and cell proliferation in human gastric cancer cells. *Lab. Invest.* **81**, 349–360 (2001).

484. Medina-Echeverz, J. *et al.* IFN-γ regulates survival and function of tumor-induced CD11b+ Gr-1high myeloid derived suppressor cells by modulating the anti-apoptotic molecule Bcl2a1. *Eur. J. Immunol.* **44**, 2457–2467 (2014).

485. Groth, C. *et al.* Immunosuppression mediated by myeloid-derived suppressor cells (MDSCs) during tumour progression. *Br. J. Cancer* **120**, 16–25 (2019).

486. Fiore, A. *et al.* Induction of immunosuppressive functions and NF-κB by FLIP in monocytes. *Nat. Commun.* **9**, 1–13 (2018).

487. Haverkamp, J. M. *et al.* Myeloid-derived suppressor activity is mediated by monocytic lineages maintained by continuous inhibition of extrinsic and intrinsic death pathways. *Immunity* **41**, 947–959 (2014).

488. Kusmartsev, S. & Gabrilovich, D. I. STAT1 Signaling Regulates Tumor-Associated Macrophage-Mediated T Cell Deletion. *J. Immunol.* **174**, 4880–4891 (2005).

489. Graubardt, N. *et al.* Ly6Chi monocytes and their macrophage descendants regulate neutrophil function and clearance in acetaminophen-induced liver injury. *Front. Immunol.* **8**, 1–17 (2017).

490. Kwak, T. *et al.* Distinct Populations of Immune-Suppressive Macrophages Differentiate from Monocytic Myeloid-Derived Suppressor Cells in Cancer. *Cell Rep.* **33**, 108571 (2020).

491. Ugel, S., De Sanctis, F., Mandruzzato, S. & Bronte, V. Tumor-induced myeloid deviation: When myeloid-derived suppressor cells meet tumor-Associated macrophages. *J. Clin. Invest.* **125**, 3365–3376 (2015).

492. Casazza, A. *et al.* Impeding Macrophage Entry into Hypoxic Tumor Areas by Sema3A/Nrp1 Signaling Blockade Inhibits Angiogenesis and Restores Antitumor Immunity. *Cancer Cell* **24**, 695–709 (2013).

493. Rivera, L. B. & Bergers, G. Location, Location, Location: Macrophage Positioning within Tumors Determines Pro- or Antitumor Activity. *Cancer Cell* **24**, 687–689 (2013).

494. Heine, A. *et al.* Generation and functional characterization of MDSC-like cells. *Oncoimmunology* **6**, e1295203 (2017).

495. Dilek, N., de Silly, R. V., Blancho, G. & Vanhove, B. Myeloid-derived suppressor cells: Mechanisms of action and recent advances in their role in transplant tolerance. *Front. Immunol.* **3**, 1–9 (2012).

496. Sinha, P., Clements, V. K., Bunt, S. K., Albelda, S. M. & Ostrand-Rosenberg, S. Cross-Talk between Myeloid-Derived Suppressor Cells and Macrophages Subverts Tumor Immunity toward a Type 2 Response. *J. Immunol.* **179**, 977–983 (2007).

497. Beury, D. W. *et al.* Cross-talk among myeloid-derived suppressor cells, macrophages, and tumor cells impacts the inflammatory milieu of solid tumors. *J. Leukoc. Biol.* **96**, 1109–1118 (2014).

498. Ostrand-Rosenberg, S., Sinha, P., Beury, D. W. & Clements, V. K. Cross-talk between myeloid-

derived suppressor cells (MDSC), macrophages, and dendritic cells enhances tumor-induced immune suppression. *Semin. Cancer Biol.* **22**, 275–281 (2012).

499. Cohen, R. *et al.* Targeting cancer cell metabolism in pancreatic adenocarcinoma. *Oncotarget* **6**, 16832–16847 (2015).

500. Carvalho, K. C. *et al.* GLUT1 expression in malignant tumors and its use as an immunodiagnostic marker. *Clinics* **66**, 965–972 (2011).

501. Singer, K. *et al.* Warburg phenotype in renal cell carcinoma: High expression of glucose-transporter 1 (GLUT-1) correlates with low CD8+ T-cell infiltration in the tumor. *Int. J. Cancer* **128**, 2085–2095 (2011).

502. Su, J. *et al.* CD147 silencing inhibits tumor growth by suppressing glucose transport in melanoma. *Oncotarget* **7**, 64778–64784 (2016).

503. Ho, P. C. *et al.* Phosphoenolpyruvate Is a Metabolic Checkpoint of Anti-tumor T Cell Responses. *Cell* **162**, 1217–1228 (2015).

504. Michalek, R. D. *et al.* Cutting Edge: Distinct Glycolytic and Lipid Oxidative Metabolic Programs Are Essential for Effector and Regulatory CD4+ T Cell Subsets. *J. Immunol.* **186**, 3299 LP – 3303 (2011).

505. Bader, J. E., Voss, K. & Rathmell, J. C. Targeting Metabolism to Improve the Tumor Microenvironment for Cancer Immunotherapy. *Mol. Cell* **78**, 1019–1033 (2020).

506. Patel, S. *et al.* Unique pattern of neutrophil migration and function during tumor progression. *Nat. Immunol.* **19**, 1236–1247 (2018).

507. Jian, S.-L. *et al.* Glycolysis regulates the expansion of myeloid-derived suppressor cells in tumor-bearing hosts through prevention of ROS-mediated apoptosis. *Cell Death Dis.* **8**, e2779 (2017).

508. Li, W. *et al.* Aerobic Glycolysis Controls Myeloid-Derived Suppressor Cells and Tumor Immunity via a Specific CEBPB Isoform in Triple-Negative Breast Cancer. *Cell Metab.* **28**, 87-103.e6 (2018).

509. Rice, C. M. *et al.* Tumour-elicited neutrophils engage mitochondrial metabolism to circumvent nutrient limitations and maintain immune suppression. *Nat. Commun.* **9**, (2018).

510. Wang, Y., Jia, A., Bi, Y., Wang, Y. & Liu, G. Metabolic Regulation of Myeloid-Derived Suppressor Cell Function in Cancer. *Cells* **9**, 1–20 (2020).

511. Pardoll, D. M. The blockade of immune checkpoints in cancer immunotherapy. *Nat. Rev. Cancer* **12**, 252–264 (2012).

512. Hodi, F. S. *et al.* Abstract CT001: Durable, long-term survival in previously treated patients with advanced melanoma (MEL) who received nivolumab (NIVO) monotherapy in a phase I trial. *Cancer Res.* **76**, CT001 LP-CT001 (2016).

513. Borghaei, H. *et al.* Nivolumab versus Docetaxel in Advanced Nonsquamous Non–Small-Cell Lung Cancer. *N. Engl. J. Med.* **373**, 1627–1639 (2015).

514. Motzer, R. J. *et al.* Nivolumab versus Everolimus in Advanced Renal-Cell Carcinoma. *N. Engl. J. Med.* **373**, 1803–1813 (2015).

515. Rosenberg, J. E. *et al.* Atezolizumab in patients with locally advanced and metastatic urothelial carcinoma who have progressed following treatment with platinum-based chemotherapy: A single-arm, multicentre, phase 2 trial. *Lancet* **387**, 1909–1920 (2016).

516. Mehra, R. *et al.* Efficacy and safety of pembrolizumab in recurrent/metastatic head and neck

squamous cell carcinoma: Pooled analyses after long-term follow-up in KEYNOTE-012. *Br. J. Cancer* **119**, 153–159 (2018).

517. Ribas, A. Adaptive Immune Resistance: How Cancer Protects from Immune Attack. *Cancer Discov.* **5**, 915–919 (2015).

518. Simeone, E. & Ascierto, P. A. Anti-PD-1 and PD-L1 antibodies in metastatic melanoma. *Melanoma Manag.* **4**, 175–178 (2017).

519. Rizvi, N. A. *et al.* Cancer immunology. Mutational landscape determines sensitivity to PD-1 blockade in non-small cell lung cancer. *Science* **348**, 124–128 (2015).

520. Snyder, A. *et al.* Genetic Basis for Clinical Response to CTLA-4 Blockade in Melanoma. *N. Engl. J. Med.* **371**, 2189–2199 (2014).

521. van Rooij, N. *et al.* Tumor Exome Analysis Reveals Neoantigen-Specific T-Cell Reactivity in an Ipilimumab-Responsive Melanoma. *J. Clin. Oncol.* **31**, e439–e442 (2013).

522. Gao, J. *et al.* Loss of IFN-γ Pathway Genes in Tumor Cells as a Mechanism of Resistance to Anti-CTLA-4 Therapy. *Cell* **167**, 397-404.e9 (2016).

523. Sucker, A. *et al.* Acquired IFNγ 3 resistance impairs anti-Tumor immunity and gives rise to T-cell-resistant melanoma lesions. *Nat. Commun.* **8**, 1–15 (2017).

524. Benci, J. L. *et al.* Tumor Interferon Signaling Regulates a Multigenic Resistance Program to Immune Checkpoint Blockade. *Cell* **167**, 1540-1554.e12 (2016).

525. Rodig, S. J. *et al.* MHC proteins confer differential sensitivity to CTLA-4 and PD-1 blockade in untreated metastatic melanoma. *Sci. Transl. Med.* **10**, (2018).

526. Restifo, N. P. *et al.* Loss of functional beta 2-microglobulin in metastatic melanomas from five patients receiving immunotherapy. *J. Natl. Cancer Inst.* **88**, 100–108 (1996).

527. Huang, L. *et al.* The RNA-binding Protein MEX3B Mediates Resistance to Cancer Immunotherapy by Downregulating HLA-A Expression. *Clin. Cancer Res.* **24**, 3366 LP – 3376 (2018).

528. Li, J., Ni, L. & Dong, C. Immune checkpoint receptors in cancer: redundant by design? *Curr. Opin. Immunol.* **45**, 37–42 (2017).

529. Duan, Q., Zhang, H., Zheng, J. & Zhang, L. Turning Cold into Hot: Firing up the Tumor Microenvironment. *Trends in Cancer* **6**, 605–618 (2020).

530. Weiss, S. A., Wolchok, J. D. & Sznol, M. Immunotherapy of melanoma: Facts and hopes. *Clin. Cancer Res.* **25**, 5191–5201 (2019).

531. Fares, C. M., Van Allen, E. M., Drake, C. G., Allison, J. P. & Hu-Lieskovan, S. Mechanisms of Resistance to Immune Checkpoint Blockade: Why Does Checkpoint Inhibitor Immunotherapy Not Work for All Patients? *Am. Soc. Clin. Oncol. Educ. B.* 147–164 (2019) doi:10.1200/edbk_240837.

532. Cassetta, L. & Pollard, J. W. Targeting macrophages: Therapeutic approaches in cancer. *Nat. Rev. Drug Discov.* **17**, 887–904 (2018).

533. Ding, A. S., Routkevitch, D., Jackson, C. & Lim, M. Targeting Myeloid Cells in Combination Treatments for Glioma and Other Tumors . *Frontiers in Immunology* vol. 10 1715 (2019).

534. Stanley, E. R. & Chitu, V. CSF-1 receptor signaling in myeloid cells. *Cold Spring Harb. Perspect. Biol.* **6**, 1–22 (2014).

535. Richardsen, E., Uglehus, R. D., Johnsen, S. H. & Busund, L.-T. Macrophage-colony stimulating factor (CSF1) predicts breast cancer progression and mortality. *Anticancer Res.* **35**, 865–874 (2015).

536. Hsu, W.-C. *et al.* CSF-1 Overexpression Predicts Poor Prognosis in Upper Tract Urothelial Carcinomas. *Dis. Markers* **2019**, 2724948 (2019).

537. Cannarile, M. A. *et al.* Colony-stimulating factor 1 receptor (CSF1R) inhibitors in cancer therapy. *J. Immunother. cancer* **5**, 53 (2017).

538. Wainberg, Z. *et al.* First-in-human phase 1 dose escalation and expansion of a novel combination, anti-CSF-1 receptor (cabiralizumab) plus anti-PD-1 (nivolumab), in patients with advanced solid tumors. *J. Immunother. Cancer* **5**, 89 (O42) (2017).

539. Hu-Lieskovan, S. *et al.* Phase 1/2a study of double immune suppression blockade by combining a CSF1R inhibitor (pexidartinib/PLX3397) with an anti PD-1 antibody (pembrolizumab) to treat advanced melanoma and other solid tumors. *Ann. Oncol.* **26**, viii5 (2015).

540. Carleton, M. *et al.* Pharmacodynamics (PD) and genomic profiling of pts treated with cabiralizumab (cabira) + nivolumab (NIVO) provide evidence of on-target tumor immune modulations and support future clinical applications. *J. Clin. Oncol.* **36**, 3020 (2018).

541. Takamatsu, H., Okuno, T. & Kumanogoh, A. Regulation of immune cell responses by semaphorins and their receptors. *Cell. Mol. Immunol.* **7**, 83–88 (2010).

542. Ch'ng, E. S. & Kumanogoh, A. Roles of Sema4D and Plexin-B1 in tumor progression. *Mol. Cancer* **9**, 1–9 (2010).

543. Delaire, S. *et al.* Biological activity of soluble CD100. II. Soluble CD100, similarly to H-SemaIII, inhibits immune cell migration. *J. Immunol.* **166**, 4348–4354 (2001).

544. Evans, E. E., Paris, M., Smith, E. S. & Zauderer, M. Immunomodulation of the tumor microenvironment by neutralization of Semaphorin 4D. *Oncoimmunology* **4**, (2015).

545. Evans, E. E. *et al.* Antibody blockade of Semaphorin 4D promotes immune infiltration into tumor and enhances response to other immunomodulatory therapies. *Cancer Immunol. Res.* **3**, 698–701 (2015).

546. Lowe, M. C. *et al.* Pilot integrated biomarker study of VX15/2503 in combination with ipilimumab and/or nivolumab in patients with resectable metastatic melanoma. *J. Clin. Oncol.* **37**, TPS9603–TPS9603 (2019).

547. Nefedova, Y. *et al.* Mechanism of all-trans retinoic acid effect on tumor-associated myeloid-derived suppressor cells. *Cancer Res.* **67**, 11021–11028 (2007).

548. Tobin, R. P. *et al.* Targeting myeloid-derived suppressor cells using all-trans retinoic acid in melanoma patients treated with Ipilimumab. *Int. Immunopharmacol.* **63**, 282–291 (2018).

549. Osada, T. *et al.* The effect of anti-VEGF therapy on immature myeloid cell and dendritic cells in cancer patients. *Cancer Immunol. Immunother.* **57**, 1115–1124 (2008).

550. Gabrilovich, D. I. *et al.* Production of vascular endothelial growth factor by human tumors inhibits the functional maturation of dendritic cells. *Nat. Med.* **2**, 1096–1103 (1996).

551. Ryzhov, S. V *et al.* Role of TGF-β signaling in generation of CD39+CD73+ myeloid cells in tumors. *J. Immunol.* **193**, 3155–3164 (2014).

552. Umansky, V., Shevchenko, I., Bazhin, A. V. & Utikal, J. Extracellular adenosine metabolism in

immune cells in melanoma. *Cancer Immunol. Immunother.* **63**, 1073–1080 (2014).

553. Allard, B., Turcotte, M. & Stagg, J. CD73-generated adenosine: Orchestrating the tumor-stroma interplay to promote cancer growth. *J. Biomed. Biotechnol.* **2012**, (2012).

554. Ryzhov, S., McCaleb, J. L., Goldstein, A. E., Biaggioni, I. & Feoktistov, I. Role of adenosine receptors in the regulation of angiogenic factors and neovascularization in hypoxia. *J. Pharmacol. Exp. Ther.* **320**, 565–572 (2007).

555. Hotson, A. *et al.* Clinical activity of adenosine 2A receptor (A2AR) inhibitor CPI-444 is associated with tumor expression of adenosine pathway genes and tumor immune modulation. *J. Immunother. Cancer* **5**, 86–86 (2017).

556. Uyttenhove, C. *et al.* Evidence for a tumoral immune resistance mechanism based on tryptophan degradation by indoleamine 2,3-dioxygenase. *Nat. Med.* **9**, 1269–1274 (2003).

557. Holmgaard, R. B., Zamarin, D., Munn, D. H., Wolchok, J. D. & Allison, J. P. Indoleamine 2,3-dioxygenase is a critical resistance mechanism in antitumor T cell immunotherapy targeting CTLA-4. *J. Exp. Med.* **210**, 1389–1402 (2013).

558. Mitchell, T. C. *et al.* Epacadostat Plus Pembrolizumab in Patients With Advanced Solid Tumors: Phase I Results From a Multicenter, Open-Label Phase I/II Trial (ECHO-202/KEYNOTE-037). *J. Clin. Oncol. Off. J. Am. Soc. Clin. Oncol.* **36**, 3223–3230 (2018).

559. Kaneda, M. M. *et al.* PI3Kγ 3 is a molecular switch that controls immune suppression. *Nature* **539**, 437–442 (2016).

560. De Henau, O. *et al.* Overcoming resistance to checkpoint blockade therapy by targeting PI3Kγ in myeloid cells. *Nature* **539**, 443–447 (2016).

561. Sullivan, R. J. *et al.* Initial results from first-in-human study of IPI-549, a tumor macrophage-targeting agent, combined with nivolumab in advanced solid tumors. *J. Clin. Oncol.* **36**, 3013 (2018).

562. Grewal, I. S. & Flavell, R. A. The Role of CD40 Ligand in Costimulation and T-Cell Activation. *Immunol. Rev.* **153**, 85–106 (1996).

563. Munroe, M. E. & Bishop, G. A. A Costimulatory Function for T Cell CD40. *J. Immunol.* **178**, 671–682 (2007).

564. Marigo, I. *et al.* T Cell Cancer Therapy Requires CD40-CD40L Activation of Tumor Necrosis Factor and Inducible Nitric-Oxide-Synthase-Producing Dendritic Cells. *Cancer Cell* **30**, 377–390 (2016).

565. Zippelius, A., Schreiner, J., Herzig, P. & Müller, P. Induced PD-L1 expression mediates acquired resistance to agonistic anti-CD40 treatment. *Cancer Immunol. Res.* **3**, 236–244 (2015).

566. Woo, S. R. *et al.* STING-dependent cytosolic DNA sensing mediates innate immune recognition of immunogenic tumors. *Immunity* **41**, 830–842 (2014).

567. Zhu, Y. *et al.* STING: A master regulator in the cancer-immunity cycle. *Mol. Cancer* **18**, 1–15 (2019).

568. Jassar, A. S. *et al.* Activation of tumor-associated macrophages by the vascular disrupting agent 5,6-dimethylxanthenone-4-acetic acid induces an effective CD8+ T-cell-mediated antitumor immune response in murine models of lung cancer and mesothelioma. *Cancer Res.* **65**, 11752–11761 (2005).

569. Zhang, C. xia *et al.* STING signaling remodels the tumor microenvironment by antagonizing

myeloid-derived suppressor cell expansion. *Cell Death Differ.* **26**, 2314–2328 (2019).

570. Weiss, J. M. *et al.* The STING agonist DMXAA triggers a cooperation between T lymphocytes and myeloid cells that leads to tumor regression. *Oncoimmunology* **6**, e1346765 (2017).

571. Iwasaki, A. & Medzhitov, R. Regulation of adaptive immunity by the innate immune system. *Science* **327**, 291–295 (2010).

572. Harris, M. R., Yu, Y. Y. L., Kindle, C. S., Hansen, T. H. & Solheim, J. C. Calreticulin and Calnexin Interact with Different Protein and Glycan Determinants During the Assembly of MHC Class I. *J. Immunol.* **160**, 5404 LP – 5409 (1998).

573. Zhang, Q. & Salter, R. D. Distinct Patterns of Folding and Interactions with Calnexin and Calreticulin in Human Class I MHC Proteins with Altered N-Glycosylation. *J. Immunol.* **160**, 831 LP – 837 (1998).

574. Basu, S., Binder, R. J., Ramalingam, T. & Srivastava, P. K. CD91 is a common receptor for heat shock proteins gp96, hsp90, hsp70, and calreticulin. *Immunity* **14**, 303–313 (2001).

575. Nilsson, A., Vesterlund, L. & Oldenborg, P.-A. Macrophage expression of LRP1, a receptor for apoptotic cells and unopsonized erythrocytes, can be regulated by glucocorticoids. *Biochem. Biophys. Res. Commun.* **417**, 1304–1309 (2012).

576. Garg, A. D. *et al.* Immunogenic cell death, DAMPs and anticancer therapeutics: an emerging amalgamation. *Biochim. Biophys. Acta* **1805**, 53–71 (2010).

577. Chen, J. *et al.* SLAMF7 is critical for phagocytosis of haematopoietic tumour cells via Mac-1 integrin. *Nature* **544**, 493–497 (2017).

578. Tridandapani, S. *et al.* Regulated expression and inhibitory function of FcγRIIb in human monocytic cells. *J. Biol. Chem.* **277**, 5082–5089 (2002).

579. Daëron, M. Fc receptor biology. *Annu. Rev. Immunol.* **15**, 203–234 (1997).

580. Bakema, J. E. & van Egmond, M. Fc receptor-dependent mechanisms of monoclonal antibody therapy of cancer. *Curr. Top. Microbiol. Immunol.* **382**, 373–392 (2014).

581. Crowley, M. T. *et al.* A critical role for Syk in signal transduction and phagocytosis mediated by Fcgamma receptors on macrophages. *J. Exp. Med.* **186**, 1027–1039 (1997).

582. Getahun, A. & Cambier, J. C. Of ITIMs, ITAMs, and ITAMis: revisiting immunoglobulin Fc receptor signaling. *Immunol. Rev.* **268**, 66–73 (2015).

583. Li, Y., Yin, Y. & Mariuzza, R. A. Structural and biophysical insights into the role of CD4 and CD8 in T cell activation. *Front. Immunol.* **4**, 1–11 (2013).

584. Barkal, A. A. *et al.* Engagement of MHC class i by the inhibitory receptor LILRB1 suppresses macrophages and is a target of cancer immunotherapy article. *Nat. Immunol.* **19**, 76–84 (2018).

585. Leone, P. *et al.* MHC Class I Antigen Processing and Presenting Machinery: Organization, Function, and Defects in Tumor Cells. *JNCI J. Natl. Cancer Inst.* **105**, 1172–1187 (2013).

586. Pollard, J. W. Tumour-educated macrophages promote tumour progression and metastasis. *Nature reviews. Cancer* vol. 4 71–78 (2004).

587. Gordon, S. R. *et al.* PD-1 expression by tumour-associated macrophages inhibits phagocytosis and tumour immunity. *Nature* **545**, 495–499 (2017).

588. Barclay, A. N. & Van Den Berg, T. K. The interaction between signal regulatory protein alpha (SIRPα) and CD47: Structure, function, and therapeutic target. *Annu. Rev. Immunol.* **32**, 25–50

(2014).

589. Seiffert, M. *et al.* Signal-regulatory protein alpha (SIRPalpha) but not SIRPbeta is involved in T-cell activation, binds to CD47 with high affinity, and is expressed on immature CD34(+)CD38(-) hematopoietic cells. *Blood* **97**, 2741–2749 (2001).

590. Okajo, J. *et al.* Regulation by Src homology 2 domain-containing protein tyrosine phosphatase substrate-1 of alpha-galactosylceramide-induced antimetastatic activity and Th1 and Th2 responses of NKT cells. *J. Immunol.* **178**, 6164–6172 (2007).

591. Bouguermouh, S. *et al.* CD47 Expression on T Cell Is a Self-Control Negative Regulator of Type 1 Immune Response. *J. Immunol.* **180**, 8073–8082 (2008).

592. Nath, P. R. *et al.* CD47 Expression in Natural Killer Cells Regulates Homeostasis and Modulates Immune Response to Lymphocytic Choriomeningitis Virus. *Front. Immunol.* **9**, 2985 (2018).

593. Jaiswal, S. *et al.* CD47 Is Upregulated on Circulating Hematopoietic Stem Cells and Leukemia Cells to Avoid Phagocytosis. *Cell* **138**, 271–285 (2009).

594. Merad, M., Sathe, P., Helft, J., Miller, J. & Mortha, A. The dendritic cell lineage: ontogeny and function of dendritic cells and their subsets in the steady state and the inflamed setting. *Annu. Rev. Immunol.* **31**, 563–604 (2013).

595. Hagnerud, S. *et al.* Deficit of CD47 results in a defect of marginal zone dendritic cells, blunted immune response to particulate antigen and impairment of skin dendritic cell migration. *J. Immunol.* **176**, 5772–5778 (2006).

596. Saito, Y. *et al.* Regulation by SIRPα of dendritic cell homeostasis in lymphoid tissues. *Blood* **116**, 3517–3525 (2010).

597. Van, V. Q. *et al.* Expression of the self-marker CD47 on dendritic cells governs their trafficking to secondary lymphoid organs. *EMBO J.* **25**, 5560–5568 (2006).

598. Roozendaal, R. & Mebius, R. E. Stromal cell-immune cell interactions. *Annu. Rev. Immunol.* **29**, 23–43 (2011).

599. Marie, P. Physiology of bone tissue. *Immuno-analyse Biol. Spécialisée* **7**, 17–24 (1992).

600. van Beek, E. M. *et al.* Inhibitory regulation of osteoclast bone resorption by signal regulatory protein alpha. *FASEB J. Off. Publ. Fed. Am. Soc. Exp. Biol.* **23**, 4081–4090 (2009).

601. Lundberg, P. *et al.* Osteoclast formation is strongly reduced both in vivo and in vitro in the absence of CD47/SIRPα-interaction. *Biochem. Biophys. Res. Commun.* **352**, 444–448 (2007).

602. Koskinen, C. *et al.* Lack of CD47 impairs bone cell differentiation and results in an osteopenic phenotype in vivo due to impaired signal regulatory protein α (SIRPα) signaling. *J. Biol. Chem.* **288**, 29333–29344 (2013).

603. Kim, D. *et al.* Anti-CD47 antibodies promote phagocytosis and inhibit the growth of human myeloma cells. *Leukemia* **26**, 2538–2545 (2012).

604. Edris, B. *et al.* Antibody therapy targeting the CD47 protein is effective in a model of aggressive metastatic leiomyosarcoma. *Proc. Natl. Acad. Sci.* **109**, 6656 LP – 6661 (2012).

605. Chao, M. P. *et al.* Therapeutic Antibody Targeting of CD47 Eliminates Human Acute Lymphoblastic Leukemia. *Cancer Res.* **71**, 1374 LP – 1384 (2011).

606. Chao, M. P. *et al.* Extranodal dissemination of non-Hodgkin lymphoma requires CD47 and is inhibited by anti-CD47 antibody therapy. *Blood* **118**, 4890–4901 (2011).

607. Willingham, S. B. *et al.* The CD47-signal regulatory protein alpha (SIRPa) interaction is a therapeutic target for human solid tumors. *Proc. Natl. Acad. Sci.* **109**, 6662–6667 (2012).

608. Mohanty, S. *et al.* Nanoparticle enhanced MRI can monitor macrophage response to CD47 mAb immunotherapy in osteosarcoma. *Cell Death Dis.* **10**, 36 (2019).

609. Wu, L. *et al.* Anti-CD47 treatment enhances anti-tumor T-cell immunity and improves immunosuppressive environment in head and neck squamous cell carcinoma. *Oncoimmunology* **7**, (2018).

610. Majeti, R. *et al.* CD47 Is an Adverse Prognostic Factor and Therapeutic Antibody Target on Human Acute Myeloid Leukemia Stem Cells. *Cell* **138**, 286–299 (2009).

611. Weiskopf, K. *et al.* CD47-blocking immunotherapies stimulate macrophage-mediated destruction of small-cell lung cancer. *J. Clin. Invest.* **126**, 2610–2620 (2016).

612. Betancur, P. A. *et al.* A CD47-associated super-enhancer links pro-inflammatory signalling to CD47 upregulation in breast cancer. *Nat. Commun.* **8**, 14802 (2017).

613. Zhang, H. *et al.* HIF-1 regulates CD47 expression in breast cancer cells to promote evasion of phagocytosis and maintenance of cancer stem cells. *Proc. Natl. Acad. Sci.* **112**, E6215 LP-E6223 (2015).

614. Casey, S. C. *et al.* MYC regulates the antitumor immune response through CD47 and PD-L1. *Science* **352**, 227–231 (2016).

615. Wiersma, V. R., Michalak, M., Abdullah, T. M., Bremer, E. & Eggleton, P. Mechanisms of Translocation of ER Chaperones to the Cell Surface and Immunomodulatory Roles in Cancer and Autoimmunity. *Front. Oncol.* **5**, 1–14 (2015).

616. Chao, M. P. *et al.* Calreticulin is the dominant pro-phagocytic signal on multiple human cancers and is counterbalanced by CD47. *Sci. Transl. Med.* **2**, (2010).

617. Matozaki, T., Murata, Y., Okazawa, H. & Ohnishi, H. Functions and molecular mechanisms of the CD47-SIRPα signalling pathway. *Trends Cell Biol.* **19**, 72–80 (2009).

618. Fujioka, Y. *et al.* A novel membrane glycoprotein, SHPS-1, that binds the SH2-domain-containing protein tyrosine phosphatase SHP-2 in response to mitogens and cell adhesion. *Mol. Cell. Biol.* **16**, 6887–6899 (1996).

619. Kodama, A. *et al.* Involvement of an SHP-2-Rho small G protein pathway in hepatocyte growth factor/scatter factor-induced cell scattering. *Mol. Biol. Cell* **11**, 2565–2575 (2000).

620. Matozaki, T., Murata, Y., Saito, Y., Okazawa, H. & Ohnishi, H. Protein tyrosine phosphatase SHP-2: a proto-oncogene product that promotes Ras activation. *Cancer Sci.* **100**, 1786–1793 (2009).

621. Matlung, H. L., Szilagyi, K., Barclay, N. A. & van den Berg, T. K. The CD47-SIRPα signaling axis as an innate immune checkpoint in cancer. *Immunol. Rev.* **276**, 145–164 (2017).

622. Tsai, R. K. & Discher, D. E. Inhibition of 'self' engulfment through deactivation of myosin-II at the phagocytic synapse between human cells. *J. Cell Biol.* **180**, 989–1003 (2008).

623. Toledano, N., Gur-Wahnon, D., Ben-Yehuda, A. & Rachmilewitz, J. Novel CD47: SIRPα Dependent Mechanism for the Activation of STAT3 in Antigen-Presenting Cell. *PLoS One* **8**, (2013).

624. Mantovani, A., Marchesi, F., Malesci, A., Laghi, L. & Allavena, P. Tumour-associated macrophages as treatment targets in oncology. *Nat. Rev. Clin. Oncol.* **14**, 399–416 (2017).

625. Chan, K. S. *et al.* Identification, molecular characterization, clinical prognosis, and therapeutic

targeting of human bladder tumor-initiating cells. *Proc. Natl. Acad. Sci. U. S. A.* **106**, 14016–14021 (2009).

626. Weiskopf, K. *et al.* Engineered SIRPα variants as immunotherapeutic adjuvants to anticancer antibodies. *Science (80-.).* **341**, 88–91 (2013).

627. Chao, M. P. *et al.* Anti-CD47 antibody synergizes with rituximab to promote phagocytosis. **142**, 699–713 (2011).

628. Pan, Y. *et al.* Endoscopic molecular imaging of human bladder cancer using a CD47 antibody. *Sci. Transl. Med.* **6**, 260ra148 (2014).

629. Zhang, M. *et al.* Anti-CD47 Treatment Stimulates Phagocytosis of Glioblastoma by M1 and M2 Polarized Macrophages and Promotes M1 Polarized Macrophages In Vivo. *PLoS One* **11**, e0153550 (2016).

630. Zhao, X. W. *et al.* CD47-signal regulatory protein-α (SIRPα) interactions form a barrier for antibody-mediated tumor cell destruction. *Proc. Natl. Acad. Sci. U. S. A.* **108**, 18342–18347 (2011).

631. Pengam, S. *et al.* SIRPα/CD47 axis controls the maintenance of transplant tolerance sustained by myeloid-derived suppressor cells. *Am. J. Transplant.* **19**, 3263–3275 (2019).

632. Ring, N. G. *et al.* Anti-SIRPα antibody immunotherapy enhances neutrophil and macrophage antitumor activity. *Proc. Natl. Acad. Sci. U. S. A.* **114**, E10578–E10585 (2017).

633. Pietsch, E. C. *et al.* Anti-leukemic activity and tolerability of anti-human CD47 monoclonal antibodies. *Blood Cancer J.* **7**, (2017).

634. Brierley, C. K. *et al.* The effects of monoclonal anti-CD47 on RBCs, compatibility testing, and transfusion requirements in refractory acute myeloid leukemia. *Transfusion* **59**, 2248–2254 (2019).

635. Catani, L. *et al.* The CD47 pathway is deregulated in human immune thrombocytopenia. *Exp. Hematol.* **39**, 486–494 (2011).

636. Mansoori, B., Mohammadi, A., Davudian, S., Shirjang, S. & Baradaran, B. The Different Mechanisms of Cancer Drug Resistance: A Brief Review. *Adv. Pharm. Bull.* **7**, 339–348 (2017).

637. Advani, R. *et al.* CD47 Blockade by Hu5F9-G4 and Rituximab in Non-Hodgkin's Lymphoma. *N. Engl. J. Med.* **379**, 1711–1721 (2018).

638. Gauttier, V. *et al.* Selective SIRPα blockade reverses tumor T cell exclusion and overcomes cancer immunotherapy resistance. *J. Clin. Invest.* **130**, 6109–6123 (2020).

639. Comu, S. *et al.* The murine P84 neural adhesion molecule is SHPS-1, a member of the phosphatase-binding protein family. *J. Neurosci.* **17**, 8702–8710 (1997).

640. Jiang, P., Lagenaur, C. F. & Narayanan, V. Integrin-associated protein is a ligand for the P84 neural adhesion molecule. *J. Biol. Chem.* **274**, 559–562 (1999).

641. Gresham, H. D. *et al.* Negative regulation of phagocytosis in murine macrophages by the Src kinase family member, Fgr. *J. Exp. Med.* **191**, 515–528 (2000).

642. Fukunaga, A. *et al.* Src Homology 2 Domain-Containing Protein Tyrosine Phosphatase Substrate 1 Regulates the Migration of Langerhans Cells from the Epidermis to Draining Lymph Nodes. *J. Immunol.* **172**, 4091–4099 (2004).

643. Verjan Garcia, N. *et al.* SIRPα/CD172a Regulates Eosinophil Homeostasis. *J. Immunol.* **187**, 2268–2277 (2011).

644. Yanagita, T. *et al.* Anti-SIRPα antibodies as a potential new tool for cancer immunotherapy. *JCI Insight* **2**, 1–15 (2017).

645. Gabrilovich, D. I. Myeloid-Derived Suppressor Cells. *Cancer Immunol. Res.* **5**, 3–8 (2017).

646. Awad, R. M., Vlaeminck, Y. De, Maebe, J. & Goyvaerts, C. Turn Back the TIMe : Targeting Tumor Infiltrating Myeloid Cells to Revert Cancer Progression. **9**, 1–22 (2018).

647. Liu, Y. & Zeng, G. Cancer and innate immune system interactions: Translational potentials for cancer immunotherapy. *J. Immunother.* **35**, 299–308 (2012).

648. Ravichandran, K. S. Find-me and eat-me signals in apoptotic cell clearance : progress and conundrums. **207**, 1807–1817 (2010).

649. Macrophage, T. Industry corner : perspectives and controversies. 1–4 (2019) doi:10.1093/annonc/mdz006.

650. Zhang, W. *et al.* Advances in Anti-Tumor Treatments Targeting the CD47/SIRPα Axis. *Front. Immunol.* **11**, 1–15 (2020).

651. Davidson, S. *et al.* Single-Cell RNA Sequencing Reveals a Dynamic Stromal Niche That Supports Tumor Growth. *Cell Rep.* **31**, 107628 (2020).

652. Yang, Y., Li, C., Liu, T., Dai, X. & Bazhin, A. V. Myeloid-Derived Suppressor Cells in Tumors: From Mechanisms to Antigen Specificity and Microenvironmental Regulation. *Front. Immunol.* **11**, 1–22 (2020).

653. Condamine, T., Ramachandran, I., Youn, J.-I. & Gabrilovich, D. I. Regulation of Tumor Metastasis by Myeloid-derived Suppressor Cells. *Annu Rev Med* 97–110 (2016) doi:10.1146/annurev-med-051013-052304.Regulation.

654. Fleming, V. *et al.* Targeting Myeloid-Derived Suppressor Cells to Bypass Tumor-Induced Immunosuppression. *Front. Immunol.* **9**, 398 (2018).

655. Li, C., Liu, T., Bazhin, A. V & Yang, Y. The Sabotaging Role of Myeloid Cells in Anti-Angiogenic Therapy: Coordination of Angiogenesis and Immune Suppression by Hypoxia. *J. Cell. Physiol.* **232**, 2312–2322 (2017).

656. Watanabe, S. *et al.* Tumor-induced CD11b+Gr-1+ myeloid cells suppress T cell sensitization in tumor-draining lymph nodes. *J. Immunol.* **181**, 3291–3300 (2008).

657. De Veirman, K. *et al.* Extracellular S100A9 protein in bone marrow supports multiple myeloma survival by stimulating angiogenesis and cytokine secretion. *Cancer Immunol. Res.* **5**, 839–846 (2017).

658. Sceneay, J. *et al.* Primary tumor hypoxia recruits CD11b+/Ly6Cmed/Ly6G+ immune suppressor cells and compromises NK cell cytotoxicity in the premetastatic niche. *Cancer Res.* **72**, 3906–3911 (2012).

659. Ai, L. *et al.* Prognostic role of myeloid-derived suppressor cells in cancers: a systematic review and meta-analysis. *BMC Cancer* **18**, 1–9 (2018).

660. Weide, B. *et al.* Myeloid-derived suppressor cells predict survival of patients with advanced melanoma: Comparison with regulatory T cells and NY-ESO-1- or melan-A-specific T cells. *Clin. Cancer Res.* **20**, 1601–1609 (2014).

661. Wang, L. *et al.* Increased Myeloid-Derived Suppressor Cells in Gastric Cancer Correlate with Cancer Stage and Plasma S100A8/A9 Proinflammatory Proteins. *J. Immunol.* **190**, 794–804 (2013).

662. Horinaka, A. *et al.* Invariant NKT cells are resistant to circulating CD15+ myeloid-derived suppressor cells in patients with head and neck cancer. *Cancer Sci.* **107**, 207–216 (2016).

663. Huang, A. *et al.* Increased CD14+HLA-DR-/low myeloid-derived suppressor cells correlate with extrathoracic metastasis and poor response to chemotherapy in non-small cell lung cancer patients. *Cancer Immunol. Immunother.* **62**, 1439–1451 (2013).

664. Lv, M., Wang, K. & Huang, X. J. Myeloid-derived suppressor cells in hematological malignancies: Friends or foes. *J. Hematol. Oncol.* **12**, 1–12 (2019).

665. Vuk-Pavlović, S. *et al.* Immunosuppressive CD14+HLA-DRlow/− monocytes in prostate cancer. *Prostate* **70**, 443–455 (2010).

666. Solito, S. *et al.* A human promyelocytic-like population is responsible for the immune suppression mediated by myeloid-derived suppressor cells. *Blood* **118**, 2254–2265 (2011).

667. Chen, M.-F. *et al.* IL-6-stimulated CD11b+ CD14+ HLA-DR- myeloid-derived suppressor cells, are associated with progression and poor prognosis in squamous cell carcinoma of the esophagus. *Oncotarget* **5**, 8716–8728 (2014).

668. Chen, H.-M. *et al.* Myeloid-Derived Suppressor Cells as an Immune Parameter in Patients with Concurrent Sunitinib and Stereotactic Body Radiotherapy. *Clin. Cancer Res.* **21**, 4073–4085 (2015).

669. Tarhini, A. A. *et al.* Immune monitoring of the circulation and the tumor microenvironment in patients with regionally advanced melanoma receiving neoadjuvant ipilimumab. *PLoS One* **9**, e87705–e87705 (2014).

670. Meyer, C. *et al.* Frequencies of circulating MDSC correlate with clinical outcome of melanoma patients treated with ipilimumab. *Cancer Immunol. Immunother.* **63**, 247–257 (2014).

671. Rose, S., Misharin, A. & Perlman, H. A novel Ly6C/Ly6G-based strategy to analyze the mouse splenic myeloid compartment. *Cytom. Part A* **81 A**, 343–350 (2012).

672. Fidler, I. J. & Nicolson, G. L. Organ selectivity for implantation survival and growth of B16 melanoma variant tumor lines. *J. Natl. Cancer Inst.* **57**, 1199–1202 (1976).

673. Ostrand-Rosenberg, S. & Fenselau, C. Myeloid-Derived Suppressor Cells: Immune-Suppressive Cells That Impair Antitumor Immunity and Are Sculpted by Their Environment. *J. Immunol.* **200**, 422–431 (2018).

674. Cance, J. C., Crozat, K., Dalod, M. & Mattiuz, R. Are conventional type 1 dendritic cells critical for protective antitomor immunity and how? *Front. Immunol.* **10**, (2019).

675. Anderson, D. A., Dutertre, C.-A., Ginhoux, F. & Murphy, K. M. Genetic models of human and mouse dendritic cell development and function. *Nat. Rev. Immunol.* 1–15 (2020) doi:10.1038/s41577-020-00413-x.

676. Ginhoux, F. & Jung, S. Monocytes and macrophages: Developmental pathways and tissue homeostasis. *Nat. Rev. Immunol.* **14**, 392–404 (2014).

677. Lee, M., Lee, Y., Song, J., Lee, J. & Chang, S. Y. Tissue-specific role of CX3CR1 expressing immune cells and their relationships with human disease. *Immune Netw.* **18**, 1–19 (2018).

678. Guo, J. *et al.* Fractalkine transgene induces T-cell-dependent antitumor immunity through chemoattraction and activation of dendritic cells. *Int. J. Cancer* **103**, 212–220 (2003).

679. Chiu, D. K. C. *et al.* Hypoxia induces myeloid-derived suppressor cell recruitment to hepatocellular carcinoma through chemokine (C-C motif) ligand 26. *Hepatology* **64**, 797–813

(2016).

680. Murray, P. J. & Wynn, T. A. Protective and pathogenic functions of macrophage subsets. *Nat. Rev. Immunol.* **11**, 723–737 (2011).

681. Lin, H. H. *et al.* The macrophage F4/80 receptor is required for the induction of antigen-specific efferent regulatory T cells in peripheral tolerance. *J. Exp. Med.* **201**, 1615–1625 (2005).

682. Chávez-Galán, L., Olleros, M. L., Vesin, D. & Garcia, I. Much more than M1 and M2 macrophages, there are also CD169+ and TCR+ macrophages. *Front. Immunol.* **6**, 1–15 (2015).

683. Sun, C., Mezzadra, R. & Schumacher, T. N. Regulation and Function of the PD-L1 Checkpoint. *Immunity* **48**, 434–452 (2018).

684. Zhang, Y. *et al.* Myeloid cells are required for PD-1/PD-L1 checkpoint activation and the establishment of an immunosuppressive environment in pancreatic cancer. *Gut* **66**, 124–136 (2017).

685. Peranzoni, E., Ingangi, V., Masetto, E., Pinton, L. & Marigo, I. Myeloid Cells as Clinical Biomarkers for Immune Checkpoint Blockade. *Front. Immunol.* **11**, 1–24 (2020).

686. Zhu, J. *et al.* Resistance to cancer immunotherapy mediated by apoptosis of tumor-infiltrating lymphocytes. *Nat. Commun.* **8**, (2017).

687. Sinha, P. *et al.* Myeloid-derived suppressor cells express the death receptor Fas and apoptose in response to T cell-expressed FasL. *Blood* **117**, 5381–5390 (2011).

688. Igney, F. H. & Krammer, P. H. Tumor counterattack: Fact or fiction? *Cancer Immunol. Immunother.* **54**, 1127–1136 (2005).

689. Grzywa, T. M. *et al.* Myeloid Cell-Derived Arginase in Cancer Immune Response. *Front. Immunol.* **11**, 1–24 (2020).

690. Miret, J. J. *et al.* Suppression of Myeloid Cell Arginase Activity leads to Therapeutic Response in a NSCLC Mouse Model by Activating Anti-Tumor Immunity. *J. Immunother. Cancer* **7**, 1–12 (2019).

691. García-Ortiz, A. & Serrador, J. M. Nitric Oxide Signaling in T Cell-Mediated Immunity. *Trends Mol. Med.* **24**, 412–427 (2018).

692. Hosoi, A. *et al.* Adoptive cytotoxic T lymphocyte therapy triggers a counter-regulatory immunosuppressive mechanism via recruitment of myeloid-derived suppressor cells. *Int. J. Cancer* **134**, 1810–1822 (2014).

693. Lyons, A. B. & Doherty, K. V. Flow cytometric analysis of cell division by dye dilution. *Curr. Protoc. Cytom.* **Chapter 9**, 1–10 (2004).

694. Millrud, C. R., Bergenfelz, C. & Leandersson, K. On the origin of myeloid-derived suppressor cells. *Oncotarget* **8**, 3649–3665 (2017).

695. Spangrude, G. J., Heimfeld, S. & Weissman, I. L. Hematopoietic Stem. *Science (80-.).* 58–62 (1988).

696. Okada, S. *et al.* In vivo and in vitro stem cell function of c-kit- and Sca-1-positive murine hematopoietic cells. *Blood* **80**, 3044–3050 (1992).

697. Rogers, P. B., Driessnack, M. G. & Hiltbold Schwartz, E. Analysis of the developmental stages, kinetics, and phenotypes exhibited by myeloid cells driven by GM-CSF in vitro. *PLoS One* **12**, 1–18 (2017).

698. Zhou, J., Nefedova, Y., Lei, A. & Gabrilovich, D. Neutrophils and PMN-MDSC: Their biological role and interaction with stromal cells. *Semin. Immunol.* **35**, 19–28 (2018).

699. Menezes, S. *et al.* The Heterogeneity of Ly6Chi Monocytes Controls Their Differentiation into iNOS+ Macrophages or Monocyte-Derived Dendritic Cells. *Immunity* **45**, 1205–1218 (2016).

700. Noman, M. Z. *et al.* PD-L1 is a novel direct target of HIF-1α, and its blockade under hypoxia enhanced MDSC-mediated T cell activation. *J. Exp. Med.* **211**, 781–790 (2014).

701. Zhu, J., Petit, P. F. & Van den Eynde, B. J. Apoptosis of tumor-infiltrating T lymphocytes: a new immune checkpoint mechanism. *Cancer Immunol. Immunother.* **68**, 835–847 (2019).

702. Steggerda, S. M. *et al.* Inhibition of arginase by CB-1158 blocks myeloid cell-mediated immune suppression in the tumor microenvironment. *J. Immunother. Cancer* **5**, 1–18 (2017).

703. Cao, Y., Feng, Y., Zhang, Y., Zhu, X. & Jin, F. L-Arginine supplementation inhibits the growth of breast cancer by enhancing innate and adaptive immune responses mediated by suppression of MDSCs in vivo. *BMC Cancer* **16**, 1–11 (2016).

704. Law, A. M. K., Valdes-Mora, F. & Gallego-Ortega, D. Myeloid-Derived Suppressor Cells as a Therapeutic Target for Cancer. *Cells* **9**, 561 (2020).

705. Heine, A. *et al.* Generation and functional characterization of MDSC-like cells. *Oncoimmunology* **6**, 1–12 (2017).

706. Metzger, P. *et al.* Systemic but not MDSC-specific IRF4 deficiency promotes an immunosuppressed tumor microenvironment in a murine pancreatic cancer model. *Cancer Immunol. Immunother.* **69**, 2101–2112 (2020).

707. Briseño, C. G. *et al.* Distinct Transcriptional Programs Control Cross-Priming in Classical and Monocyte-Derived Dendritic Cells. *Cell Rep.* **15**, 2462–2474 (2016).

708. Stachelek, S. J. *et al.* The effect of CD47 modified polymer surfaces on inflammatory cell attachment and activation. *Biomaterials* **32**, 4317–4326 (2011).

709. Heine, A. *et al.* Generation and functional characterization of MDSC-like cells. *Oncoimmunology* **6**, (2017).

710. Washio, K. *et al.* Dendritic cell SIRPα regulates homeostasis of dendritic cells in lymphoid organs. *Genes to Cells* **20**, 451–463 (2015).

711. Murata, Y., Kotani, T., Ohnishi, H. & Matozaki, T. The CD47-SIRPα signalling system: Its physiological roles and therapeutic application. *J. Biochem.* **155**, 335–344 (2014).

712. Hayes, B. H. *et al.* Macrophages show higher levels of engulfment after disruption of cis interactions between CD47 and the checkpoint receptor SIRPα. *J. Cell Sci.* **133**, (2020).

713. Oldenborg, P. A., Gresham, H. D. & Lindberg, F. P. CD47-signal regulatory protein α (SIRPα) regulates Fcγ and complement receptor-mediated phagocytosis. *J. Exp. Med.* **193**, 855–861 (2001).

714. Blazar, B. R. *et al.* CD47 (Integrin-associated Protein) Engagement of Dendritic Cell and Macrophage Counterreceptors Is Required to Prevent the Clearance of Donor Lymphohematopoietic Cells. **194**, (2001).

715. Greenberg, S. & Grinstein, S. Phagocytosis and innate immunity Greenberg and Grinstein 137. 136–145 (2002).

716. Sick, E. *et al.* CD47 update : a multifaceted actor in the tumour microenvironment of potential therapeutic. (2012) doi:10.1111/j.1476-5381.2012.02099.x.

717. Liu, X. *et al.* CD47 blockade triggers T cell-mediated destruction of immunogenic tumors. *Nat. Med.* **21**, 1209–1215 (2015).

718. Zilionis, R. *et al.* Single-Cell Transcriptomics of Human and Mouse Lung Cancers Reveals Conserved Myeloid Populations across Individuals and Species. *Immunity* **50**, 1317-1334.e10 (2019).

719. Kerdidani, D. *et al.* Tumor MHCII immunity requires in situ antigen presentation by cancer-associated fibroblasts. *bioRxiv* 2020.03.24.005355 (2020) doi:10.1101/2020.03.24.005355.

720. Haeryfar, S. M. M. & Hoskin, D. W. Thy-1: More than a Mouse Pan-T Cell Marker. *J. Immunol.* **173**, 3581–3588 (2004).

721. Katsumata, L. W., Miyajima, A. & Itoh, T. Portal fibroblasts marked by the surface antigen Thy1 contribute to fibrosis in mouse models of cholestatic liver injury. *Hepatol. Commun.* **1**, 198–214 (2017).

722. Johnston, R. J. *et al.* VISTA is an acidic pH-selective ligand for PSGL-1. *Nature* **574**, 565–570 (2019).

723. Candas-Green, D. *et al.* Dual blockade of CD47 and HER2 eliminates radioresistant breast cancer cells. *Nat. Commun.* **11**, 1–15 (2020).

724. Liu, R. *et al.* CD47 promotes ovarian cancer progression by inhibiting macrophage phagocytosis. *Oncotarget* **8**, 39021–39032 (2017).

725. Martinez-Marin, D., Jarvis, C., Nelius, T. & Filleur, S. Assessment of phagocytic activity in live macrophages-tumor cells co-cultures by Confocal and Nomarski Microscopy. *Biol. Methods Protoc.* **2**, 1–7 (2017).

726. Uribe-Querol, E. & Rosales, C. Phagocytosis: Our Current Understanding of a Universal Biological Process. *Front. Immunol.* **11**, 1–13 (2020).

727. Ohnishi, H., Kubota, M., Ohtake, A., Sato, K. & Sano, S. I. Activation of protein-tyrosine phosphatase SH-PTP2 by a tyrosine-based activation motif of a novel brain molecule. *J. Biol. Chem.* **271**, 25569–25574 (1996).

728. Barclay, A. N. & Brown, M. H. The SIRP family of receptors and immune regulation. *Nat. Rev. Immunol.* **6**, 457–464 (2006).

729. Morrissey, M. A. & Vale, R. D. CD47 suppresses phagocytosis by repositioning SIRPA and preventing integrin activation. *bioRxiv* 752311 (2019) doi:10.1101/752311.

730. Yu, H., Kortylewski, M. & Pardoll, D. Crosstalk between cancer and immune cells: role of STAT3 in the tumour microenvironment. *Nat. Rev. Immunol.* **7**, 41–51 (2007).

731. Trovato, R. *et al.* Immunosuppression by monocytic myeloid-derived suppressor cells in patients with pancreatic ductal carcinoma is orchestrated by STAT3. *J. Immunother. Cancer* **7**, 1–16 (2019).

732. Su, Y. L., Banerjee, S., White, S. V. & Kortylewski, M. STAT3 in tumor-associated myeloid cells: Multitasking to disrupt immunity. *Int. J. Mol. Sci.* **19**, (2018).

733. De Haas, N. *et al.* STAT family protein expression and phosphorylation state during moDC development is altered by platinum-based chemotherapeutics. *J. Immunol. Res.* **2019**, (2019).

734. Auten, R. L. & Davis, J. M. Oxygen toxicity and reactive oxygen species: The devil is in the details. *Pediatr. Res.* **66**, 121–127 (2009).

735. Aggarwal, V. *et al.* Role of reactive oxygen species in cancer progression: Molecular

mechanisms and recent advancements. *Biomolecules* **9**, (2019).

736. Baumann, T. *et al.* Regulatory myeloid cells paralyze T cells through cell–cell transfer of the metabolite methylglyoxal. *Nat. Immunol.* **21**, 555–566 (2020).

737. Cekic, C., Day, Y. J., Sag, D. & Linden, J. Myeloid expression of adenosine a2A receptor suppresses T and NK cell responses in the solid tumor microenvironment. *Cancer Res.* **74**, 7250–7259 (2014).

738. Cohen, H. B. *et al.* TLR stimulation initiates a CD39-based autoregulatory mechanism that limits macrophage inflammatory responses. *Blood* **122**, 1935–1945 (2013).

739. Jin, D. *et al.* CD73 on tumor cells impairs antitumor T-cell responses: A novel mechanism of tumor-induced immune suppression. *Cancer Res.* **70**, 2245–2255 (2010).

740. Murata, Y. *et al.* Autoimmune animal models in the analysis of the CD47-SIRPα signaling pathway. *Methods* **65**, 254–259 (2014).

741. Chao, M. P. *et al.* Calreticulin is the dominant pro-phagocytic signal on multiple human cancers and is counterbalanced by CD47. *Sci. Transl. Med.* **2**, 63ra94 (2010).

742. Ishikawa-sekigami, T. *et al.* Enhanced phagocytosis of CD47-deficient red blood cells by splenic macrophages requires SHPS-1. **343**, 1197–1200 (2006).

743. Okazawa, H. *et al.* Negative Regulation of Phagocytosis in Macrophages by the CD47-SHPS-1 System. (2021) doi:10.4049/jimmunol.174.4.2004.

744. Huang, Y. *et al.* SHP2 associates with nuclear localization of STAT3 : significance in progression and prognosis of colorectal cancer. 1–10 (2017) doi:10.1038/s41598-017-17604-7.

745. Kim, M., Morales, L. D., Jang, I., Cho, Y. & Kim, D. J. Protein Tyrosine Phosphatases as Potential Regulators of STAT3 Signaling. **3**, 1–19.

746. Murciano-goroff, Y. R., Warner, A. B. & Wolchok, J. D. The future of cancer immunotherapy : microenvironment- targeting combinations. *Cell Res.* (2020) doi:10.1038/s41422-020-0337-2.

747. Feng, R., Zhao, H., Xu, J. & Shen, C. CD47: the next checkpoint target for cancer immunotherapy. *Crit. Rev. Oncol. Hematol.* **152**, 103014 (2020).

748. Gaudino, S. J. & Kumar, P. Cross-Talk Between Antigen Presenting Cells and T Cells Impacts Intestinal Homeostasis , Bacterial Infections , and Tumorigenesis. **10**, 1–14 (2019).

749. Kratky, W., Reis, C., Oxenius, A. & Spörri, R. Direct activation of antigen-presenting cells is required for CD8 + T-cell priming and tumor vaccination. (2011) doi:10.1073/pnas.1108945108/-/DCSupplemental.www.pnas.org/cgi/doi/10.1073/pnas.1108945108.

750. Smith-garvin, J. E., Koretzky, G. A. & Jordan, M. S. T Cell Activation. doi:10.1146/annurev.immunol.021908.132706.

751. Buatois, V. *et al.* Preclinical development of a bispecific antibody that safely and effectively targets CD19 and CD47 for the treatment of B-cell lymphoma and leukemia. *Mol. Cancer Ther.* **17**, 1739–1751 (2018).

752. Huang, Y., Ma, Y., Gao, P. & Yao, Z. Targeting CD47: The achievements and concerns of current studies on cancer immunotherapy. *J. Thorac. Dis.* **9**, E168–E174 (2017).

753. Ouzounova, M. *et al.* Monocytic and granulocytic myeloid derived suppressor cells differentially regulate spatiotemporal tumour plasticity during metastatic cascade. *Nat. Commun.* **8**, 1–13 (2017).

754. Cassetta, L. *et al.* Differential expansion of circulating human MDSC subsets in patients with cancer, infection and inflammation. *J. Immunother. Cancer* **8**, (2020).

755. Talmadge, J. E., Gabrilovich, D. I. & Immunology, T. T. History of myeloid derived suppressor cells (MDSCs) in the macro- and micro-environment of tumour-bearing hosts. *Nat. Rev. Cancer* **13**, 739–752 (2013).

756. Roche, P. A. & Furuta, K. The ins and outs of MHC class II-mediated antigen processing and presentation. *Nat. Rev. Immunol.* **15**, 203–216 (2015).

757. Clark, W. H. *et al.* Model Predicting Survival in Stage I Melanoma Based on Tumor Progression. *J. Natl. Cancer Inst.* 1893–1904 (1989).

758. Clemente, C. G. *et al.* Prognostic value of tumor infiltrating lymphocytes in the vertical growth phase of primary cutaneous melanoma. *Cancer* **77**, 1303–1310 (1996).

759. Curiel, T. J. *et al.* Specific recruitment of regulatory T cells in ovarian carcinoma fosters immune privilege and predicts reduced survival. *Nat. Med.* **10**, 942–949 (2004).

760. Miracco, C. *et al.* Utility of tumour-infiltrating CD25+FOXP3+ regulatory T cell evaluation in predicting local recurrence in vertical growth phase cutaneous melanoma. *Oncol. Rep.* **18**, 1115–1122 (2007).

761. Mougiakakos, D. *et al.* Intratumoral forkhead box p3-positive regulatory t cells predict poor survival in cyclooxygenase-2-positive uveal melanoma. *Cancer* **116**, 2224–2233 (2010).

762. Hori, S., Nomura, T. & Sakaguchi, S. Control of regulatory T cell development by the transcription factor Foxp3. *J. Immunol.* **198**, 981–985 (2017).

763. Fontenot, J. D., Gavin, M. A. & Rudensky, A. Y. Foxp3 programs the development and function of CD4+CD25+ regulatory T cells. *J. Immunol.* **198**, 986–992 (2017).

764. Soncin, I. *et al.* The tumour microenvironment creates a niche for the self-renewal of tumour-promoting macrophages in colon adenoma. *Nat. Commun.* **9**, (2018).

765. Ma, Y., Shurin, G. V., Peiyuan, Z. & Shurin, M. R. Dendritic cells in the cancer microenvironment. *J. Cancer* **4**, 36–44 (2013).

766. Laviron, M. & Boissonnas, A. Ontogeny of Tumor-Associated Macrophages. *Front. Immunol.* **10**, 1799 (2019).

767. Polyak, S. *et al.* Impaired class II expression and antigen uptake in monocytic cells after HIV-1 infection. *J. Immunol.* **175**, 8444–8444 (2005).

768. Daro, E. *et al.* Polyethylene Glycol-Modified GM-CSF Expands CD11b high CD11c high But Not CD11b low CD11c high Murine Dendritic Cells In Vivo: A Comparative Analysis with Flt3 Ligand . *J. Immunol.* **165**, 49–58 (2000).

769. Neefjes, J., Jongsma, M. L. M., Paul, P. & Bakke, O. Towards a systems understanding of MHC class i and MHC class II antigen presentation. *Nat. Rev. Immunol.* **11**, 823–836 (2011).

770. Devin Dersh, Jonathan W. Yewdell, and J. W. A SIINFEKL-Based System to Measure MHC Class I Antigen Presentation Efficiency and Kinetics Devin. *Springer Nat. 2019* **1897**, 44–45 (1989).

771. Böttcher, J. P. & Reis e Sousa, C. The Role of Type 1 Conventional Dendritic Cells in Cancer Immunity. *Trends in cancer* **4**, 784–792 (2018).

772. Antohe, M. *et al.* Tumor infiltrating lymphocytes: The regulator of melanoma evolution (Review). *Oncol. Lett.* **17**, 4155–4161 (2019).

773. Park, J. *et al.* Immune checkpoint inhibitor-induced reinvigoration of tumor-infiltrating CD8+ T cells is determined by their differentiation status in glioblastoma. *Clin. Cancer Res.* **25**, 2549–2559 (2019).

774. So, Y. K. *et al.* An increase of CD8+ T cell infiltration following recurrence is a good prognosticator in HNSCC. *Sci. Rep.* **10**, 1–9 (2020).

775. Wang, Y. *et al.* PD-L1 expression and CD8+ T cell infiltration predict a favorable prognosis in advanced gastric cancer. *J. Immunol. Res.* **2018**, (2018).

776. Calmeiro, J. *et al.* Dendritic cell vaccines for cancer immunotherapy: The role of human conventional type 1 dendritic cells. *Pharmaceutics* **12**, 1–20 (2020).

777. Kim, H.-Y. *et al.* Discovery of potential biomarkers in human melanoma cells with different metastatic potential by metabolic and lipidomic profiling. *Sci. Rep.* **7**, 8864 (2017).

778. Livingstone, E., Zimmer, L., Vaubel, J. & Schadendorf, D. Current advances and perspectives in the treatment of advanced melanoma. *J. der Dtsch. Dermatologischen Gesellschaft = J. Ger. Soc. Dermatology JDDG* **10**, 319–325 (2012).

779. Pflugfelder, A. *et al.* Malignant melanoma S3-guideline 'diagnosis, therapy and follow-up of melanoma'. *J. der Dtsch. Dermatologischen Gesellschaft = J. Ger. Soc. Dermatology JDDG* **11 Suppl 6**, 1-116,1-126 (2013).

780. Kanterman, J., Sade-Feldman, M. & Baniyash, M. New insights into chronic inflammation-induced immunosuppression. *Semin. Cancer Biol.* **22**, 307–318 (2012).

781. Umansky, V. & Sevko, A. Melanoma-induced immunosuppression and its neutralization. *Semin. Cancer Biol.* **22**, 319–326 (2012).

782. Ostrand-Rosenberg, S. Myeloid-derived suppressor cells: more mechanisms for inhibiting antitumor immunity. *Cancer Immunol. Immunother.* **59**, 1593–1600 (2010).

783. Meyer, C. *et al.* Chronic inflammation promotes myeloid-derived suppressor cell activation blocking antitumor immunity in transgenic mouse melanoma model. *Proc. Natl. Acad. Sci. U. S. A.* **108**, 17111–17116 (2011).

784. Navarini-Meury, A. A. & Conrad, C. Melanoma and innate immunity active inflammation or just erroneous attraction? Melanoma as the source of leukocyte-attracting chemokines. *Semin. Cancer Biol.* **19**, 84–91 (2009).

785. Mairhofer, D. G. *et al.* Impaired gp100-Specific CD8(+) T-Cell Responses in the Presence of Myeloid-Derived Suppressor Cells in a Spontaneous Mouse Melanoma Model. *J. Invest. Dermatol.* **135**, 2785–2793 (2015).

786. Raber, P. L. *et al.* Subpopulations of myeloid-derived suppressor cells impair T cell responses through independent nitric oxide-related pathways. *Int. J. Cancer* **134**, 2853–2864 (2014).

787. Mishra, R. *et al.* Tumor progression is associated with increasing CD11b+ Cells and CCL2 in Lewis rat sarcoma. *Anticancer Res.* **35**, 703–711 (2015).

788. Chen, X. *et al.* CCL2/CCR2 Regulates the Tumor Microenvironment in HER-2/neu-Driven Mammary Carcinomas in Mice. *PLoS One* **11**, e0165595 (2016).

789. Lee, C. *et al.* Targeting of M2-like tumor-associated macrophages with a melittin-based pro-apoptotic peptide. *J. Immunother. Cancer* **7**, 1–14 (2019).

790. Tamás, R. Understanding th Mysterious M2 macrophage through activation markers and effector mechanism. *Mediators Inflamm.* **2015**, 16 (2015).

791. Bian, Z. *et al.* Arginase-1 is neither constitutively expressed in nor required for myeloid-derived suppressor cell-mediated inhibition of T-cell proliferation. *Eur. J. Immunol.* **48**, 1046–1058 (2018).

792. Ma, Z. *et al.* Overexpression of Arginase-1 is an indicator of poor prognosis in patients with colorectal cancer. *Pathol. - Res. Pract.* **215**, 152383 (2019).

793. Czystowska-Kuzmicz, M. *et al.* Small extracellular vesicles containing arginase-1 suppress T-cell responses and promote tumor growth in ovarian carcinoma. *Nat. Commun.* **10**, 1–16 (2019).

794. You, J. *et al.* The Oncogenic Role of ARG1 in Progression and Metastasis of Hepatocellular Carcinoma. *Biomed Res. Int.* **2018**, 2109865 (2018).

795. Yélamos, O. & Gerami, P. Predicting the outcome of melanoma: Can we tell the future of a patient's melanoma? *Melanoma Manag.* **2**, 217–224 (2015).

796. Alderson, M. R. *et al.* Fas ligand mediates activation-induced cell death in human T lymphocytes. *J. Exp. Med.* **181**, 71–77 (1995).

797. Peyvandi, S. *et al.* Fas ligand deficiency impairs tumor immunity by promoting an accumulation of monocytic myeloid-derived suppressor cells. *Cancer Res.* **75**, 4292–4301 (2015).

798. Stiff, A. *et al.* Nitric oxide production by myeloid-derived suppressor cells plays a role in impairing Fc receptor–mediated natural killer cell function. *Clin. Cancer Res.* **24**, 1891–1904 (2018).

799. Padgett, E. L. & Pruett, S. B. Evaluation of nitrite production by human monocyte-derived macrophages. *Biochem. Biophys. Res. Commun.* **186**, 775–781 (1992).

800. Thwe, P. M. & Amiel, E. The role of nitric oxide in metabolic regulation of Dendritic cell immune function. *Cancer Lett.* **412**, 236–242 (2018).

801. Gabrilovich, D. I., Velders, M. P., Sotomayor, E. M. & Kast, W. M. Mechanism of Immune Dysfunction in Cancer Mediated by Immature Gr-1 + Myeloid Cells. *J. Immunol.* **166**, 5398–5406 (2001).

802. Sinha, P., Clements, V. K. & Ostrand-Rosenberg, S. Interleukin-13-regulated M2 macrophages in combination with myeloid suppressor cells block immune surveillance against metastasis. *Cancer Res.* **65**, 11743–11751 (2005).

803. Lesokhin, A. M. *et al.* Monocytic CCR2 + myeloid-derived suppressor cells promote immune escape by limiting activated CD8 T-cell infiltration into the tumor microenvironment. *Cancer Res.* **72**, 876–886 (2012).

804. Zagorulya, M., Duong, E. & Spranger, S. Impact of anatomic site on antigen-presenting cells in cancer. *J. Immunother. Cancer* **8**, 23–26 (2020).

805. Zhou, Z. *et al.* Development and function of myeloid-derived suppressor cells generated from mouse embryonic and hematopoietic stem cells. *Stem Cells* **28**, 620–632 (2010).

806. Okada, S. L. *et al.* Conditioned media from the renal cell carcinoma cell line 786.O drives human blood monocytes to a monocytic myeloid-derived suppressor cell phenotype. *Cell. Immunol.* **323**, 49–58 (2018).

807. Jayaraman, P. *et al.* TGF-β1 programmed myeloid-derived suppressor cells (MDSC) acquire immune-stimulating and tumor killing activity capable of rejecting established tumors in combination with radiotherapy. *Oncoimmunology* **7**, 1–16 (2018).

808. Younis, R. H., Han, K. L. & Webb, T. J. Human Head and Neck Squamous Cell Carcinoma–

Associated Semaphorin 4D Induces Expansion of Myeloid-Derived Suppressor Cells. *J. Immunol.* **196**, 1419–1429 (2016).

809. Park, M. Y. *et al.* GM-CSF promotes the expansion and differentiation of cord blood myeloid-derived suppressor cells, which attenuate xenogeneic graft-vs.-host disease. *Front. Immunol.* **10**, 1–15 (2019).

810. Ma, N., Liu, Q., Hou, L., Wang, Y. & Liu, Z. MDSCs are involved in the protumorigenic potentials of GM-CSF in colitis-associated cancer. *Int. J. Immunopathol. Pharmacol.* **30**, 152–162 (2017).

811. Bazhin, A. V, von Ahn, K., Fritz, J., Werner, J. & Karakhanova, S. Interferon-α Up-Regulates the Expression of PD-L1 Molecules on Immune Cells Through STAT3 and p38 Signaling . *Frontiers in Immunology* vol. 9 2129 (2018).

812. Nam, S., Lee, A., Lim, J. & Lim, J. S. Analysis of the expression and regulation of PD-1 protein on the surface of myeloid-derived suppressor cells (MDSCs). *Biomol. Ther.* **27**, 63–70 (2019).

813. Nguyen, T. & Russell, J. The regulation of FasL expression during activation-induced cell death (AICD). *Immunology* **103**, 426–434 (2001).

814. Peter, M. E. *et al.* The role of CD95 and CD95 ligand in cancer. *Cell Death Differ.* **22**, 549–559 (2015).

815. Zhang, Y. *et al.* Fas signal promotes lung cancer growth by recruiting myeloid-derived suppressor cells via cancer cell-derived PGE2. *J. Immunol.* **182**, 3801–3808 (2009).

816. Lee, G. K. *et al.* Tryptophan deprivation sensitizes activated T cells to apoptosis prior to cell division. *Immunology* **107**, 452–460 (2002).

817. Munn, D. H. *et al.* Expression of indoleamine 2,3-dioxygenase by plasmacytoid dendritic cells in tumor-draining lymph nodes. *J. Clin. Invest.* **114**, 280–290 (2004).

818. Curti, A. *et al.* Modulation of tryptophan catabolism by human leukemic cells results in the conversion of CD25- into CD25+ T regulatory cells. *Blood* **109**, 2871–2877 (2007).

819. Wang, L. *et al.* VISTA is highly expressed on MDSCs and mediates an inhibition of T cell response in patients with AML. *Oncoimmunology* **7**, e1469594 (2018).

820. Le Mercier, I. *et al.* VISTA Regulates the Development of Protective Antitumor Immunity. *Cancer Res.* **74**, 1933–1944 (2014).

821. Kondo, Y. *et al.* Differential contribution of three immune checkpoint (VISTA, CTLA-4, PD-1) pathways to antitumor responses against squamous cell carcinoma. *Oral Oncol.* **57**, 54–60 (2016).

822. Deng, J. *et al.* Hypoxia-Induced VISTA Promotes the Suppressive Function of Myeloid-Derived Suppressor Cells in the Tumor Microenvironment. *Cancer Immunol. Res.* **7**, 1079–1090 (2019).

823. Johnston, R. J. *et al.* VISTA is an acidic pH-selective ligand for PSGL-1. *Nature* **574**, 565–570 (2019).

824. Ingram, J. R. *et al.* Localized CD47 blockade enhances immunotherapy for murine melanoma. *Proc. Natl. Acad. Sci. U. S. A.* **114**, 10184–10189 (2017).

825. Weiskopf, K. Cancer immunotherapy targeting the CD47/SIRPα axis. *Eur. J. Cancer* **76**, 100–109 (2017).

826. Jayaraman Rukmini, S. *et al.* Inducing Tumor Suppressive Microenvironments through Genome Edited CD47−/− Syngeneic Cell Vaccination. *Sci. Rep.* **9**, 1–12 (2019).

827. Manna, P. P., Dimitry, J., Oldenborg, P.-A. & Frazier, W. A. CD47 augments Fas/CD95-mediated apoptosis. *J. Biol. Chem.* **280**, 29637–29644 (2005).

828. Manna, P. P. & Frazier, W. A. The Mechanism of CD47-Dependent Killing of T Cells: Heterotrimeric Gi-Dependent Inhibition of Protein Kinase A. *J. Immunol.* **170**, 3544 LP – 3553 (2003).

829. Taheri, F. *et al.* L-Arginine Regulates the Expression of the T-Cell Receptor ζ Chain (CD3ζ) in Jurkat Cells. *Clin. Cancer Res.* **7**, 958–966 (2001).

830. Tal, M. C. *et al.* Upregulation of CD47 Is a Host Checkpoint Response to Pathogen Recognition. *MBio* **11**, e01293-20 (2020).

831. Cui, L. *et al.* Activation of JUN in fibroblasts promotes pro-fibrotic programme and modulates protective immunity. *Nat. Commun.* **11**, (2020).

832. Kojima, Y. *et al.* CD47-blocking antibodies restore phagocytosis and prevent atherosclerosis. *Nature* **536**, 86–90 (2016).

833. Cheng, Y. *et al.* Cancer-associated fibroblasts induce PDL1+ neutrophils through the IL6-STAT3 pathway that foster immune suppression in hepatocellular carcinoma. *Cell Death Dis.* **9**, (2018).

834. Green, J., Endale, M., Auer, H. & Perl, A. K. T. Diversity of interstitial lung fibroblasts is regulated by platelet-derived growth factor receptor a kinase activity. *Am. J. Respir. Cell Mol. Biol.* **54**, 532–545 (2016).

835. Dooling, L. J. *et al.* Solid Tumor Cures by Complete Disruption of the CD47:SIRPa Macrophage Checkpoint, Tumor Opsonization, and 'Phagocytic Feed- back'. *Biophysj* **120**, 89a (2021).

836. Dolgin, E. CD47 checkpoint data supercharge Stanford spinout IPO. *Nat. Biotechnol.* **36**, 671–672 (2018).

837. Wei, J., Zhang, M. & Zhou, J. Myeloid-derived suppressor cells in major depression patients suppress T-cell responses through the production of reactive oxygen species. *Psychiatry Res.* **228**, 695–701 (2015).

838. Kim, H., Bang, S., Jee, S., Paik, S. S. & Jang, K. Clinicopathological significance of CD47 expression in hepatocellular carcinoma. *J. Clin. Pathol.* **74**, 111–115 (2021).

839. Zumerle, S. *et al.* Intercellular Calcium Signaling Induced by ATP Potentiates Macrophage Phagocytosis. *Cell Rep.* **27**, 1-10.e4 (2019).

840. Ohta, A. A metabolic immune checkpoint: Adenosine in Tumor Microenvironment. *Front. Immunol.* **7**, 1–11 (2016).

841. Linnemann, C. *et al.* Adenosine regulates CD8 T-cell priming by inhibition of membrane-proximal T-cell receptor signalling. *Immunology* **128**, (2009).

842. Li, J. *et al.* CD39/CD73 upregulation on myeloid-derived suppressor cells via TGF-β-mTOR-HIF-1 signaling in patients with non-small cell lung cancer. *Oncoimmunology* **6**, (2017).

843. Piccione, E. C. *et al.* A bispecific antibody targeting CD47 and CD20 selectively binds and eliminates dual antigen expressing lymphoma cells. *MAbs* **7**, 946–956 (2015).

844. Du, K. *et al.* A bispecific antibody targeting GPC3 and CD47 induced enhanced antitumor efficacy against dual antigen-expressing HCC. *Mol. Ther.* (2021) doi:https://doi.org/10.1016/j.ymthe.2021.01.006.

845. Adams, S. Signal-regulatory protein is selectively expressed by myeloid and neuronal cells. *The journal of immunology.* vol. 161 1853–1859 (1998).

846. Ovacik, M. & Lin, K. Tutorial on Monoclonal Antibody Pharmacokinetics and Its Considerations in Early Development. *Clin. Transl. Sci.* **11**, 540–552 (2018).

847. Di Blasio, S. *et al.* The tumour microenvironment shapes dendritic cell plasticity in a human organotypic melanoma culture. *Nat. Commun.* **11**, 1–17 (2020).

848. Niess, J. H. *et al.* CX3CR1-mediated dendritic cell access to the intestinal lumen and bacterial clearance. *Science (80-.).* **307**, 254–258 (2005).

849. Schulz, O. *et al.* Intestinal CD103+, but not CX3CR1+, antigen sampling cells migrate in lymph and serve classical dendritic cell functions. *J. Exp. Med.* **206**, 3101–3114 (2009).

850. Nagaraj, S. *et al.* Antigen-specific CD4 + T cells regulate function of myeloid- derived suppressor cells in cancer via retrograde MHC class II signaling. *Cancer Res.* **72**, 928–938 (2012).

851. Zhang, Y. L. *et al.* Different subsets of tumor infiltrating lymphocytes correlate with NPC progression in different ways. *Mol. Cancer* **9**, 1–11 (2010).

852. Yi, T. *et al.* Splenic Dendritic Cells Survey Red Blood Cells for Missing Self-CD47 to Trigger Adaptive Immune Responses. *Immunity* **43**, 764–775 (2015).

853. Zipfel, P. F. & Skerka, C. Complement regulators and inhibitory proteins. *Nat. Rev. Immunol.* **9**, 729–740 (2009).

854. Pio R, Corrales L, L. J. *The role of complement in tumor growth*. *Advances in Experimental Medicine and Biology* vol. 772 (2014).

855. Markiewski, M. M. *et al.* Modulation of the antitumor immune response by complement. *Nat. Immunol.* **9**, 1225–1235 (2008).

856. Wang, Y. *et al.* Autocrine Complement Inhibits IL10-Dependent T-cell–Mediated Antitumor Immunity to Promote Tumor Progression. *Cancer Discov.* **6**, 1022 LP – 1035 (2016).

857. Cho, M. S. *et al.* Autocrine effects of tumor-derived complement. *Cell Rep.* **6**, 1085–1095 (2014).

858. Wang, Y., Zhang, H. & He, Y. W. The Complement Receptors C3aR and C5aR Are a New Class of Immune Checkpoint Receptor in Cancer Immunotherapy. *Front. Immunol.* **10**, 1574 (2019).

859. Kwak, J. W. *et al.* Complement Activation via a C3a Receptor Pathway Alters CD4+T Lymphocytes and Mediates Lung Cancer Progression. *Cancer Res.* **78**, 143 LP – 156 (2018).

860. Emmerich, J. *et al.* IL-10 directly activates and expands tumor-resident CD8(+) T cells without de novo infiltration from secondary lymphoid organs. *Cancer Res.* **72**, 3570–3581 (2012).

861. Nabizadeh, J. A. *et al.* The Complement C3a Receptor Contributes to Melanoma Tumorigenesis by Inhibiting Neutrophil and CD4+ T Cell Responses. *J. Immunol.* **196**, 4783 LP – 4792 (2016).

862. Corrales, L. *et al.* Anaphylatoxin C5a creates a favorable microenvironment for lung cancer progression. *J. Immunol.* **189**, 4674–4683 (2012).

863. Ajona, D. *et al.* A Combined PD-1/C5a Blockade Synergistically Protects against Lung Cancer Growth and Metastasis. *Cancer Discov.* **7**, 694–703 (2017).

864. Schreiber, A. D. & Frank, M. M. Role of antibody and complement in the immune clearance and destruction of erythrocytes. II. Molecular nature of IgG and IgM complement-fixing sites and effects of their interaction with serum. *J. Clin. Invest.* **51**, 583–589 (1972).

865. McBride, J. M., Jung, T., de Vries, J. E. & Aversa, G. IL-10 alters DC function via modulation of cell surface molecules resulting in impaired T-cell responses. *Cell. Immunol.* **215**, 162–172

(2002).

866. Mittal, S. K., Cho, K.-J., Ishido, S. & Roche, P. A. Interleukin 10 (IL-10)-mediated Immunosuppression: MARCH-I INDUCTION REGULATES ANTIGEN PRESENTATION BY MACROPHAGES BUT NOT DENDRITIC CELLS. *J. Biol. Chem.* **290**, 27158–27167 (2015).

867. O'Farrell, A.-M., Liu, Y., Moore, K. W. & Mui, A. L.-F. IL-10 inhibits macrophage activation and proliferation by distinct signaling mechanisms: evidence for Stat3-dependent and -independent pathways. *EMBO J.* **17**, 1006–1018 (1998).

868. Lopes, R. L., Borges, T. J., Zanin, R. F. & Bonorino, C. IL-10 is required for polarization of macrophages to M2-like phenotype by mycobacterial DnaK (heat shock protein 70). *Cytokine* **85**, 123–129 (2016).

869. Hsu, B. E. *et al.* C3a elicits unique migratory responses in immature low-density neutrophils. *Oncogene* **39**, 2612–2623 (2020).

870. Myers, L. M. *et al.* A functional subset of CD8 + T cells during chronic exhaustion is defined by SIRPα expression. *Nat. Commun.* **10**, (2019).

871. He, Y. M. *et al.* Transitory presence of myeloid-derived suppressor cells in neonates is critical for control of inflammation. *Nat. Med.* **24**, 224–231 (2018).

872. Wei, L. *et al.* Lactoferrin deficiency induces a pro-metastatic tumor microenvironment through recruiting myeloid-derived suppressor cells in mice. *Oncogene* **39**, 122–135 (2020).

873. Ward, P. P., Mendoza-meneses, M., Cunningham, G. A. & Conneely, O. M. Iron Status in Mice Carrying a Targeted Disruption of Lactoferrin. **23**, 178–185 (2003).

874. Francis, D. M. *et al.* Blockade of immune checkpoints in lymph nodes through locoregional delivery augments cancer immunotherapy. *Sci. Transl. Med.* **12**, 1–12 (2020).

8 APPENDIX

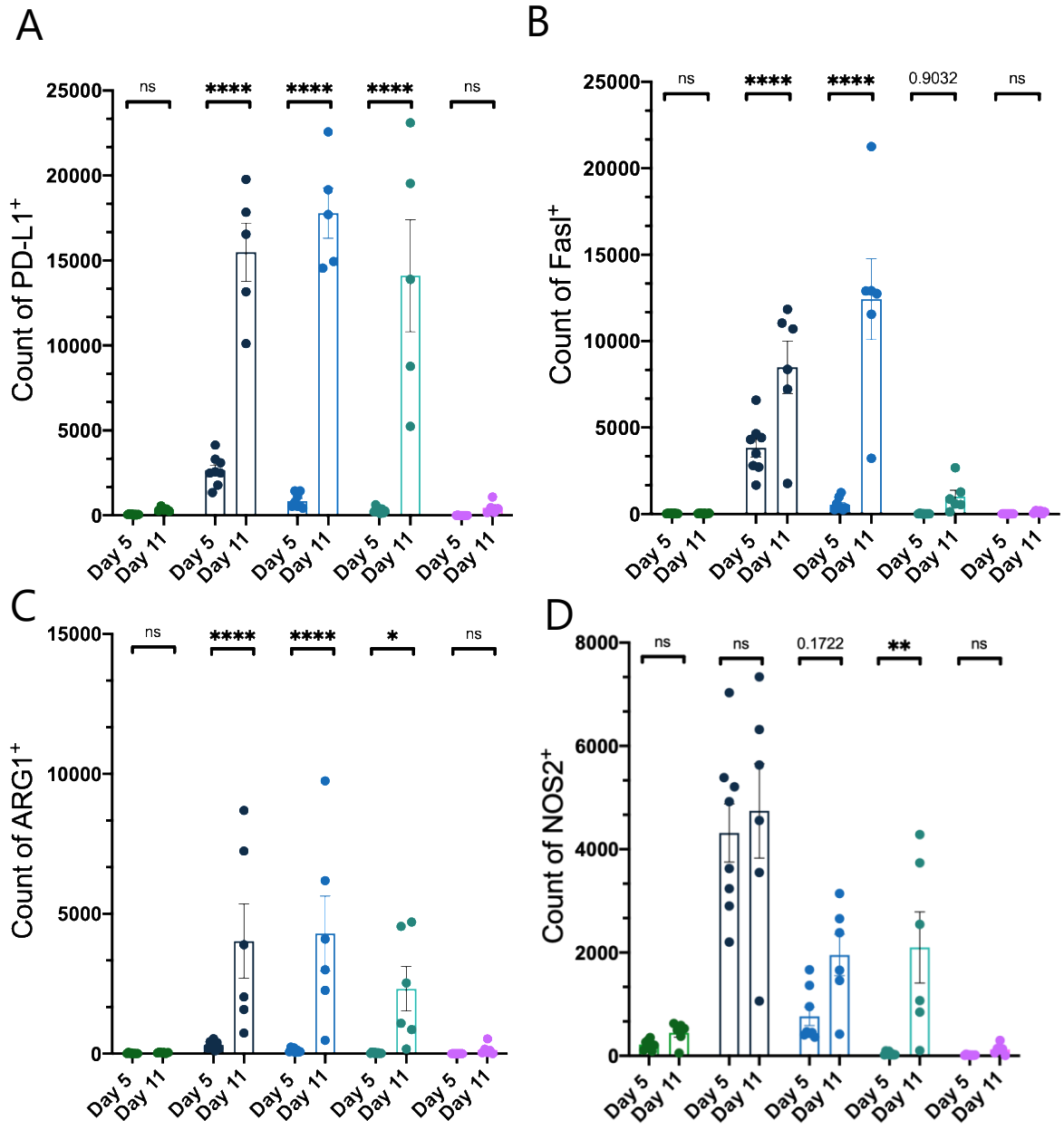

Appendix 8.1. Analysis of function associated markers in the evolving myeloid cells Myeloid immune modulators count of positive increases along tumour evolution. Myeloid cells were extracted at the fifth and eleventh day of tumour development and markers associated with immunosuppression quantified by flow cytometry. The count of positive for **(A)** PD-L1 expression, **(B)** FasL expression, **(C)** ARG1 expression and **(D)** NOS2 expression for each myeloid cluster was assessed is shown. Data are mean ± SEM; * = p < 0.05, ** = p < 0.01, *** = p < 0.001, **** =

p<0.0001 using two-way ANOVA with a Sidak's multiple comparison post hoc test. Mice n=4 (day5) and n=3 (Day 11) in two independent experiments.

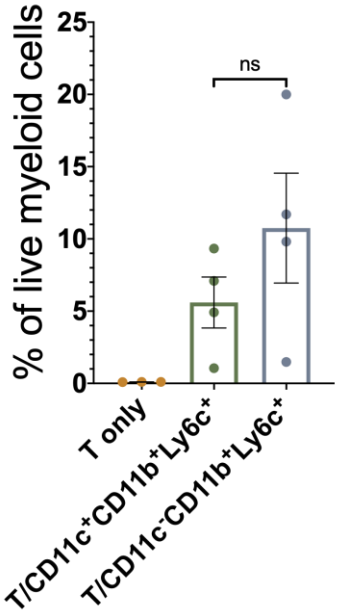

Appendix 8.2. The sorted myeloid cells died along the experiment. The graph shows the percentage of live moDC ($CD11c^{+}CD11b^{+}Ly6C^{+}$) and M-MDSC ($CD11c^{-}CD11b^{+}Ly6C^{+}$) at the end of the T cells proliferation assay. Data are mean ± SEM; * = p < 0.05, ** = p < 0.01, *** = p < 0.001, **** = p<0.0001 using Unpaired test. Experiments n=2 in duplicate.

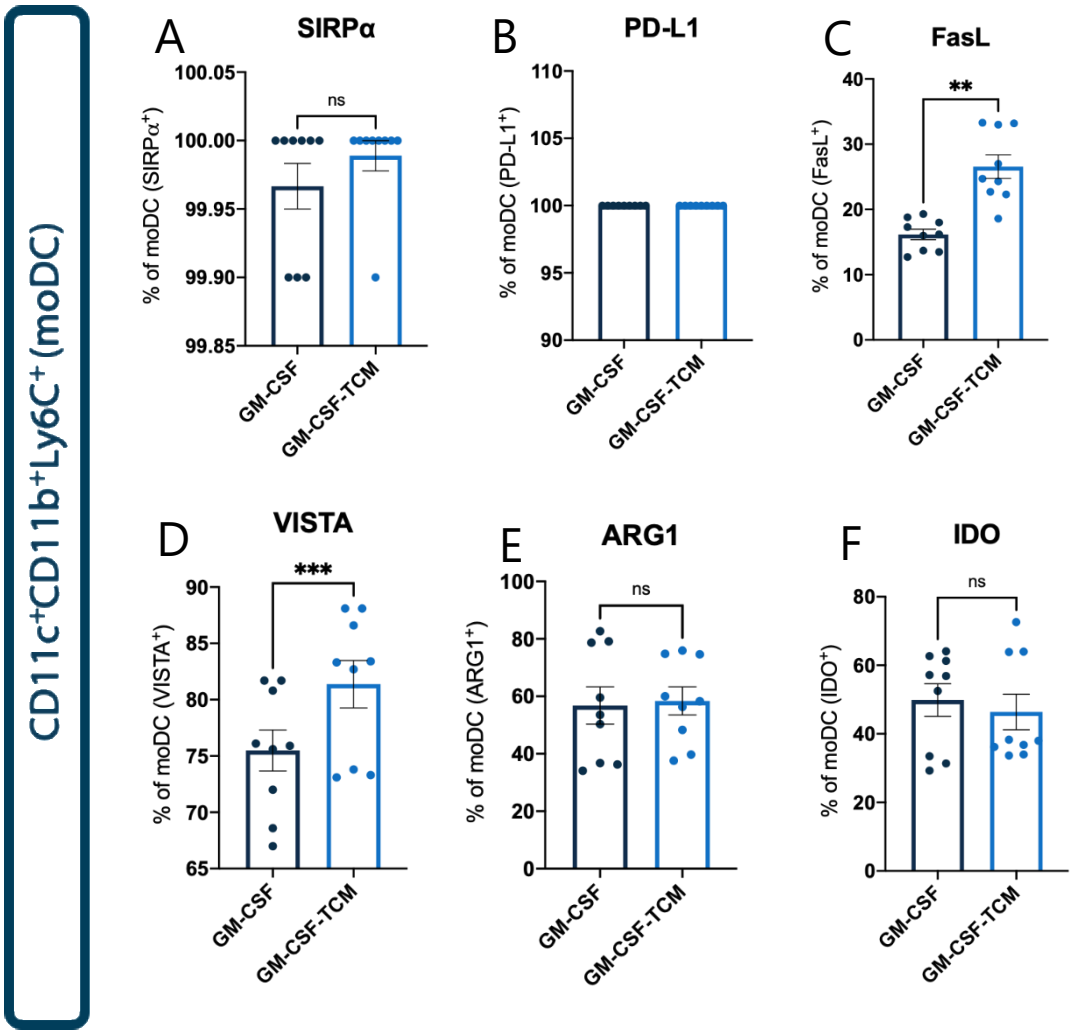

Appendix 8.3. Modulation of suppressive molecule expression in moDCs (CD11c⁺CD11b⁺Ly6c⁺) by GM-CSF-TCM. Flow cytometric quantification of the % of positive of moDSCs cultured in GM-CSF vs GM-CSF-TCM for **(A)** signal-regulatory protein alpha, Sirpα, **(B)** programmed death-ligand 1, Pdl1, **(C)** type-II transmembrane protein FAS ligand, **(D)** V-domain Ig suppressor of T cell activation VISTA, **(E)** arginase 1, ARG1 and **(F)** indoleamine 2,3-dioxygenase, IDO1. Data are mean ± SEM; * = $p < 0.05$, ** = $p < 0.01$, *** = $p < 0.001$, **** = $p<0.0001$ using Paired t test. Experiments n=3 in triplicates.

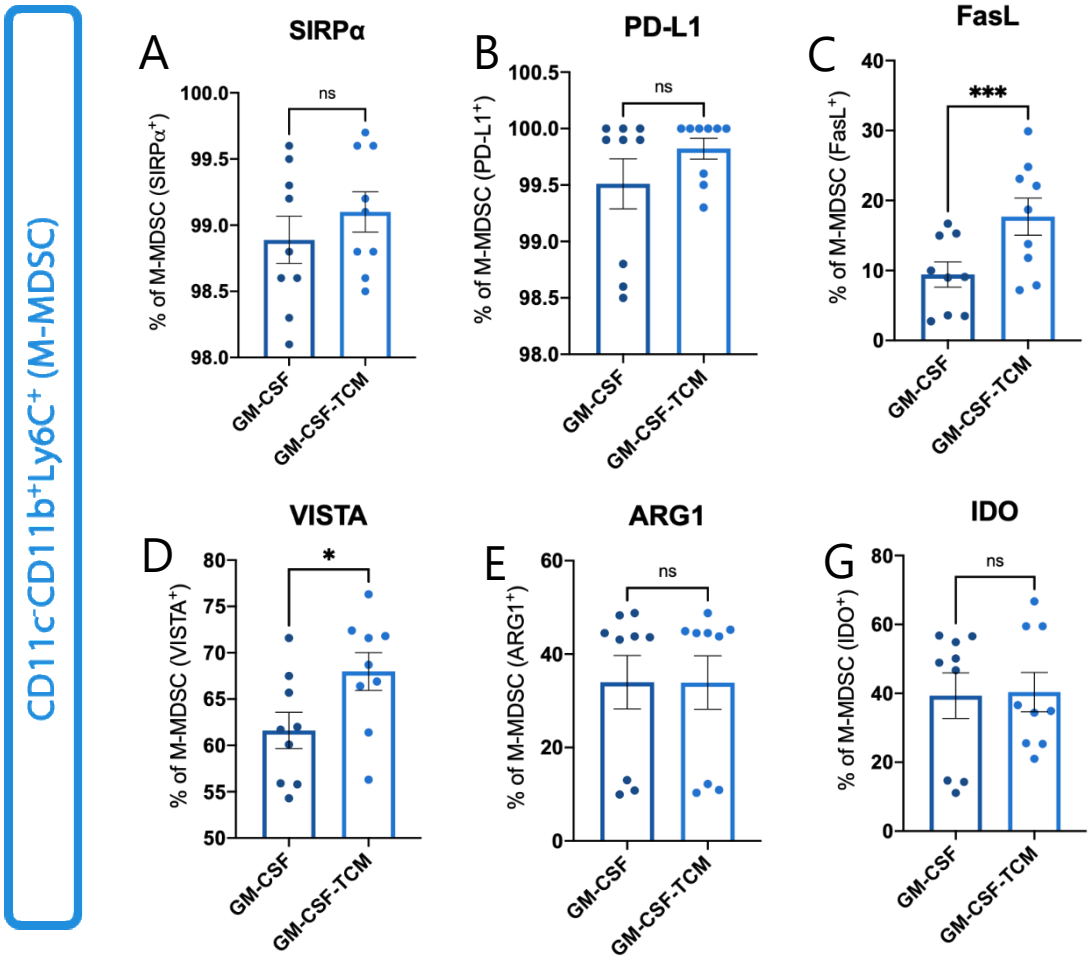

Appendix 8.4. Modulation of suppressive molecule expression in M-MDSCs ($CD11c^{-}CD11b^{+}Ly6C^{+}$) by GM-CSF-TCM. Flow cytometric quantification of the % of positive of M-MDSCs cultured in GM-CSF vs GM-CSF-TCM for **(A)** signal-regulatory protein alpha, Sirpα, **(B)** programmed death-ligand 1, Pdl1, **(C)** type-II transmembrane protein FAS ligand, **(D)** V-domain Ig suppressor of T cell activation VISTA, **(E)** arginase 1, ARG1 and **(F)** indoleamine 2,3-dioxygenase, IDO1. Data are mean ± SEM; * = $p < 0.05$, ** = $p < 0.01$, *** = $p < 0.001$, **** = $p<0.0001$ using Paired t test. Experiments n=3 in triplicates.

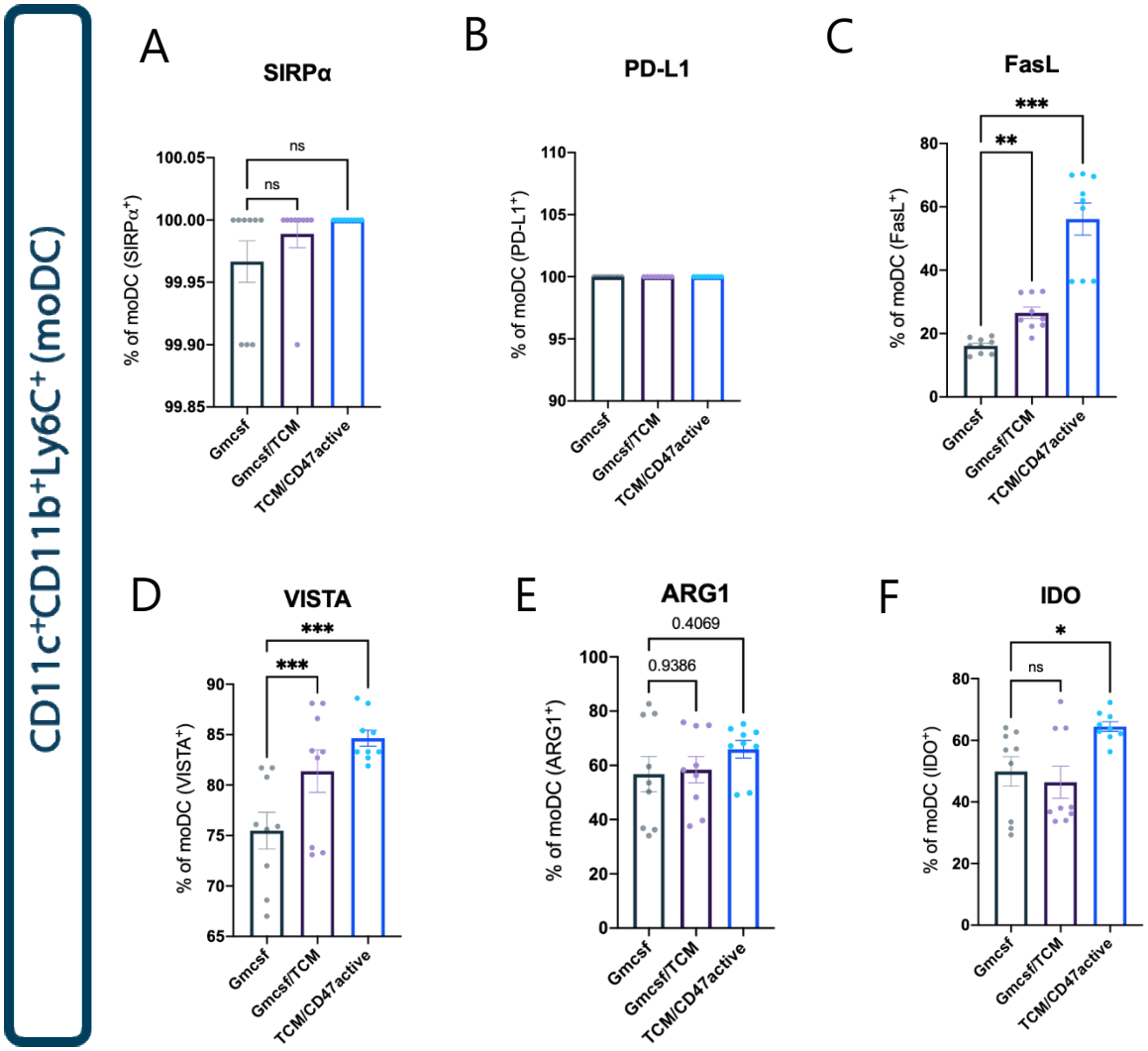

Appendix 8.5. Increased population percentage expressing FasL, VISTA and IDO in moDCs ($CD11c^+CD11b^+Ly6c^+$) cultured in GM-CSF-TCM-CD47. Flow cytometric quantification of the %

of positive of moDSCs cultured in GM-CSF vs GM-CSF-TCM and GM-CSF-TCM-CD47 for **(A)** signal-regulatory protein alpha, SIRPα, **(B)** programmed death-ligand 1, PD-L1, **(C)** type-II transmembrane protein FAS ligand, **(D)** V-domain Ig suppressor of T cell activation VISTA, **(E)** arginase 1, ARG1 and **(F)** indoleamine 2,3-dioxygenase, IDO1. Data are mean ± SEM; * = p < 0.05, ** = p < 0.01, *** = p < 0.001, **** = p<0.0001 using ordinary one-way ANOVA with Dunnett's post hoc test. Experiments n=3 in triplicates.

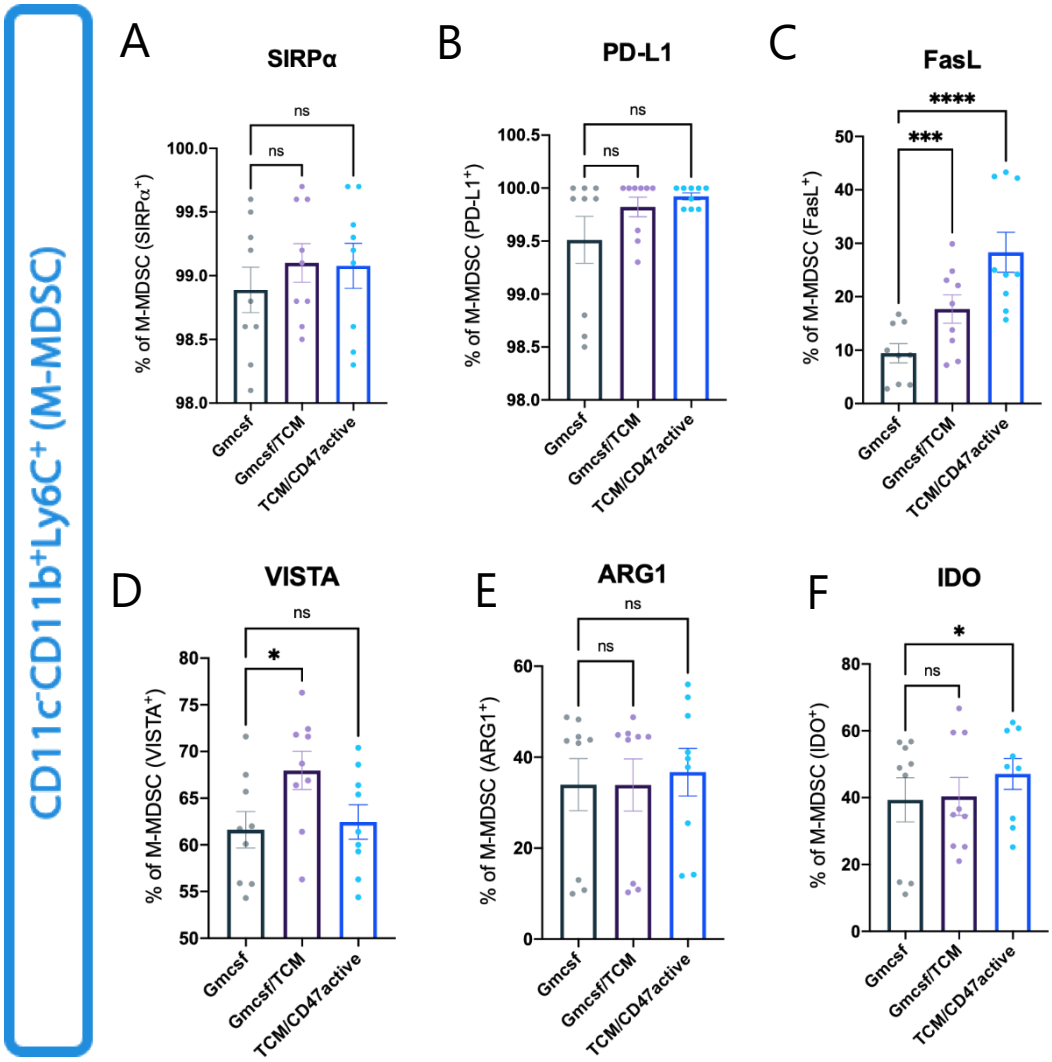

Appendix 8.6. Increased population percentage expressing FasL and IDO in M-MDSCs ($CD11c^{-}CD11b^{+}Ly6c^{+}$) cultured in GM-CSF-TCM-CD47. Flow cytometric quantification of the % of positive of M-MDSCs cultured in GM-CSF vs GM-CSF-TCM and GM-CSF-TCM-CD47 for **(A)** signal-regulatory protein alpha, SIRPα, **(B)** programmed death-ligand 1, PD-L1, **(C)** type-II transmembrane protein FAS ligand, **(D)** V-domain Ig suppressor of T cell activation VISTA, **(E)** arginase 1, ARG1 and **(F)** indoleamine 2,3-dioxygenase, IDO. Data are mean ± SEM; * = $p < 0.05$, ** = $p < 0.01$, *** = $p < 0.001$, **** = $p<0.0001$ using ordinary one-way ANOVA with Dunnett's post hoc test. Experiments n=3 in triplicates.

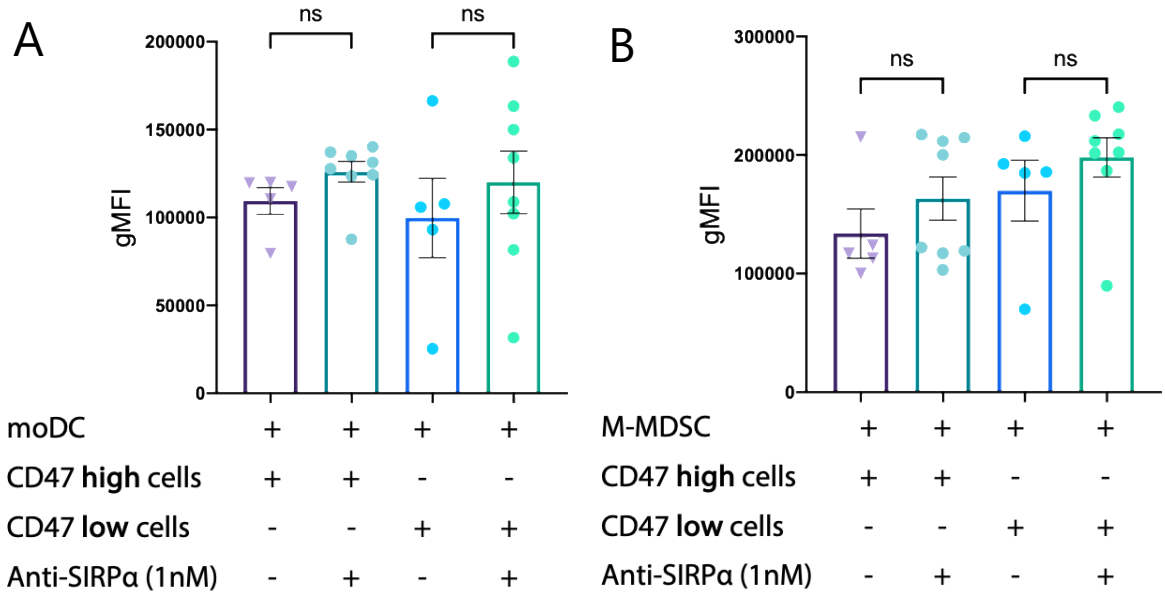

Appendix 8.7. The gMFI signal output of phagocytosis by M-MDSC and moDC cells very high and can't distinguish variable intensity. (A) Flow cytometry quantification of the gMFI signal of labelled CD47-high or -low cell debris by moDCs and **(B)** M-MDSCs obtained in presence of CD47-SIRPα engagement and blockade. Data are mean ± SEM; * = $p < 0.05$, ** = $p < 0.01$, *** = $p < 0.001$, **** = $p<0.0001$ using ordinary one-way ANOVA with Dunnett's post hoc test. Assays n=3 at least in duplicate.

A B

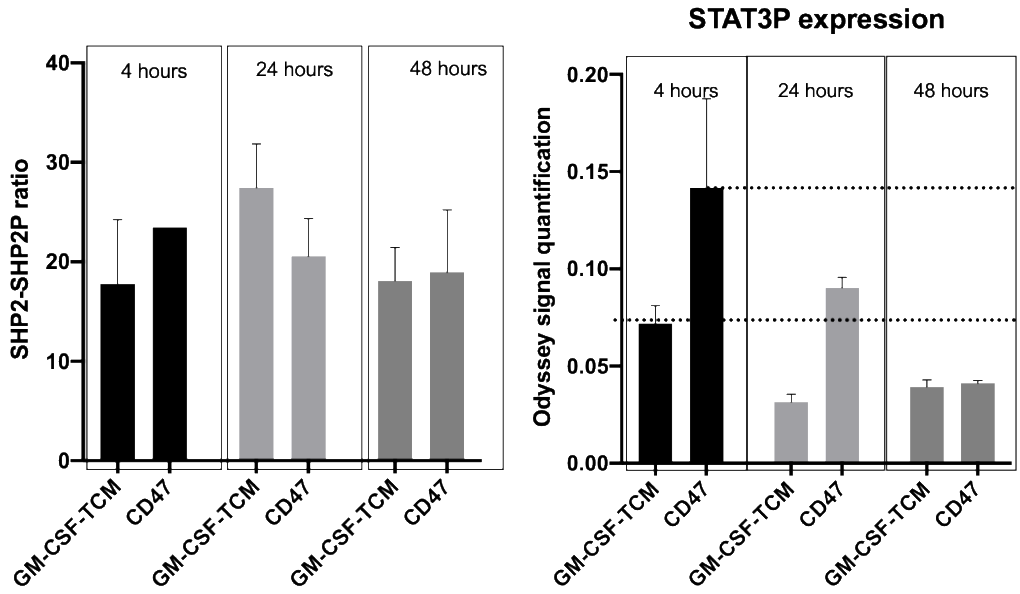

Appendix 8.8. The best detection of the difference between SHP2, STAT3 and respective phosphorylated versions was at 4 hours of the experiment. Western immunoblot quantification was performed using Odyssey CLx (Li-Cor) of **(A)** SHP2 and SHP2-P protein and of **(B)** STAT3 and STAT3-P.

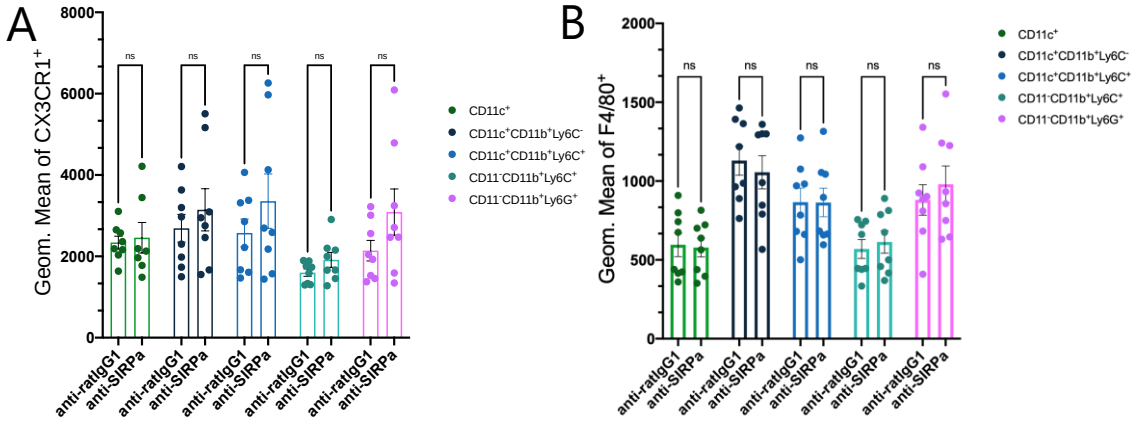

Appendix 8.9. The markers CX3CR1 and F4/80 intensities don't vary upon SIRPα blockade. Myeloid cells gMFI quantification for **(A)** the monocytic marker CX3CR1 and **(B)** the macrophage marker F4/80 comparing SIRPα blockade to rat-IgG1 injected controls. Data are mean ± SEM; * = $p < 0.05$, ** = $p < 0.01$, *** = $p < 0.001$, **** = $p<0.0001$ using two-way ANOVA with a Sidak's multiple comparison post hoc test. Assay n=4 mice for each group in two independent experiments.

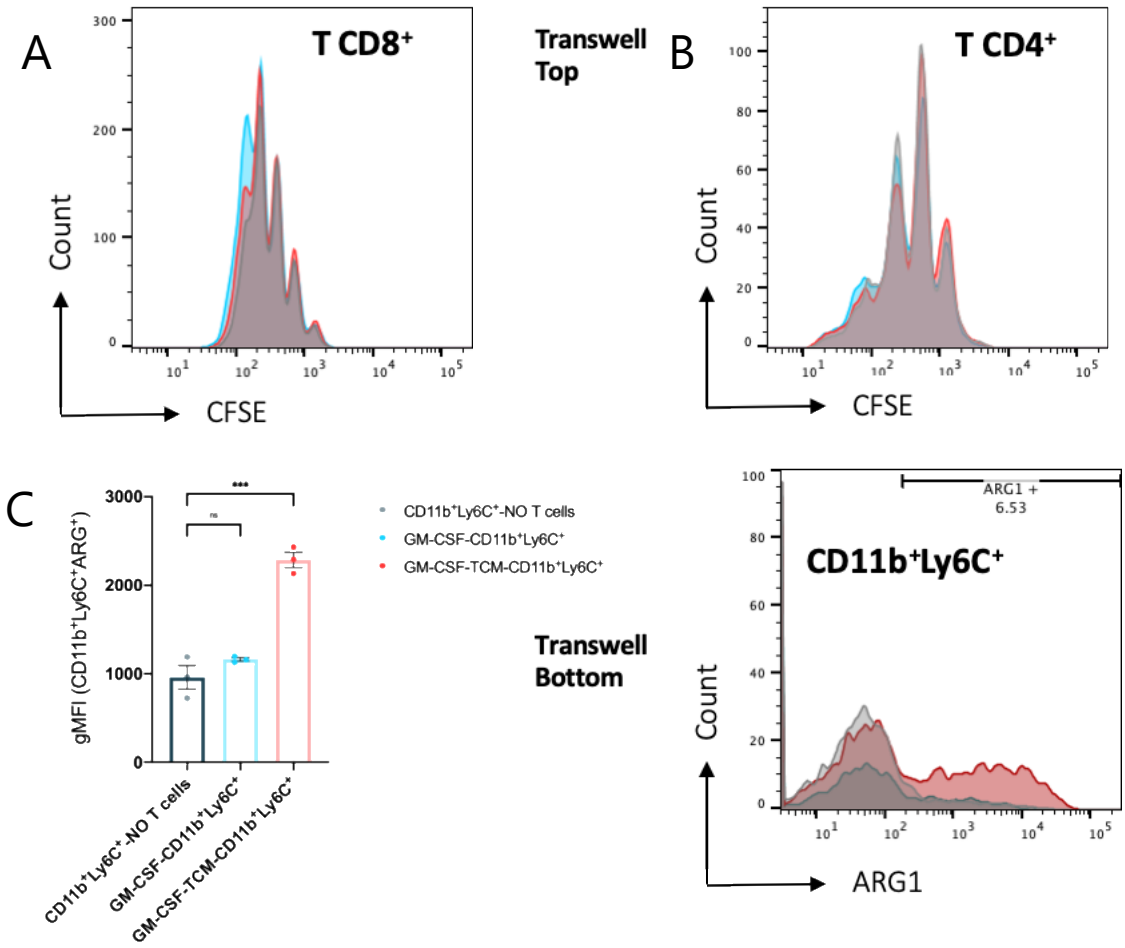

Appendix 8.10 The ARG1 increase doesn't affect T cells proliferation in a transwell experiment. GM-CSF and GM-CSF-TCM grown moDC and M-MDSC cells were seeded at the bottom and activated CFSE stained T cells at the top of a transwell plate. **(A-B)** Representative plots showing the proliferation of $CD8^+$ and $CD4^+$ T cells seeded at the top of a transwell. **(C)** Graph showing the quantification of ARG1 gMFI of $CD11b^+Ly6C^+$ cells seeded at the bottom of a transwell. (D) Representative plots showing the histogram of the ARG1 signal. Data are mean ± SEM; * = $p < 0.05$, ** = $p < 0.01$, *** = $p < 0.001$, **** = $p<0.0001$ using the one-way ANOVA with a Dunnett's post hoc test. Assays n=1.

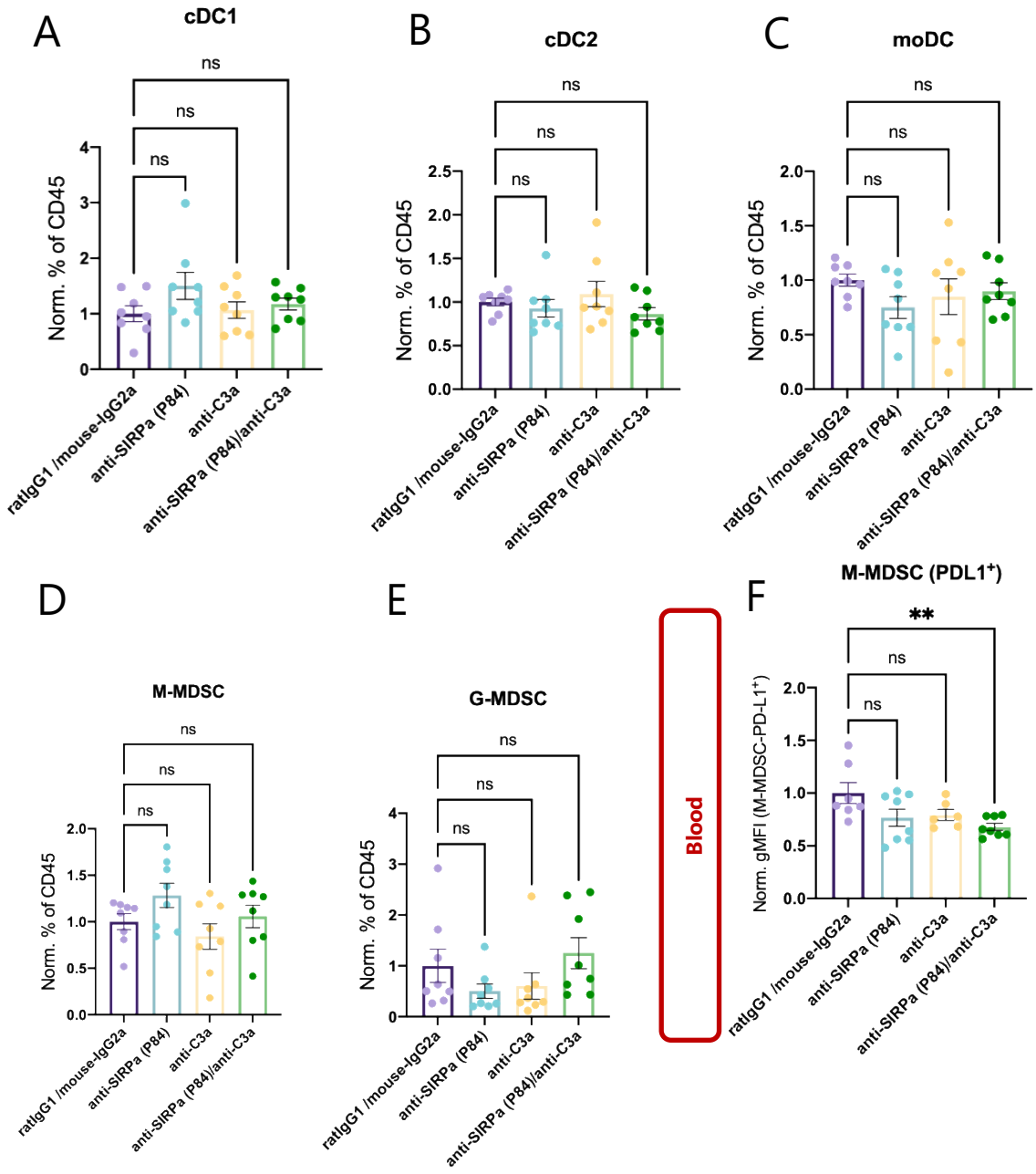

Appendix 8.11. The combination of C3a and SIRPα blockade results in an opposing myeloid remodelling obtained with the single agents but reduces PD-L1$^+$ M-MDSCs in the blood. The graphs show the **(A)** cDC1 (CD11c$^+$XCR1$^+$), **(B)** cDC2 (CD11c$^+$CD11b$^+$Ly6C$^-$), **(C)** moDC (CD11c$^+$CD11b$^+$Ly6C$^+$), **(D)** M-MDSC (CD11c$^-$CD11b$^+$Ly6C$^+$) and **(E)** G-MDSC (CD11c$^-$CD11b$^+$Ly6G$^+$) cells calculated as percentage of total CD45$^+$ cells for mice groups injected with rat-IgG1 and mouse-IgG2a (violet), anti-SIRPα-P84 antibody (light blue), anti-C3a antibody (yellow) and with the combination of the two (green). **(F)** the graph shows the normalised gMFI to control

of PD-L1 expressed by M-MDSCs in the mice blood injected with the respective drugs. The data were normalised by the signal detected for the control injected mice samples. Data are mean ± SEM; * = $p < 0.05$, ** = $p < 0.01$, *** = $p < 0.001$, **** = $p<0.0001$ using the (A to E) RM one-way ANOVA with a Dunnett's post hoc test and (F) ordinary one-way ANOVA. Assays mice n=4 for each group in two independent experiments.

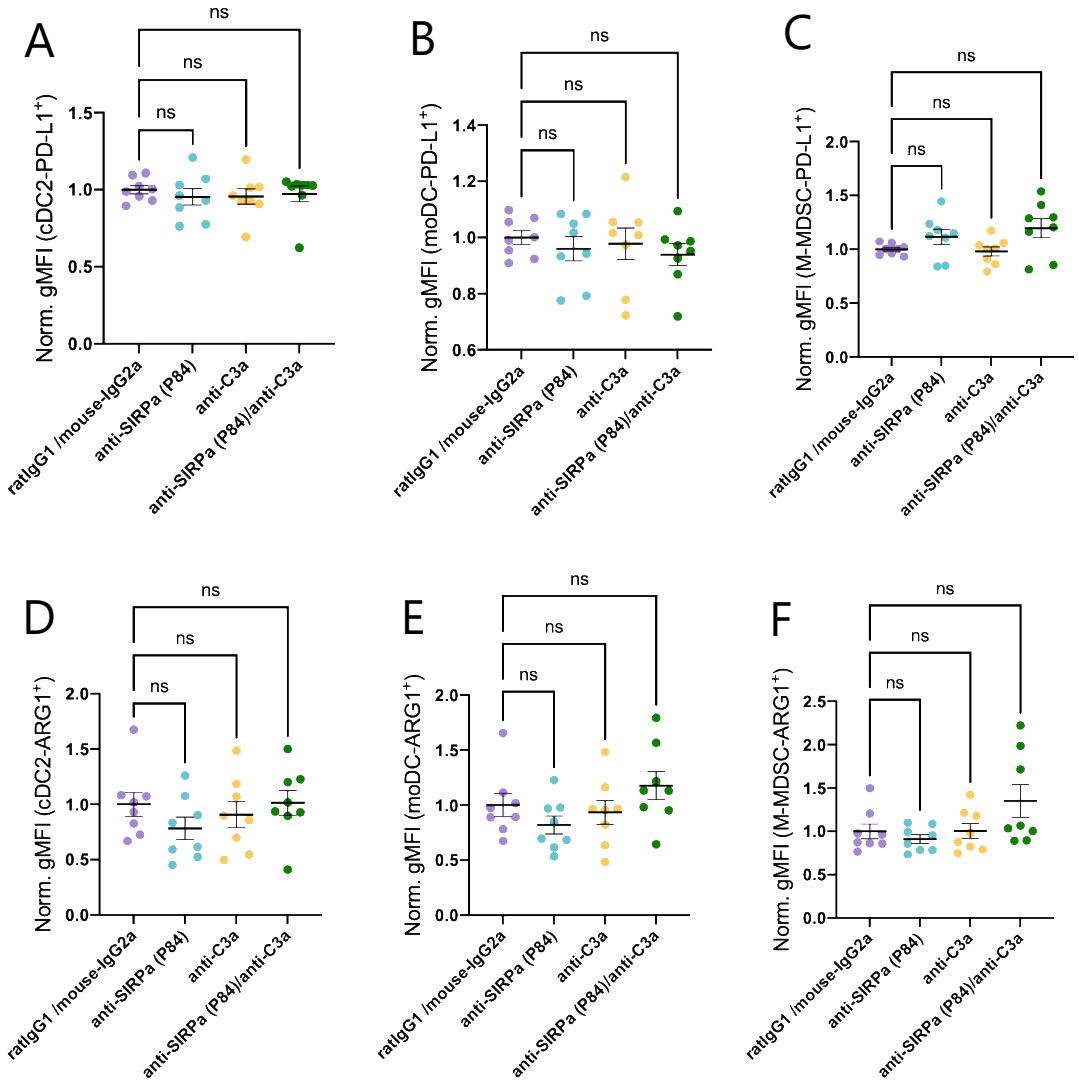

Appendix 8.12. The SIRPα and C3a blockade may partially modulate PD-L1 and ARG1 expression. The graphs show **(A to C)** PD-L1, **(D to F)** ARG1, gMFI variation associated to cDC2, moDC and M-MDSC cells in mice groups injected with rat-IgG1/mouse-IgG2a (control), anti-SIRPα-P84 anti-C3a and the antibodies combination. (A to F) The data were normalised by the signal detected in the control samples. Data are mean ± SEM; * = $p < 0.05$, ** = $p < 0.01$, *** = $p < 0.001$, **** = $p<0.0001$ using the one-way ANOVA with a Dunnett's post hoc test. Mice n=4 per group in duplicate.

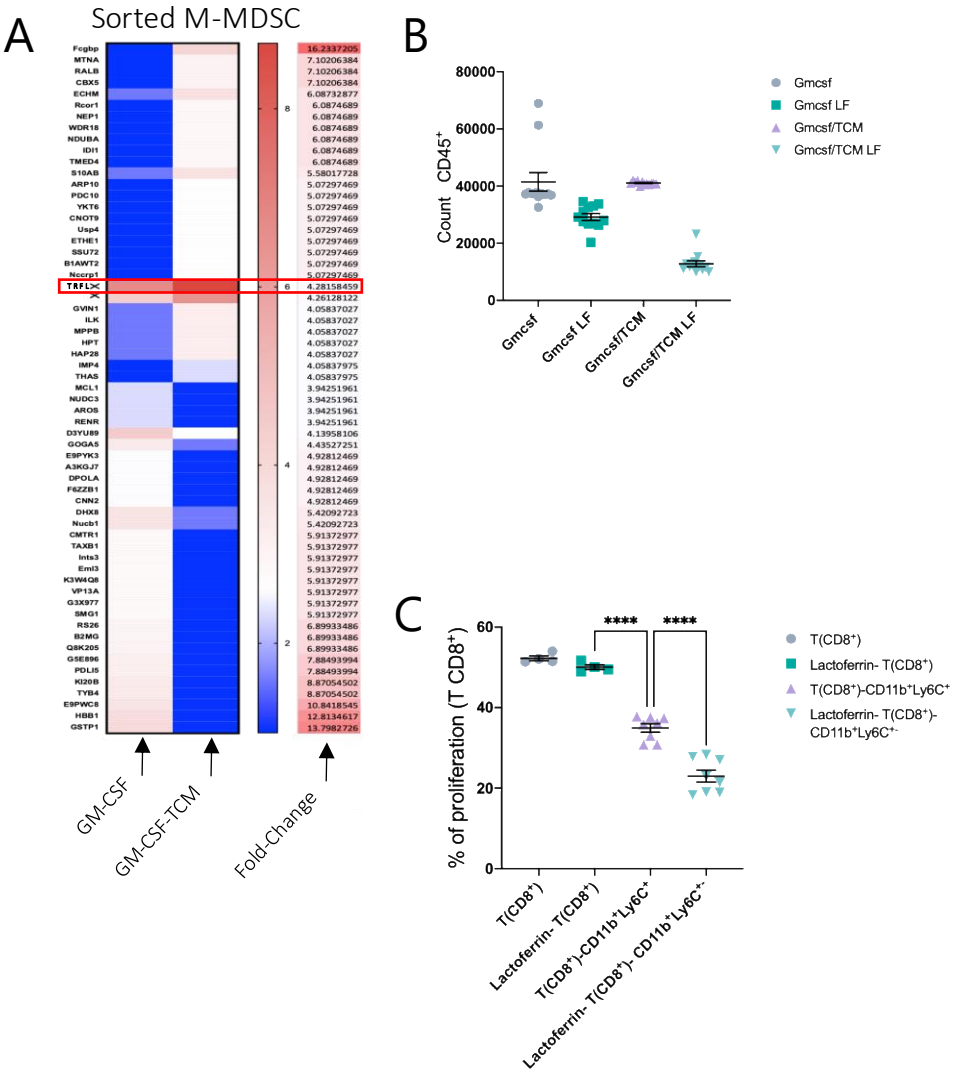

Appendix 8.13. Lactoferrin enhances the suppressive potency of M-MDSCs. (A) Differential proteins expression in sorted M-MDSCs grown in GM-CSF and GM-CSF-TCM analysed by mass spectrometry. The relative intensity of each protein is indicated by the coloured bar next to the heatmap. Fold-changes are indicated on the extreme right of the image. **(B)** Count of total CD45 positive cells after 5 days of cell culture in GM-CSF and GM-CSF-TCM with Lactoferrin addition. **(C)** T CD8$^+$ cells % of proliferation in co-culture with CD11b$^+$Ly6C$^+$ cells in GM-CSF-TCM and GM-CSF-TCM-Lactoferrin. Data are mean ± SEM; * = p < 0.05, ** = p < 0.01, *** = p < 0.001, **** = p<0.0001 using the one-way ANOVA with a Dunnett's post hoc test. Assays n=2 at least in duplicate.